An investigation of nucleation and crystallisation phenomena in lithia-alumina-silica glasses

Hunt, R. P.

AN INVESTIGATION OF NUCLEATION AND CRYSTALLISATION PHENOMENA IN LITHIA-ALUMINA-SILICA GLASSES

by

R.P. HUNT, B.Sc.
(Hatfield)

A thesis presented in candidature for the degree of Doctor of Philosophy in the University of Durham

JUNE
1973

ACKNOWLEDGEMENTS

I would like to express thanks to my supervisor, Dr. K.N.R. Taylor, for continued assistance throughout this work. Also I am indebted to the Science Research Council for a C.A.P.S. award which was in conjunction with James A. Jobling and Company Limited. I gratefully acknowledge the co-operation from the Staff of the latter. In addition my appreciation must go to the entire Staff of the Physics Department, particularly to the Head, Professor G.D. Rochester. Finally I wish to thank all others who have given support in particular Mrs. Albury for typing the manuscript.

A B S T R A C T

An outline of the use of titanium in glass ceramic production is given. To investigate the role of titanium in this process a variety of procedures were necessary. These included X-ray diffraction, Electron microscopy, Optical measurements and Electron spin resonance.

Two main approaches to the investigation have been adopted, the first is through the observation of the effects of crystallisation on gadolinium introduced into the glass matrix. The interpretation of the electron spin resonance for gadolinium in terms of a spin hamiltonian has led to the suggestion of two sites for this rare earth ion.

A crystal growth inhibition has been found to be produced by the incorporation of gadolinium in the lithia alumina silica glass ceramics.

The alternative method of investigation is concerned with X-ray induced defects and the results have been interpreted in terms of local well ordered domains existing within the glass.

Glossary of Terms

Dragation - rapid quenching with water.

Solarisation - production of defects by irradiation

Non-bridging oxygen ions - oxygen ions in a glass which are bonded to only one ion.

β-eucrypitite - a crystalline form of lithium aluminium silicate

Seed - small air bubbles found in glass.

CONTENTS

CONTENTS (cont'd)

LIST OF FIGURES

LIST OF FIGURES (CONT'D)

LIST OF FIGURES (CONT'D)

LIST OF TABLES

CHAPTER 1.

1.1 Introduction

Although a universally accepted definition of a glass is yet to be found the definition given by Mackenzie (1.1) will be sufficient in the context of this work. "A glass is any isotropic material, organic or inorganic, in which three-dimensional atomic periodicity is absent and the viscosity of which is greater than 10^{14} poise". It is the degree of periodicity of the basic structural units that distinguishes between the glassy and crystalline states. The rapid cooling techniques usual in glass production, result in the freezing in of liquid disorder, the type and amount of this disorder depending upon the temperature of the melt and the cooling conditions. A great number of glass systems are now known to exist, but the most common are those which incorporate alkali or alkaline earth oxides with phosphorus, silicon or boron, together with large amounts of oxygen. A useful introduction to the complex subject of glass can be found in the review by Weyl and Marboe (1.2).

For many years glass has been used with its manufacture based on empirical methods and an understanding of the scientific nature of glass formation can be considered to begin with the work of Zachariasen (1.3). In 1932 he proposed the random network theory in which the oxides B_2O_3, SiO_2, GeO_2, P_2O_5 and As_2O_5 were designated "glass formers" and the alkali and alkaline earth oxides were called "network modifiers". This concept of a continuous random glass lattice was found to be useful to glass technologists for many years, but a more detailed look at ionic environments led to the development of a new crystallite theory by

Valenkov and Porai-Koshits (1.4). In contrast to Zachariasen's idea of a continuous network this theory favours the existence of domains in which a high degree of local ordering occurs. These regions can be considered to be small distorted crystals separated by zones of less order.

These two theories represent extremes in the variety of possible glass-like structures and it appears that the extent to which one or other applies depends upon the particular system one is observing. Structural interpretation in the glass world is difficult as even the nature of pure vitreous silica and of many complex silicate crystals is still to be completely determined (1.5)(1.6). It is thus clear that in a complex system like the lithium aluminium silicates a certain amount of information is still required to provide clarification. This particular system has become important in recent years as it forms the basis of many commercial ceramics.

This new field of glass technology has initiated a reversal of the age old problem of glass technologists to prevent devitrification. However the devitrification of glass must be effectively controlled to produce the optimum beneficial properties possible. Stookey's (1.7) discovery that TiO_2 can act as a catalyst in the formation of desirable crystalline phases which produce pyroceram, a ceramic material of high mechanical strength and low thermal expansion, has led to the widespread use of titanium dioxide in glass ceramic production. Much research has been directed towards the elucidation of the role played by titania in the glass phase and in the glass to crystal transition and the requirements for fine grained ceramic formation. Although it is evident

from the literature that titanium dioxide nucleation occurs efficiently in many glass systems the lithium aluminium silica system has been the major consideration in this present work as it is known to produce ceramics of great practical importance.

1.2 Nature of Titanium Dioxide Nucleation

When titanium is added to fused silica the direct substitution of titanium ions for silicon ions would seem a reasonable possibility if one considers the similarity in both physical and chemical properties of these oxides. However geometric considerations reveal a remarkable dissimilarity. Whereas the Ti^{4+} ion has an ionic radius of 0.64 a.u. which requires a co-ordination number of six, the Si^{4+} ion is known to exist with tetragonal co-ordination. Coupled with the inability (1.8) of experimentalists to dope rutile crystals with any significant amount of SiO_2 or a crystal of silica with TiO_2, and the general lack of Ti^{4+} replacement of Si^{4+} in silicate minerals the four-fold co-ordination of Ti^{4+} in glasses seems unlikely. Turnbull and Lawrence (1.9) conclude that a constant six-fold co-ordination occurs for Ti^{4+} in Na_2O - SiO_2 - TiO_2 glasses, whilst Rao (1.10) shows the existence of both four-fold co-ordination of Ti^{4+} leading to a strengthening of the structure and a six-fold co-ordination leading to a weakening of the structure in a binary alkali - TiO_2 system. It appears that titania incorporation into glass depends as expected upon the exact nature of the glass system but is usually in the six-fold co-ordination state.

This six co-ordination state as required by the larger titanium ion produces a relative weakening of the glass structure in the vicinity of the titanium ion. A resulting reduction in the viscosity is observed

and may be one of the causes for enhancement of crystallisation by allowing the rapid re-arrangement of ions in the glass. The effects produced by TiO_2 in glass systems have been summarised by Beal (1.8) and it is evident that more than one method must be considered to explain the increased and fine grained nature, of the crystallisation induced by the heat treatment of TiO_2 containing glass systems.

It is known (1.11) that regions exist in the Li-Al-Si system in which lithium rich phases can develop, thus providing the possibility that titanium dioxide could influence the component distribution in a glass leading to phase separation. Regions may then occur in which a composition close to a crystal or in which a super-saturation of a given crystal exist and may result in precipitation. The resulting crystals could act as centres of crystal growth for the bulk crystallisation of the glass, the numerous nucleation sites ensuring the production of a fine grained ceramic. Such a mechanism has been suggested (1.12) to explain the role of titania in a Li_2O - AL_2O_3 - SiO_2 glass.

An alternative approach (1.13) is that the addition of titanium produces a super-saturated condition for some titanate compound without phase separation. Upon increase of temperature, the resulting reduction in viscosity allows the re-organisation of molecules and results in the precipitation of titanate compounds. These precipitates are again thought to act as nucleation centres for bulk crystallisation of the glass.

A further local ordered domain theory has been applied (1.14) to some compositions in the Li-Al-Si system. Titanium is said to associate with non-bridging oxygen ions around regions of high order. This is

reasonable since the titanium could more easily obtain the required six co-ordination in the presence of non-bridging oxygens. The existence of non-bridging oxygens is a requirement of the charge imbalance between uneven atomic distribution of positive and negative charges in glass. These well ordered regions can then be thought of as nucleation centres with the titanium acting as a catalyst at the crystal growth front.

It has become apparent that the variability and complexity of glasses with their dependence on thermal history and impurities makes the universal application of one mechanism to explain the effect of TiO_2, even in one system, unlikely.

1.3 Aim Of This Work

The aim of this study was to obtain information relevant to the production of glass ceramics and in particular to the influence of titanium dioxide in the glass to crystal conversion. A variety of techniques were employed as the very nature of glass prohibits a clear interpretation of any one set of experimental results.

Two main approaches to the problem were considerd, the first was by the introduction of an ionic probe to be monitored during the crystallisation specifically by electron spin resonance. Naturally, advantage was taken of any additional information gained by the introduction of such a probe. The second was through the study of X-ray induced defects.

1.4 Previous Investigations

The incorporation of transition ions to investigate structural

changes in glass has been a useful technique for a number of years (1.15)(1.16). Sands (1.17) was the first to study the e.s.r. of these ions in glasses, and his unexpected discovery of resonances at $g \approx 6.0$ and $g \approx 4.2$ was later explained by Castner, Newell, Holton and Slichter (1.18) as due to an Fe^{3+} impurity. Since then Fe^{2+}, Fe^{3+}, Mn^{2+}, Cr^{5+} and V^{5+} have been used as dopants.

Observation of the effect of even small concentrations of transition metal ions in some glass systems is evidence of the non-neutrality of the transition ions, which is an undesirable property of an "inert" probe used to observe structural changes. For example recently iron and chromium oxides when added in small percentages to glasses, in the $CaO - MgO - Al_2O_3 - SiO_2$ quaternary system, have been shown by Rogerson (1.19) to affect both the rate of nucleation and the rate of crystal growth during heat treatment. The number of commercial glass-ceramics employing one or other of the transition ions as a nucleation catalyst has rapidly increased. These facts indicate that it is extremely doubtful that transition ions, TiO_2 in particular, can act as inert dopants in glasses.

Until recently the use of the 4f ions of the lanthanide series as paramagnetic dopants in this area of research has been very limited, a fact which may be associated with the reduced effects of the crystal field on these ions compared with the 3d-transition metal ions. It is probable that there is less distortion of the glass structure about a 4f impurity ion than about a 3d ion since the 4f electrons are deeply buried in the ion and consequently well screened from the crystalline electrostatic field. The lanthanide ions may thus prove more satisfactory as inert structure-sensitive probes than the transition metal ions though the effects of crystallisation are expected to be correspondingly reduced.

In order to use the rare-earths as probes in the crystallisation process one must have some knowledge of their environment in the glass. It is known that glass lacks definite long range order and it seems reasonable to expect that the rare-earth may influence its immediate surroundings.

Previous workers have associated the average environment for rare-earth ions in oxide glasses with the equivalent rare-earth oxide structure. Mann (1.20) found the energy levels of Neodymium in glass, to correlate closely with those determined from oxide crystals and concluded that the ions occupy sites of low symmetry. The spectral line half widths, of approximately 100 cm^{-1}, were attributed to inhomogeneity of the glass structure.

Work by Rice and Deshazer (1.21) compared the fluorescence and absorption spectra of europium ions in glass with the spectra of europium in single crystals of gadolinium oxide. Some absorption lines, for example the $^7F_o \longrightarrow {}^5D_2$ line, of europium in the gadolinium crystals were found to consist of three groups of lines indicating that three preferential sites exist for the Eu^{3+} ion. This agrees with the three kinds of Eu^{3+} ion sites in europium sesquioxide with point-group symmetries of C_3. This rather complex monoclinic structure is also found for gadolinium sesquioxide and by direct comparison three sites might be expected for gadolinium in a glassy environment. Further work by Mann and Deshazer on Neodymium in glass suggests that the Nd^{3+} ion locates in only one average environment site in glass, mirroring the fact that there is only one kind of Nd^{3+} ion site in the trigonal neodymium sesquioxide.

All of the information mentioned so far, concerning rare-earth sites

in glass, has been obtained from optical observations. The use of e.s.r. has been very limited, however the Eu^{3+} and Gd^{3+} ions produce resonances at room temperature and are relatively easily obtained. Yarif' yanov et al. first studied Gd^{3+} as well as Cr^{3+}, Cr^{5+} and Mn^{2+} (in various glasses) but the interpretation of the results was not at all clear. The first theoretical explanation of the e.s.r. spectra of Gd^{3+} ions in a glass matrix appears to be that of Nicklin (1.22). By using a spin Hamiltonian approach and restricting the magnetic field to the x, y and z directions he was able to account for the main details of the X-band resonance. His postulate of one site for gadolinium, however, led to discrepancies which he could not explain at frequencies away from X-band. Further no correlation was found between the intensities of the various parts of the experimental resonances from his calculations.

It is thus necessary to clarify the nature of the environment of the Gd^{3+} ion in the glass matrix if the maximum advantage is to be taken of this paramagnetic probe in the investigation of glass crystallisation.

The alternative approach to the problem through X-ray induced defects is also not well developed. It is well known that one of the effects of ionizing radiation on solids is to produce free electrons and holes which are ultimately trapped to form a type of defect centre. The optical absorption and magnetic resonance spectra of these centres have been extensively studied in an effort to understand the nature of the centres and the kinetics of their formation (1.23) (1.24) (1.25) (1.26) (1.27). The optical absorption and resonance studies of trapped holes suggest that the same kind of hole traps occur in many silicate, phosphate and borate glasses having tetrahedrally co-ordinated network

formers. Most models propose that the main hole traps are associated with non-bridging oxygen ions in the glass forming tetrahedra in which the electrons are placed. For silicate glasses, placing these levels in the vitreous silica band gap relates the electronic band structure of binary silicate glasses to that of vitreous silica (1.28).

In contrast to the optical and e.s.r. studies of irradiated glasses little work has so far been done in connection with the thermoluminescence properties of glasses (1.29) (1.30). It was considered that thermoluminescence would prove a useful technique in the context of the present work as it provides a sensitive tool for investigating defect energy levels in either glassy or crystalline solids.

CHAPTER 2.

TECHNIQUES AND EXPERIMENTAL METHODS

2.1 Specimen Preparation

All the glasses used in this work were prepared from high purity materials which included acid washed, 180 micron mesh Brazilian quartz; 99.9% lithium carbonate; acid washed, crushed sapphire; 99.95% rare earth oxides and B.D.H. grade titanium dioxide with less than 0.05% Fe.

Compositions were chosen from the Li_2O-Al_2O_3-SiO_2 phase diagram Fig. (2.1), for the base L.A.S. glasses. The amount of additions of Gd_2O_3 and TiO_2 to these L.A.S. base glasses depended upon the considerations outlined in Chapter 3. Mixtures of the constituents, to give the compositions required, were prepared and ground together in an agate mortar to assist dispersion before melting. Electrically heated furnaces were used to melt approximately 100 gm. batches of the individual glasses in 95% platinum 5% rhodium crucibles. The Kanthal heating elements allowed the temperature to be governed by a Eurotherm control system. There was no attempt made to alter the atmosphere surrounding the melt, although this has been used to produce oxidation and reduction of ions in glass melts by other workers. The use of a lid on the crucibles and a constant air environment for the melt was assumed to give an adequately constant oxidation condition.

Glasses were maintained in the molten state for several hours with intermediate dragation, with distilled water, to promote the production of a homogeneous glass and the removal of seed. When the

FIG. 2.1

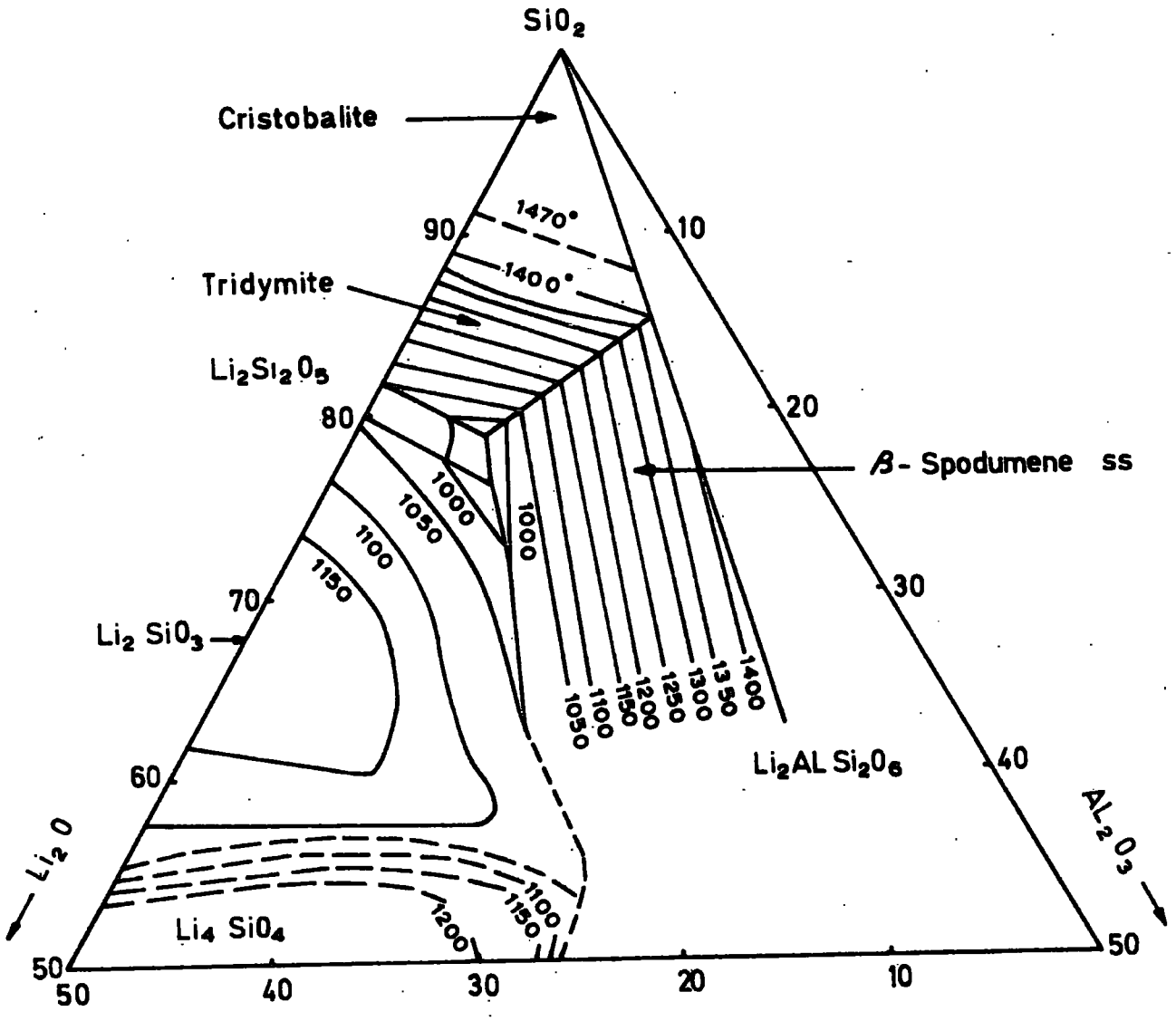

Li_2O - AL_2O_3 - SiO_2 Phase Diagram

after R.A. Eppler, J. Am. Ceram. Soc., 46 [2] 100 (1963)

melt was seen to be reasonably 'seed-free', the glass was cooled rapidly to room temperature by chilling on metal blocks. For some glasses preheating of the metal blocks to 200-300°C was necessary to prevent shattering of the glass on cooling. The temperature and time of melting varied with glass composition but was typically 1600°C for 10-20 hours for glasses in the L.A.S. system. All the samples produced in this way were found to be totally glassy by X-ray diffraction.

Additions were calculated and added to 100% of the base glass. Standard wet chemical analysis, performed on a selection of the glasses at James A. Jobling Advanced Research Unit, gave the composition of the glasses within a few percent of the batch compositions. These slight changes may be due to volatilisation in the melt or inhomogeneity in the glass. The small differences have been assumed negligible and the glass composition taken as that of the original batch when analysis results were not available. Table (2.1) shows the compositions for all the glasses used.

Samples required for specific experiments were specially prepared: for use in optical absorption measurements, specimens were ground flat and polished to a one micron finish with diamond paste after being cut to the required shape and size.

Preliminary heat treatment studies were made on samples placed in a temperature gradient furnace. More precise heat treatment was obtained by placing the samples directly into a preheated furnace and they were returned to room temperature as rapidly as possible after the required period of soaking at the set temperatures. The

TABLE 2.1

GLASS COMPOSITIONS

SAMPLE NOS.	MOLE % OF					
	SiO_2	Al_2O_3	Li_2O	TiO_2	Gd_2O_3	Nd_2O_3
1022	60	20	20	-	-	-
1023	60	20	20	0.1	-	-
1035	60	20	20	5.0	-	-
1036	60	20	20	5.0	1.0	-
1057	60	20	20	0.1	1.0	-
1058	60	20	20	-	1.0	-
1059	60	20	20	5.0	-	1.0
1060	60	20	20	-	-	1.0
1129	60	20	20	5.0	0.18	-
1130	60	20	20	5.0	0.09	-
1022/1	60	20	20	0.01	-	-
1022/2	60	20	20	0.05	-	-
1022/3	60	20	20	0.10	-	-
1022/4	60	20	20	0.50	-	-
1022/5	60	20	20	1.00	-	-
1022/6	60	20	20	5.00	-	-
1022/0/1	90	5	5	-	-	-
1022/0/2	80	10	10	-	-	-
1022/0/3	70	15	15	-	-	-
1022/0/4	50	25	25	-	-	-
1022/0/5	80	0	20	-	-	-
1022/0/6	70	10	20	-	-	-
1022/0/7	50	30	20	-	-	-
1022/0/8	80	20	0	-	-	-
1022/0/9	70	20	10	-	-	-
1022/0/10	50	20	30	-	-	-

temperatures were estimated to be within 2°C of the stated values.

2.2 Differential Thermal Analysis

2.2.1 Outline of Theory

Differential thermal analysis was used to observe thermal effects accompanying chemical changes and structural transformations during the crystallisation of the glasses. The temperature differential between a sample and a thermally inert reference sample of aluminium oxide is recorded whilst both undergo an identical, constant rate of temperature increase.

It has been shown (2.1) that if K is a temperature normalising coefficient between the sample and the reference material, r is the heating rate, T_r is the temperature of the reference junction, $\Delta T = T_r - T_s$, C_p is the heat content of the sample and its support and ΔH is the amount of heat associated with the reaction, then assuming C_p and K are not temperature-dependent over the interval involved during a time period dt when the reaction is occurring, the heat balance equation is

$$C_p \, d\Delta T = d\Delta H - K \Delta T \, dt \qquad (2\text{-}1)$$

If t_1 and t_2 are the times at the beginning and end of a peak then it follows from equation (2-1) that

$$\Delta H = K \int_{t_1}^{t_2} \Delta T \; dt \qquad (2\text{-}2)$$

$$= K \text{ peak area (A)} \qquad (2\text{-}3)$$

K is a function of sample and furnace geometry and is complicated by specimen contraction and temperature non-uniformity arising from problems of thermal transfer.

From equation (2-1) between temperatures t_1 and t_2

$$\int_{t_1}^{t_2} K \left(T_1 - T_s \right) dt = \int_{t_1}^{t_2} C_p \, dT_s + \int_{t_1}^{t_2} d \, \Delta H \qquad (2\text{-}4)$$

since $$T_r = T_s + rt, (t_1 \leqslant t \leqslant t_2) \qquad (2\text{-}5)$$

$$\Delta T_{max} = r \left(t_2 - t_1 \right) \qquad (2\text{-}6)$$

from equation (2-4) $$\frac{K r \left(t_1 - t_2 \right)^2}{2} = \Delta H \qquad (2\text{-}7)$$

$$\Delta T_{max} = \sqrt{\frac{2r \, \Delta H}{K}} \qquad (2\text{-}8)$$

From equations (2-3) and (2-8) it can be seen that the heat associated with a given reaction is proportional to the peak area, whilst the maximum temperature span is proportional to the square root of the product of the heating rate and the peak area.

By keeping experimental procedures as constant as possible the temperature normalising coefficient, K, can be assumed constant. This entailed constant weights and size of particles for specimen and reference materials. A constant geometrical apparatus arrangement was also used. As the heating rate r was kept constant, from

equations (2-3) and (2-8) it can been seen that the area and width of the differential peak give a measure of the thermal changes occurring in the sample.

2.2.2 Experimental

A commercial Standata 5-50 D.T.A. apparatus, a schematic diagram of which is shown in Fig. (2.2), was used in this study. 0.30 grams of specimen and reference material were placed in separate matched platinum crucibles, after being passed through a 250 micron mesh sieve to ensure uniform grain size, and each was gently vibrated to avoid air inclusions. A Pt/Rh thermocouple was used to record the furnace temperature whilst a second thermocouple measured the temperature differential. The e.m.f. outputs were displayed on a chart recorder. A consistency check with two identical specimens in two different sets of differential thermal analysis apparatus showed the temperatures recorded to differ by less than 2^{o} C.

2.3 X-ray Diffraction

A regular crystalline arrangement is not required for the production of diffraction effects as was first pointed out by Debye (2.2). In contrast to the sharp diffraction effects of crystalline materials it is found that liquids and glasses generate only one or more broad diffuse halos. This is to be expected as the well-defined lattice parameters, necessary to produce sharp diffraction lines, are absent.

In the present study the progress of the glasses towards

FIG. 2·2

DIFFERENTIAL THERMAL ANALYSIS APPARATUS

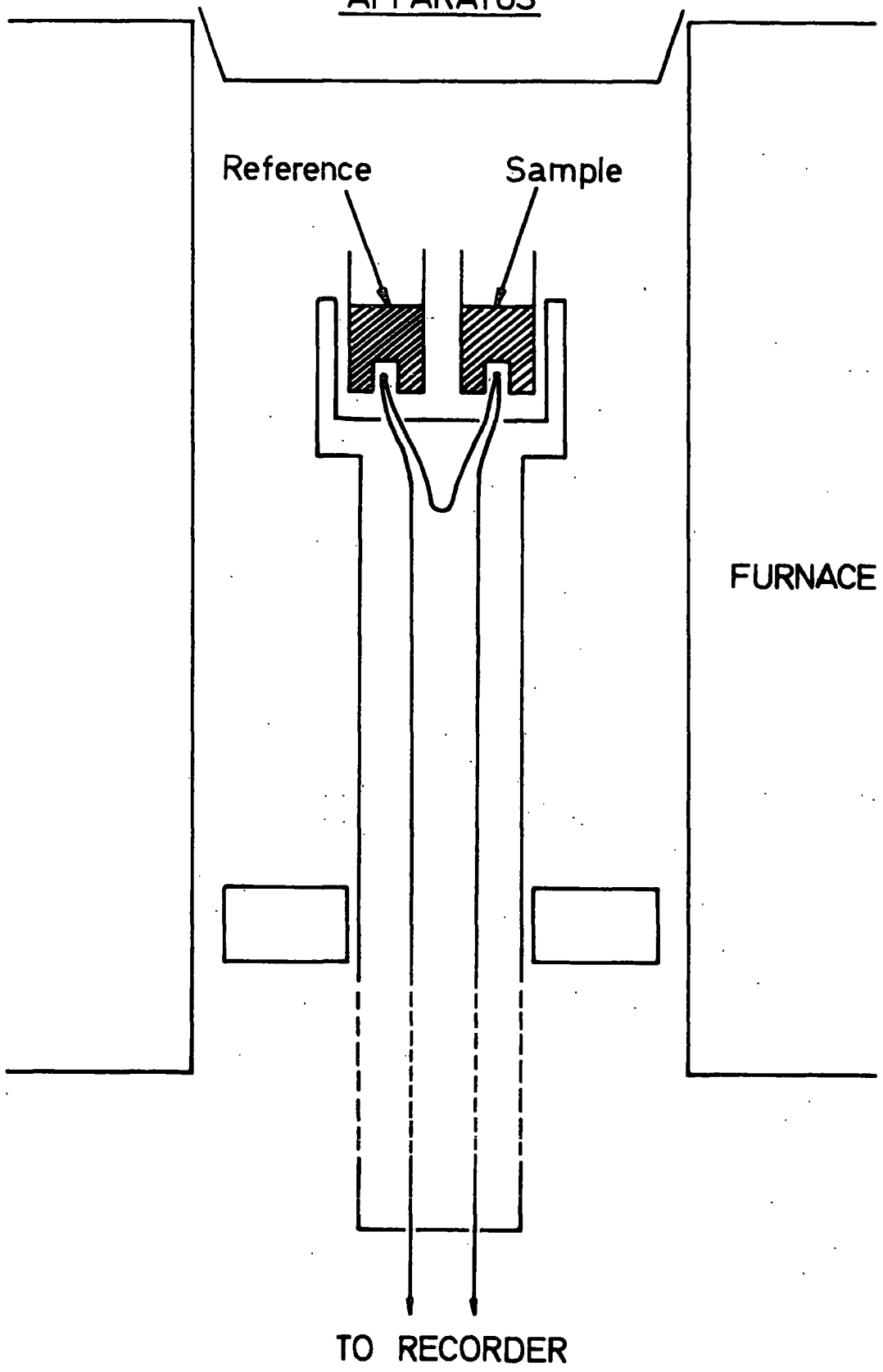

crystallinity, with heat treatment, was monitored by the emergence of the crystalline diffraction lines. X-ray measurements were obtained using either an A.E.I. Raymax RX3 or a Philips commercial X-ray camera operated with a Cu Kα tube.

As it was desirable to use the diffraction line intensities as a semi-quantitative measure of the extent of crystallisation a constant procedure was followed. This included three-hour exposures with X-ray tube settings of 35 kV and 15 mA in conjunction with Kodak industrial G film. An inert hyspin oil binder was used to hold the samples, which had been ground in an agate mortar and passed through a 250 micron mesh sieve. After standard X-ray film development, the negatives were processed by use of a Joyce Loebl optical densitometer operated with a 100 micron step interval. Both a graphical and a punched tape output were obtained, the latter being analysed on an I.B.M. 1130 computer to find the appropriate d-values. These d-values were then compared with the A.S.T.M. index values of the expected crystalline structures.

As no sharp dividing line exists between crystalline and so-called amorphous materials a quantitative measure of the crystallisation was estimated from either the graphical optical densitometer output or from the computer processed data.

2.4 Electron Microscopy

Preliminary observations of heat-treated glasses were made with a Tesla BS 242E electron microscope. This reduced the number of specimens which required the higher magnification obtainable with a Philips E.M. 300 electron microscope. Samples were examined by

observation of replicas taken from freshly fractured surfaces. For the highest resolution it was found that transmission through thin chips provided the clearest pictures. For both microscopes a similar double-stage specimen preparation was followed. Advantage of the different solubility of the glassy and the crystalline phases in dilute hydrofluoric acid was taken to enhance the image resolution. Careful control was required to obtain the maximum possible advantage of the different solubilities. After several test runs a procedure was adopted in which freshly fractured surfaces were etched with 0.2% HF for several seconds. Plastic replication, using acetone softening of the plastic, was followed by carbon coating of the replica in an evacuated atmosphere. This carbon film was then released by dissolving the plastic in 5% HF for several minutes. It was then washed in acetone and distilled water and floated onto a copper grid. The copper grid could then be mounted in the electron microscope.

Although structure greater than 1,000 A could be observed by the replication technique finer detail required transmission electron microscopy. It was found that the double-stage preparation of the samples allowed observation by the transmission process, since small fragments of specimen remained on the replicas. At large magnification, greater than one hundred and fifty thousand times, heat generated by the electron beam was found to cause some structural alterations. This could only be avoided by use of the replica technique, which produced very poor resolution at this magnification, or by use of low electron beam intensities and short exposure periods with the electron transmission measurements.

As the latter gave the best results it was the method normally followed.

2.5 Optical Measurements

Several instruments were used to investigate the optical properties of the glasses. Within the 170mμ to 1,000mμ region an Optika spectrophotometer was used whilst a Perkin-Elmer 137 E sodium chloride absorption spectrophotometer covered the 15μ to 25μ region. For higher energies a Perkin-Elmer U.V. spectrometer was used.

When necessary, for example in the measurement of luminescence spectra, the spectrometer output was corrected for the quantum efficiency of the detectors used. Both thin film and KI/pellet techniques were used in the infra red region, the latter being required for crystallised samples.

2.6 Thermoluminescence

Thermoluminescence (glow curve) spectra were obtained using a specially designed cryostat (see Fig. 2.3) capable of working in the temperature range from 80^{o}K to 860^{o}K in conjunction with an E.M.I. photo multiplier tube (type 9514 B). 2 mm thick polished samples approximately 1.2 x 7 mm were used and subjected to various periods of radiation, at set temperatures, from a Co. tube target operating at 20 mA and 15 kV. Radiation was supplied to the samples through a $\frac{1}{4}$ inch diameter hole in the brass cryostat, masked to allow evacuation. Specimens were mounted on a copper block and the temperature measured by direct contact of the thermocouple to the

FIG. 2.3

THERMOLUMINESCENCE APPARATUS

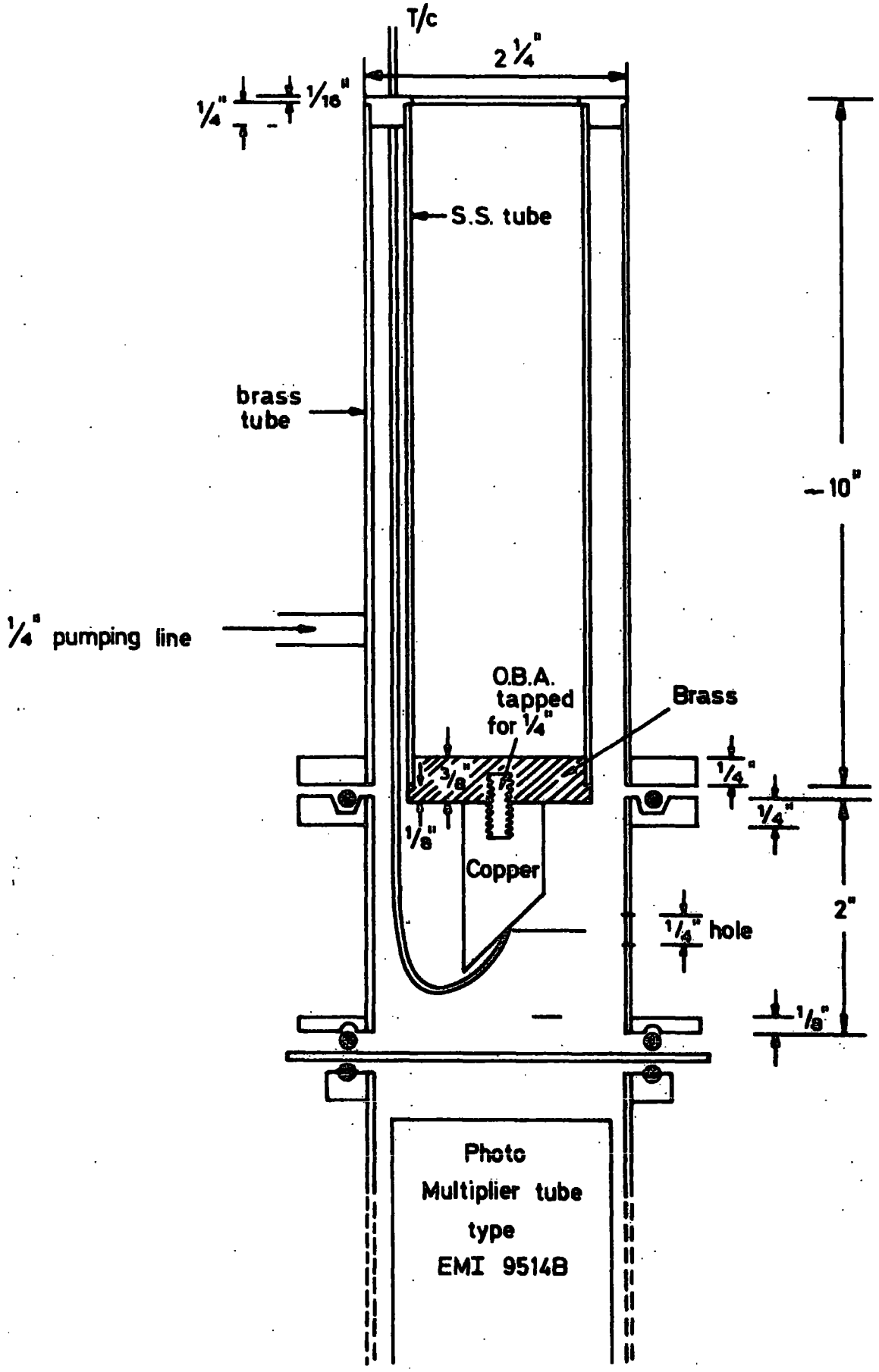

glass surface away from the copper. Since the glasses had a low thermal conductivity the temperature of this side, which has the greater probability of defects, was deemed to be most appropriate.

After solarisation, samples were warmed at a constant rate by a Kanthal-wire electrical heater, optically screened from the photo multiplier. As the sample was heated, the thermal release of trapped electrons resulted in the release of optical photons, which were detected by the photo-multiplier. Amplification of this signal was by means of the circuit shown in Fig.(2.4). The output from the anode was fed directly to the Y axis of an X-Y recorder, the X axis being driven by the output from a copper/constantan thermocouple, with reference junction at $77^{o}K$, attached directly to the specimen. By the use of an internal time base the X-Y recorder could also be used to display the luminescence intensity, at a particular temperature, as a function of the time after switching the excitation radiation on or off.

Spectral resolution of the thermoluminescence output was obtained by incorporation of a series of optical filters between the sample and the photo multiplier, correction being made for the spectral sensitivity of the detector.

2.7 Electron Spin Resonance

2.7.1 Introduction

The fundamental resonance condition is given by

$$h\nu = g\mu_B H \qquad (2\text{-}9)$$

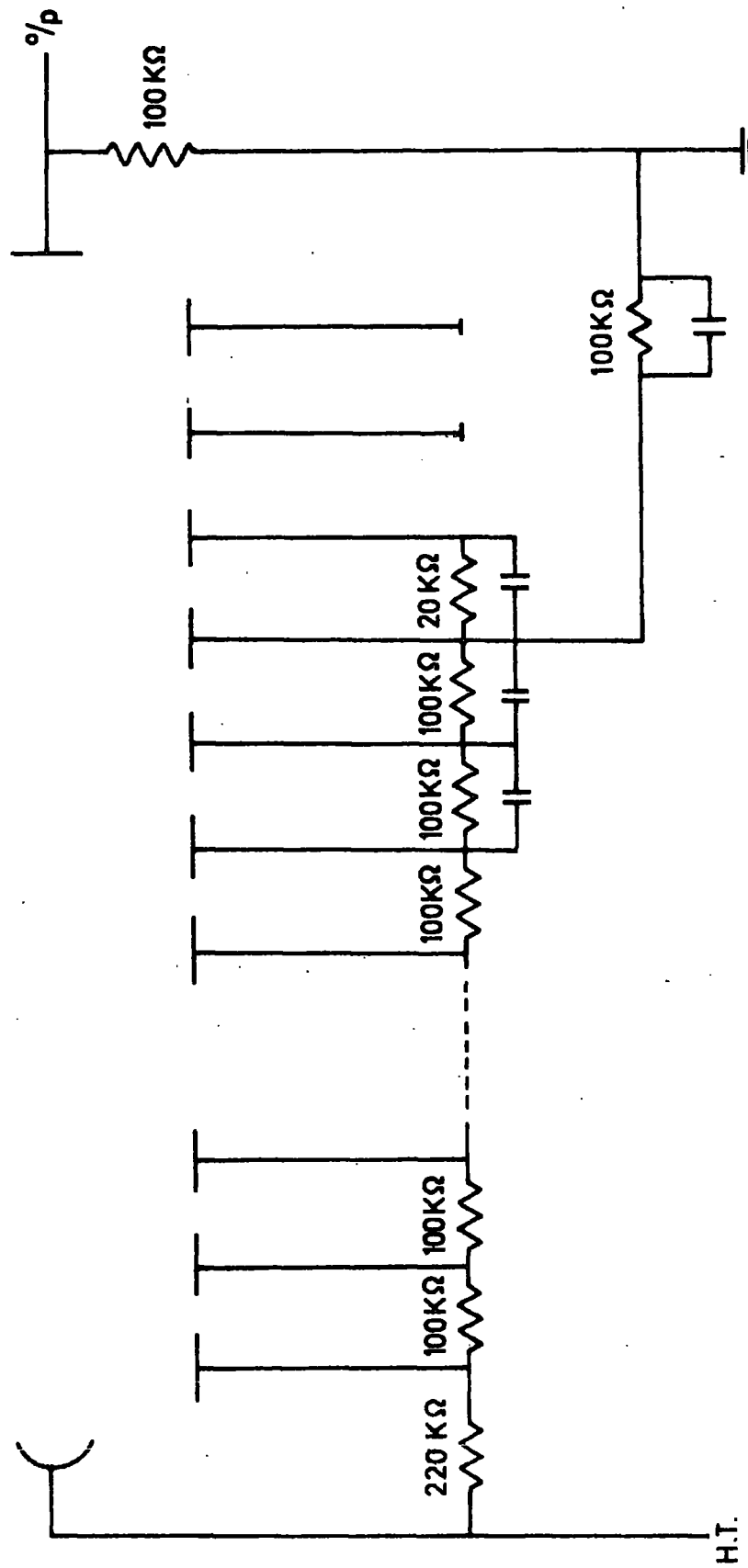

PHOTO MULTIPLIER BASE CIRCUIT.

FIG. 24

where $\mu_B = \frac{e\hbar}{2mc}$

from equation (2-9)

$$g = \frac{21.4178}{H\lambda} \qquad (2\text{-}10)$$

Where H is in kilogauss

and λ is in centimetres

Experiments are normally carried out in the centimetre microwave range as the higher magnetic fields necessary at shorter wavelengths are prohibitive, whilst at higher values of wavelengths the resolution of the spectrum becomes poor due to long relaxation times.

In Fig.(2.5 a,b) can be seen a comparision of the absorption and the derivative spectra for a typical gadolinium-containing lithium aluminium silicate glass. The greatly-increased resolution of the e.s.r. absorption lines obtained by using the derivative technique was found necessary due to the broad nature of the lines found in glass.

Two major causes are responsible for the limitation of resolution in the e.s.r. spectra of single crystals. The first is the spin-lattice relaxation time τ, which is a measure of the time for energy transfer to the lattice. τ is found (2.3) to be inversely proportional to temperature and gives rise to a half width, for the resonance lines, at half intensity of the order of $\frac{1}{2\pi\tau}$ sec.$^{-1}$. Low temperatures are often employed to assist

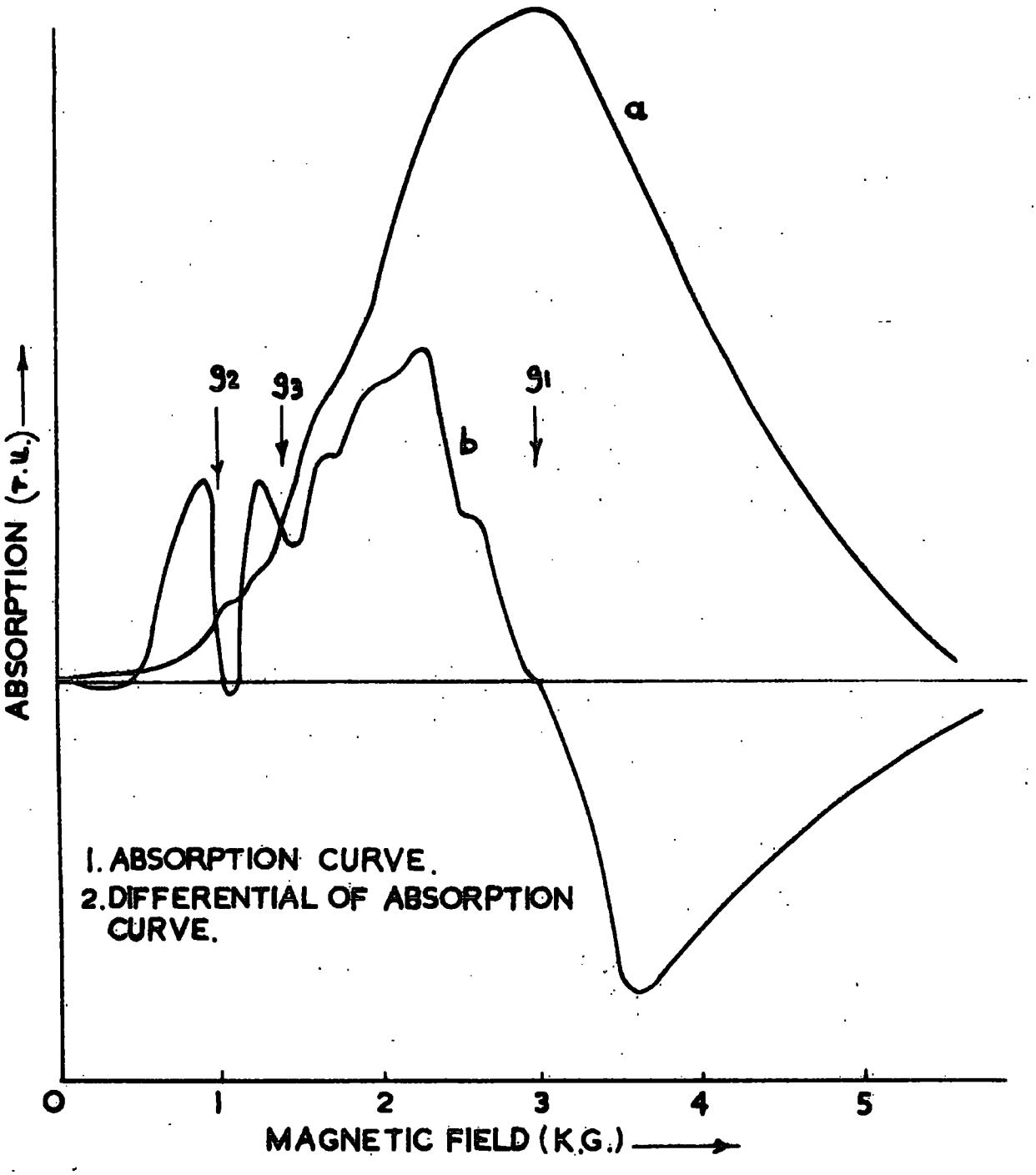

FIG 2.5 COMPARISON OF DERIVATIVE AND INTEGRAL E.S.R. ABSORPTION FOR L.A.S.1058 AT 300°K.

resolution for this reason. A second broadening mechanism is due to the temperature independent spin-spin relaxation time which can only be reduced by dilution of the relevant paramagnetic ions. Theoretical determinations are given by Van Vleck (2.4) and Pryce and Stevens (2.5).

The first spin-lattice mechanism may be discounted as the main cause of broadening in the glass samples as no improved resolution was obtained upon reduction of the temperature of measurement from 300 K to 4.2 K. Also the use of varying concentrations of paramagnetic Gd^{3+} ions in the glass showed that the second spin-spin relaxation was not responsible for the broadening as no change in line width occurred. This also discounts the possibility of dipolar broadening. It is more likely that the random orientation and distortions of the ionic sites within the glasses studied provided the majority of the line width.

The magnet employed produced a magnetic field which had a high degree of uniformity over the volume of the samples and negligible change was produced in the e.s.r. spectrum when the field was rotated.

2.72 X-Band E.S.R. Spectrometer

A conventional superheterodyne X-band reflection spectrometer with 180 Hz. field modulation allowed observation of the e.s.r. signal. Fig. (2.6) is a block diagram representing the apparatus used for these measurements and the relevant circuitry is shown in Figs. (2.7) and (2.8). Microwave power is obtained from a 20 kHz. frequency

FIG. 2·6

BLOCK DIAGRAM OF E.S.R. SPECTROMETER.

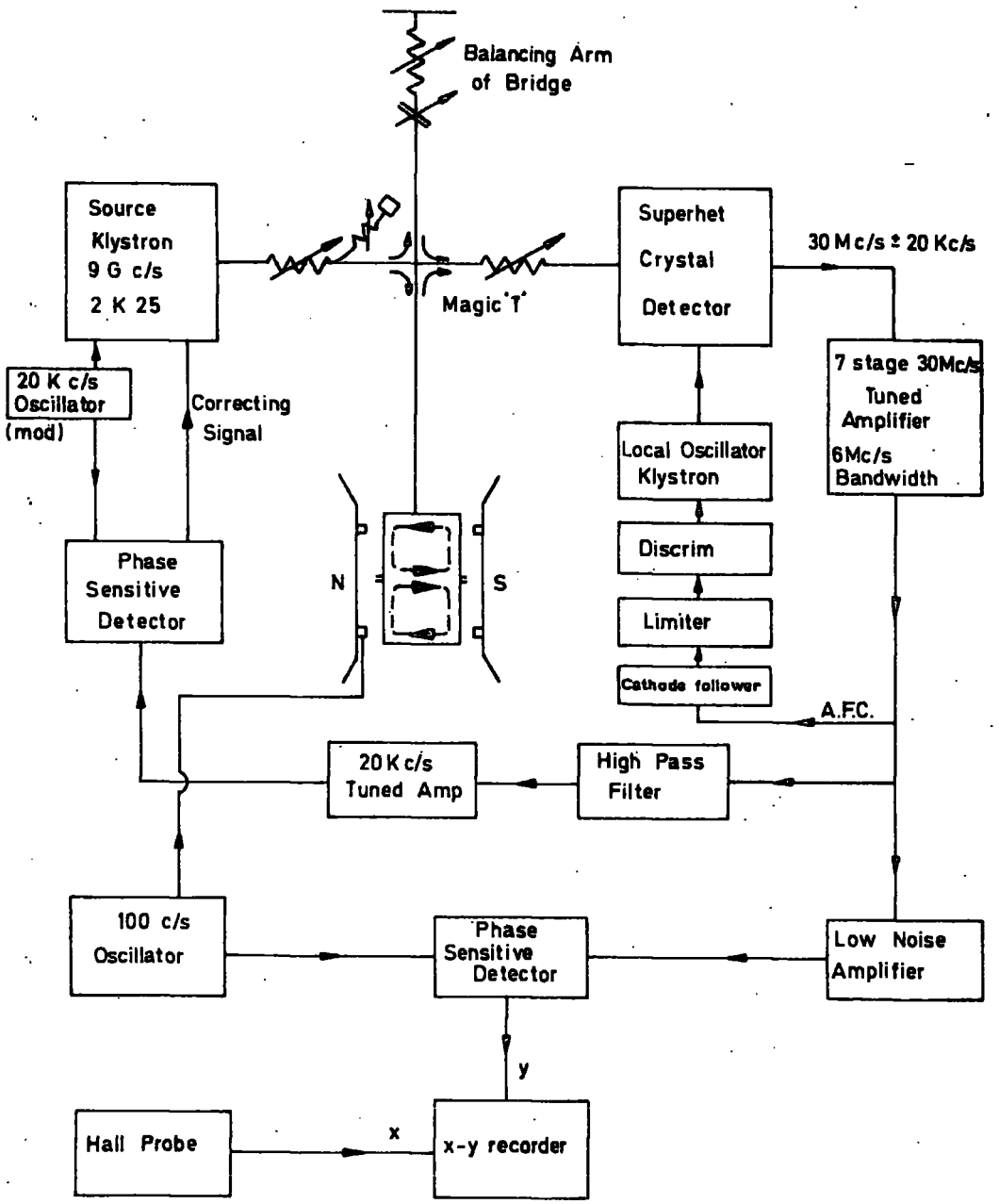

FIG. 2·7

Source Klystron / Cavity Locking System.

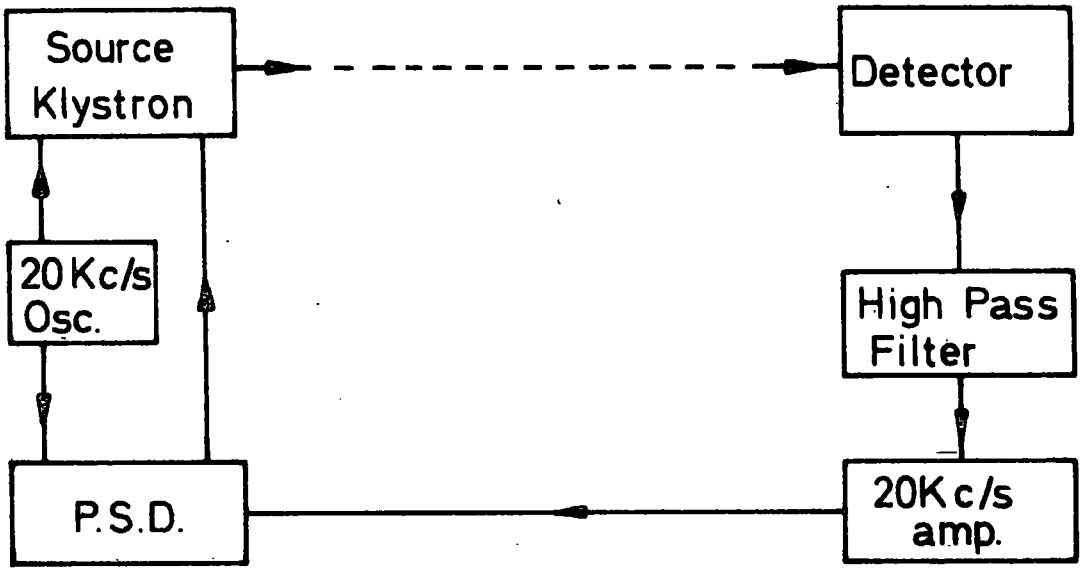

FILTER AND TUNED AMP.

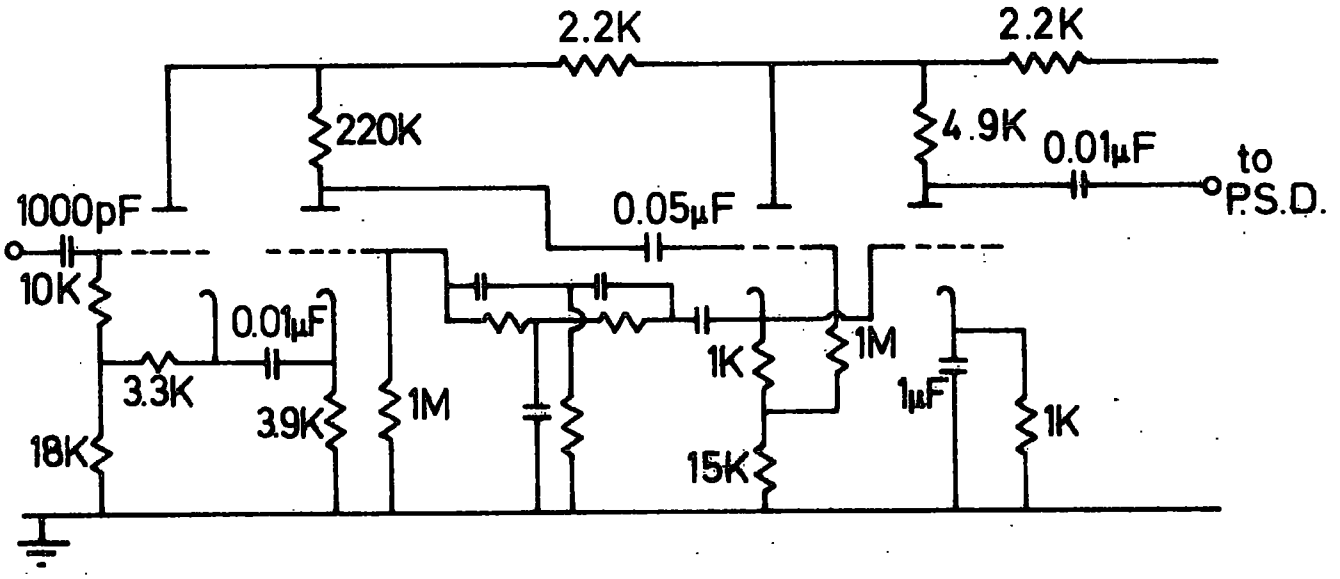

FIG. 2·8

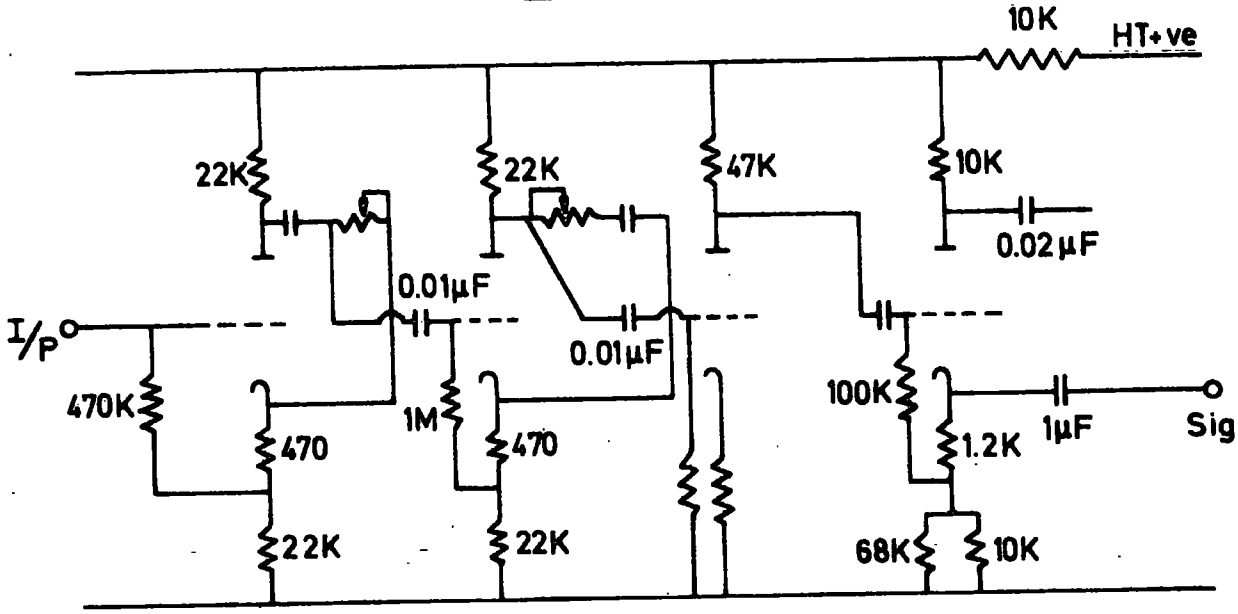

PHASE SENSITIVE DETECTOR

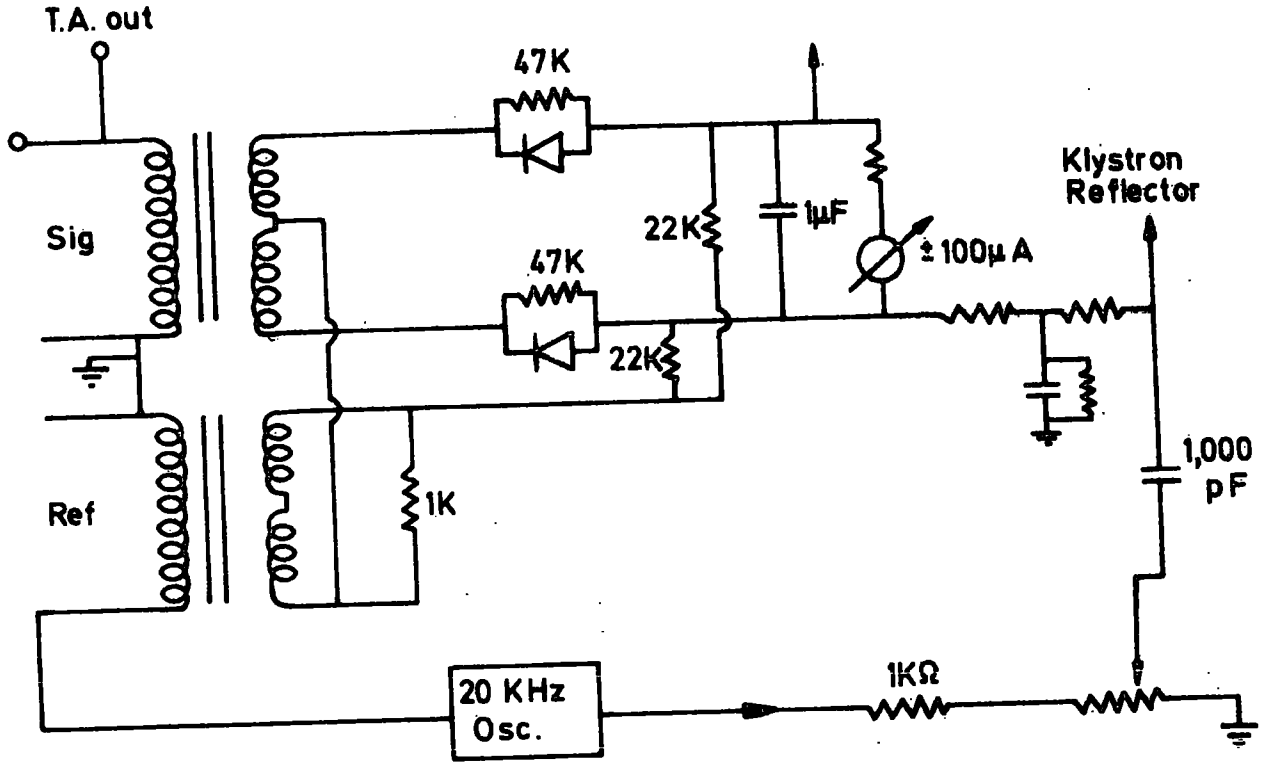

20KHz STABILSING SIGNAL.

modulated 9.8 GHz. Mullard Klystron (type 2K 25) which has a stabilised voltage supply. The klystron was mechanically tunable to match the microwave frequencies of the sample cavities employed.

In order to measure the frequency, and hence calculate g-values, a fraction of the microwave power was coupled out of the initial waveguide which feeds power to a magic T. At this magic T the power is equally divided between the sample arm and the balancing arm. In this second arm an adjustable attenuator and phase shifter allow the bridge to be balanced. The reflected power from these two arms will completely cancel when the bridge is balanced and then no power leaves by the fourth arm of the magic T. This fourth arm leads to the signal detection circuits.

As the magnetic field is increased and the resonance condition reached, the sample absorbs microwave power causing the bridge to become unbalanced. This produces an out-of-balance signal in the fourth arm of the magic T which leads to the crystal detector. Here a local oscillator klystron supplies a mixing frequency to the incoming signal to allow the reduction of frequency to a value at which normal electronic amplification can be applied. This mixing changes the input signal to 30 MHz. still retaining the 20 kHz. modulation. This 30 MHz. is now selectively amplified by means of a tuned amplifier with centre frequency of 30 MHz. and a 6 MHz. bandwidth. A sample of this amplified signal is used to obtain frequency locking of the local oscillator klystron by feeding it back to this klystron via a cathode follower, limiter and discriminator.

The source klystron is also locked to the resonant cavity. This is achieved by taking a sample of the 30 MHz. amplified signal, which has a 20 kHz. modulation component, passing it through a high pass filter and a 20 kHz. tuned amplifier to a phase sensitive detector. This p.s.d. with its reference signal from the 20 kHz. source klystron modulation oscillator, provides a signal which is proportional to the frequency difference between the klystron and the cavity, thus providing a locking-in signal.

The magnetic field is modulated at 180 Hz. by a pair of Helmholtz coils connected to the D.C. magnet pole pieces. Detection of this modulated signal via a low noise amplifier and phase sensitive detector allows the display of the differential of the absorption signal on an X-Y recorder. The X-axis is driven by the output from a Hall probe.

The magnetic field sweep rate and range were controlled by a remote control unit Fig. (2.9) attached to a Brentford stabilised D.C. power supply (type GRDAQX 95/04), which operated in the 0 to 250 volts and 0 to 300 amps. range, to produce available fields up to 15 koe.

The magnetic field was calibrated with a nuclear magnetic resonance method. Additional evaluation of the field was provided by the inclusion of a sample of diphenyl picryl hydrazyl (D.P.P.H.).

FIG. 2·9 REMOTE CONTROL UNIT FOR BRENTFORD POWER SUPPLY.

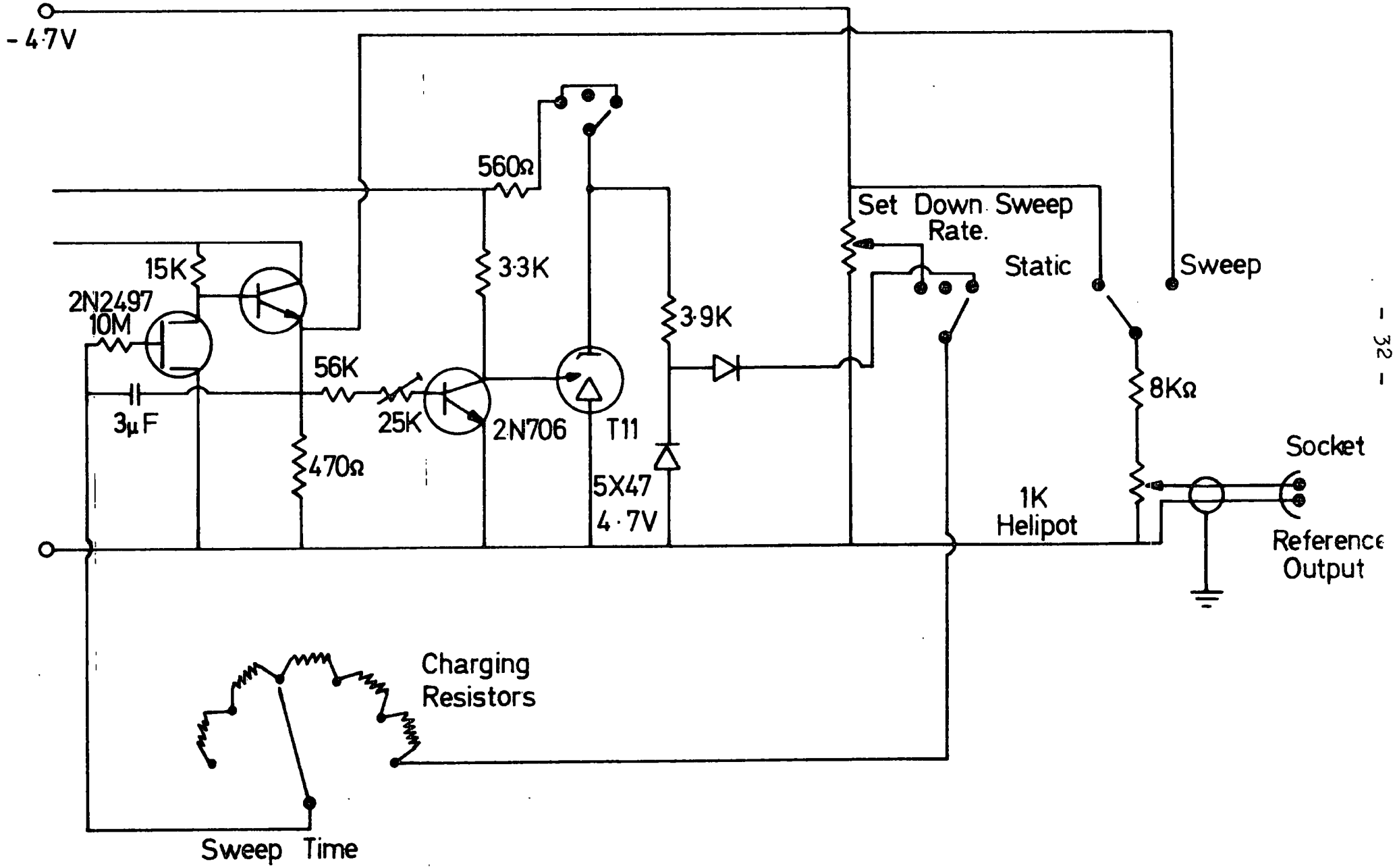

CHAPTER 3.

RESULTS AND DISCUSSION (Part I)

A. Structural Properties

3.1 Differential Thermal Analysis

Initial establishment of the extent of nucleation and crystallisation in the glasses was made by the use of differential thermal analysis (D.T.A.). Low temperature endothermic peaks were found which are known to correspond to the nucleation process (3.1) occurring some tens of degrees below the dominant exothermic, crystallisation peak T_c. In all cases the lower peak is at least an order of magnitude smaller than the crystallisation peak and as a result the nucleation transition was frequently difficult to detect.

Several interesting features for the L.A.S. 1022 series are shown in Fig. 3.1 (a-h). The base glass shows a small broad exothermic peak at 824°C with some indication of another exothermic peak on the high temperature side. Also observable is a small poorly resolved endothermic peak near 760°C indicative of a nucleation process. Observation of Fig. 3.1 (a-c) shows the effect of adding 0, 0.1, and 5.0% TiO_2 to this base glass. Although the initial small addition produced virtually no change, the presence of 5% TiO_2 in the glass causes a reduction of the crystallisation temperature by approximately 50°C and at the same time drastically reduces the width of the corresponding peak in the D.T.A. output. It is known that TiO_2 can reduce the viscosity of a glass melt and it is natural to consider that the

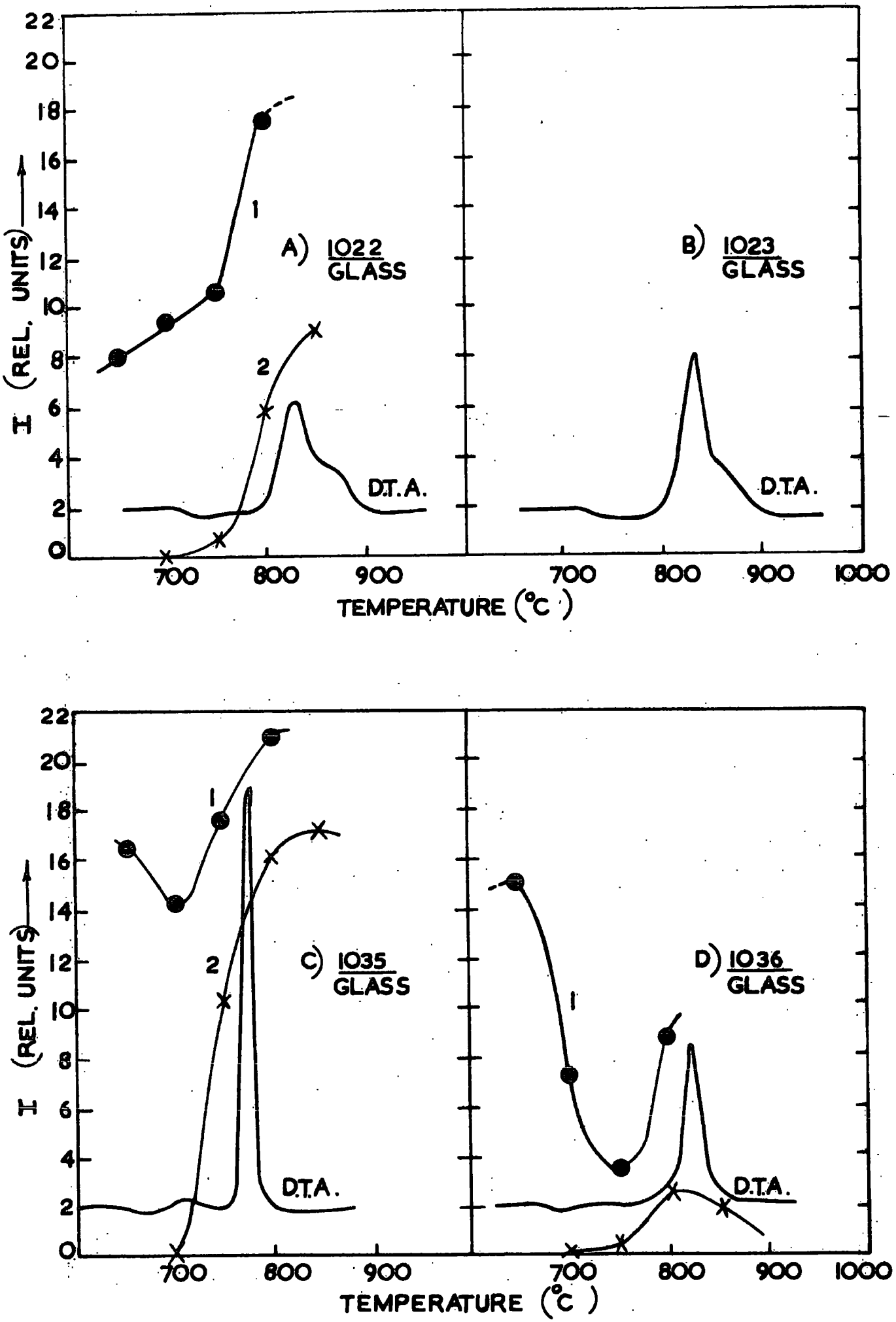

FIG 3.1 D.T.A. OUTPUT AND CRYSTALLIZATION EXTENT.

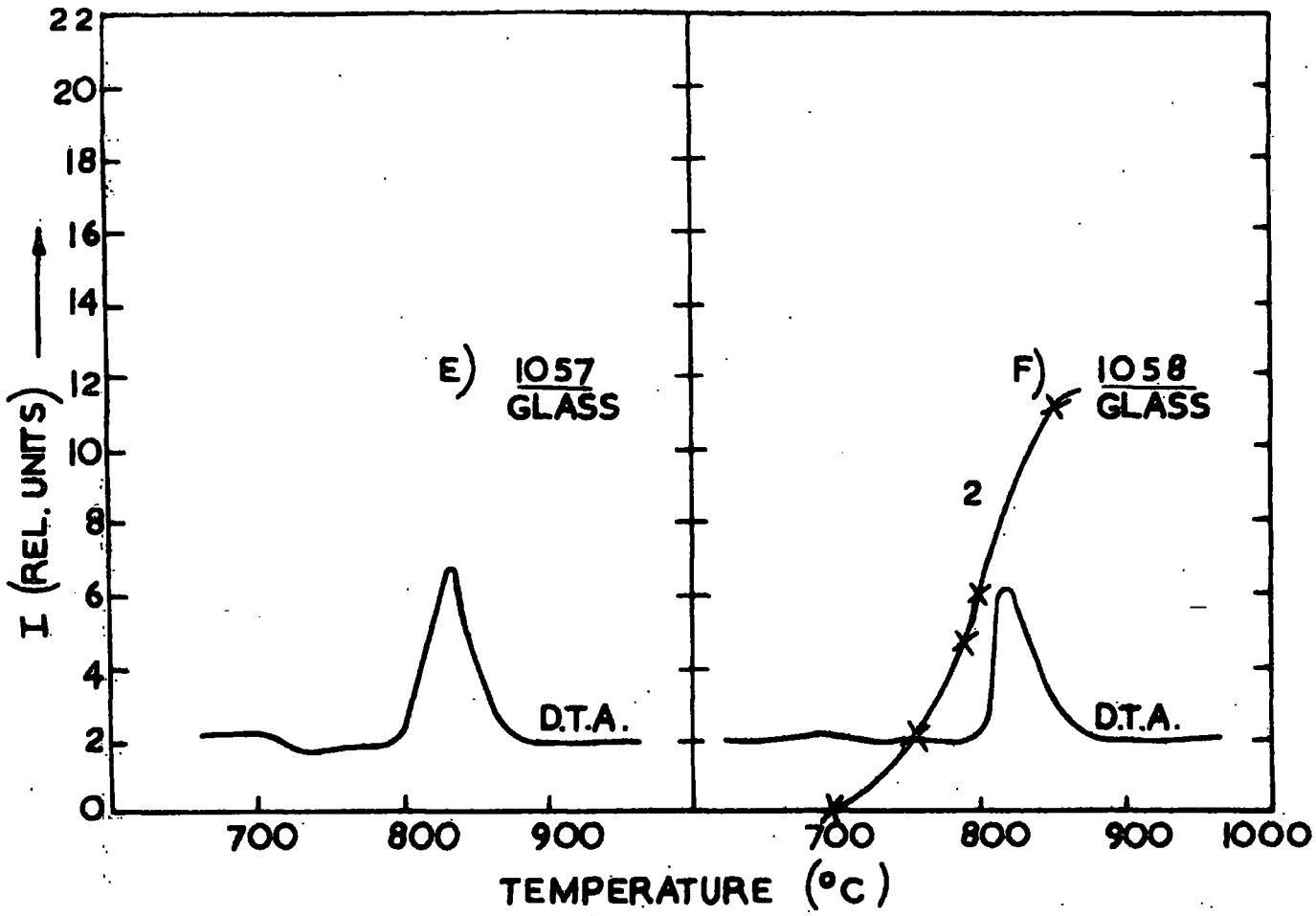

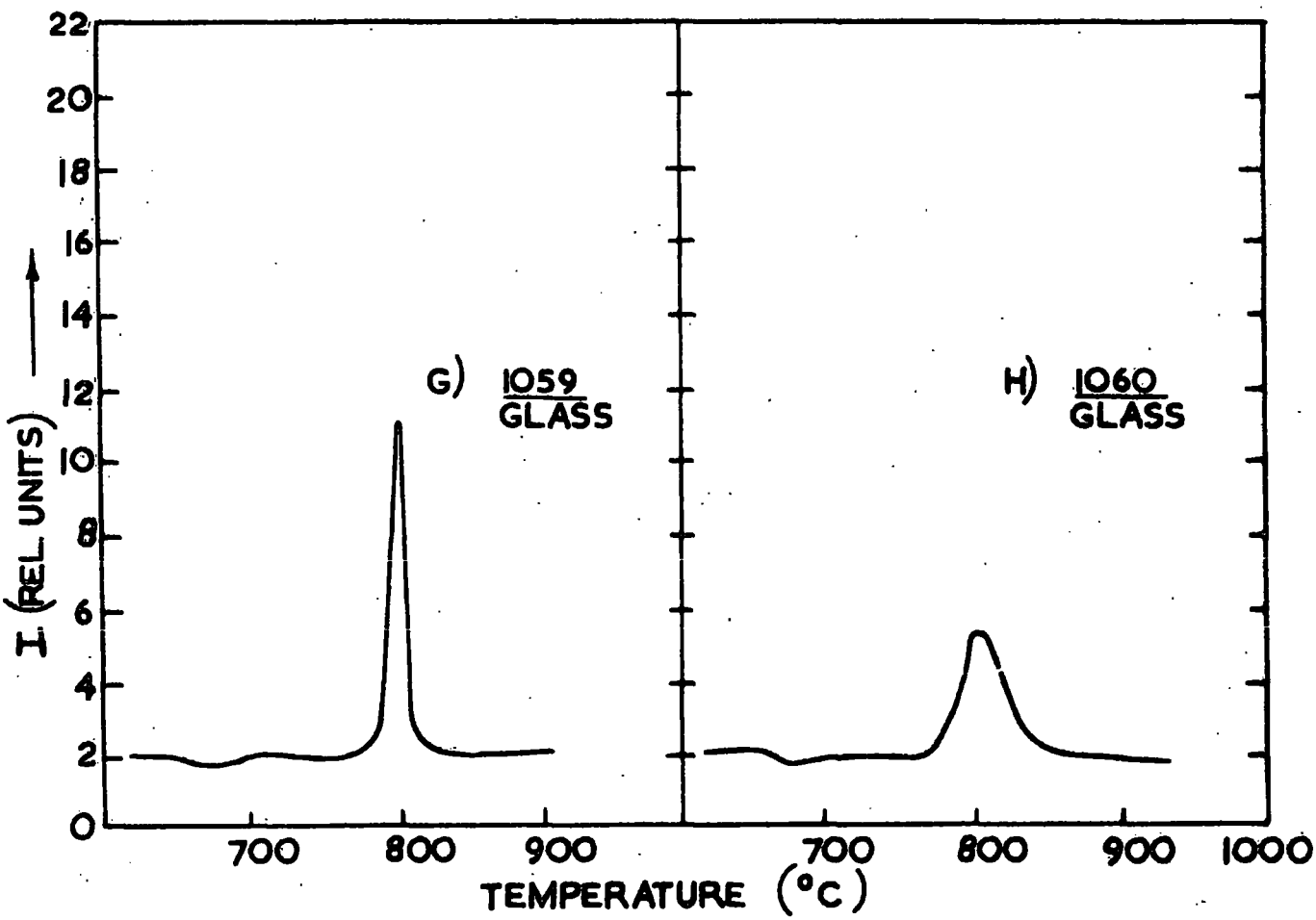

FIG. 3.1 (CONT'D.) D.T.A. OUTPUT AND CRYSTALLIZATION EXTENT.

effects of TiO_2 on the crystallisation mechanism can, in part, be explained by the increased mobility of the ions at a reduced temperature. Unfortunately this reduced viscosity should lead to an easier diffusion of ions to the crystal growth front and hence produce relatively large crystals. By electron microscopy it is shown later that apart from increasing the size of crystals formed there is a remarkable reduction in the size and an increase in the number of crystals. It is this very fact that gives the ceramics their desirable physical properties. It is thus necessary to consider additional or alternative methods of crystallisation enhancement. As the greatest barrier to crystal formation is known to be the formation and growth of nuclei to a critical radius, the formation of nuclei by the titanium seems to be a feasible process.

To clarify the effects of a foreign ion in the glass 1% Gd_2O_3 and 1% Nd_2O_3 were added separately to the base glass and to the base glass with 5% TiO_2 to be monitored specifically by e.s.r. and optical absorption. The effects on the D.T.A. output can be seen in Fig. 3.1. It is evident that neither gadolinium nor neodymium alone, appreciably alters the form of the crystallisation. When, in addition to 5% TiO_2, 1% of the rare earths is present the temperature of crystallisation is returned to the value corresponding to the base glass and the transition is again broadened.

A broad low intensity endothermic peak was found in all the glasses and is an indication of a nucleation region. Although this peak is more clearly defined whenever 5% TiO_2 is present, it is less obviously affected by other additions to the base glass. The enhancement of the nucleation region

by 5% TiO_2 was found, irrespective of the presence of the rare earths. It would appear that whereas the nucleation produced by the titania is unaffected by additional ions, the enhanced crystallisation so produced is effectively inhibited. This can be understood if the glass is considered to have regions with compositions close to the resulting crystal, then only a small amount of local rearrangement is required to produce nucleation and is enhanced by the reduced viscosity in the neighbourhood of the titanium ions. However the crystal growth requires the diffusion of ions to and from the growth front to allow composition compatibility. The inhibition of the process by the rare earths may be due to their large co-ordination requirements preventing ionic diffusion.

3.2 Electron Microscopy

The type and form of the crystallisation in the L.A.S. glasses was followed by observation of the samples after heat treatment, by the use of electron microscopy. Both transmission and replica techniques were used in conjunction with a variety of etching procedures. A comparison of the effects of different specimen preparation is shown in Fig. 3.2 (a-e) in which the same sample has been subjected to the preparations shown. For detail greater than 1,000 A the replica technique proved most useful but the fine grained crystallisation induced by the presence of TiO_2 required observation by transmission microscopy. A two stage plastic/carbon replication method was found to be the most useful, as explained earlier. A comparison of the effects

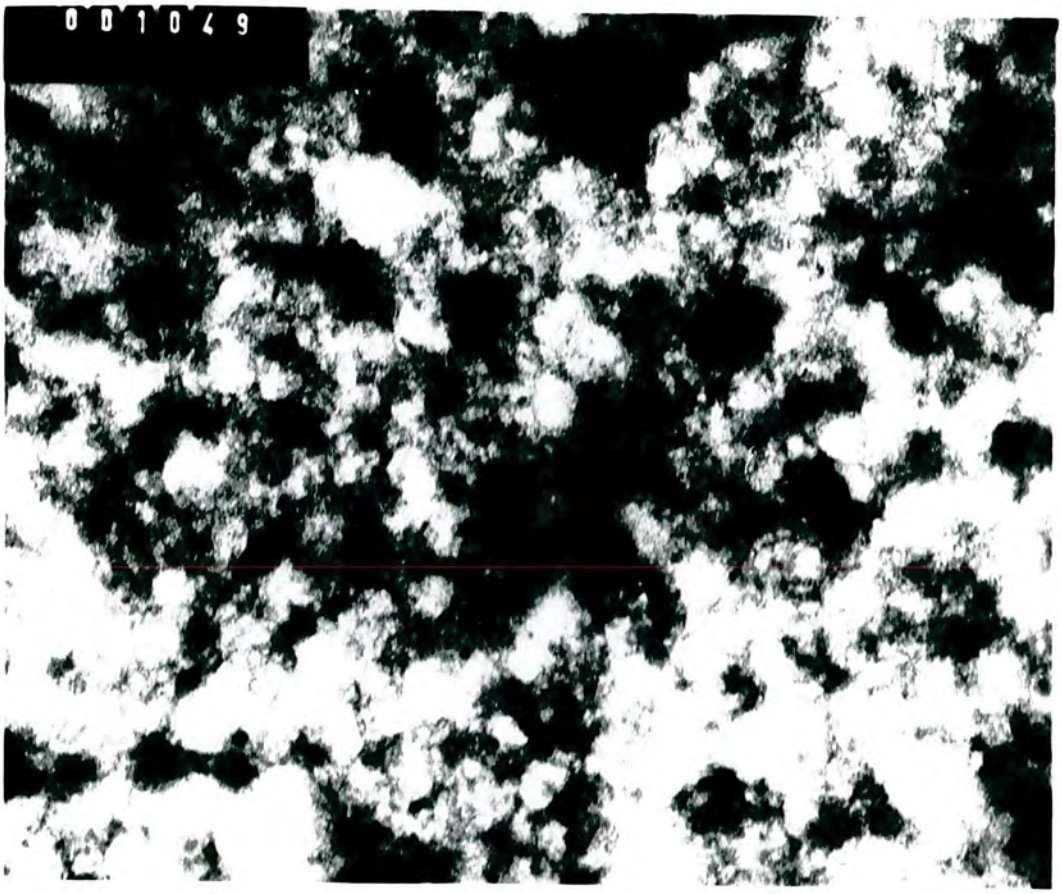

Fig. 3.2 a Carbon replication after 20 sec. 0.2% HF etch. x 224,000

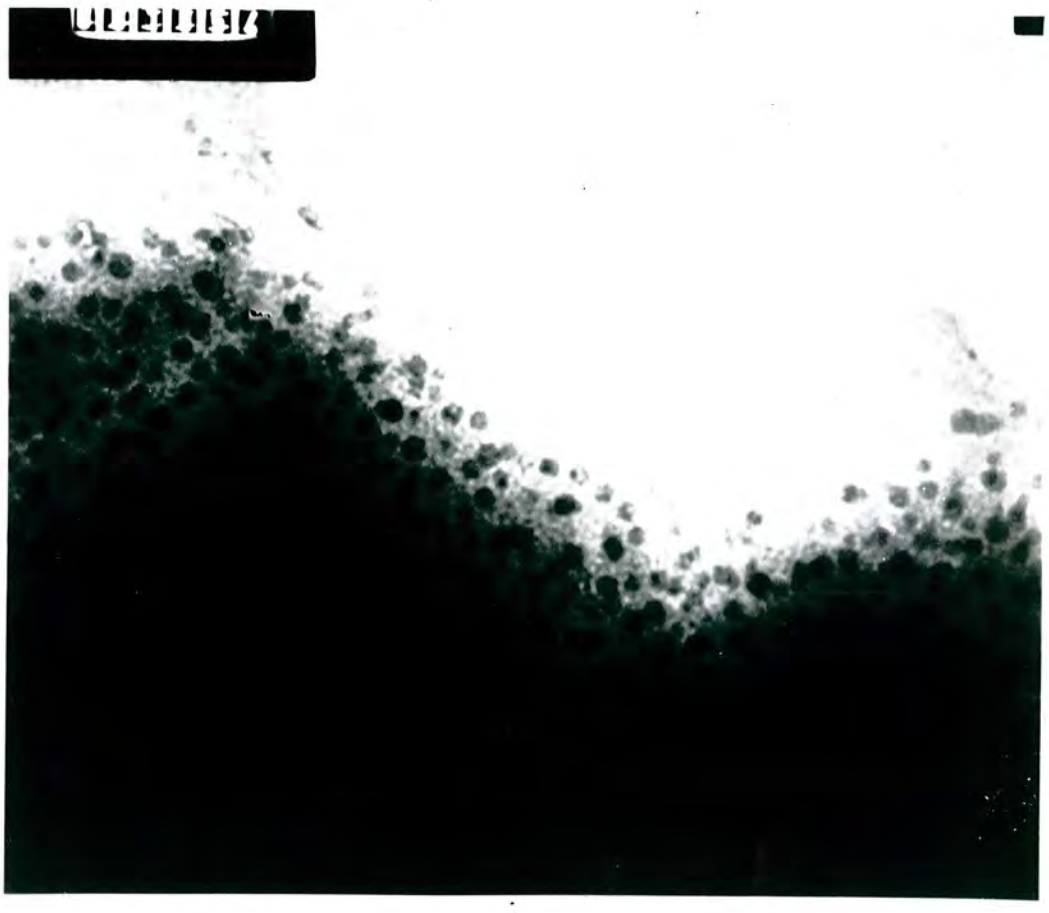

Fig. 3.2 b Small fragment of sample on carbon film x 224,000

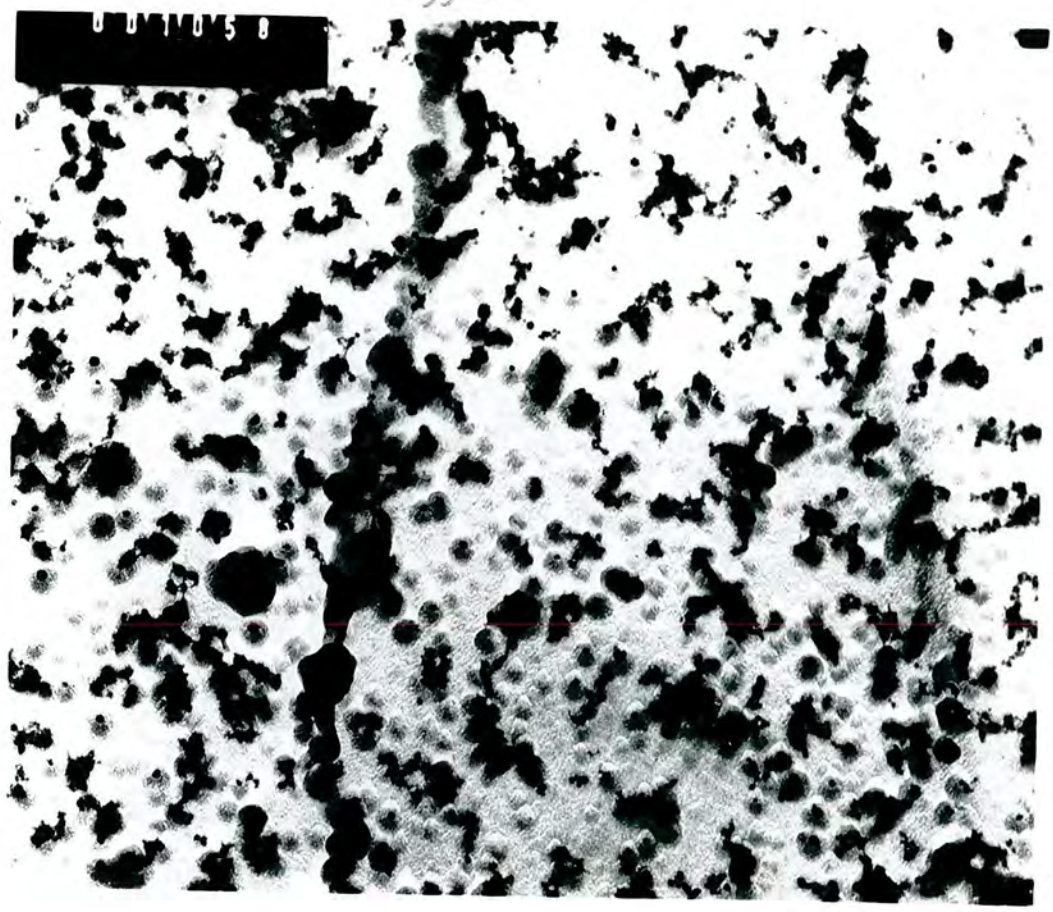

Fig. 3.2 c Carbon replication after 20 sec. 0.2% HF etch. released in 0.2% HF for 45 sec. x 110,000

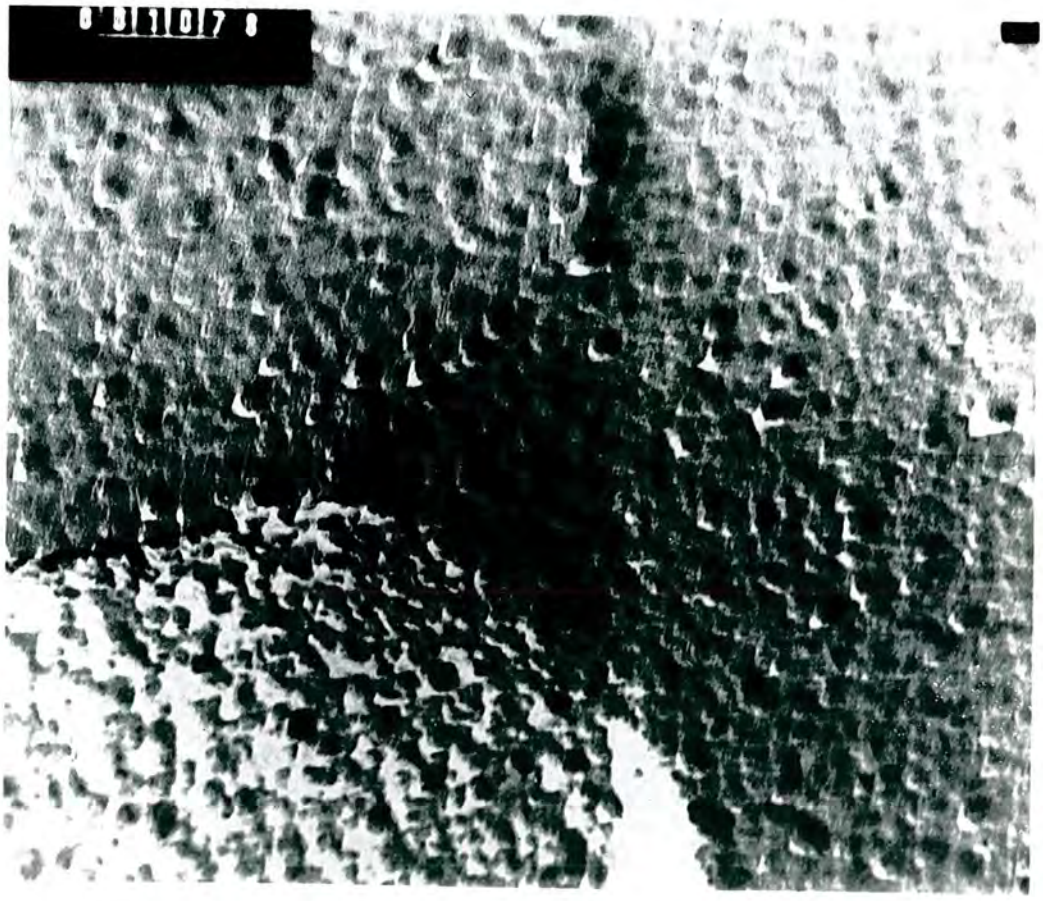

Fig. 3.2 d 2-stage plastic/carbon replication of a fracture surface x 172,000

Fig. 3.2 e 2-stage plastic/carbon replication after 0.2% HF etch for 10 sec. x 55,300

All the samples in Fig. 3.2 are 1036 that had been heat treated at 767^{o}C for one hour. The sample had a hazy appearance and X-ray diffraction patterns showed the emergence of β -eucryptite lines.

of magnification on the sample in Fig. 3.2 with the same sample preparation , is shown in Fig. 3.3 (a-e) and it can be seen that electron transmission and high magnification are necessary to observe the smallest structures.

From Fig. 3.2 (a-e) it is clear that for an interpretation of the electron micrographs a consistent method of sample preparation must be followed. By a comparison of the appearance of the X-ray diffraction patterns Fig. 3.5 the structures observed are known to be the early development of β -eucryptite crystals. The onset of crystallisation in this region is also seen to correspond to the D.T.A. output. It is evident that structural development was observable by electron microscopy before the diffraction lines developed. Samples were subjected to a series of heat treatments based on the information derived from the D.T.A. These consisted of either a single stage heating, at set temperatures from 600°C to 800°C for one hour, or a double stage heating in which samples initially subjected to the single stage were subsequently held at 850°C for one hour. Samples were brought as quickly as possible to these temperatures by placing them in a preheated furnace and immediately after the heat treatment the samples were chilled to room temperature by removal from the furnace. By use of this procedure it was hoped to observe the development of the crystallisation as a function of the heat treatment and also to observe changes produced by the incorporation of titania and the rare earths.

Fig. 3.3 a L.A.S. 1036 at 767°C for 1 hour x 32,600

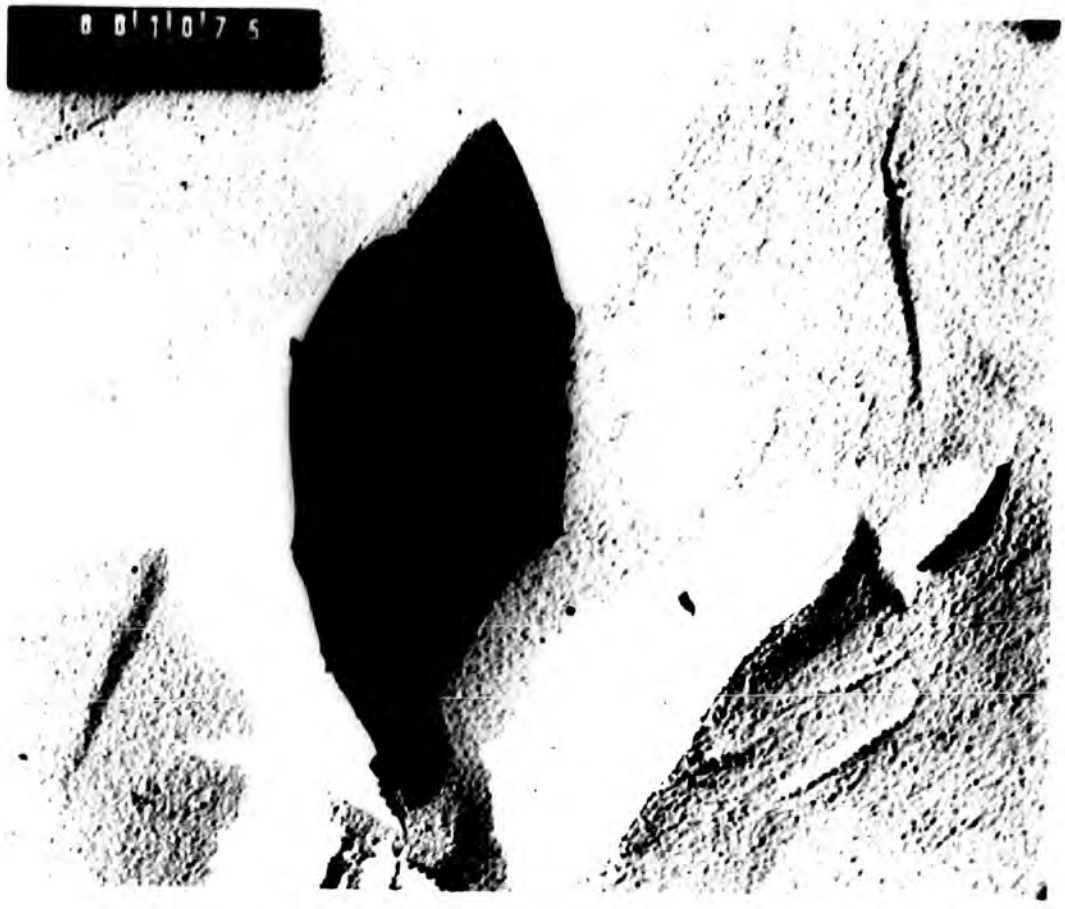

Fig. 3.3 b L.A.S. 1036 at 767°C for 1 hour x 55,300

Fig. 3.3 c L.A.S. 1036 x 135,000

Fig. 3.3 d L.A.S. 1036 at 767°C for 1 hour x 172,000

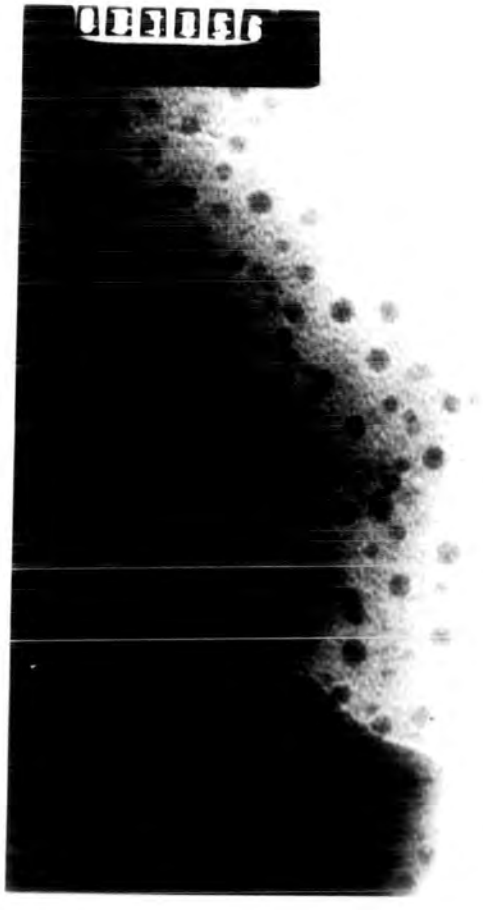

Fig. 3.3 c L.A.S. 1056 at 767°C for 1 hour x 224,000

The results of the electron microscopy, in terms of crystal size and number, together with an indication of the X-ray diffraction observation of crystallinity, are summarised in table 3.1. Examples of the observed structures are given in Fig. 3.4 (a-l), from which it can be seen that spherically shaped structures appear after the single stage heating. As stated above, these can be identified with the development of β-eucryptite crystallites. The average size of these structures, although varying slightly, was about 5,000 A for samples of L.A.S. 1022 subjected to the single heat treatment. For an initial temperature of 650°C the two stage heating produced similar sized structures; however above this temperature of initial heating much larger spherical structures developed with radial dimensions up to 20,000 A. These spherical regions showed internal structure which can be associated with non-uniform development of the crystallite growth front. The large extent of these regions intermingled with glassy regions typifies inefficient crystal nucleation; a fact which is also evident from the relative ease of glass formation within this composition.

When 0.1% TiO_2 was added to the previous glass a small but significant reduction in the spherical structure was produced when samples had undergone a similar, single stage heat treatment up to 800°C. If the initial heating was at 850°C then the crystallites, with diameters from 1,000 - 2,000 A were found to be extended to 20,000 A, reminiscent of the structures produced by the double stage heat treatment of L.A.S. 1022. This double stage heating of the glass with 0.1% TiO_2 produced

TABLE 3. 1

ELECTRON MICROSCOPY RESULTS

Glass No.	Heat Treatment at stated Temperatures for one hour	X-ray Observation of crystallisation	Size of Crystallisation	Relative No. of Structures in unit volume
1022	650°C	None	-	-
	700°C	Small Amount	5,000A	28
	750°C	Crystalline	5,000A	14
	800°C	"	2,000A	200 - 250
	850°C	"	6,500A	9
	650°C then 850°C	"	5,000A	25
	700°C then 850°C	"	18,000A	3 - 4
	750°C then 850°C	"	10,000A-20,000A	20
	800°C then 850°C	"	10,000A-20,000A	10
1023	650°C	None	1,000A	200
	700°C	"	2,000A	120
	750°C	"	1,000A	500
	800°C	Small Amount	1,500A	250
	850°C	Crystalline	5,000A-20,000A	5
	650°C then 850°C	"	1,000A	500
	700°C then 850°C	"	2,500A	60
	750°C then 850°C	"	3,000A	60
	800°C then 850°C	"	3,000A	60

TABLE 3.1 (continued)

ELECTRON MICROSCOPY RESULTS

Glass No.	Heat Treatment at stated Temperatures for one hour	X-ray Observation of Crystallisation	Size of Crystallisation	Relative No. of Structures in unit Volume
1035	650°C	None	1,500A	25
	700°C	Small Amount	500A	Large No.
	750°C	Crystalline	0-1,000A	1,500
	800°C	"	100 A	Large No.
	850°C	"	1,000A	Less
	650°C then 850°C	"	1,000A	Large No.
	700°C then 850°C	"	1,000A-1,500A	"
	750°C then 850°C	"	1,000A-2,000A	"
	800°C then 850°C	"	8,000A	"
1036	650°C	None	1,000A	Large No.
	700°C	None	1,000A	"
	750°C	Small Amount	1,000A	"
	800°C	Crystalline	2,000A	"
	850°C	"	5,000A	"
	650°C then 850°C	"	500A	"
	700°C then 850°C	"	1,000A	"
	750°C then 850°C	"	-	"
	800°C then 850°C	"	500A	"

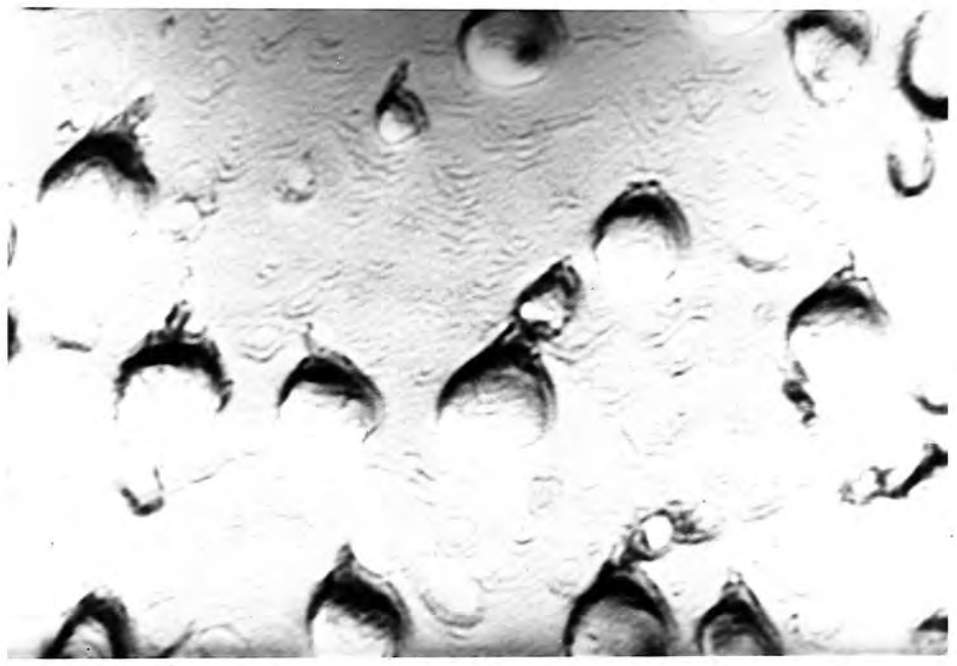

Fig. 3.4 a Sample 1022 at 700°C for 1 hour x 23,600

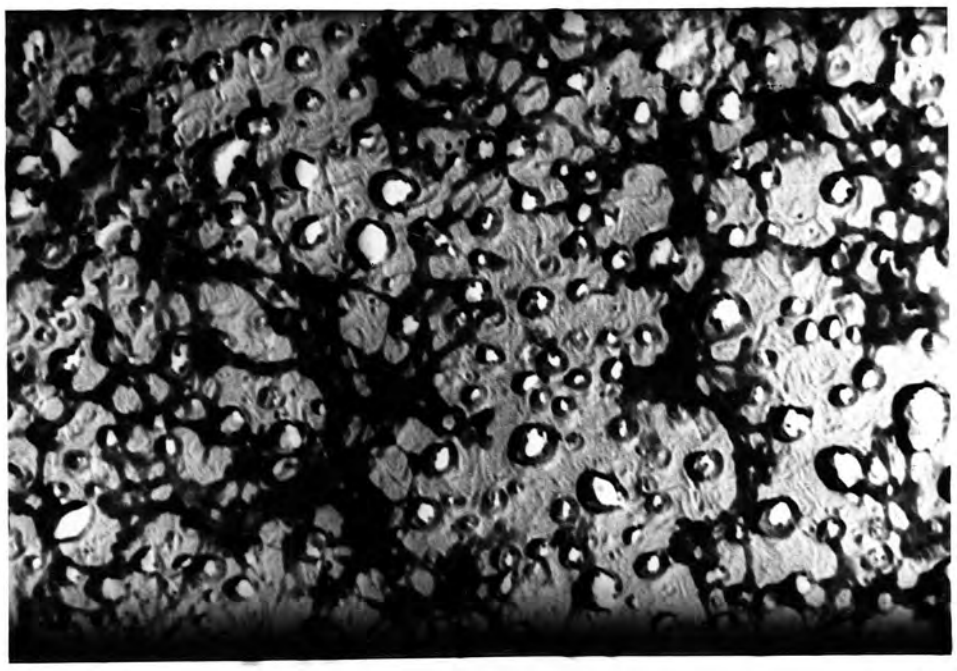

Fig. 3.4 b Sample 1022 at 800°C for 1 hour x 23,600

Fig. 3.4 c Sample 1022 at 850°C for 1 hour x 23,600

Fig. 3.4 d Sample 1022 at 800°C for 1 hour then at 850°C for 1 hour x 23,600

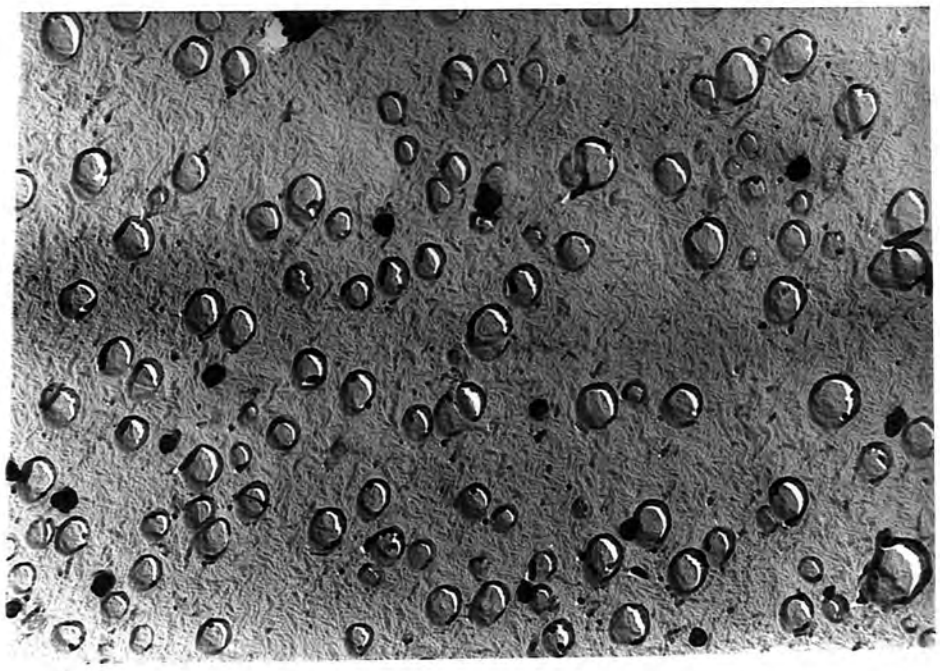

Fig. 3.4 e Sample 1023 at 700°C for 1 hour x 23,600

Fig. 3.4 f Sample 1023 at 850°C for 1 hour x 23,600

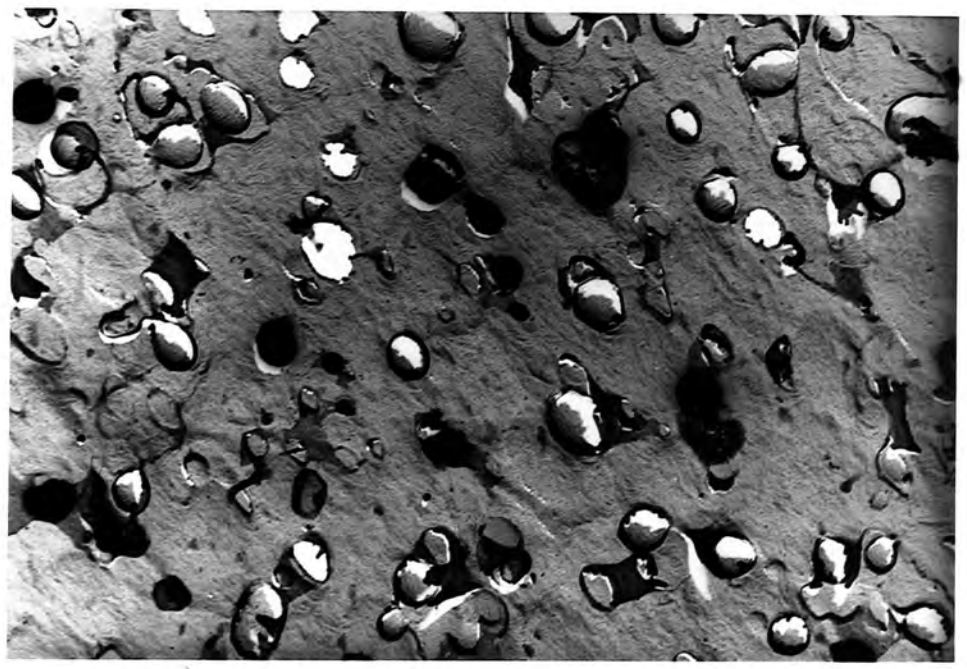

Fig. 3.4 g Sample 1023 at 700°C for 1 hour then at 850°C for 1 hour x 23,600

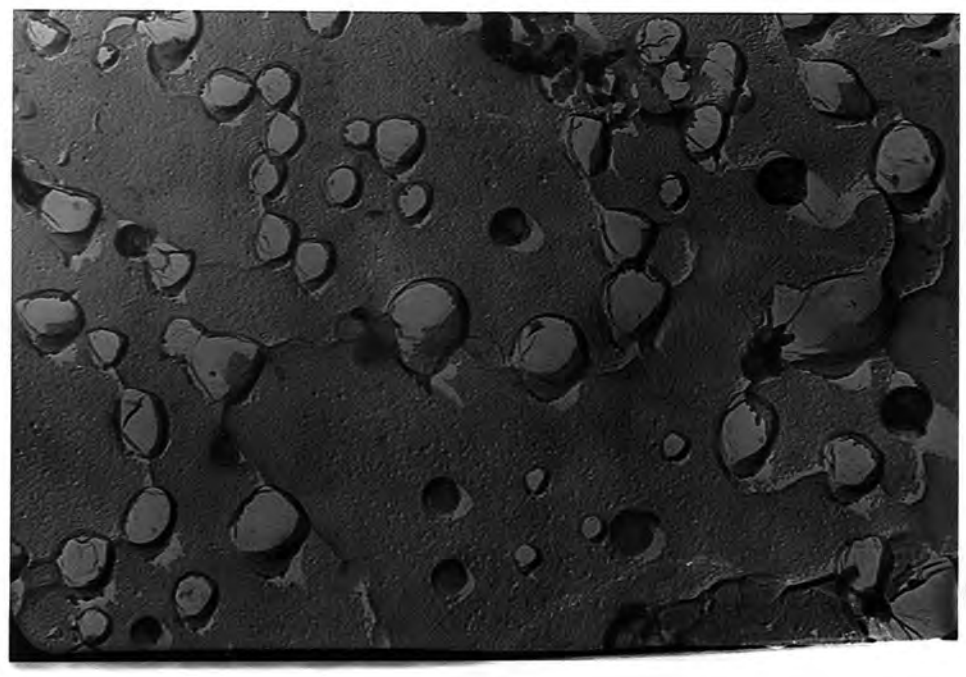

Fig. 3.4 h Sample 1023 at 800°C for 1 hour then at 850°C for 1 hour x 23,600

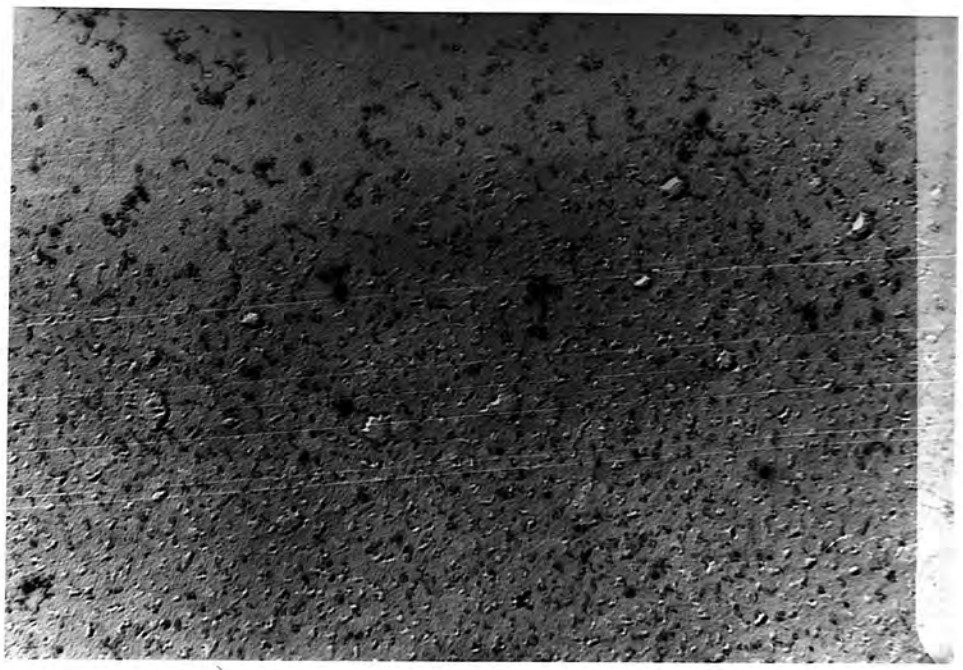

Fig. 3.4 i Sample 1035 at 750°C for 1 hour x 23,600

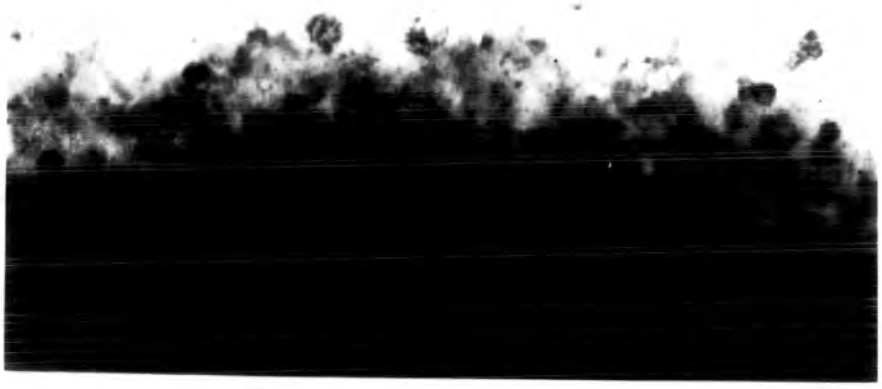

Fig. 3.4 j L.A.S. 1035 at 850°C for 1 hour x 50,050

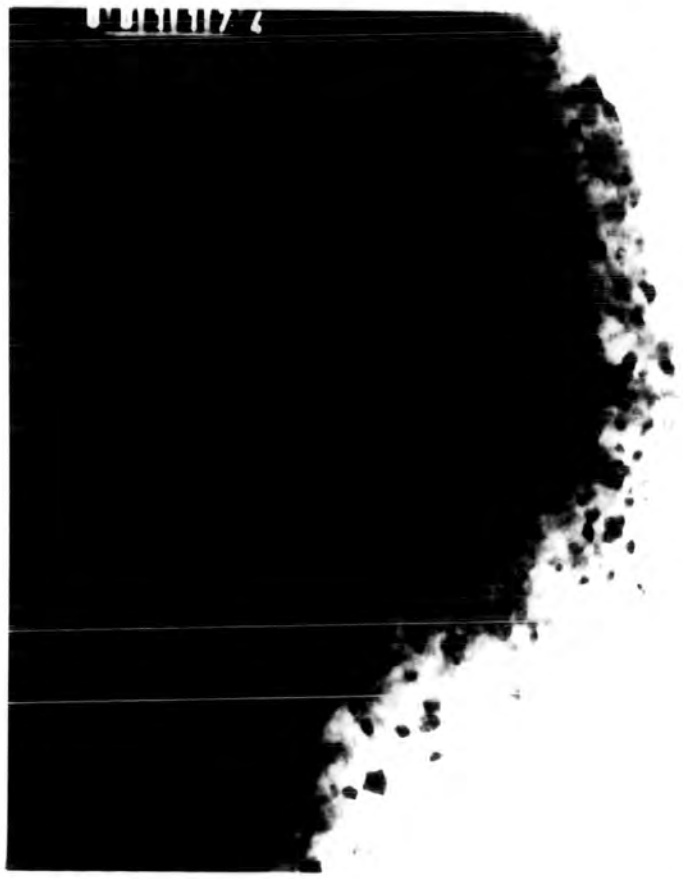

Fig. 3.4 k 1035 at 750°C for 1 hour then at 850°C for 1 hour x 27,600

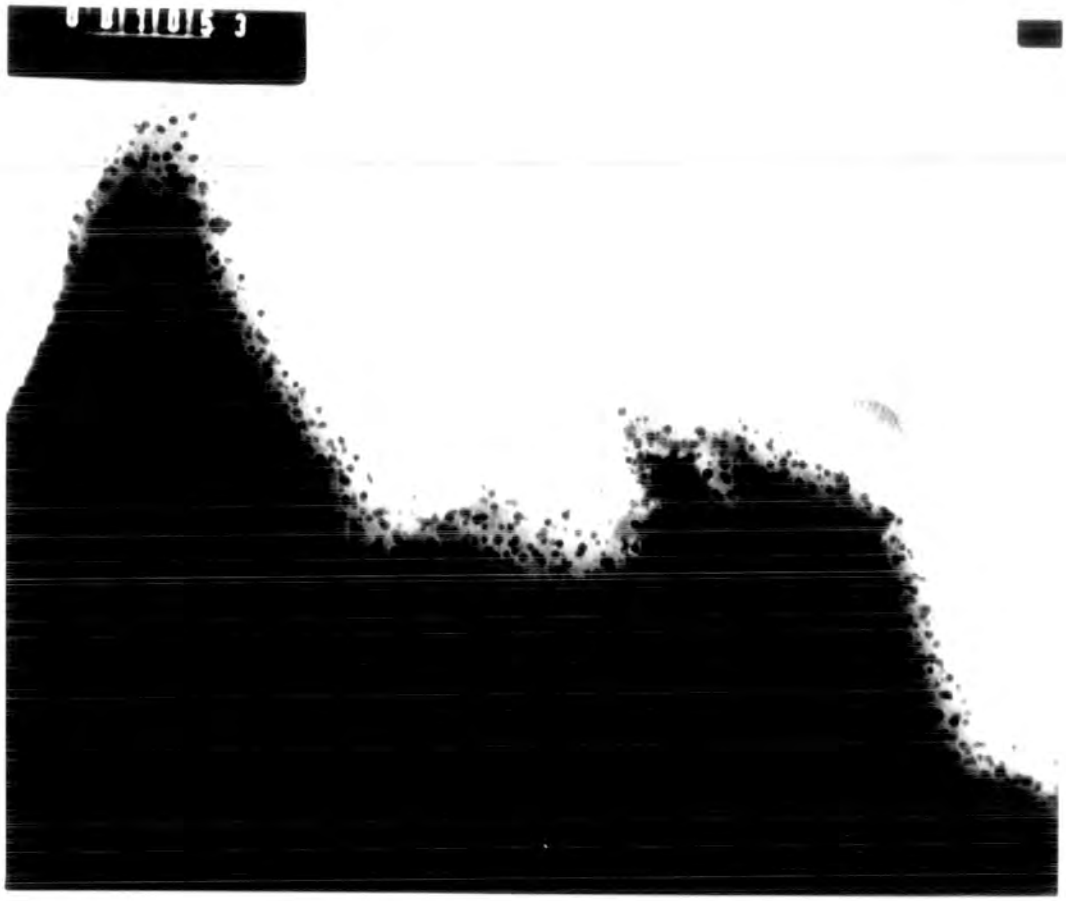

Fig. 3.4 1 1036 at 767°C for 1 hour x 86,000

spherical structures with an average size of 2,500 A and the large (20,000 A) spherical regions with internal structure, found in the base glass, were notably absent. This indicated that nucleation had been increased by the presence of titania.

When either 5% TiO_2 or 5% TiO_2 and 1% Gd_2O_3 was incorporated in the base L.A.S. glass, the crystallisation process produced such a fine grain structure after the heat treatments that the replication method for structural observation became inapplicable. In this case greater resolution was obtainable with the transmission method previously mentioned. If only titania was present, a large number of spherical crystallites were observed after the first stage heat treatment, the average size of which was under 1,000 A.

The two stage heating was found to produce structures with sizes which increased from 1,000 A to 8,000 A with the temperature of the initial heating. This is interpreted as the reduction of the nucleation efficiency and increased crystal growth at the elevated temperatures.

In all the cases considered so far the double stage heating resulted in an increase in the crystal dimensions compared with the single stage process. It is interesting to note that when 1% Gd_2O_3 is added in addition to 5% TiO_2 the double heating produced a reduction in the diameter of the structure compared to that of the single heating which produced structures of about 1,000 A extent.

From the above it is evident that 0.1% TiO_2 does influence the crystallisation by increasing the nucleation efficiency; however the much greater effects produced by 5% TiO_2 are more likely to produce the fine grained crystallisation required for useful ceramic production. The assumption of nucleation and crystal growth regions would appear to be justified by the results for the single and double heat treatments. A nucleation region exists below 800°C while near 850°C rapid crystal growth occurs. It is not suggested that these regions are completely distinct as the ability to nucleate crystals and propagate crystal growth must depend on similar activation energies. They are considered more as broad overlapping regions, as found in other systems (3.2). If we accept the existence of these regions, the role of Gd_2O_3 in the crystallisation process is again seen to be ineffective in the nucleation zone and inhibitive in the region of crystal growth.

As one of the theories of TiO_2 nucleated crystallisation suggests that phase separation plays an active role in the process it is important to note that at no stage in any of the L.A.S. glasses observed was any indication of phase separation observed. Phase separation may have occurred on a scale too small to be observed in the present investigation, although this would appear unlikely as previous observations of phase separation in glasses, has shown that structural units with dimensions well within the limits of observability here, are formed.

3.3 X-ray Diffraction

Standard powder X-ray diffraction procedures were followed to investigate the extent and nature of the crystal formation in the glasses subjected to the various heat treatments. Identification of the crystallisation product was made by a comparison of the observed d-values, for the lattice planes giving the most intense lines, with the expected value for β-eucryptite. Agreement was normally found to be within 1% and a typical comparison is shown in Table 3.2 for L.A.S. 1022 after heat treatment at 850°C for one hour.

All the crystallisation products, produced by heating glasses with L.A.S. 1022 as the base, gave diffraction lines which could be attributed to the β-eucryptite crystal lattice. This means that the various additions of titania and rare earths although effecting the extent, did not affect the morphology of the final crystallisation product. The investigation of the effect of TiO_2 is thus simplified to the consideration of only one observable crystalline development. As no indication of titanate compound formation was found in the early stages of titania-nucleated crystallisation, the precipitation of titanium compounds seems unlikely to be of major importance.

Unit cell dimensions have been calculated for some of the heat treated glasses and are given in Table 3.3. No systematic change in the fluctuations seen about the value expected for β-eucryptite was found, confirming that β-eucryptite was the only crystallisation product on a scale large enough to be

TABLE 3.2

REFLECTION H	K	L	D CALCULATED	SAMPLE 1022 AT 850°C FOR 1 HR. D OBSERVED	D.O. - D.C.
1	0	0	4.521	4.544	0.023
1	0	2	3.485	3.489	0.004
1	1	0	2.610	2.621	0.011
1	0	4	2.340	2.343	0.003
2	0	0	2.260	2.267	0.007
1	1	3	2.122	2.096	- 0.026
2	0	3	1.921	1.891	- 0.030
2	1	2	1.631	1.636	0.005
2	1	4	1.449	1.453	0.004
2	0	6	1.419	1.422	0.003

TABLE 3.3

HEAT TREATMENT	SAMPLE							
	1022		1023		1035		1036	
	a	c	a	c	a	c	a	c
800°C for 1 hr.	5.17	10.99	5.25	11.98	5.26	10.97	5.28	11.17
850°C for 1 hr.	5.22	10.94	5.22	11.11	5.26	11.01	5.17	11.22
650°C for 1 hr. + 850°C for 1 hr.	5.26	11.17	5.25	10.99	5.27	10.94	5.24	11.10
700°C for 1 hr. + 850°C for 1 hr.	5.18	10.98	5.25	10.99	5.40	11.15	5.28	11.13
750°C for 1 hr. + 850°C for 1 hr.	5.25	10.97	5.14	10.98	5.23	11.23	5.20	10.96
800°C for 1 hr. + 850°C for 1 hr.	5.21	11.08	5.24	10.97	5.11	11.00	5.25	11.03

detected by this technique.

The lattice parameters of the heat treated glasses showed no correlation with the temperature of crystallisation or with the single and double heat treatments. However, a small but definite increase occurred in the observed cell dimensions when titania was present. Although this effect is only just observable it may indicate the stretching of the crystal lattice by the incorporation of titanium. No equivalent expansion of the cell dimensions was found when gadolinium was present. This would suggest that gadolinium is located in the glassy part of the specimen and hence could act as a barrier to the crystal growth front.

The height of the most prominent diffraction peaks found from densitometer traces, have been used as a measure of the degree of crystallisation. This is feasible as the procedure of obtaining the diffraction patterns was made as constant as possible from sample to sample. The relative intensities of crystallisation for the single (2) and double (1) heat treatments are shown superimposed on the D.T.A. output in Fig. 3.1 (a-h). For a single heat treatment, little crystallisation was detected at temperatures less than those corresponding to the crystallisation peak. Above T_c however, the percentage crystallisation rose rapidly before passing through a maximum. Again there is a marked difference between the L.A.S. 1035 (TiO_2 only) and L.A.S. 1036 (TiO_2 + Gd_2O_3) glasses; for the latter composition the maximum amount of the crystalline phase was almost an order of

magnitude less than that of the specimens containing only TiO_2.

Further evidence for the inhibition of the crystallisation process by gadolinium comes from the results obtained for specimens subjected to the double heat treatment. The glasses containing TiO_2 show a double peak in the percentage crystallisation curve in agreement with other workers (3.2); however, when Gd_2O_3 is also added to the glass the amount of crystallisation developed by the second heating at temperatures above 700°C is much less than for the glasses containing only TiO_2.

A graphical form of the densitometer output for some typical samples is shown in Fig. 3.5 (a-h). Large amounts of glassy scattering can be observed with all samples of L.A.S. before heat treatment except when both 5% TiO_2 and 1% Gd_2O_3 are present, when very little glassy scattering was observed. The ratio of crystalline diffraction to glassy scattering was increased as the temperature and time of heat treatment increased, but for the L.A.S. base glass 1022 and for the glass with only 01% TiO_2 a small amount of scattering remained after quite high heat treatment temperatures. The incorporation of 5% TiO_2 reduced this to almost zero after the two stage heating.

The above confirms that titanium produces both increased nucleation and crystal growth and also that when gadolinium is present the crystal growth is reduced. A similar phenomenon has been noted recently (3.3) in the production of a barium titanate ceramic. Here the starting materials are crystalline and sintering occurs to produce the final product which is found to

FIG 3.5 X-RAY DIFFRACTION CURVES.

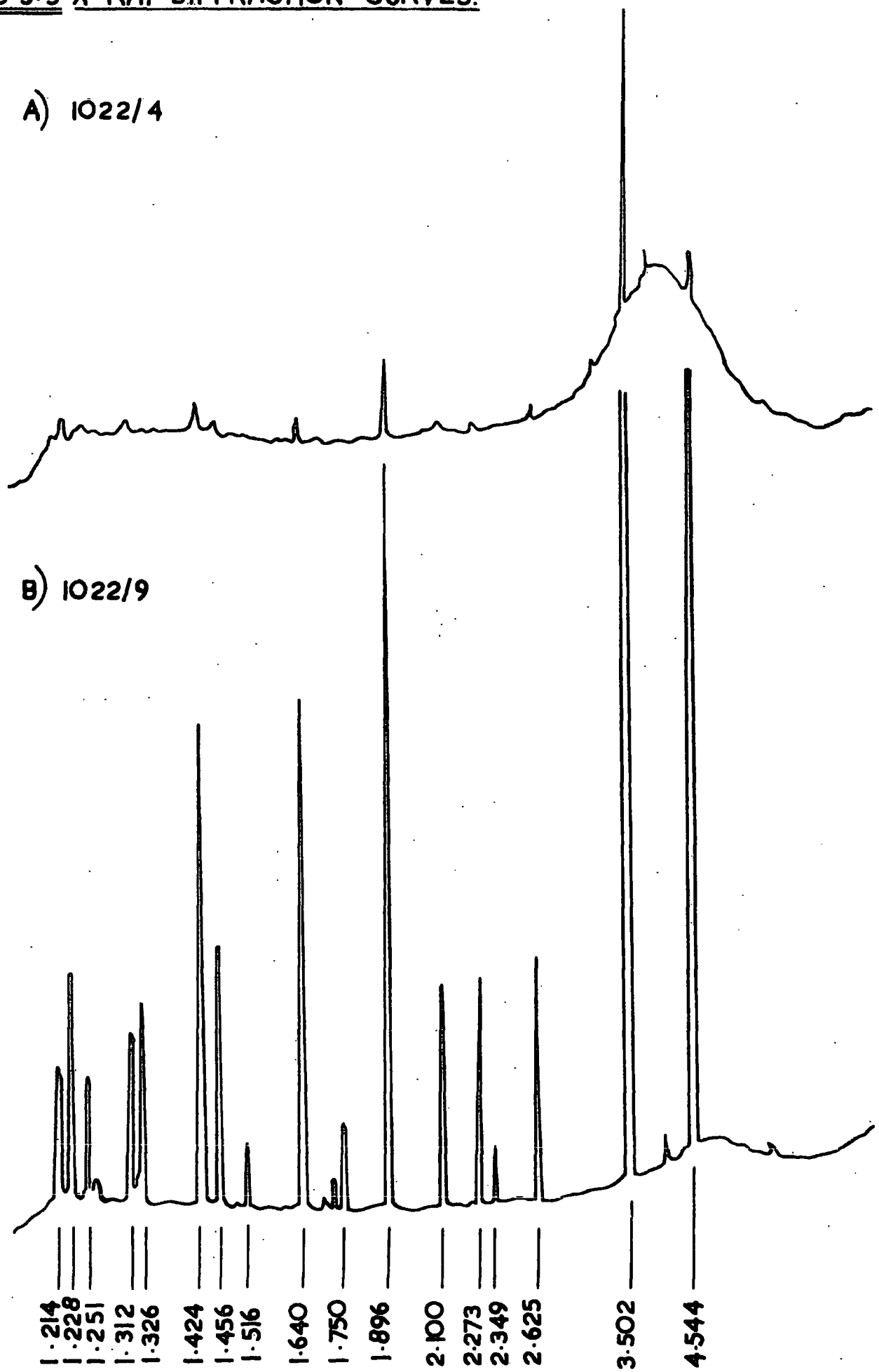

FIG. 3.5 (CONT'D.)

E) 1035/0

F) 1035/9

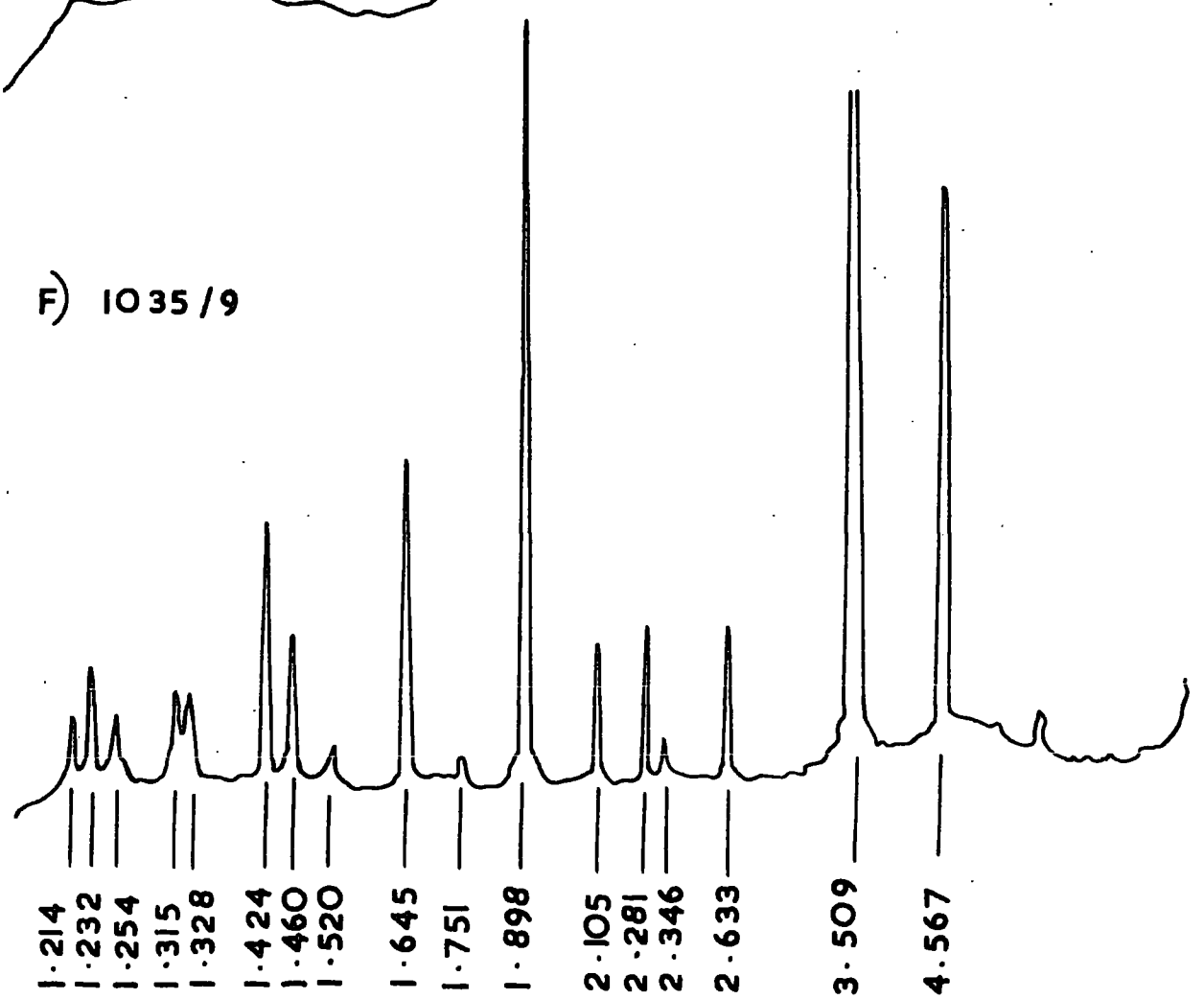

FIG 3.5 (CONTD)

G) 1036/0

H) 1036/9

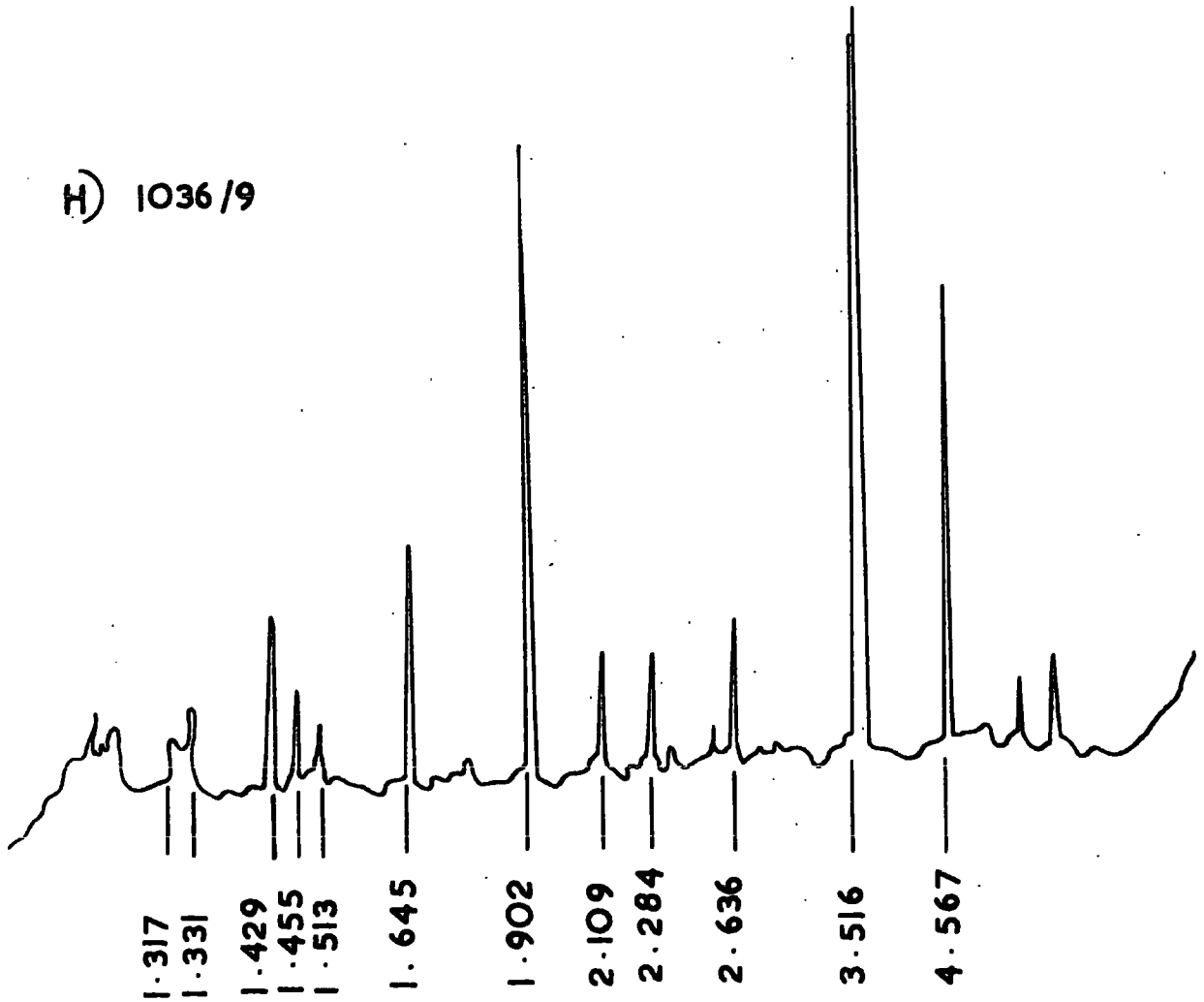

be affected by the prescence of Gd_2O_3. It is evident that some form of crystal growth inhibition is produced by the rare earth in the production of the enhanced properties, and its role may be similar to that indicated by the effects observed in this work.

The absence of glassy scatter before heat treatment in all the specimens with TiO_2 and Gd_2O_3 present is difficult to explain. Glassy scatter is due to the random nature of the glass lattice and the creation of a well ordered structure when TiO_2 and Gd_2O_3 are present cannot account for the absence of this scattering as crystalline diffraction lines do not appear. As yet this phenomenon is not understood.

B. Electron Spin Resonance

3.4 Electron Spin Resonance of Gd^{3+} in glass

3.4.1 Theory of Resonance Phenomenon

Electron paramagnetic resonance is dependent on the existence of unpaired electrons in an atom or molecule. This is because a non-zero total angular momentum $\underline{J}$ is required to produce a moment $\underline{\mu}$ which is given by:

$$\underline{\mu} \quad \alpha \quad h \quad \underline{J} \qquad (3\text{-}1)$$

$$= -\gamma \quad g \quad \underline{J} \qquad (3\text{-}2)$$

$$= -g_L \beta \quad \underline{J} \qquad (3\text{-}3)$$

where g_L is the Landé g-factor,

and $\beta = \frac{e\hbar}{2mc}$ is the Bohr magneton.

By applying a magnetic field $\underline{H}$ to the ion an energy level can be defined as

$$E = g_L \beta \, \underline{H}.\underline{J} \qquad (3\text{-}4)$$

and a pair of levels with different energies corresponding to $\pm J$ states result. For a particular J value the energy difference, $\Delta\varepsilon$, can be obtained, for example if $J=\frac{1}{2}$ then

$$\Delta E = g_L \beta H_z \qquad (3\text{-}5)$$

The application of electromagnetic radiation of frequency ν can cause an electronic transition between the levels if

$$h\nu = g_L \beta H_z \qquad (3\text{-}6)$$

Equation (3-6) represents the basic resonance condition.

Although a free ion may justify the use of equation (3-6), an ion is normally located within a solid and cannot be considered to be free. A variety of forces influence ions in solids and it is found convenient to define an effective g-value such that

$$h\nu = g_{eff}\,\beta H \qquad (3\text{-}7)$$

At temperatures normally used in e.s.r. experiments only the ground state is appreciably occupied and effective g-values can be used to reflect the location of paramagnetic ions in materials. In this way the complex interactions between the paramagnetic ions and their surroundings can be represented by a single experimental parameter.

3.4.2. The Hamiltonian

In order to understand the experimental results obtained some attempt must be made to derive the g-values theoretically. This requires a knowledge of the energy levels of the paramagnetic ion and these can be found by considering the total hamiltonian of the ion in the particular solid.

Although only small coupling exchange forces exist in paramagnetic systems, the orbital and spin interactions must be considered. In the iron group, with incomplete 3d shells, the 3d electrons are locked into the field of the neighbouring ions. This effective quenching of the orbital motion results in a spin-only magnetism. The protected, incomplete, inner 4f shell of the rare earths however, allows both orbital and spin

contributions to the ionic magnetism.

Whenever the unfilled shell is half filled, a spherical distribution of the charge cloud occurs and should result in no orbital state degeneracy for the free ion. In the $3d^5\ {}^6S$ state of the iron group and in the $4f^7\ {}^8S$ state of the rare earths this would appear to be the case, but observed resonances in crystals give conflicting evidence (3.4) (3.5). To explain this anomaly a spin-spin interaction has been suggested with the form

$$\sum_4 \beta^2 \left[\frac{S_j . S_k}{r_{jk}^3} - \frac{3(r_{jk} . S_j)(r_{jk} . S_k)}{r_{jk}^5} \right] \qquad (3\text{-}8)$$

which assumes an ellipsoidal distortion of the electron cloud. A spin hamiltonian, $\mathcal{H}(s)$ can thus be written to represent the spin-spin interaction with the form given below

$$\mathcal{H}(s) = aS_x^2 + bS_y^2 + cS_z^2 \qquad (3\text{-}9)$$

where a, b and c are real.

In e.s.r it is not possible to obtain the absolute values of the energy levels but only the relative separations and splittings in a magnetic field. The spin hamiltonian of equation (3-9) can be considered to define the energy levels before a magnetic field is applied. It is also possible to add a term, symmetric in S_x, S_y and S_z to equation (3-9) which will

only alter its absolute value without affecting the relevancy to e.s.r. It has become common to subtract a term $\frac{1}{3}(a+b+c)S^2$ from the right hand side of the equation (3-9) to enable the hamiltonian to be subdivided in terms of two crystal field parameters D and E. This then gives

$$\mathcal{H}(S) = D(S_Z^2 - \tfrac{1}{3}S(S+1)) + E(S_x^2 - S_y^2) \qquad (3\text{-}10)$$

where $D = \frac{3}{2}c$ and $E = \frac{1}{2}(a-b)$

From equation (3-10) the axial fields due to trigonal or tetragonal symmetry can be seen to be represented by D whilst the result of lower symmetry orthorhombic crystal fields give rise to the E term. The application of a magnetic field produces a Zeeman term $g\beta H.S$ which must be added to equation (3-10) to give the following hamiltonian for the conditions encountered in e.s.r.

$$\mathcal{H}(S) = g\beta H.S + D(S_z^2 - \tfrac{1}{3}S(S+1)) + E(S_x^2 - S_y^2) \qquad (3\text{-}11)$$

Equation (3-11) is considered as the starting point for an interpretation of the e.s.r. phenomenon found in glasses and the solution, as applicable to this work, is outlined below.

3.4.3 Discussion of Spin Hamiltonian Solution

The application of the spin hamiltonian approach to polycrystals is made difficult by the fact that the observed spectra contain spatial averages over all possible crystal orientations relative to the applied field. In a glass matrix the situation

is even more complex as it is not at all certain that the paramagnetic ion is in only one site. At best one can probably assume similar co-ordinations for the probe ions, but the inter-ionic spacing in the immediate vicinity of the probe ions will differ throughout the sample. Consequently a second average must be made in attempting to reproduce the observed resonances and such an analysis may be of little value unless a great deal of structural information is also known about the glass matrix.

A broad $g \simeq 2$ resonance is to be expected for transitions between two pure states, but to account for the high g-value resonances found in glasses containing Gd^{3+}, consideration must be given to forbidden ($|\Delta M_S| > 1$) transitions, which require the presence of strong crystal field effects to remove the limiation imposed by the selection rules. The low field transitions are then effectively those between the crystal-field-split doublets of the $J = \frac{7}{2}$ state.

The hamiltonian of equation (3-11) can be written

$$\mathcal{H}(S) = g_{\parallel}\beta H_z S_z + g_{\perp}\beta (H_x S_x + H_y S_y) + D(S_z^2 - \tfrac{1}{3}S(S+1)) + E(S_x^2 - S_y^2) \qquad (3\text{-}12)$$

A simplification can be made by assuming g isotropic with $g_{\parallel} = g_{\perp} = g$ which gives

$$\mathcal{H}(S) = g\beta (H_z S_z + H_x S_x + H_y S_y) + D(S_z^2 - \tfrac{1}{3}S(S+1)) + E(S_x^2 - S_y^2) \qquad (3\text{-}13)$$

Classical mechanical angular momentum can be represented by a vector whose direction corresponds to the sense and axis of rotation and whose magnitude corresponds to the value of the angular momentum about this axis. However quantum mechanics limits the available knowledge to the magnitude of the angular momentum and its component in one direction. The relationship between the components of S may be expressed in a definite form if these component vectors are represented as operators which obey the following commutation relations.

$$[S_x,S_y] = iS_z; [S_y,S_z] = iS_x; [S_z,S_x] = iS_y \qquad (3\text{-}14)$$

where $[S_i,S_j] \equiv S_iS_j - S_jS_i$ (3-15)

and the magnitude of S is $\sqrt{S(S+1)}$ where $S^2 = S_x^2+S_y^2+S_z^2$ (3-16)

Two operators A and B are said to commute if $[A,B] \equiv 0$ which means that A and B may be precisely known at the same time and can be represented by diagonal matrices. It has also been shown (3.6) that in a representation where S^2 and S_z are diagonal, the operators S^2, S_z, S_x and S_y have the following properties:

$$S^2 \mid M\rangle = S(S+1) \mid M\rangle \qquad (3\text{-}17)$$

$$S_z \mid M\rangle = M \mid M\rangle, \qquad (3\text{-}18)$$

$$S_+ \mid M\rangle = \left(S(S+1)-M(M+1)\right)^{\frac{1}{2}} \mid M+1\rangle \qquad (3\text{-}19)$$

$$S_- \mid M\rangle = \left(S(S+1)-M(M-1)\right)^{\frac{1}{2}} \mid M-1\rangle \qquad (3\text{-}20)$$

where $S_+ = S_x + iS_y$ and $S_- = S_x - iS_y$ (3-21)

and $\mid M\rangle$ represents a spin state.

From (3-13) and (3-21) the spin hamiltonian becomes:

$$\mathcal{H}(S) = g\beta\left(H_z S_z + H_x \frac{(S_+ + S_-)}{2}\right) + D(S_z^2 - \tfrac{1}{3}S(S+1)) + E\frac{(S_+^2 - S_-^2)}{2} \qquad (3\text{-}22)$$

Now since we can represent the applied field H in terms of components along the z and x directions such that $H_z = H\cos\theta$ and $H_x = H\sin\theta$ we have

$$\mathcal{H}(S) = g\beta\left(H\cos\theta\ S_z + \tfrac{1}{2}H\sin\theta\ (S_+ + S_-)\right) + \frac{D}{3}(3S_z^2 - S(S+1)) + \frac{E}{2}(S_+^2 - S_-^2) \qquad (3\text{-}23)$$

Matrix elements can be found from equation (3-23) by applying the rules given in equations (3-17) to (3-21) to the $J = \frac{7}{2}$ gadolinium ground state. The matrix elements can be calculated by the use of 'operator equivalents' as described fully by Stevens (3.7) and Bleaney and Stevens (3.8). These calculations have been made once and for all and are tabulated (3.9). The formation of the matrix using these values is outlined below.

Firstly the diagonal components are given by

$$\left\langle -\tfrac{7}{2} \right| H(S) \left| -\tfrac{7}{2} \right\rangle = g\,\beta\,H\cos\theta\,(-\tfrac{7}{2}) + \tfrac{D}{3} \qquad (7.3)$$

$$\left\langle -\tfrac{5}{2} \right| H(S) \left| -\tfrac{5}{2} \right\rangle = g\,\beta\,H\cos\theta\,(-\tfrac{5}{2}) + \tfrac{D}{3} \qquad (1.3)$$

$$\left\langle -\tfrac{3}{2} \right| H(S) \left| -\tfrac{3}{2} \right\rangle = g\,\beta\,H\cos\theta\,(-\tfrac{3}{2}) + \tfrac{D}{3} \qquad (-9)$$

$$\left\langle -\tfrac{1}{2} \right| H(S) \left| -\tfrac{1}{2} \right\rangle = g\,\beta\,H\cos\theta\,(-\tfrac{1}{2}) + \tfrac{D}{3} \qquad (-15)$$

(3-24)

$$\left\langle \tfrac{1}{2} \right| H(S) \left| \tfrac{1}{2} \right\rangle = g\,\beta\,H\cos\theta\,(\tfrac{1}{2}) + \tfrac{D}{3} \qquad (-15)$$

$$\left\langle \tfrac{3}{2} \right| H(S) \left| \tfrac{3}{2} \right\rangle = g\,\beta\,H\cos\theta\,(\tfrac{3}{2}) + \tfrac{D}{3} \qquad (-9)$$

$$\left\langle \tfrac{5}{2} \right| H(S) \left| \tfrac{5}{2} \right\rangle = g\,\beta\,H\cos\theta\,(\tfrac{5}{2}) + \tfrac{D}{3} \qquad (1.3)$$

$$\left\langle \tfrac{7}{2} \right| H(S) \left| \tfrac{7}{2} \right\rangle = g\,\beta\,H\cos\theta\,(\tfrac{7}{2}) + \tfrac{D}{3} \qquad (7.3)$$

next the first order off diagonal elements are

$$\left\langle -\tfrac{5}{2} \right| H(S) \left| -\tfrac{7}{2} \right\rangle = \tfrac{1}{2} g\,\beta\,H\sin\theta \left(\tfrac{63}{4} - \tfrac{35}{4}\right)^{\frac{1}{2}}$$

$$\left\langle -\tfrac{3}{2} \right| H(S) \left| -\tfrac{5}{2} \right\rangle = \tfrac{1}{2} g\,\beta\,H\sin\theta \left(\tfrac{63}{4} - \tfrac{15}{4}\right)^{\frac{1}{2}}$$

$$\left\langle -\tfrac{7}{2} \right| H(S) \left| -\tfrac{5}{2} \right\rangle = \tfrac{1}{2} g\,\beta\,H\sin\theta \left(\tfrac{63}{4} - \tfrac{35}{4}\right)^{\frac{1}{2}}$$

$$\left\langle -\tfrac{1}{2} \right| H(S) \left| \tfrac{1}{2} \right\rangle = \tfrac{1}{2} g\,\beta\,H\sin\theta \left(\tfrac{63}{4} + \tfrac{1}{4}\right)^{\frac{1}{2}}$$

$$\langle -\tfrac{5}{2} \mid H(S) \mid -\tfrac{3}{2} \rangle = \tfrac{1}{2} g \beta H \sin\theta \left(\tfrac{63}{4} - \tfrac{15}{4}\right)^{\frac{1}{2}}$$

$$\langle \tfrac{1}{2} \mid H(S) \mid -\tfrac{1}{2} \rangle = \tfrac{1}{2} g \beta H \sin\theta \left(\tfrac{63}{4} + \tfrac{1}{4}\right)^{\frac{1}{2}}$$

$$\langle -\tfrac{3}{2} \mid H(S) \mid -\tfrac{1}{2} \rangle = \tfrac{1}{2} g \beta H \sin\theta \left(\tfrac{63}{4} - \tfrac{3}{4}\right)^{\frac{1}{2}}$$

$$\langle \tfrac{3}{2} \mid H(S) \mid \tfrac{1}{2} \rangle = \tfrac{1}{2} g \beta H \sin\theta \left(\tfrac{63}{4} - \tfrac{3}{4}\right)^{\frac{1}{2}}$$

$$\langle -\tfrac{1}{2} \mid H(S) \mid -\tfrac{3}{2} \rangle = \tfrac{1}{2} g \beta H \sin\theta \left(\tfrac{63}{4} - \tfrac{3}{4}\right)^{\frac{1}{2}}$$

$$\langle \tfrac{5}{2} \mid H(S) \mid \tfrac{3}{2} \rangle = \tfrac{1}{2} g \beta H \sin\theta \left(\tfrac{63}{4} - \tfrac{15}{4}\right)^{\frac{1}{2}} \qquad (3\text{-}25)$$

$$\langle \tfrac{1}{2} \mid H(S) \mid \tfrac{3}{2} \rangle = \tfrac{1}{2} g \beta H \sin\theta \left(\tfrac{63}{4} - \tfrac{3}{4}\right)^{\frac{1}{2}}$$

$$\langle \tfrac{7}{2} \mid H(S) \mid \tfrac{5}{2} \rangle = \tfrac{1}{2} g \beta H \sin\theta \left(\tfrac{63}{4} - \tfrac{35}{4}\right)^{\frac{1}{2}}$$

$$\langle \tfrac{3}{2} \mid H(S) \mid \tfrac{5}{2} \rangle = \tfrac{1}{2} g \beta H \sin\theta \left(\tfrac{63}{4} - \tfrac{15}{4}\right)^{\frac{1}{2}}$$

$$\langle \tfrac{5}{2} \mid H(S) \mid \tfrac{7}{2} \rangle = \tfrac{1}{2} g \beta H \sin\theta \left(\tfrac{63}{4} - \tfrac{35}{44}\right)^{\frac{1}{2}}$$

and finally the second order off diagonal elements are

$$\langle \pm \tfrac{7}{2} \mid H(S) \mid \pm \tfrac{3}{2} \rangle = \frac{E}{2} \sqrt{21}$$

$$\langle \pm \tfrac{5}{2} \mid H(S) \mid \pm \tfrac{1}{2} \rangle = \frac{E}{2} .3 \sqrt{5}$$

$$\langle \pm \tfrac{3}{2} \mid H(S) \mid \mp \tfrac{1}{2} \rangle = \frac{E}{2} .2 \sqrt{15}$$

$$\langle \pm \tfrac{1}{2} \mid H(S) \mid \mp \tfrac{3}{2} \rangle = \frac{E}{2} .2 \sqrt{15}$$

$$\left\langle \pm \frac{1}{2} \right| H(S) \left| \pm \frac{5}{2} \right\rangle = \frac{E}{2} \cdot 3\sqrt{5}$$

$$\left\langle \pm \frac{3}{2} \right| H(S) \left| \pm \frac{7}{2} \right\rangle = \frac{E}{2}\sqrt{21}$$

The resulting 8 x 8 matrix becomes:

	$\left\vert -\frac{7}{2}\right\rangle$	$\left\vert -\frac{5}{2}\right\rangle$	$\left\vert -\frac{3}{2}\right\rangle$	$\left\vert -\frac{1}{2}\right\rangle$	$\left\vert \frac{1}{2}\right\rangle$	$\left\vert \frac{3}{2}\right\rangle$	$\left\vert \frac{5}{2}\right\rangle$	$\left\vert \frac{7}{2}\right\rangle$
$\left\vert -\frac{7}{2}\right\rangle$	$-\frac{7}{2}G+7D$	$G'\sqrt{\frac{28}{2}}$	$E\sqrt{\frac{21}{2}}$	0	0	0	0	0
$\left\vert -\frac{5}{2}\right\rangle$	$G'\frac{\sqrt{28}}{2}$	$-\frac{5}{2}G+D$	$G'\sqrt{\frac{48}{2}}$	$E\frac{3\sqrt{5}}{2}$	0	0	0	0
$\left\vert -\frac{3}{2}\right\rangle$	$E\sqrt{\frac{21}{2}}$	$G'\sqrt{\frac{48}{2}}$	$-\frac{3}{2}G-3D$	$G'\sqrt{\frac{60}{2}}$	$E\sqrt{15}$	0	0	0
$\left\vert -\frac{1}{2}\right\rangle$	0	$E'\frac{3\sqrt{5}}{2}$	$G'\sqrt{\frac{60}{2}}$	$-\frac{1}{2}G-5D$	$G'\ 4$	$E\sqrt{15}$	0	0
$\left\vert \frac{1}{2}\right\rangle$	0	0	$E\sqrt{15}$	$G'\ 4$	$\frac{1}{2}G-5D$	$G'\sqrt{\frac{60}{2}}$	$E\frac{3\sqrt{5}}{2}$	0
$\left\vert \frac{3}{2}\right\rangle$	0	0	0	$E\sqrt{15}$	$G'\sqrt{\frac{60}{2}}$	$\frac{3}{2}G-3D$	$G'\sqrt{\frac{48}{2}}$	$E\sqrt{\frac{21}{2}}$
$\left\vert \frac{5}{2}\right\rangle$	0	0	0	0	$E\frac{3\sqrt{5}}{2}$	$G'\sqrt{\frac{48}{2}}$	$\frac{5}{2}G+D$	$G'\sqrt{\frac{28}{2}}$
$\left\vert \frac{7}{2}\right\rangle$	0	0	0	0	0	$E\sqrt{\frac{21}{2}}$	$G'\sqrt{\frac{28}{2}}$	$\frac{7}{2}G+7D$

where $G = g\beta H\cos\theta$ and $G' = \frac{1}{2} g\beta H\sin\theta$

It was found convenient during computation to divide this matrix into three submatrices which are given below. This allowed the crystal field parameters D and E to be varied.

The E matrix becomes

E	$\left\|-\frac{7}{2}\right\rangle$	$\left\|-\frac{5}{2}\right\rangle$	$\left\|-\frac{3}{2}\right\rangle$	$\left\|-\frac{1}{2}\right\rangle$	$\left\|\frac{1}{2}\right\rangle$	$\left\|\frac{3}{2}\right\rangle$	$\left\|\frac{5}{2}\right\rangle$	$\left\|\frac{7}{2}\right\rangle$
$\left\|-\frac{7}{2}\right\rangle$	0	0	2.292	0	0	0	0	0
$\left\|-\frac{5}{2}\right\rangle$	0	0	0	3.354	0	0	0	0
$\left\|-\frac{3}{2}\right\rangle$	2.292	0	0	0	3.873	0	0	0
$\left\|-\frac{1}{2}\right\rangle$	0	3.354	0	0	0	3.873	0	0
$\left\|\frac{1}{2}\right\rangle$	0	0	3.873	0	0	0	3.354	0
$\left\|\frac{3}{2}\right\rangle$	0	0	0	3.873	0	0	0	2.292
$\left\|\frac{5}{2}\right\rangle$	0	0	0	0	3.354	0	0	0
$\left\|\frac{7}{2}\right\rangle$	0	0	0	0	0	2.292	0	0

and the D matrix is

D	$\left\|-\frac{7}{2}\right\rangle$	$\left\|-\frac{5}{2}\right\rangle$	$\left\|-\frac{3}{2}\right\rangle$	$\left\|-\frac{1}{2}\right\rangle$	$\left\|\frac{1}{2}\right\rangle$	$\left\|\frac{3}{2}\right\rangle$	$\left\|\frac{5}{2}\right\rangle$	$\left\|\frac{7}{2}\right\rangle$
$\left\|-\frac{7}{2}\right\rangle$	7	0	0	0	0	0	0	0
$\left\|-\frac{5}{2}\right\rangle$	0	1	0	0	0	0	0	0
$\left\|-\frac{3}{2}\right\rangle$	0	0	-3	0	0	0	0	0
$\left\|-\frac{1}{2}\right\rangle$	0	0	0	-5	0	0	0	0
$\left\|\frac{1}{2}\right\rangle$	0	0	0	0	-5	0	0	0
$\left\|\frac{3}{2}\right\rangle$	0	0	0	0	0	-3	0	0
$\left\|\frac{5}{2}\right\rangle$	0	0	0	0	0	0	1	0
$\left\|\frac{7}{2}\right\rangle$	0	0	0	0	0	0	0	7

whilst finally the D and E independent terms become

	$\left\|-\frac{7}{2}\right\rangle$	$\left\|-\frac{5}{2}\right\rangle$	$\left\|-\frac{3}{2}\right\rangle$	$\left\|-\frac{1}{2}\right\rangle$	$\left\|\frac{1}{2}\right\rangle$	$\left\|\frac{3}{2}\right\rangle$	$\left\|\frac{5}{2}\right\rangle$	$\left\|\frac{7}{2}\right\rangle$
$\left\|-\frac{7}{2}\right\rangle$	0	2.646	0	0	0	0	0	0
$\left\|-\frac{5}{2}\right\rangle$	2.646	0	3.464	0	0	0	0	0
$\left\|-\frac{3}{2}\right\rangle$	0	3.464	0	3.873	0	0	0	0
$\left\|-\frac{1}{2}\right\rangle$	0	0	3.873	0	4.0	0	0	0
$\left\|\frac{1}{2}\right\rangle$	0	0	0	4.0	0	3.873	0	0
$\left\|\frac{3}{2}\right\rangle$	0	0	0	0	3.873	0	3.464	0
$\left\|\frac{5}{2}\right\rangle$	0	0	0	0	0	3.464	0	2.646
$\left\|\frac{7}{2}\right\rangle$	0	0	0	0	0	0	2.646	0

By solution of the sum of these three submatrices for a particular set of values of E, D and θ an energy level scheme can be found for the gadolinium ion for a definite value of the external magnetic field H. As H is varied an energy level diagram of the type shown in Fig. (3.6) is produced. It is then possible to predict the magnetic field values of possible transitions. On Fig. (3.6) all the possible X-band transitions are indicated; however since in glasses an averaging process must be employed to account for the observed spectrum it is necessary to find a measure of the expected relative intensities, which depend on the transition probabilities.

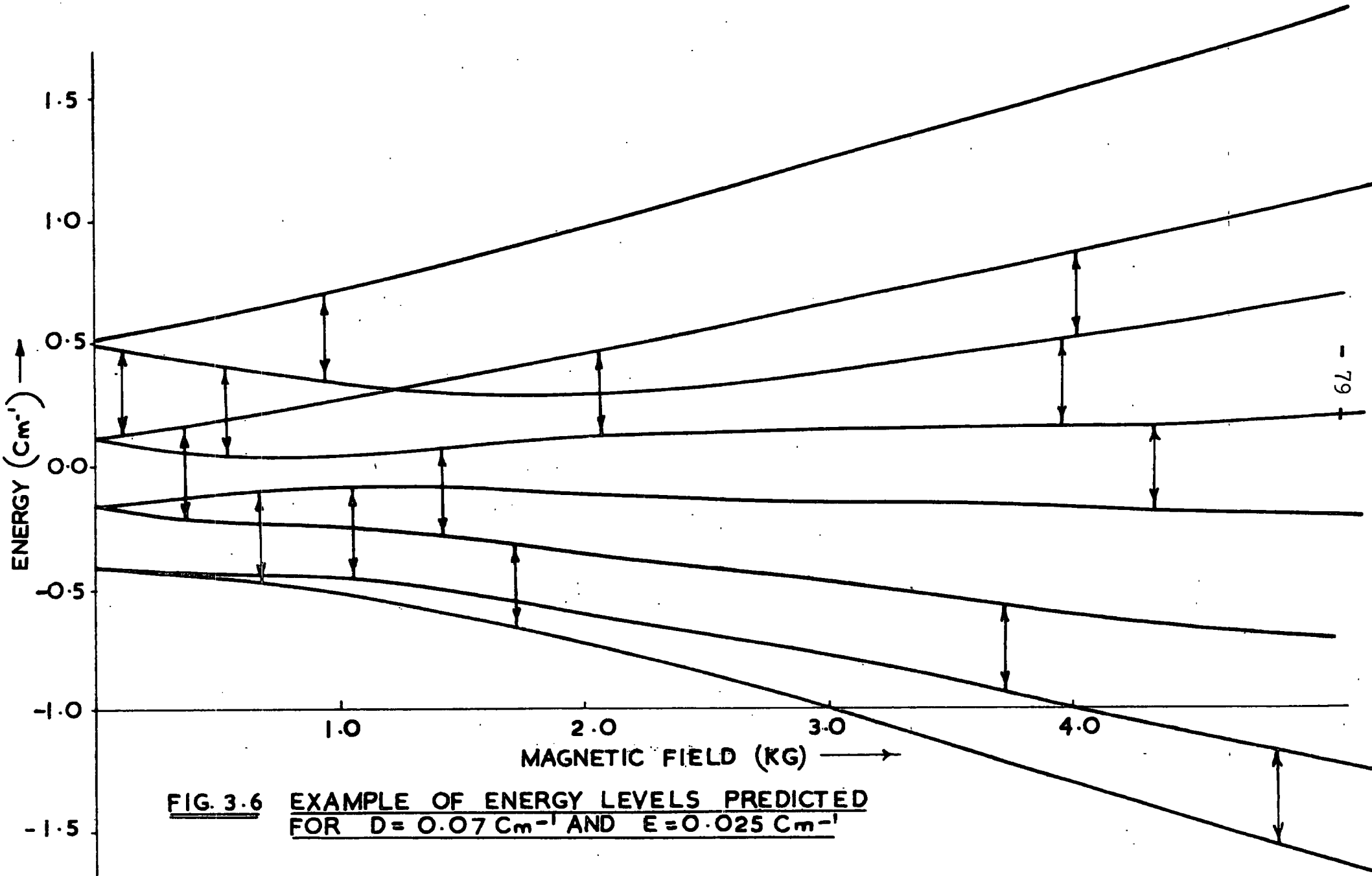

FIG. 3.6 EXAMPLE OF ENERGY LEVELS PREDICTED FOR $D = 0.07\ Cm^{-1}$ AND $E = 0.025\ Cm^{-1}$

3.4.4. Transition Probabilities

It is well known (3.10) that transition probabilities can be calculated by adding a perturbation to the hamiltonian. From equation (3-13) by adding $H_1^2 \cos \omega t$ the hamiltonian becomes:

$$\mathcal{H}(S) = g\beta \left(S_x \underline{i} + S_y \underline{j} + S_z \underline{k} \right) . \; h2 \cos\omega t (\cos\alpha \, \underline{i} + \sin\alpha \, \underline{j}) \qquad (3\text{-}27)$$

where $H_1 \cos \omega t$ represents the oscillatory magnetic component of the microwave energy and where α gives the orientation of h in the x-y plane.

The probability $\omega_{mm'}$ per unit time that a paramagnetic ion initially in the state $|m\rangle$ will be found in the state $|m'\rangle$ is given by Pake (3.11) as

$$\omega_{mm'} = |\langle m' | H_1' | m \rangle|^2 g(\nu) \qquad (3\text{-}28)$$

where $g(\nu)$ represents the resonance line shape distribution. However, the nature of $g(\nu)$ is not important in the calculation of relative line intensities which are given by

$$P_{mm'} = |\langle m' | H_1' | m \rangle|^2 \qquad (3\text{-}29)$$

When the crystal field is such as to cause mixing of the basis states it is possible to represent the mixed states as linear combinations of the eight basis states.

For example two such mixed states can be of the form

$$|a\rangle = \sum_{m'} a_{m'} |m'\rangle \qquad (3\text{-}30)$$

$$|b\rangle = \sum_{m} b_{m} |m\rangle \qquad (3\text{-}31)$$

In this case the transition probability as given by equation (3-29) becomes

$$P_{ab} = \left(\tfrac{1}{2} h g \beta\right)^2 \left(\cos\alpha \langle a| S_+ + S_- |b\rangle - i \sin\alpha \langle a| S_+ - S_- |b\rangle\right)^2 \qquad (3\text{-}32)$$

$$= \left(\tfrac{1}{2} h g \beta\right)^2 \left(\cos^2\alpha \langle a| S_+ + S_- |b\rangle^2 + \sin^2\alpha \langle a| S_+ - S_- |b\rangle^2\right) \qquad (3\text{-}33)$$

The variable site occupation means that in a glass all orientations have equal probability so an average must be taken over all possible values of α . Since the average values of $\sin^2\alpha$ and $\cos^2\alpha$ is $\frac{1}{2}$, equation (3-31) becomes

$$P_{ab} = \left(\tfrac{1}{2} h g \beta\right)^2 \left(\tfrac{1}{2} \langle a| S_+ + S_- |b\rangle^2 + \tfrac{1}{2} \langle a| S_+ - S_- |b\rangle^2\right) \qquad (3\text{-}34)$$

$$= \left(\tfrac{1}{2} h g \beta\right)^2 \left(\langle a| S_+ |b\rangle^2 + \langle a| S_- |b\rangle^2\right) \qquad (3\text{-}35)$$

It has been possible with the aid of a computer programme given in Appendix I to calculate all the energy level differences

between predicted energy levels with the $J = \frac{7}{2}$ state for particular magnetic field values. This energy difference is compared with the microwave energy applied and if it is within a specified tolerance the probability is calculated to give a measure of both field position and intensity of the expected transitions.

The computed output can be drawn as a histogram of transition intensities against field for particular values of the field orientation. Again since all orientations of the glass sites have equal probability a summation must be made for all field orientations. Since isotropy in the x-y directions has been assumed in the derivation, a weighting factor of $2 \sin\theta + \cos\theta$ must be used to correct the relative transition probabilities. Evaluation of the results of these calculations are presented in the Section 3.4.6.

The spin hamiltonian of equation (3.11) will be seen later to lead to an explanation of some of the structure found in the electron spin resonance signal of the gadolinium containing glass. However, the approximation of symmetry in the x-y plane may lead to some inaccuracies. In order to evaluate the effect of non uniformities in the x-y plane an alternative hamiltonian was considered in which the external magnetic field is restricted to the x-y plane. The hamiltonian (3.11) thus becomes

$$\mathcal{H}(s) = g\beta\left(H_z S_z + H_x S_x + H_y S_y\right) + D\left(S_z^2 - \tfrac{1}{3}S(S+1)\right) + E\left(S_x^2 - S_y^2\right)$$

where we assume $g_{//} = g_{\perp} = g$

Let $H_z = 0$

$H_x = H \cos\theta$

$H_y = H \sin\theta$

then $$\mathcal{H}(S) = g\beta H(\cos\theta S_x + \sin\theta S_y) + D(S_z^2 - \tfrac{1}{3}S(S+1)) + E(S_x^2 - S_y^2) \qquad (3-36)$$

using $S_y = \frac{1}{2i}(S_+ - S_-)$ and $S_x = \frac{1}{2}(S_+ + S_-)$

and substituting into equation (3-36) gives

$$\mathcal{H}(S) = \tfrac{1}{2}g\beta H(\sin\theta + i\cos\theta)S_+ - \tfrac{1}{2}g\beta H(\sin\theta - i\cos\theta)S_- + \frac{D}{3}(3S_z^2 - S(S+1)) + \frac{E}{2}(S_+^2 + S_-^2) \qquad (3-37)$$

Equation (3-37) can now be solved in a similar way to equation (3-23). Again spatial averages over all possible angles for the external field must be made and transition probabilities calculated. This results in a histogram of transition intensity versus magnetic field for a particular crystal field value. To obtain the observed form of the resonance absorption this x-y intensity variation must be added to the result for the x-z plane. The results of this further calculation are presented in Section (3.4.6).

3.4.5. Results

E.s.r. absorption was anticipated only for glasses containing Gd^{3+} ions, however, specimens of all the glasses prepared were

examined in order to eliminate the possible existence of impurity resonances (for example from Fe^{3+}) which might interfere with the Gd^{3+} spectra. Resonances were never found in any specimen which did not contain gadolinium, a feature which also confirmed that the titanium ions, when added to the glasses, were predominately in the non-magnetic Ti^{4+} state. Consequently any possible influence of these ions on the observed spectrum due to cross relaxation phenomena can be ruled out. In further support of this conclusion the temperature dependence of the spectra for glasses containing both gadolinium and titanium ions was not typical of that to be expected for a resonance spectrum dominated by cross relaxation (3.5).

The resonance spectra for three gadolinium concentrations (0.09%, 0.2% and 1.0%) were examined in preliminary measurements in order to determine the optimum conditions for the present investigations. The general form of the spectra in the range from H = 0 to 8 $k\theta a$ is the same for all the compositions with relatively sharp resonances at $g \approx 5.9$ and 4.3 and a much broader high-intensity resonance with its centre field corresponding to $g \approx 2.0$. This is shown for the glass L.A.S. 1058 (1.0% Gd) in Fig. (3.6). There is also evidence of some further structure associated with this large peak in the vicinity of $g \approx 2$ but it has so far proved impossible to resolve this satisfactorily.

The only variation evident from decreasing the gadolinium concentration is associated with the broad central resonance which decreases in intensity but has a constant half-width. There is no

corresponding change in the higher g value line intensities and again their half-widths are independent of composition; consequently it can be assumed that there are no appreciable interactions between the Gd^{3+} ions leading to exchange narrowing of the lines in the concentrations studied. These features are typical of those found by earlier workers with gadolinium doped glasses, and the use of 1.0% gadolinium concentration employed in the previous investigations of other workers allows a more meaningful direct comparison of the various sets of results.

The resonance spectrum of the 1% Gd^{3+} sample Fig (3.7) is similar to that found by these earlier workers (3.12) (3.13) (3.14) using other types of glass matrix. Differences due to the glass matrix were found when the differential of the e.s.r. absorption of 1% Gd^{3+} in lithium aluminium silicate, sodium silicate and sodium borosilicate glass were compared. These are shown in Fig. (3.8) and will be discussed later.

The main interest in this study was in the lithium aluminium silicate glasses and it was found for gadolinium-doped glasses in this system that after heat treatment the intensities of the g_2($g \approx 5.9$) and g_3 ($g \approx 4.3$) resonances (see Fig.(3.7)) decreased with respect to the g_1 resonance as the heat treatment is increased above about 600 ^{o}C. This decrease, which is shown in Fig. (3.9) occurred for both the L.A.S. 1036 (Gd and Ti doped) and L.A.S. 1058 (Gd doping only) glasses. However, the detailed variation of the intensity ratio of the g_2 and g_3 resonances (I_2/I_3) depends upon the composition of the glass under investigation. For the L.A.S. 1058 glasses, increasing the temperature of heat treatment led to

FIG 3.7 E.S.R. DIFFERENTIAL ABSORPTION SPECTRUM.

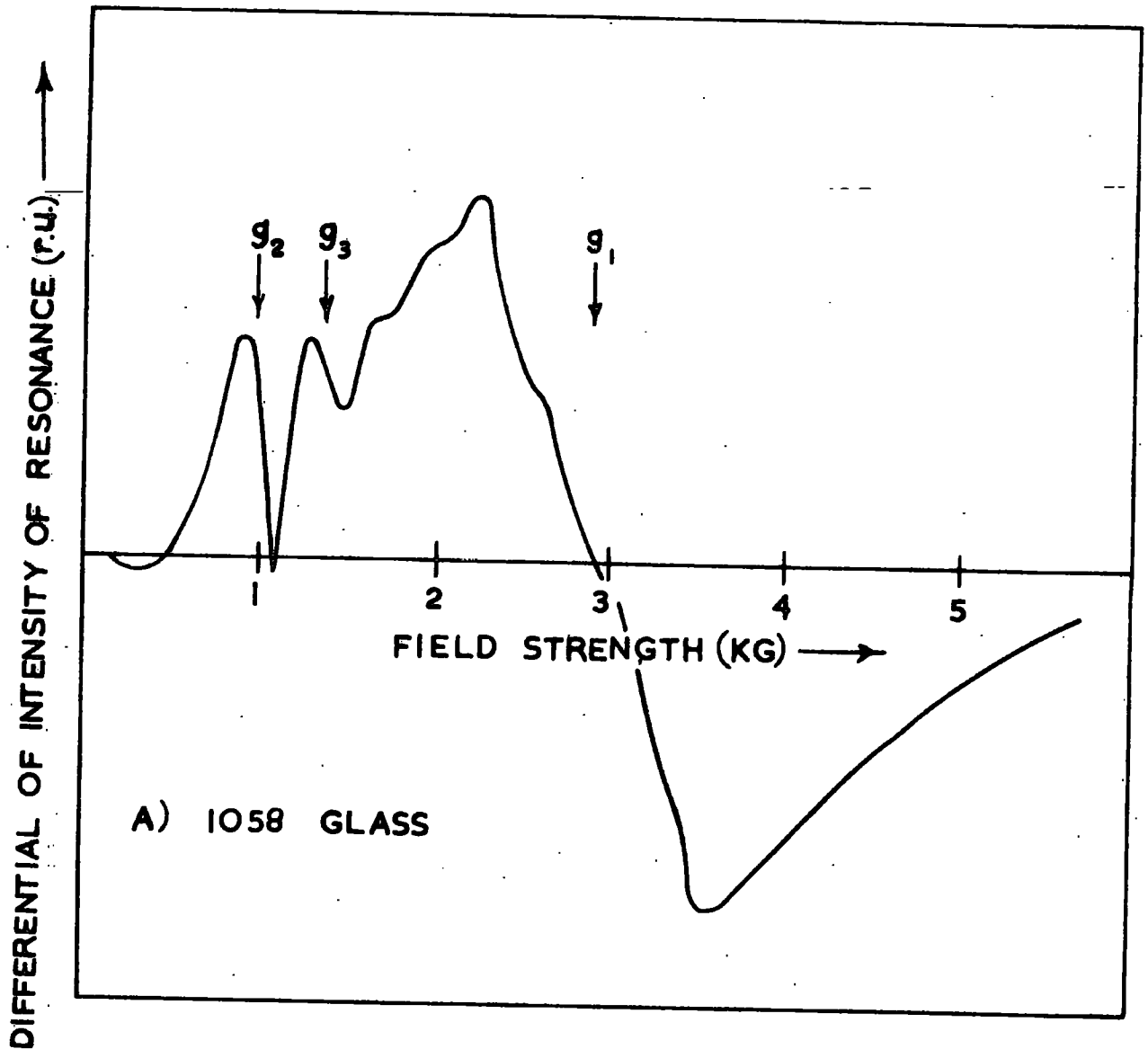

FIG 3.8 E.S.R. DIFFERENTIAL ABSORPTION SPECTRUM

A) Gd_2O_3 IN BORO SILICATE GLASS

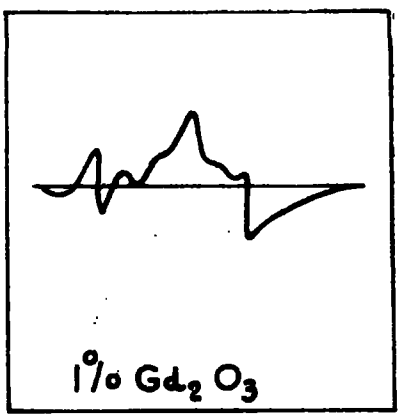

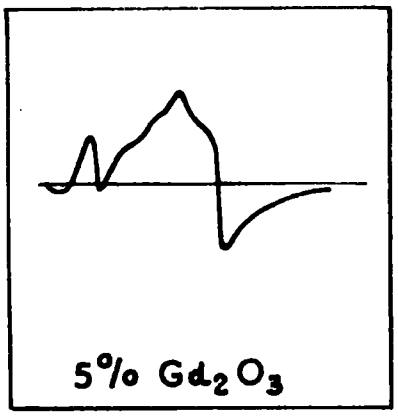

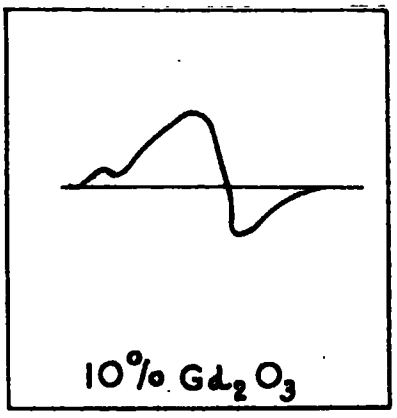

B) Gd_2O_3 IN SODIUM SILICATE GLASS.

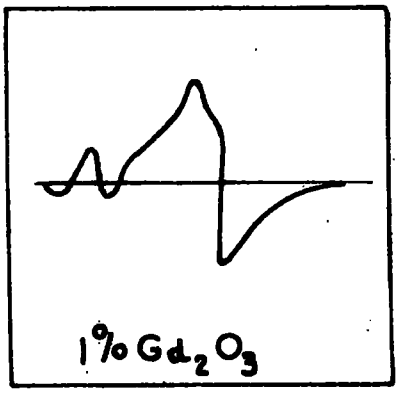

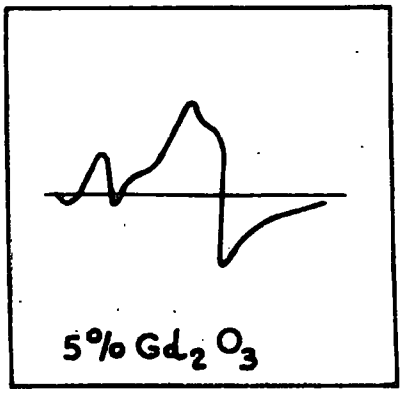

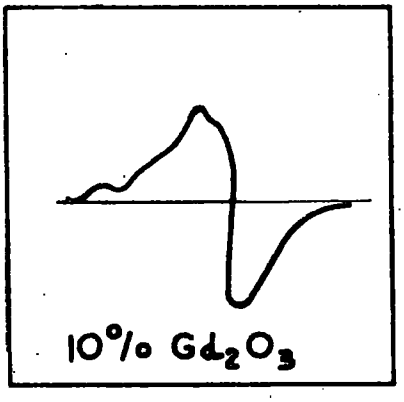

C) Gd_2O_3 IN LITHIUM ALUMINIUM SILICATE GLASS.

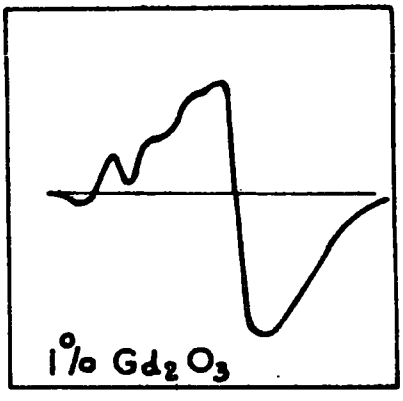

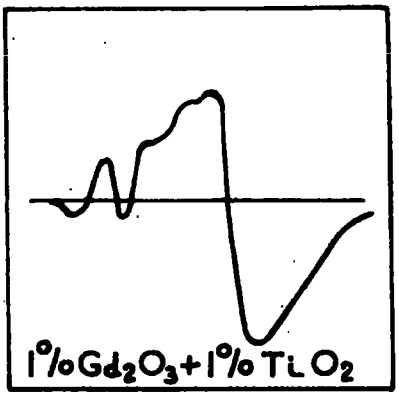

FIG 3.9 E.S.R. INTENSITY VARIATION WITH HEAT TREATMENT.

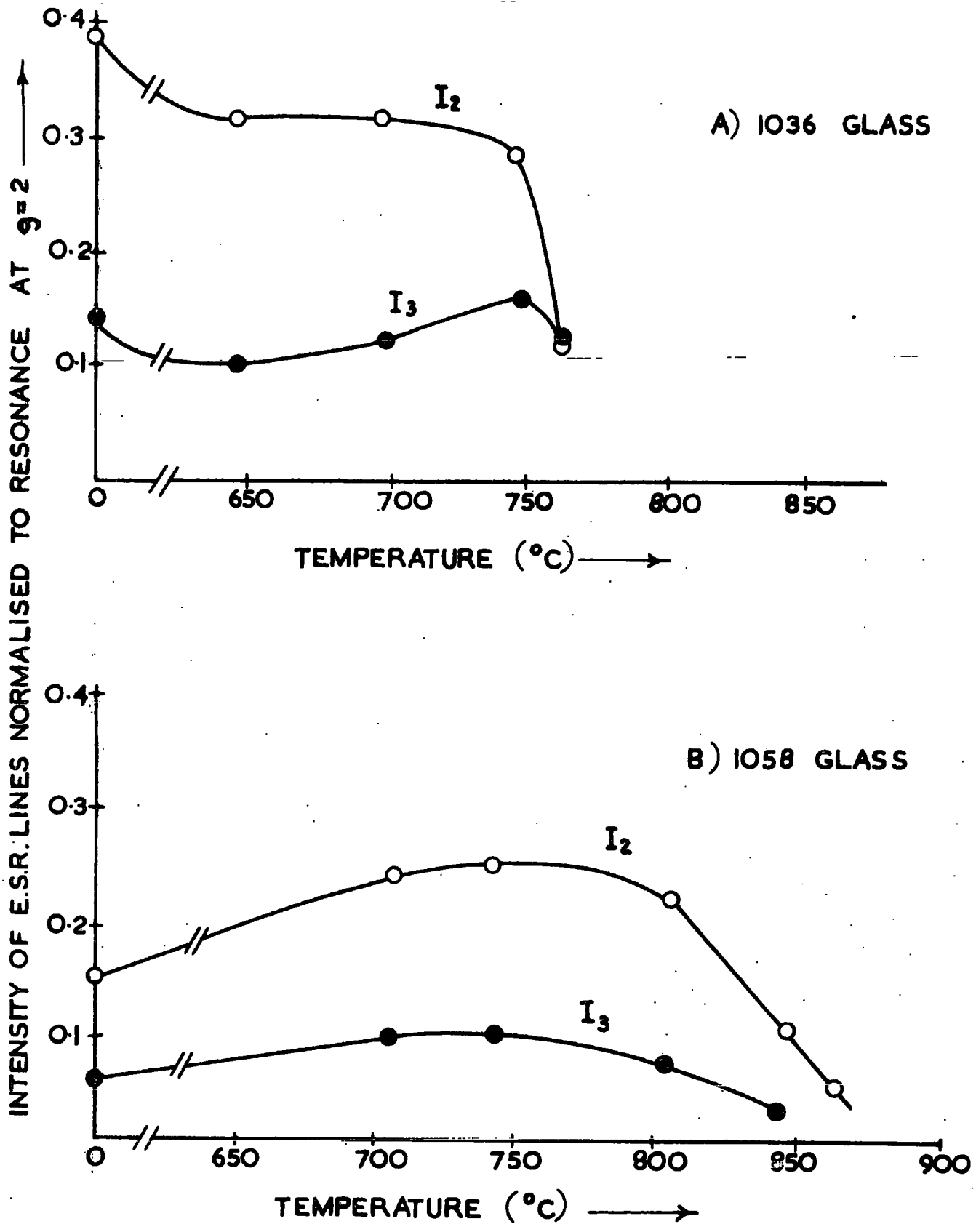

a sudden increase in I_2/I_3 above about 800^{o}C. This temperature corresponds to the onset of crystallisation as described earlier. Fig. (3.10) shows the variation of this ratio with increasing heat treatment temperature. Fig. (3.10) shows also the behaviour of the glasses containing both titanium and gadolinium for which the results are obviously different, the I_2/I_3 ratio decreasing with increasing nucleation heat treatment temperature. Comparison with the D.T.A. and crystallisation data of Fig. (3.1) suggests that these variations in the intensity ratio are associated with the onset of crystallisation, differences occurring due to the different methods of nucleation.

The observation of Gd^{3+} spectra in other glass matrices shown in Fig. (3.8) shows that although the resonance line positions appear to be independent of the glass host the relative intensities of these lines change from one matrix to another. The relative reduction in the broad g_1 ($g \approx 2$) resonance produced a greater resolution of the individual lines when the glass host was changed from lithium aluminium silicate to sodium silicate and finally to sodium borosilicate. This increased resolution correlates with a reduction in the viscosities at comparable temperatures for these three glasses. As the presence of TiO_2 in L.A.S. glass, also makes the Gd^{3+} spectra more easily resolvable and since titania is known to reduce the viscosity, the correlation seems reasonable.

Measurements made of the resonance spectrum on a single sample at 77 K and 4.2 K did not differ appreciably from those made at room temperature. From this and the fact that below 1% Gd_2O_3 concentrations

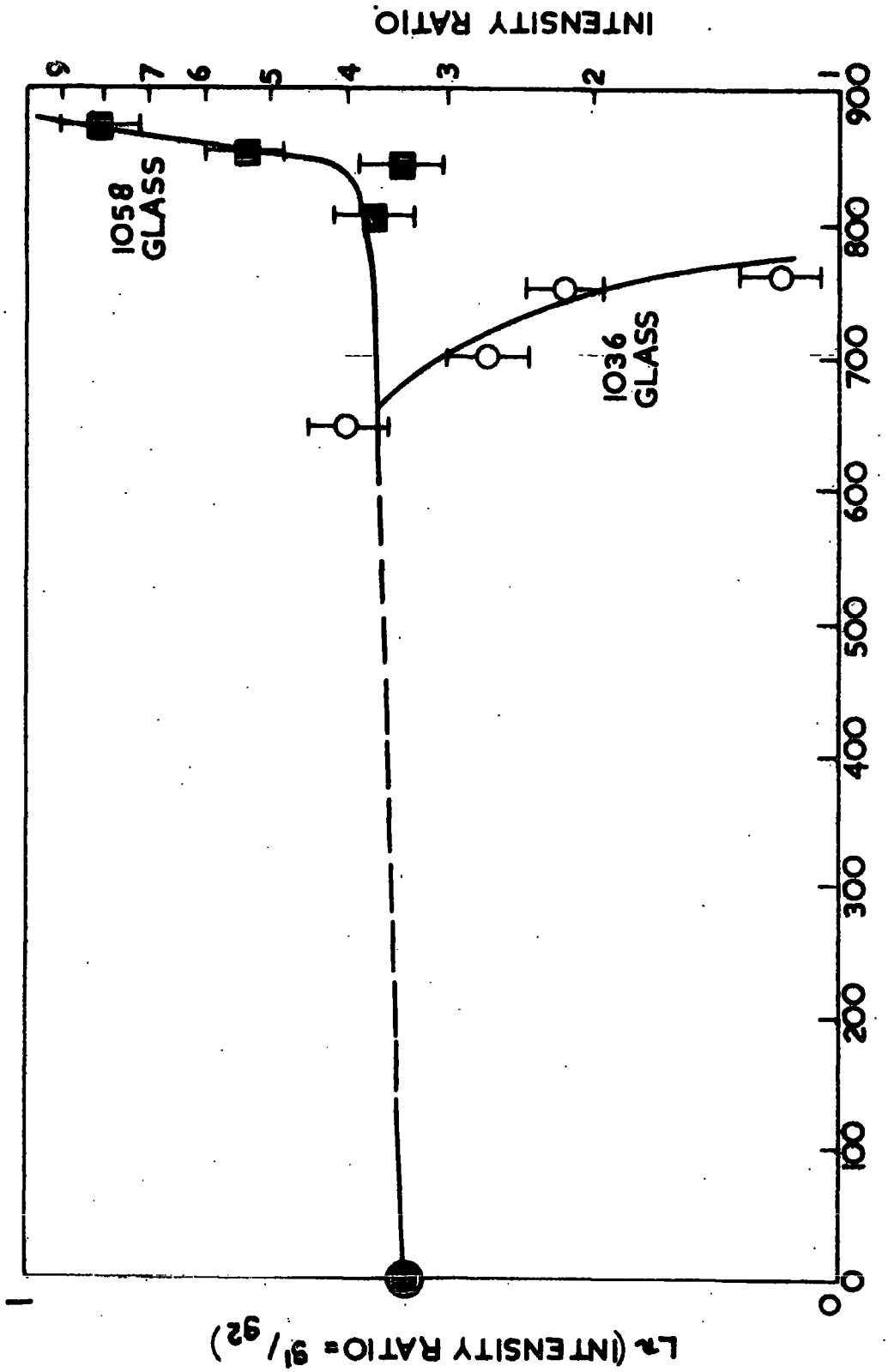

FIG 3.10 VARIATION OF g_1/g_2 RATIO WITH HEAT TREATMENT FOR LAS.1058.AND LA.S.1036.

no line narrowing of the spectra was observed, it can be concluded that the broad nature of resonance lines was due to the non-uniformity in the rare earth crystal field environment and the random orientation of the ion sites within the glass.

Measurements showed that the high g value structure produced by the Gd^{3+} at X-band was absent at Q band frequency. This is in agreement with the observations of Nicklin (3.14) who found that at frequencies away from X-band, resolution of the spectra gradually decreased. This is shown in Fig. (3.11).

3.4.6. Results of the Crystal Field Calculations

The solution of equation (3-23) produced a series of energy levels, for the external field set in various directions with respect to the x-z plane. It was necessary to have a measure of the crystal field parameters D and E which could then be varied to allow a simulation of the experimental results. For the X-band measurements as discussed previously the high g value resonances are indicative of crystal field mixing of the basis states. To observe the mixed states the microwave energy must be comparable with the crystal field energy. Consequently the value of the microwave energy could be used as a starting value for the crystal field parameters D and E. It was also considered likely that the crystal field would show some degree of axial symmetry, inherent in the initial assumption of isotropic g values. This allowed the variation of D and E to be semi-systematic. Even so, values of D and E were chosen across the entire range from the strong crystal field case, when zero field resonances predominated, to the low crystal field, pure Zeeman region.

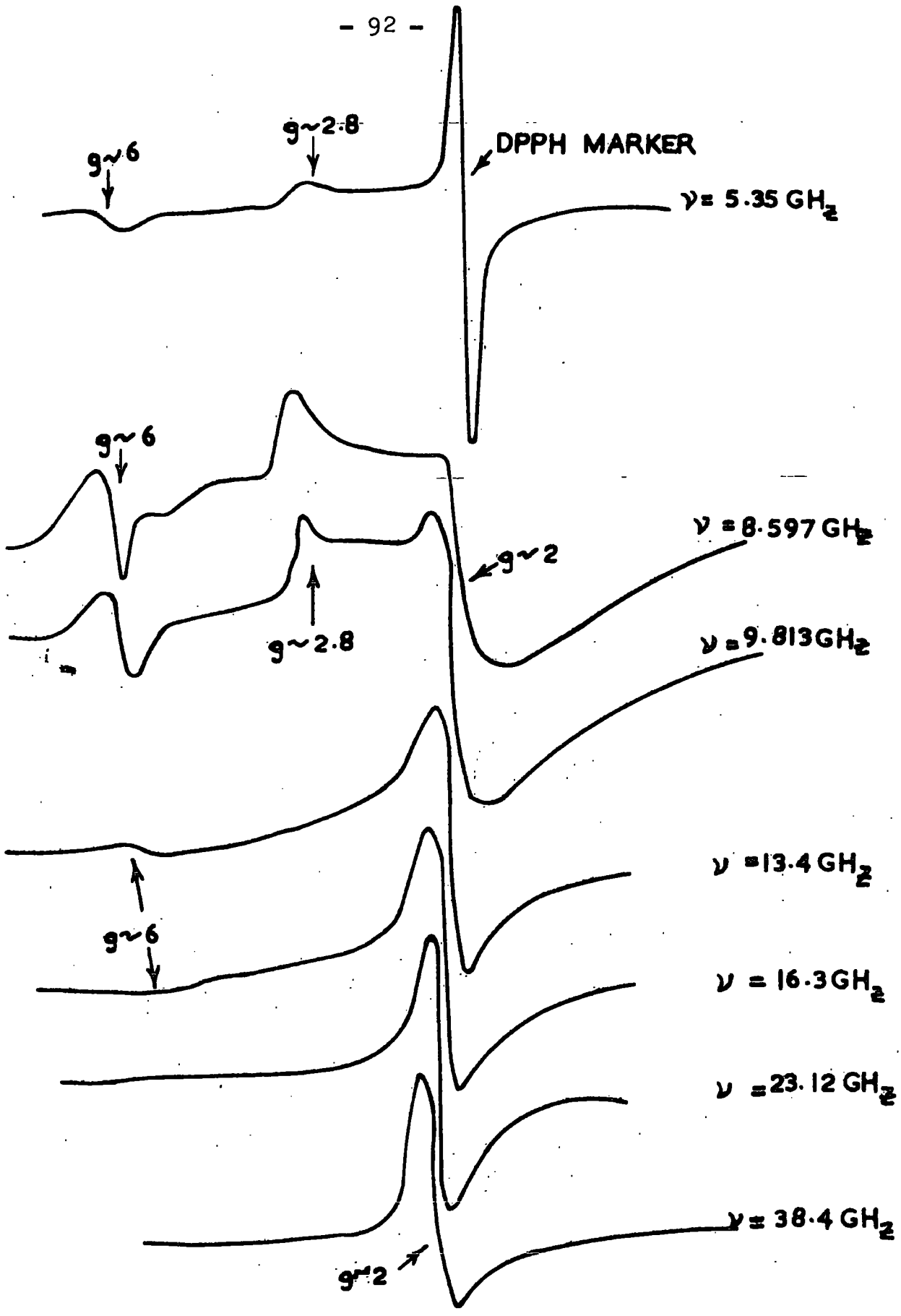

FIG 3.11

THE ESR DERIVATIVE ABSORPTION OF GADOLINIUM IN SODIUM SILICATE GLASS AS A FUNCTION OF FREQUENCY AFTER NICKLIN

Although eigenvalues, eigenvectors and transition probabilities were found en route to the final expected transition intensities only an indication of their values for a few typical cases are given in Table (3.4). It is more appropriate to consider the histograms obtained by summation of the spatial orientations for individual crystal field parameters. Some of the histograms formed in this manner are shown in Fig. (3.12). By a comparison of Fig. (3.12) with the numerically integrated differential absorption spectrum of Gd^{3+} in lithium aluminium silicate glass it is apparent that no single set of D and E values adequately accounts for the observed results. However, it can also be seen that the dominant broad peak at $g \approx 2$ requires a summation over relatively low crystal field values. This is to be expected as in the pure Zeeman limit the basis states must remain pure. Transitions then occur with the normal "free ion", $|\Delta M_s| = 1$ selection rule which produces g values with magnitudes close to 2. The broadening is then thought to be due, as discussed earlier, to random orientation and crystal field fluctuations of the Gd^{3+} environment in the glass matrix.

It was found that a relatively narrow, well defined region of high transition probability occurred in the region of $g \approx 6$ for a range of crystal field values. The remarkable stability of this absorption with respect to the crystal field could account for the relative narrow form of this line in the glasses. A dual site occupation must be suggested to account for the two different resonance lines (g_1,g_2) as no individual crystal field value was found to describe both position and intensity of these two distinct

TABLE 3.4

Example of Predicted Transitions at X-band for Gadolinium in a High Crystal Field

Crystal Field Parameters D = 0.07 cm^{-1} E = 0.025 cm^{-1}

Magnetic Field = 0.60 kG. in Z Direction

Predicted Eigen Values

-0.43	-0.41	-0.22	-0.11	-0.04	0.22	0.30	0.69

Eigen Vectors

0.0000	0.0520	-0.0849	0.0000	0.0000	-0.0188	0.9949	0.0000
-0.2177	0.0000	0.0000	-0.4058	0.8876	0.0000	0.0000	0.0005
0.0000	-0.6410	0.7611	0.0000	0.0000	0.0125	0.0987	0.0000
0.9288	0.0000	0.0000	0.1932	0.3162	0.0000	0.0000	0.0070
0.0000	0.7588	0.6344	0.0000	0.0000	0.1463	0.0172	0.0000
-0.2995	0.0000	0.0000	0.8910	0.3339	0.0000	0.0000	0.0706
0.0000	-0.1032	-0.1051	0.0000	0.0000	0.9890	0.0151	0.0000
0.0148	0.0000	0.0000	-0.0642	-0.0263	0.0000	0.0000	0.9975

Moments

0.82	0.62	1.32	-1.54	3.68	-4.88	6.92	-6.94

Predicted X-band Transitions

Eigen Values

-9.92295E-02 -4.19270E-01

Transition Probability = 9.2109

Eigen Values

2.21498E-01 -9.92295E-02

Transition Probability = 10.7572

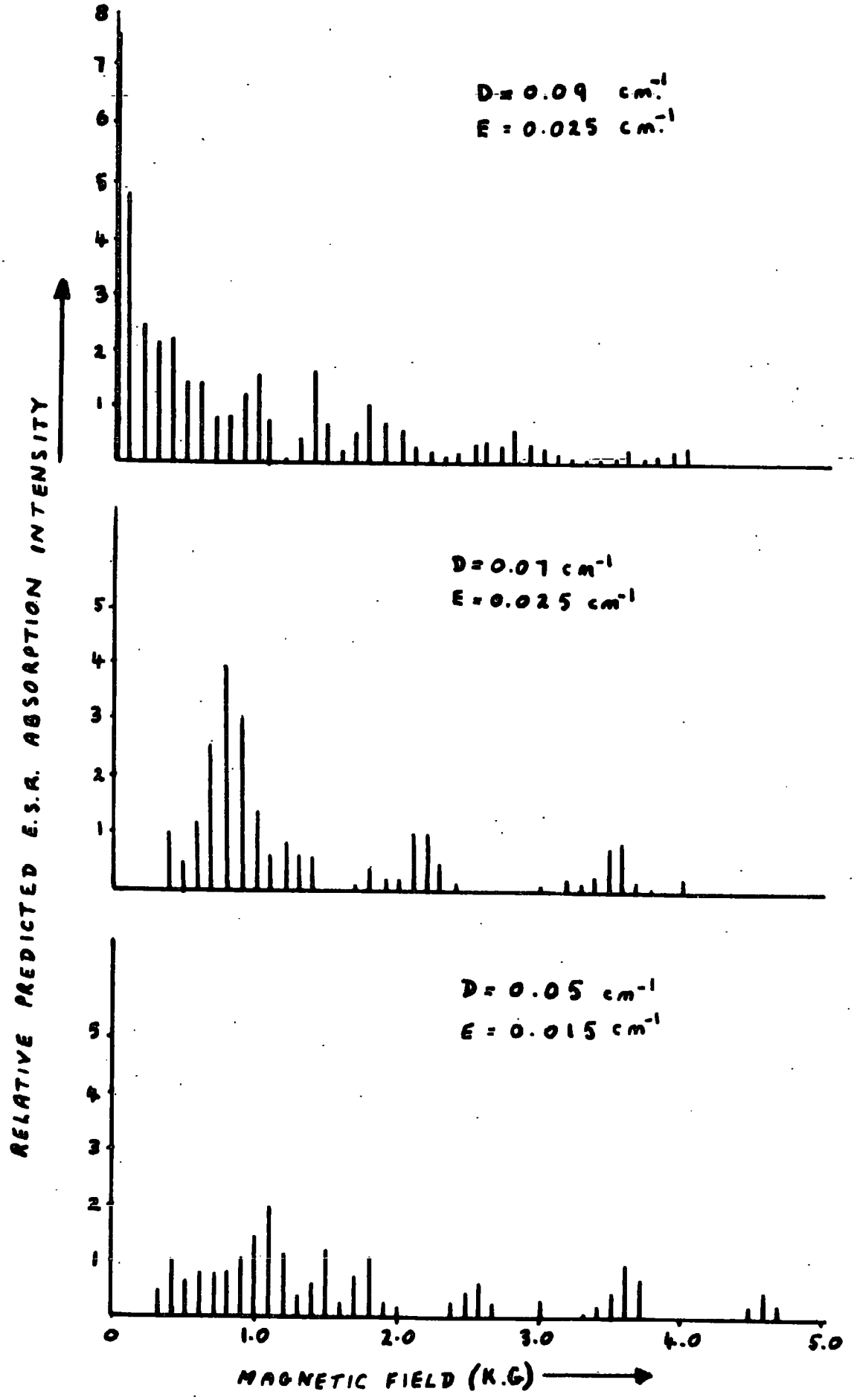

Fig 3.12 SIMPLIFIED HISTOGRAMS OF PREDICTED E.S.R. ABSORPTION INTENSITY FOR CRYSTAL FIELDS WITH NO X-Y ANISOTROPY

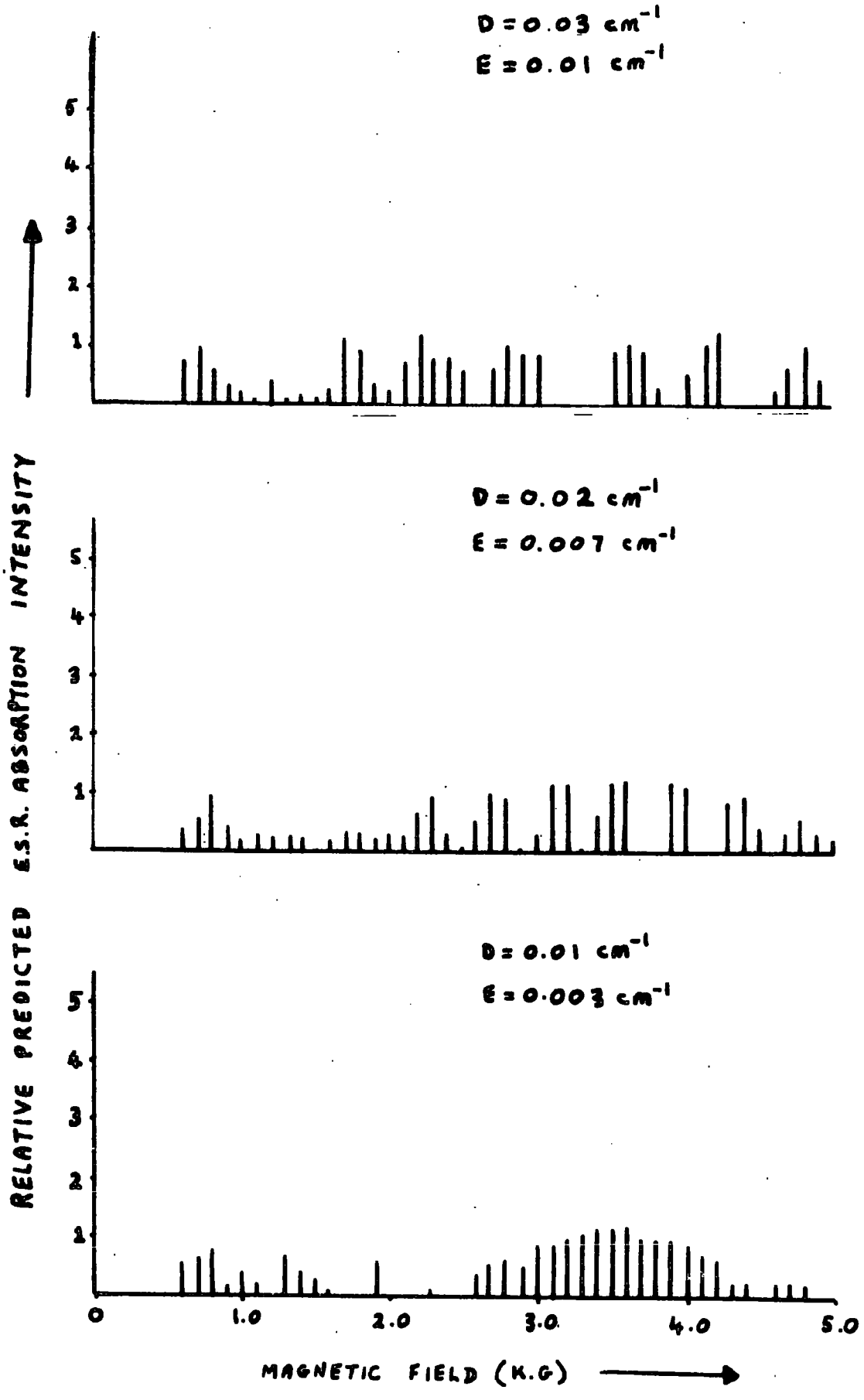

Fig 3.12 (CONTINUED)

Gd^{3+} resonance features. Certain discontinuities in the calculated histograms arise due to the mesh size used for the computation in both magnetic field value and orientation interval. These irregularities will be smoothed out by a reduction in these increments but no new features appear to be developed.

From the integrated spectrum Fig. (3.13) it can be seen that the resolution is greatly reduced compared to the experimental differential curve. This together with the broad nature of the curves and the necessity for a finer mesh for computation means that an exact fit with the experimental results will require extensive computation. However, the summation of transition intensities due to crystal field values around D = 0.06 cm^{-1} and E = 0.015 cm^{-1} whilst accounting for the resonance with $g \approx 5.9$ also produced absorption peaks at either side of the $g \approx 2$ region as shown in Fig. (3.13). It is suggested that this accounts for the poorly resolved structure in the $g \approx 2$ region for Gd^{3+} doped L.A.S. glass which may be similar to that observed for the equivalently doped sodium borosilicate glass. If this is so then the absorption with $g \approx 4.3$ is not yet explained. However, when the hamiltonian (3-37) representing the assymmetry in the x-y plane was solved the low crystal field values of D and E produced a marked absorption in the region of $g \approx 4.3$. It is therefore suggested that two sites exist for the gadolinium, one with a high crystal field and the other with a much lower crystal field.

To enable a good fit to be obtained with the experimental results a gaussian distribution in the crystal field parameters was

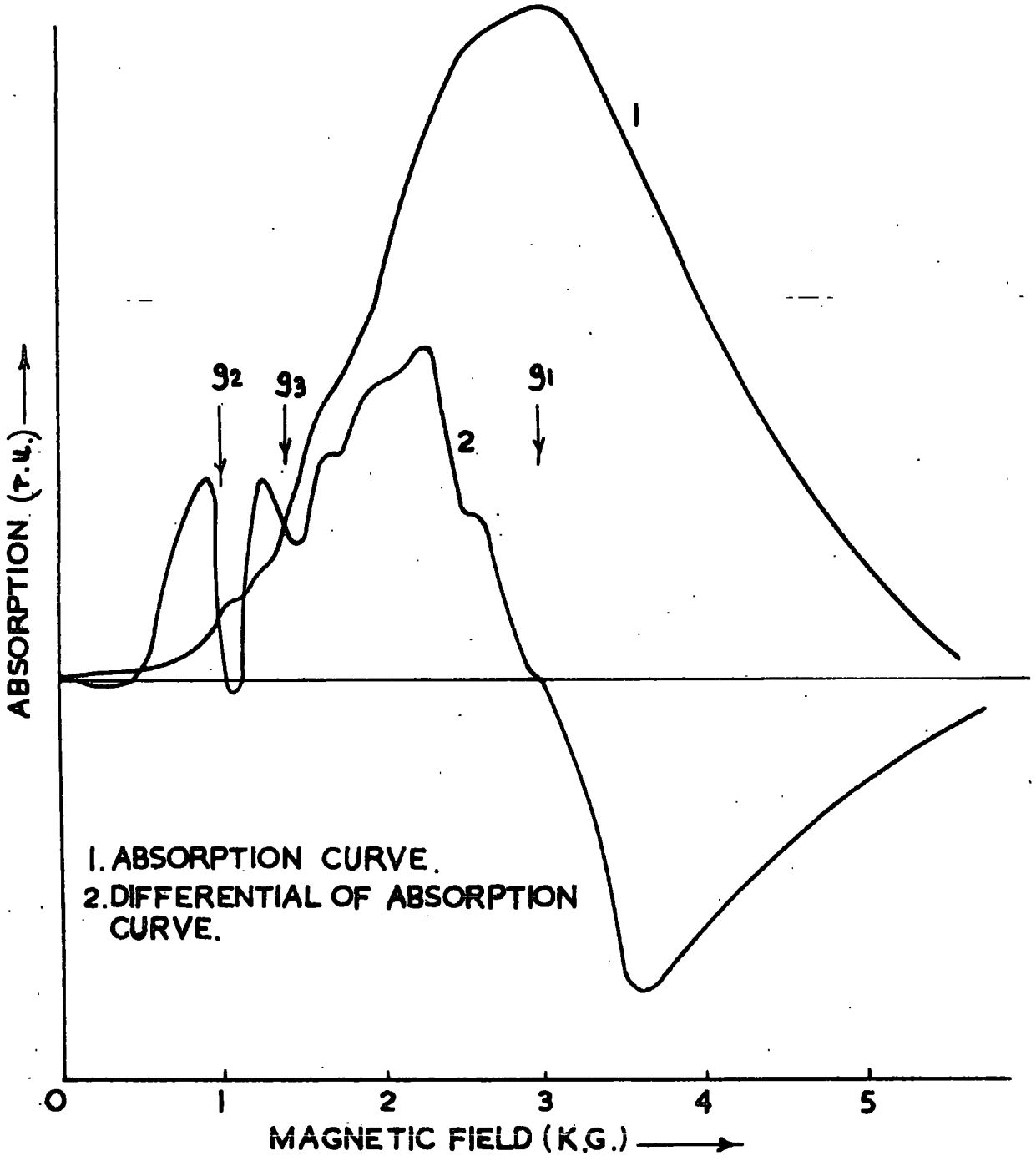

FIG 3-13 COMPARISON OF DERIVATIVE AND INTEGRAL E.S.R. ABSORPTION FOR L.A.S.1058 AT 300°K.

used. The resultant values for the low crystal field site were found to be D = 0.018 $\pm$ 0.004 , E = 0.005 $\pm$ 0.002 whilst the other site had D = 0.065 $\pm$ 0.005 E = 0.025 $\pm$ 0.005 cm^{-1}. Although an exact fit with the experimental results requires more extensive computation, the averaging procedures adopted have obviously predicted the main features of the experimental data.

From the overall integrated absorption intensity an estimate can be made of the relative occupation for the two proposed sites. This is found to be approximately 1:20 for the high and low crystal field sites respectively with 1.0 mole % gadolinium in a lithium aluminium silicate glass.

To verify the values of the crystal field parameters found measurements of e.s.r. absorption were made at Q-band frequencies ($\sim 4 \times 10^{10}$ Hz). A broad low intensity absorption was found in the region of g $\approx$ 2 with no high g value absorption lines. Microwave energies which corresponded to Q-band frequencies were used to calculate the expected intensity and position of the transitions for the level scheme corresponding to the high and low crystal field values found to explain best the results at x-band. In agreement with the experimental results only a broad low intensity absorption in the region of g $\approx$ 2 was predicted.

Various useful information has been obtained by employing the spin hamiltonian approach to account for the main resonances of the glasses containing Gd^{3+} but an alternative method of analysis is possible. This has been described by Koster and Statz (3.15) (3.16) and uses the fact that the matrix elements

contained in the expression for the oscillator strengths suggest that a great many transitions may occur between the eight levels, including some at very low field values. The hamiltonian used in this treatment is formed by using basis wave functions of the correct symmetry and Koster and Statz have shown that the matrix elements of H_z between two states Γ_i and Γ_j may be written

$$\langle \Gamma_i | H_z | \Gamma_j \rangle = \mu_\beta g_z^{ij} \left(H_x U_x^1 + H_y U_y^1 + H_z U_z^1 \right) + \mu_\beta g_z^{ij} \left(H_x U_x^2 + H_y U_y^2 + H_z U_z^2 \right) \qquad (3-36)$$

Where the g^{ij}'s are fitting parameters and the U's are matrices which have been derived once and for all for many symmetries by Koster and Statz. The zero field splittings are assumed to exist ab initio and the level separations are then also used as fitting parameters. Unlike the spin hamiltonian approach the g values are not related by simple constants and there is, in consequence, considerably more flexibility in fitting observed resonances using this method. Due to the difficulty of interpretation of the glass spectra this procedure was not followed and is only given as an outline of a possible alternative method.

3.4.7. Discussion

In the light of the randqm orientation of the distorted

environments about the Gd^{3+} ions making the spectra interpretation incomplete, it was found more useful to attempt to employ the characteristics of the resonance spectra themselves (i.e. line width, resonance field and line intensity) as a means of obtaining information indicating possible correlations between the structural and electronic properties of the glasses.

The most sensitive feature of the spectrum, Fig. (3.7) the low field resonances and, as has been shown, the relative intensities of these lines vary with heat treatment, the detailed variation depending upon the composition. However, the line widths and resonance fields are essentially constant. If the increase in the I_2/I_3 ratio with heat treatment temperature observed for the L.A.S. 1058 glasses is taken as the normal behaviour then the sudden drop in this quantity in the titanium-containing L.A.S. 1036 glasses must be taken as an indication of an interaction between the Gd^{3+} and Ti^{4+} ions.

If the Gd^{3+} is in only one site in the glass and the low field resonances arise from transitions between the strongly hybridized doublets of the $J = \frac{7}{2}$ manifold it is difficult to see why the presence of titanium ions during crystallisation should affect one of the resonance lines more than another. It is possible that at Gd^{3+} sites, which have a Ti^{4+} ion in the nearest neighbour shell, the change in the crystal field is sufficient to change the eigenfunctions of the levels involved in the low field transitions and hence the transition probability between them. Changes of this type would normally be accompanied

by changes in the energies of the levels concerned and consequently in the resonance field values. As this is not observed any changes must be such as to leave the average resonance position the same. The spin hamiltonian approach coupled with the preceding considerations again suggests that a two site model is to be preferred.

In this case, it is convenient to consider the $g \approx 5.9$ and $g \approx 4.3$ resonances as being produced by Gd^{3+} ions at two different sites. The structural evidence described earlier suggests that on crystallisation with titanium present, the gadolinium and titanium ions may become jointly involved in complexes in the crystallising glass. If this is so, then the zero field splitting of the ground state may be modified by the presence of the quadrivalent titanium ions as described previously. These changes will depend on the location of the Ti^{4+} ions with respect to the symmetry axis of the local electrostatic field at the Gd^{3+} site.

Under these conditions the observed changes in the resonance line intensities would seem to suggest that (i) titanium is incorporated into one site in preference to another or (ii) the crystal field is less sensitive to the presence of Ti^{4+} at one of the sites compared with the other, or finally (iii) that the Gd^{3+} ions are ejected from one of the sites as crystallisation develops. It is also interesting to consider the overall reduction found in gadolinium-containing glasses, irrespective of titanium presence when the glasses are subjected to the heat

treatments causing crystallisation. Eventually only a broad $g \approx 2$ absorption is found after crystallisation. The development of a well-defined crystalline structure as the glass crystallises will produce an increased influence on the Gd^{3+} ion. Ultimately the rare earth ion may be located within the crystalline phase or in the residual glassy phase. Either process could give rise to the observed spectra as in both cases the Gd^{3+} ion is expected to be subject to a greater crystal field by the developing crystals. It is clear from the discussion and from the results of previous workers (3.12) (3.13) (3.14) with various glass matrices that the observed spectra are predominately produced by the rare earth ions. So it cannot yet be decided whether the Gd^{3+} ion will be finally located in the crystalline or residual glassy environment. However, the electron spin resonance of commercial gadolinium oxide powder shows a broad $g \approx 2$ absorption. This is to be associated with the polycrystalline state of the sample but gives a measure of the width of the Gd^{3+} resonance under these conditions. The result of crystallisation of the glass is to reduce the Gd^{3+} resonance to a similar structure to that found with gadolinium oxide. This similar structure due to a high symmetry, low crystal field environment for the Gd^{3+} ion indicates that a crystalline environment may result for the gadolinium ion in a glass ceramic. It is difficult to describe the two sites suggested for the gadolinium in detail, as the parameters D and E used in the calculations cover a broad range of possible crystal field environments. It may be that the low crystal field site is

produced when gadolinium directly substitutes for a silicon ion whilst the other site is more likely to be due to the gadolinium located in an interstitial position.

The observed change in the Gd^{3+} spectra as the glass matrix changes, shown in Fig. (3.8) can thus be explained by either a crystal field distortion or a site occupancy change. The latter is preferred as no change in the effective g values was found when the host lattice changed. From the observation of gadolinium in a borosilicate glass it would appear that the direct substitution of gadolinium into a symmetric site is less likely than in the lithium aluminium silicates. Alternatively the reduced viscosity at an equivalent temperature of borosilicates, may favour the production of interstitial positions for gadolinium ions.

A comparison of the computed absorption for gadolinium in a high crystal field environment, with the observed absorption from this crystal field component for gadolinium in a borosilicate glass is given in Fig. (3.14).

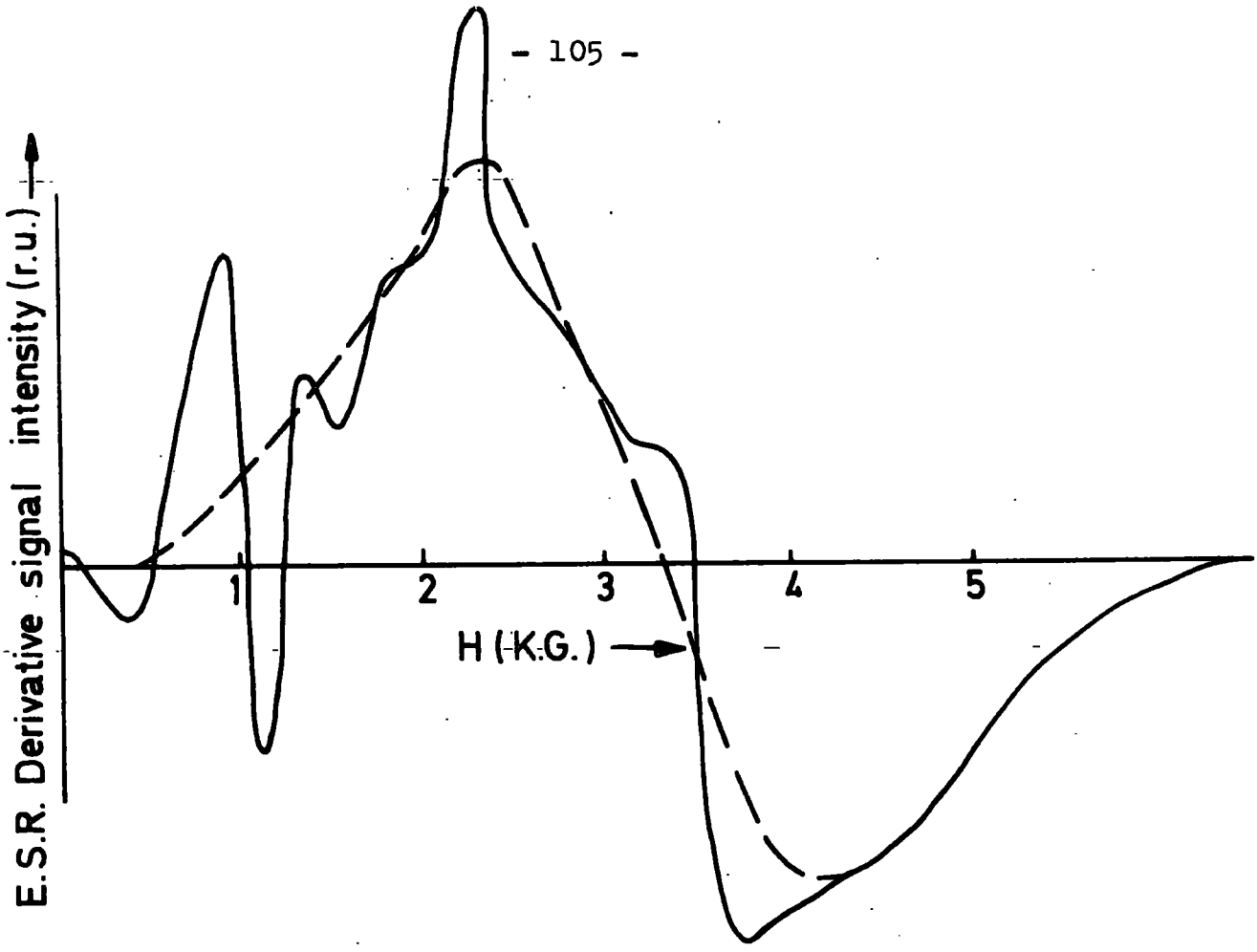

FIG.3.14(a) Derivative of E.S.R. signal for 1% Gd_2O_3 in a Borosilicate glass with a broad g = 2 component indicated by the broken curve.

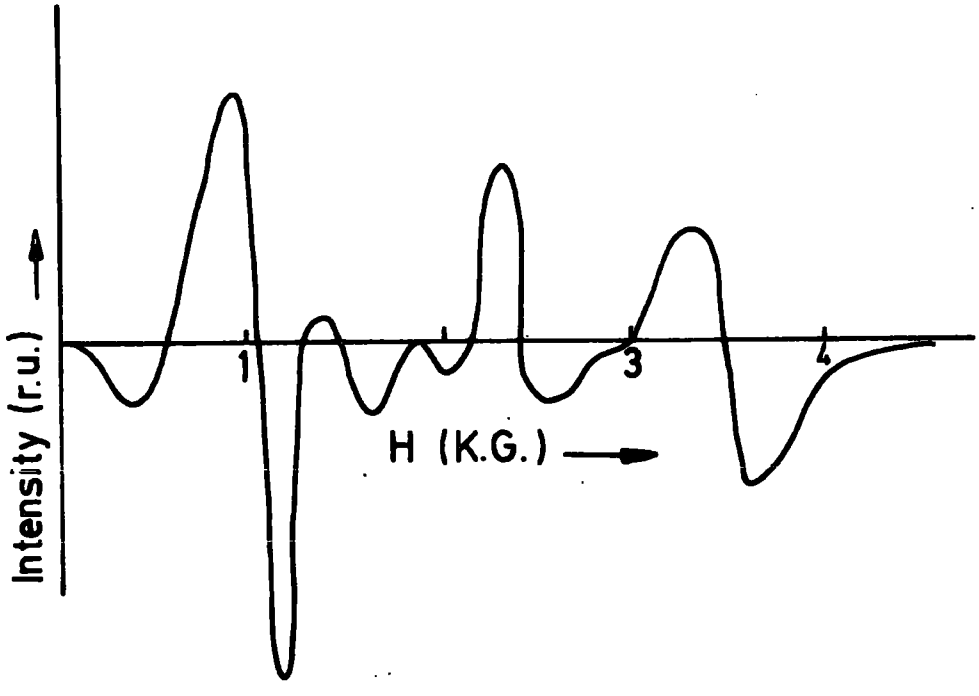

(b) Difference of the curves in fig (a)

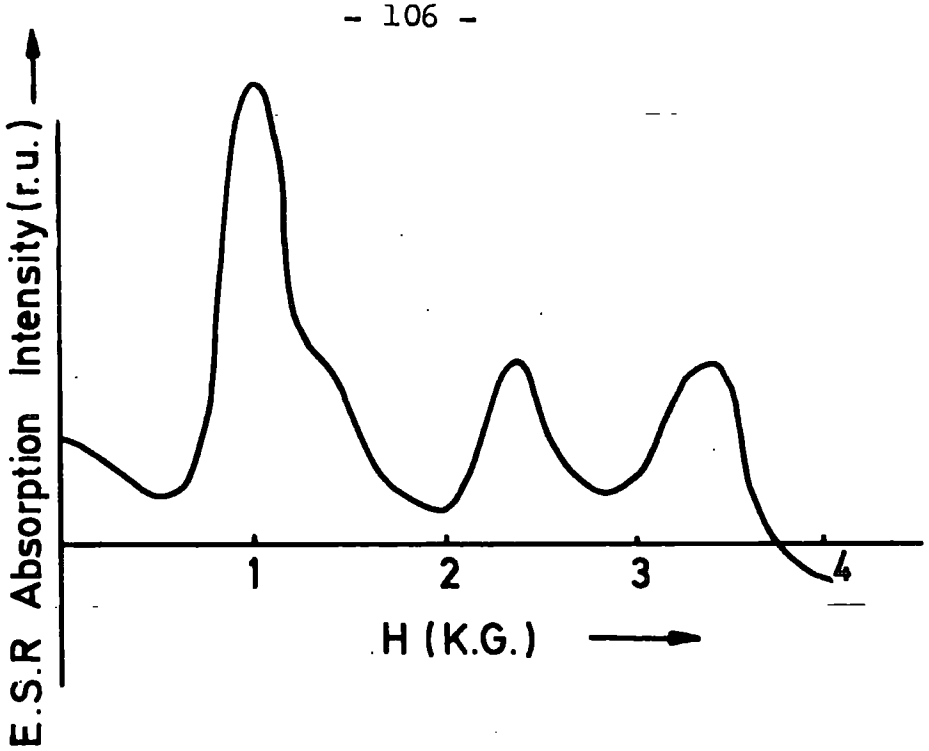

FIG. 3.14(c) Numerical integrated form of curve shown in fig(b).

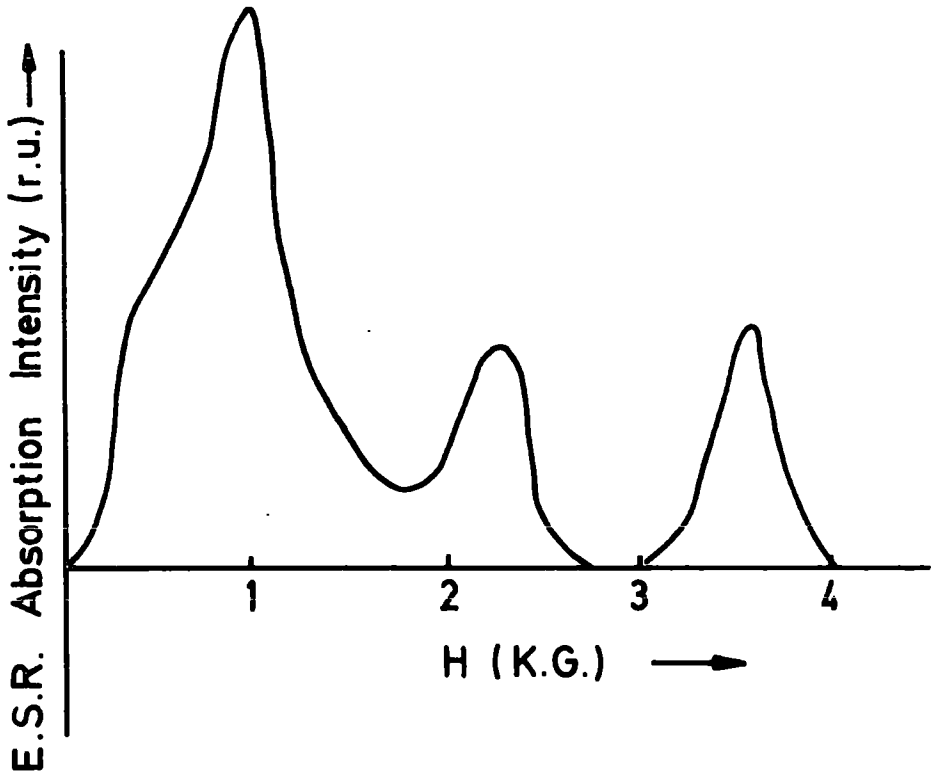

(d) Computed absorption for Gadolinium in crystal field with D=0.06 and E=0.015

CHAPTER 4.

RESULTS AND DISCUSSION (Part 2)

4.1 Introduction

It is evident that the results outlined in Chapter 3 do not provide a complete understanding of the role played by the gadolinium and titanium in the crystallisation of the L.A.S. glass composition chosen. To clarify the position an alternative approach to the e.s.r. monitoring of rare earth ions was considered. This second method can be summarised as the observation of induced defects produced in the glass matrix by X-ray radiation. Additional information could be obtained by this method as electron spin resonance signals were known to be associated with the defects and the titanium ions, if the latter could be converted to the paramagnetic Ti^{3+} state. Defect production was also thought likely to reflect the glass matrix stability and hence elucidate the mechanism of nucleation and initial crystal growth. Since both gadolinium and titanium were seen earlier to play relevant roles in the crystallisation process, information obtained from the defects should lead to some clarification of the problem. X-ray irradiation was chosen as this energy is sufficient to produce internal ionization in the glass specimens, but not to produce ionic displacements which would complicate the investigation.

In addition to the observation of the defects by e.s.r use was made of thermoluminescence and optical phenomena. Luminescence

characteristics of glasses containing various rare earth ions were measured as a preliminary to carrying out the thermoluminescence measurements. X-ray luminescence spectra of Pr^{3+}, Sm^{3+}, Tb^{3+} and Dy^{3+} doped Soda glass are shown in Fig. (4.1), and the positions of the emission bands are listed in Table (4.1) along with the overall colour of the luminescence after Shulgin et al. (4.1). U.V. excitation has been reported (4.2) (4.3) to produce spectra of the same form. This is to be expected as all the observed peaks are related to electronic transitions between Stark components of the energy levels of the tripositive rare earth ions. As can be seen from table (4.1) the gadolinium ions gave a single emission band at 313-315 nm. The luminescence intensity of this band was found to be an order of magnitude greater for the same Gd_2O_3 concentration when the base glass was changed from sodium silicate to lithium aluminium silicate. A lower absorption coefficient in this wavelength range for the L.A.S. glass accounts for this increased intensity. Measurements of the total luminescence emission with increasing temperature showed that the observed intensity is appreciable to above 650 K. For example fig. (4.2a) shows the temperature dependence of the Dy^{3+} (490 nm peak) Tb^{3+} (553 nm peak) and Gd^{3+} (314 nm peak) luminescence in soda glass. The data for Gd^{3+} and Dy^{3+} is replotted in fig. (4.2b) as a function of reciprocal temperature and it is evident that the thermal quenching of the luminescence is given by the relation (4.4) below.

$$I(T) = I_o(I + C\exp(-W/kT))^{-1} \qquad (4\text{-}1)$$

where W is the activation energy of the quenching process. For

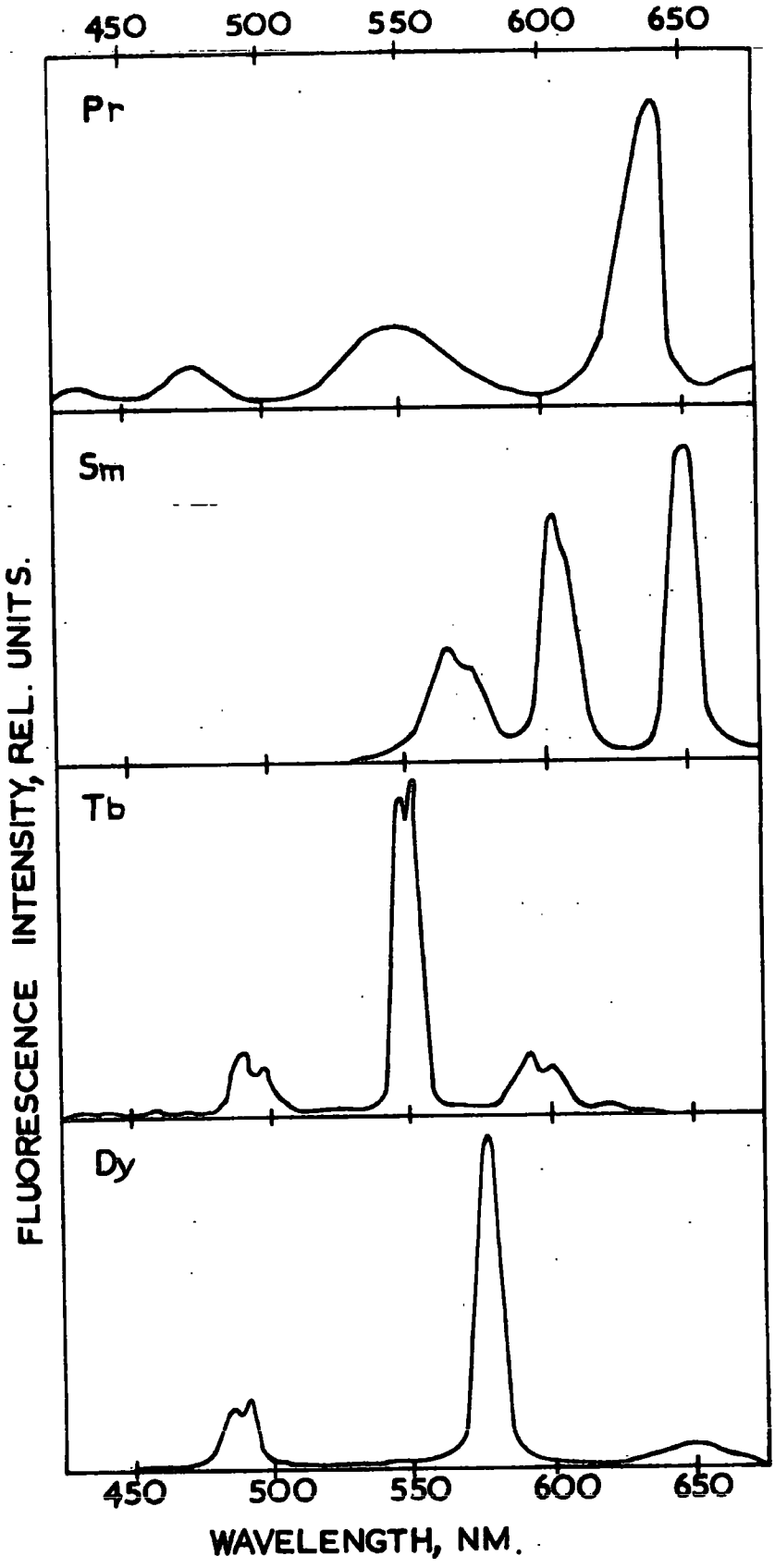

FIG 4.1 X-RAY LUMINESCENCE SPECTRA OF RARE EARTH DOPED SODIUM SILICATE GLASS.

TABLE 4.1

Activator	Colour	Luminescence Peaks (nm)
Pr^{3+}	White	420-430 530-550 620-645
Sm^{3+}	Orange	560 573 604 650
Tb^{3+}	Blue/Green	382 416 450 490 550 590
Dy^{3+}	White	485 490 587
Gd^{3+}		313-315

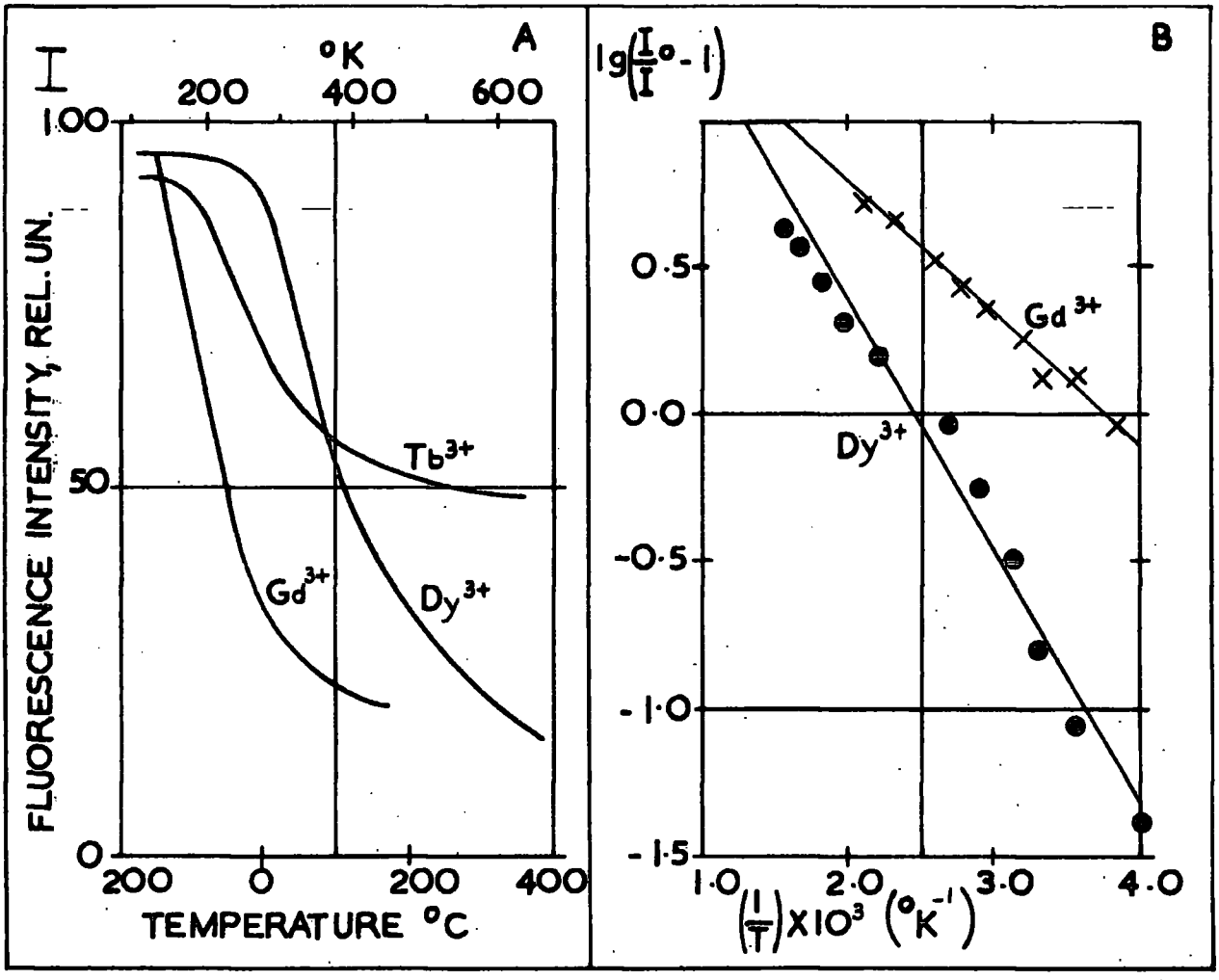

FIG 4.2 TEMPERATURE DEPENDENCE OF LUMINESCENCE IN SODIUM SILICATE GLASS.

the case of Dy^{3+} in sodium silicate glass the data gives $W = 0.20 \pm 0.03$ eV, and for Gd^{3+} in L.A.S. glasses $W = 0.1 \pm 0.03$ eV. The persistence of luminescence emission to the high temperatures observed justifies the choice of a rare earth probe as an indicator during the thermoluminescence measurements.

The results for Tb^{3+} do not follow this classical behaviour and no attempt has been made to interpret them. It is noted, however, that Bieringer and Montgomery (4.5), in a study of radiation induced absorbance in rare earth doped silica also observed abnormalities specific to the terbium doped sample. This was attributed to the production of dopant-associated traps and may be the origin of the failure of equation (4-1) to fit the experimental thermal quenching results of terbium in sodium silicate and L.A.S. glasses.

4.2 Thermoluminescence

4.2.1 Theory

Thermoluminescence involves the thermal activation of electrons and/or holes from traps and their radiative recombination. Although energy gaps are normally associated with the periodic nature of the crystalline state it can be seen from the optical absorption of glasses that an equivalent gap exists in the glassy state. Recent work (4.6) has attempted to derive a theoretical model for band-gaps in amorphous materials but this requires material inhomogeneities to exist within the sample. The band edges are not well defined in the amorphous state with the density of states tailing into the gap, since this band gap is

forbidden only when there is perfect order. Electron transitions are considered to occur within this forbidden band. Electrons can be raised from the valence band to the conduction band by application of sufficiently high energy radiation. Excited electrons, so produced, may either recombine directly with the created holes or remain in traps located near the conduction band. A schematic diagram of the hole and electron traps is shown in Fig. (4.3a). As the temperature of the irradiated sample is increased and sufficient thermal energy is supplied the trapped electrons can be released. By their recombination with holes these freed electrons can produce an optical frequency emission whose intensity is a measure of the trap population whilst the temperature of emission gives an indication of the depth of the trap. Electron traps can be located at point defects, substitutional defects, impurity defects etc., and in general the recombination site may be different from the production site due to migration of the defect or energy transfer processes.

In order to establish an applicable theory for this process the number and occupancy of the electron and hole traps must be known together with the degree of charge transfer between these levels. Several approximations can be made to facilitate the procedure. The U.R.W. formalism due to Urbach (4.7), Randall and Wilkins (4.8) is commonly adopted, in which electron escape from trapping centres and subsequent emission of radiation is assumed to be a thermally activated process of first order. The probability per unit time of this process is

$$P = b\exp(-E/kT) \qquad (4\text{-}2)$$

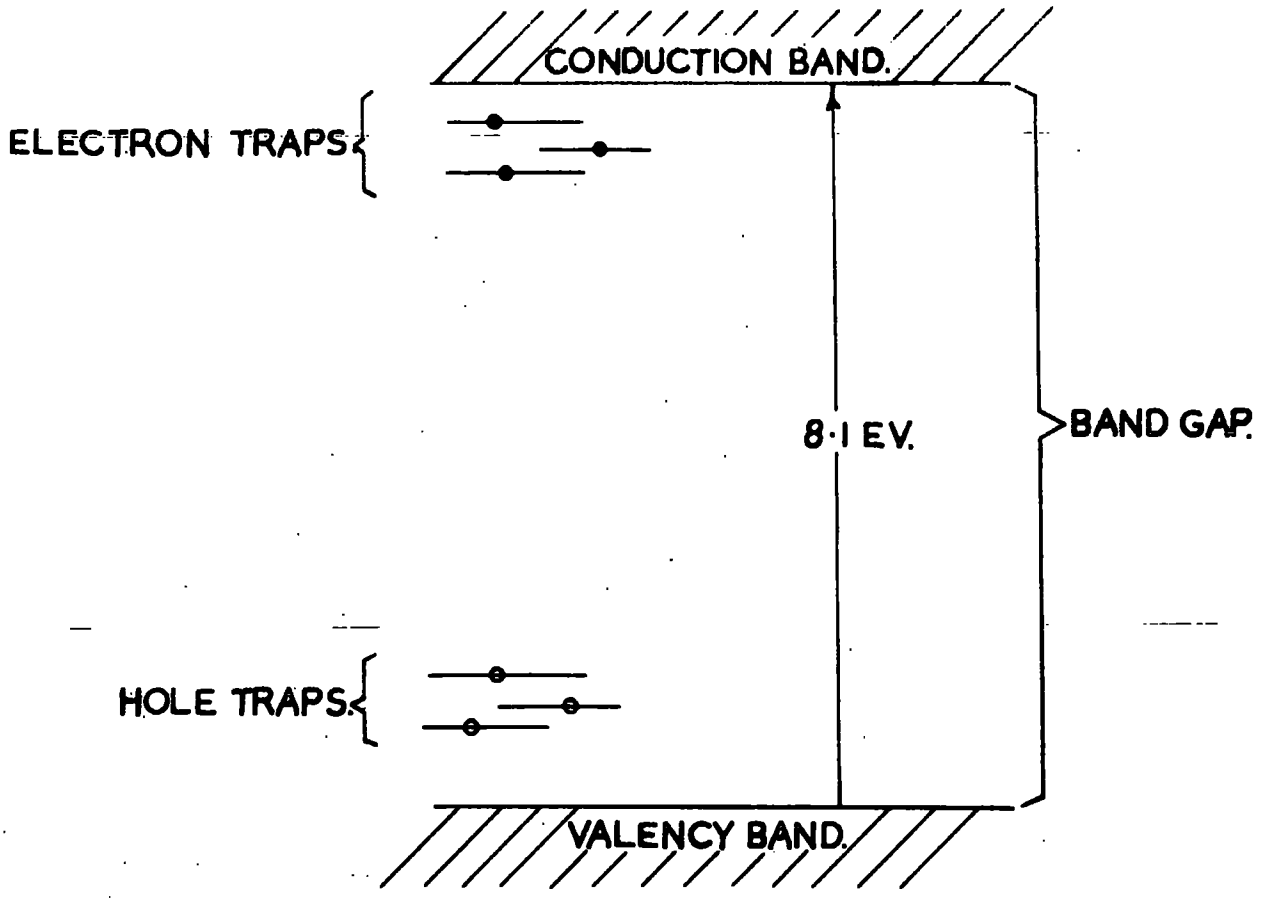

b

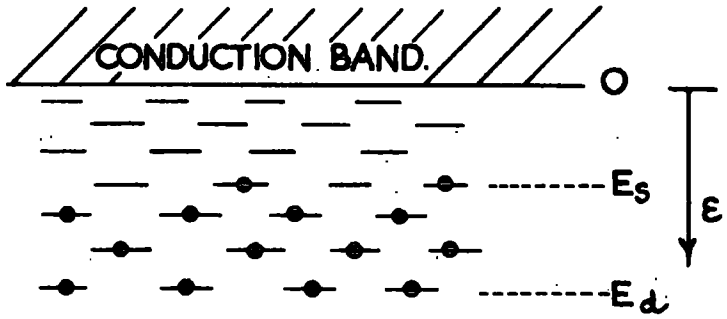

FIG 4.3 SCHEMATIC DIAGRAM OF HOLE AND ELECTRON TRAPS IN GLASS.

where E is an activation energy and b is the so-called "frequency factor" (4.7). If n(t) represents the number of filled traps at time t, then

$$-dn/dt = b\exp(-E/kT)\, n \qquad (4\text{-}3)$$

For an initial number n_o of traps at a constant temperature T_o

$$n(t,T_o) = n_o\exp(-P_o t) \qquad (4\text{-}4)$$

where $P_o = b\exp(-E/kT_o)$ (4-5)

and $$-dn/dt = P_o n_o \exp(-P_o t) \qquad (4\text{-}6)$$

represents the intensity of the light emitted after a time t. An exponential decay is predicted.

The integration of equation (4-3) for a linear increase in temperature, gives the shape of the glow curve. The solution is given by G. Bonfiglioli (4.9) in terms of the parameters E and β as

$$\beta E/kT^{*2} = \exp(-E/kT^{*}) \qquad (4\text{-}7)$$

where the temperature T* corresponds to the maximum of the glow peak and β represents the speed of warming. An exponential increase in the emission is caused by the thermal depopulation of the defects and ceases when the number of electrons in the traps becomes small, the light output falling to zero when the traps are empty. The above calculation assumes only one electron trap and one hole trap, but there is no a priori reason why the number of holes and traps should be equal or limited to one, particularly in the glassy state.

Yokota (4.10) used thermoluminescence in the investigation of fused quartz and later Kikuchi (4.11) noted that the broad low temperature glow peak in fused quartz and other glasses was not found in crystalline quartz. This broad peak followed the temperature of irradiation to the lowest temperatures available and led him to suggest that this band of the glow curve is due to many shallow electron traps whose levels are distributed over a wide range.

The rate of decay of luminescence after the incident radiation is removed has been found not to resemble that of a bimolecular process. Several attempts have been made to obtain a theoretical fit to the experimental decay curves. Kikuchi (4.11) proceeded as follows:

Let ε represent the depth of a trapping level from the bottom of the conduction band and the density of electron occupied trapping levels from ε to $\varepsilon + d\varepsilon$ immediately after the removal of the X-ray irradiation be $z(\varepsilon)d\varepsilon$. Then the intensity of the luminescence I(t), t secs. after the irradiation ceases is given by (4-10).

$$I(t) = \int_0^\infty Cb \exp(-bt \exp(-\varepsilon/kT)\, z(\varepsilon)d\varepsilon \qquad (4\text{-}8)$$

where b is a frequency factor, k is Boltzmann's constant, T is the absolute temperature and C is a constant.

If we assume that the trapped electron distribution to be uniform from levels E_d to E_s as shown in Fig. (4.3b)

$$\left.\begin{array}{lll} \text{i.e.} & 0 < \varepsilon < E_s, & z(\varepsilon) = 0 \\ & E_s \leq \varepsilon \leq E_d, & z(\varepsilon) = A \\ & E_d < \varepsilon & z(\varepsilon) = 0 \end{array}\right\} \qquad (4\text{-}9)$$

where E_s and E_d are the most shallow and the deepest trapping levels occupied by the electrons respectively at t = 0, then substitution of (4-9) in (4-8) gives

$$I(t) = \int_{E_s}^{E_d} A.Cb \exp(-\varepsilon/kT)\exp(-bt \exp(-\varepsilon/kT))d\varepsilon \qquad (4\text{-}10)$$

$$= I_o \frac{\exp(-bx_d t)\,(1 - \exp(-b(x_s - x_d)t))}{b(x_s - x_d)t} \qquad (4\text{-}11)$$

where $x_s = \exp(-E_s/kT)$; $x_d = \exp(-E_d/kT)$;

and I_o is the luminescence intensity at t = 0

Since $x_s \gg x_d$, (4-11) becomes

$$I(t) = I_o \frac{1 - \exp(-bx_s t)}{bx_s t} \qquad (4\text{-}12)$$

An estimation of the trap depth can be made by finding a best fit for E_s and T, if b is fixed. However, the agreement of equation (4-12) with the experimental decay curves at various temperatures is not very good. The discrepancy is no doubt caused by the assumption of only one type of site in the glass and it may be necessary to assume a non-uniform electron distribution over many traps. This would probably be the case in our systems as the perturbation of local short range structure in glass makes the existence of a series

of discrete traps with a relatively narrow range of energies possible. If this is to be the starting point for the analysis, the algebraic computations become rapidly more complex as the number of different sites increases and has prohibited the formation of a more relevant theoretical fit.

Even the estimate of the trap depth, from a glow curve in crystals, is far from straight-forward. This can be seen in a recent review of methods for determining trap depths from glow curves by Shalgaonkar and Narlikar (4.12). In this review more than a dozen alternative methods were considered. Due to the difficulty in applying several methods to one specimen no estimate of the range of possible trap depths for a single peak was given. This degree of flexibility of interpretation, coupled with the broad nature of the glow peaks justifies the use of an approximate equation in the case of glasses.

Equation (4-3) representing the rate of change of filled traps in the U.R.W. formalism is

$$-dn/dt = b \exp(-E/kT)\, n \qquad (4\text{-}3)$$

Now for a heating rate β the solution of (4-3) becomes

$$(\ln n)_{n_o}^{n} = -\frac{b}{\beta}\int_{T_o}^{T} \exp(-E/kT)dT \qquad (4\text{-}13)$$

$$n = n_o \exp\left(\left(-\frac{b}{\beta}\right)\int_{T_o}^{T} \exp(-E/kT)dT\right) \qquad (4\text{-}14)$$

The intensity, I, of the thermoluminescence peak is given by

$$I = -C\, dn/dt$$

$$= Cbn \exp(-E/kT) \qquad (4\text{-}15)$$

where C is a proportionality constant.

Substituting from (4-14) leads to

$$I = Cbn_o \exp(-E/kT) \exp((-\tfrac{b}{\beta})\int_{T_o}^{T} \exp(-E/kT))dt \qquad (4\text{-}16)$$

The position of maximum intensity can now readily be obtained by differentiating equation (4-16) with respect to T and equating to zero. This gives

$$Cn_o b \exp(-E/kT)(-\tfrac{b}{\beta} \exp(-E/kT) \exp((-\tfrac{b}{\beta})\int_{T_o}^{T} \exp(-E/kT)dT))$$

$$+ \exp((-\tfrac{b}{\beta})\int_{T_o}^{T} \exp(-E/kT)dT)Cn_o bE/kT^2 \exp(-E/kT) = 0 \qquad (4\text{-}17)$$

After cancellation this equation is simplified to

$$E/kT_m^2 = \tfrac{b}{\beta} \exp(-E/kT_m) \qquad (4\text{-}18)$$

Upon rewriting this becomes

$$E = kT_m \ln\left\{\frac{bkT_m^2}{\beta E}\right\} \qquad (4\text{-}19)$$

This equation can be solved numerically to find the trap depth E from a knowledge of the peak temperature and an estimate of b, the escape frequency factor. However, for the case of glasses it is reasonable to apply an approximation to allow direct solution of (4-19). To first order $E = kT_m$ which upon substitution in the logarithmic term of (4-19) yields

$$E = kT_m \ln\left\{\frac{bT_m}{\beta}\right\} \qquad (4\text{-}20)$$

4.2.2. Results

Thermoluminescence measurements were made on the various

glasses after X-ray irradiation in an attempt to understand the nature of the defects formed. False peaks appeared occasionally just above the temperature of irradiation which were assumed to be due to thermal annealing of lower peaks whilst the sample was irradiated. This could be overcome for all the peaks, by observation after irradiation at a lower temperature, except for peaks near 77 K, which was the lowest temperature obtainable.

Glow curves obtained for N.S. and L.A.S. glasses were found to be essentially the same for any rare earth activator and moreover similar to one another. Further similarities can be found between the L.A.S. and N.S. glow curves on the one hand and those of quartz and fused silica (4,13) on the other (see table(4.2)). Especially good agreement is found for the position of the main peak at 165 K. However, a more detailed observation of the L.A.S. glass did reveal some differences in the glow curves.

The base L.A.S. glass gave three distinct thermoluminescence peaks when warmed after irradiation at temperatures from 77 K to 300 K. These peaks occurred at 150 K, 260 K and 433 K. Addition of 1% Gd_2O_3 to the base glass produced peaks at 170 K, 310 K and 455 K.

The depth of the traps ε , estimated by the approximate equation (4-20)

$$E = kT_m \frac{\ln bT_m}{\beta}$$

are given in Table (4.2)

TABLE 4.2

SAMPLE	Position of Thermoluminescence Peaks (^{o}K)							
1022	160	-	270	-	430	-	-	-
1058	-	170	-	320	-	450	-	-
N.S. + 8.16 wt % Tb	175	205	-	-	405	475	530	-
O.C.	165	-	260	350	-	-	-	-
C.H.	165	-	260	350	-	-	500	600
S.C.	190	210	260	350	-	-	500	600
	Equivalent Trap Depths For Above Peaks (e.v.)							
1022	0.36	-	0.60	-	0.96	-	-	-
1058	-	0.42	-	0.71	-	1.00	-	-
N.S. + 8.16 wt %Tb	0.39	0.46	-	-	0.90	1.01	1.12	-
O.C.	0.37	-	0.58	0.78	-	-	-	-
C.H.	0.37	-	0.58	0.78	-	-	1.11	1.33
S.C.	0.42	0.47	0.58	0.78	-	-	1.11	1.33

For low temperature irradiation of the L.A.S. glasses, the most intense peak is at 160 - 170 K while the intensity of peaks above 300 K is very small. In contrast the specimens irradiated at room temperature show an intense thermoluminescence at high temperatures. It would appear from these results that the shallow traps involved in the thermoluminescence have a bigger cross section than the deeper traps and in consequence are filled first during irradiation. Further it is evident that there is little energy transfer between one type of trap and another. Addition of titanium dioxide to the glass quenched the thermoluminescence considerably and only if less than 0.5% TiO_2 was added could a measurable signal be obtained. However, for 0.1% TiO_2, peaks occurred at 150 K and 260 K as in the base glass, but above room temperature there was evidence of peaks at 415 K and 475 K compared to the 433 K base glass peak.

When both 0.1% TiO_2 and 1% Gd_2O_3 are present the signal is still further quenched with peaks at 150 K and 260 K, although the double structure in the high temperature peak of L.A.S. 1023 becomes single and was found to be at 460 K again. These results are summarised in Fig. (4.4).

In order to investigate the dependence, if any, of the glow curves on the L.A.S. glass constituents, various base glasses were made. Table (4.1) gives a list of all the glasses prepared. Initially thermoluminescence was only observed after irradiation at room temperature. It was found convenient to keep one of the constituents constant whilst considering the results obtained

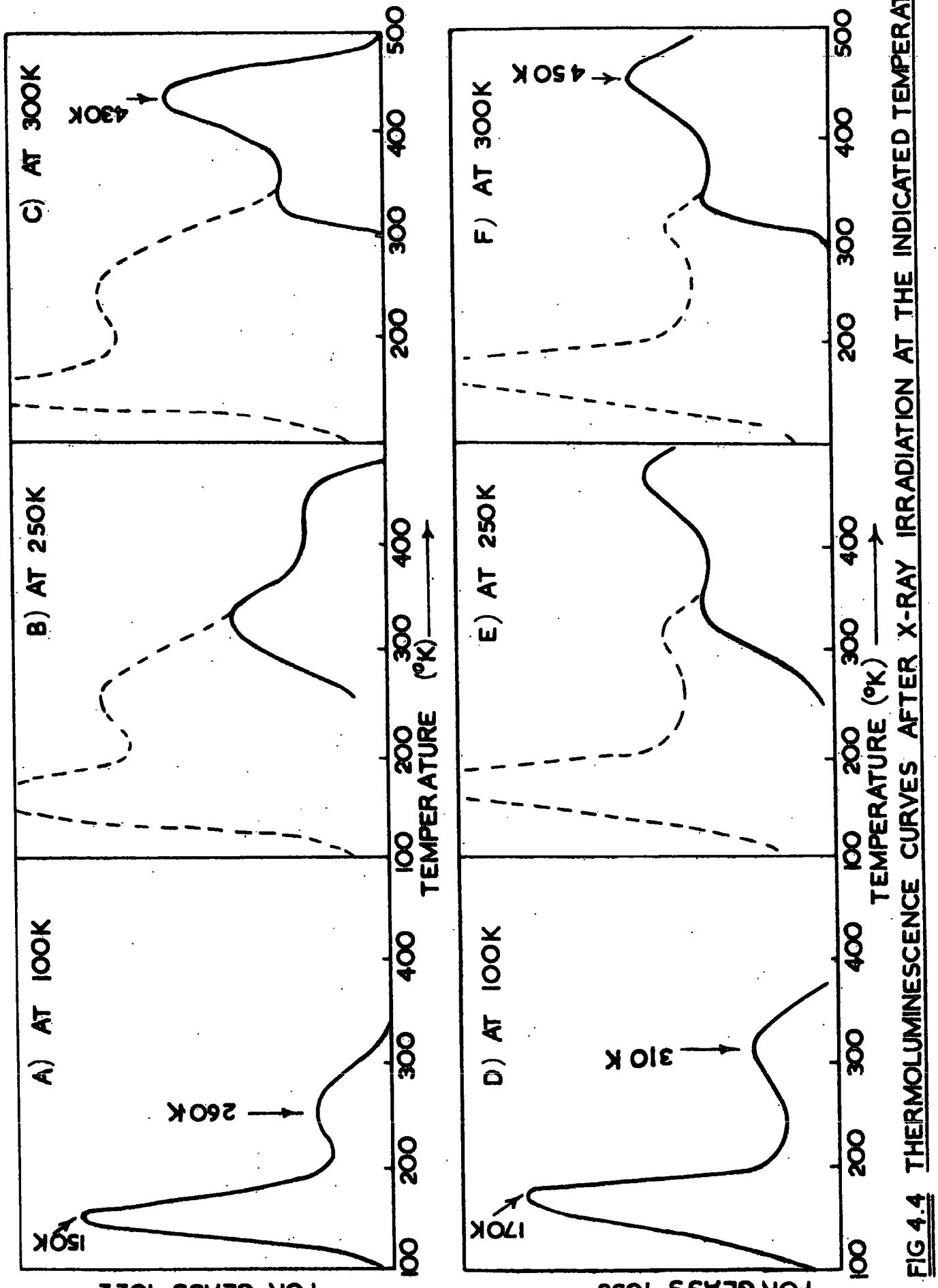

FIG 4.4 THERMOLUMINESCENCE CURVES AFTER X-RAY IRRADIATION AT THE INDICATED TEMPERATURES.

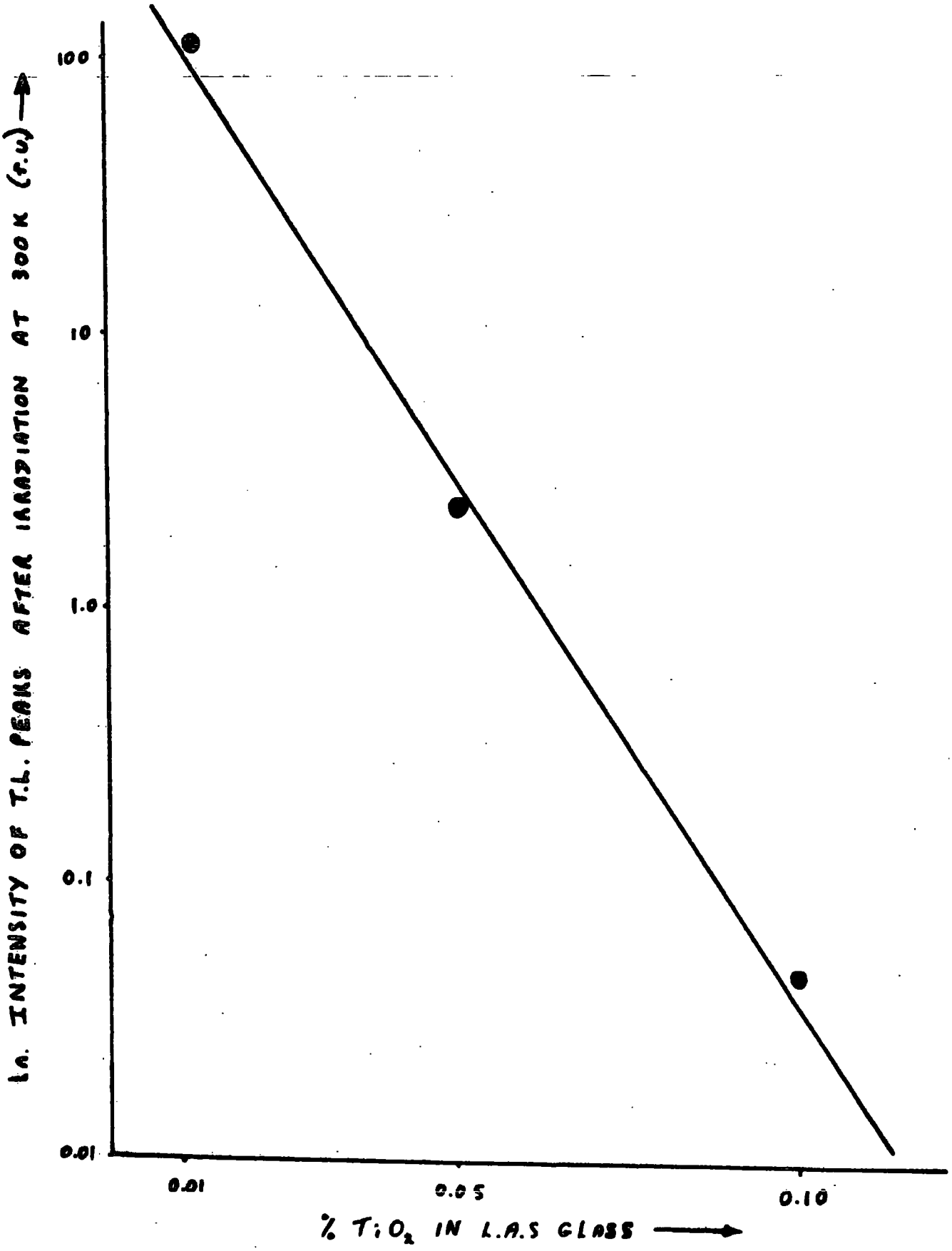

Fig 4.4 b EFFECT OF TiO_2 CONCENTRATION ON THERMOLUMINESCENCE INTENSITY

with various base glasses. The position of the glow peak above room temperature was found to be almost independent of the base L.A.S. glass composition whilst the intensity was found to depend upon the various component concentrations. For the glasses with 20% Li_2O the glow peak intensity increased exponentially with Al_2O_3 concentration as shown in Fig. (4.5). The less systematic results found for constant values of Al_2O_3 and SiO_2 concentration are summarised in Fig. (4.6)(a-d). The general trend appears to be an increase in glow peak intensity with an increase in the relative amount of Al_2O_3 present. Observation of the thermoluminescence peaks at 150 K after irradiation at 100 K gives a reversal of this trend i.e. the peak intensity at 150 K increases with increase in lithium concentration. This suggests the association of the 433 K L.A.S. glow peak with aluminium and the 150 K peak with lithium.

The mechanism involved in thermoluminescence involves both the removal of an electron from a trap and a recombination process. The glow peak temperature has been shown to be a function of the trap depth but the intensity is also dependent on the recombination rate. One method of investigating the recombination is through the glow peak intensity but the spectral resolution of the glow peaks may sometimes resolve a double stage in the recombination process. With this in mind the spectral distribution of the L.A.S. 1022 thermoluminescence peaks was found after irradiation at 77 K by the use of a series of optical filters. Optical absorption characteristics of the filters used are shown in Fig. (4.7). The low intensity of the emitted light prevented the spectral resolution being obtained with a spectrometer.

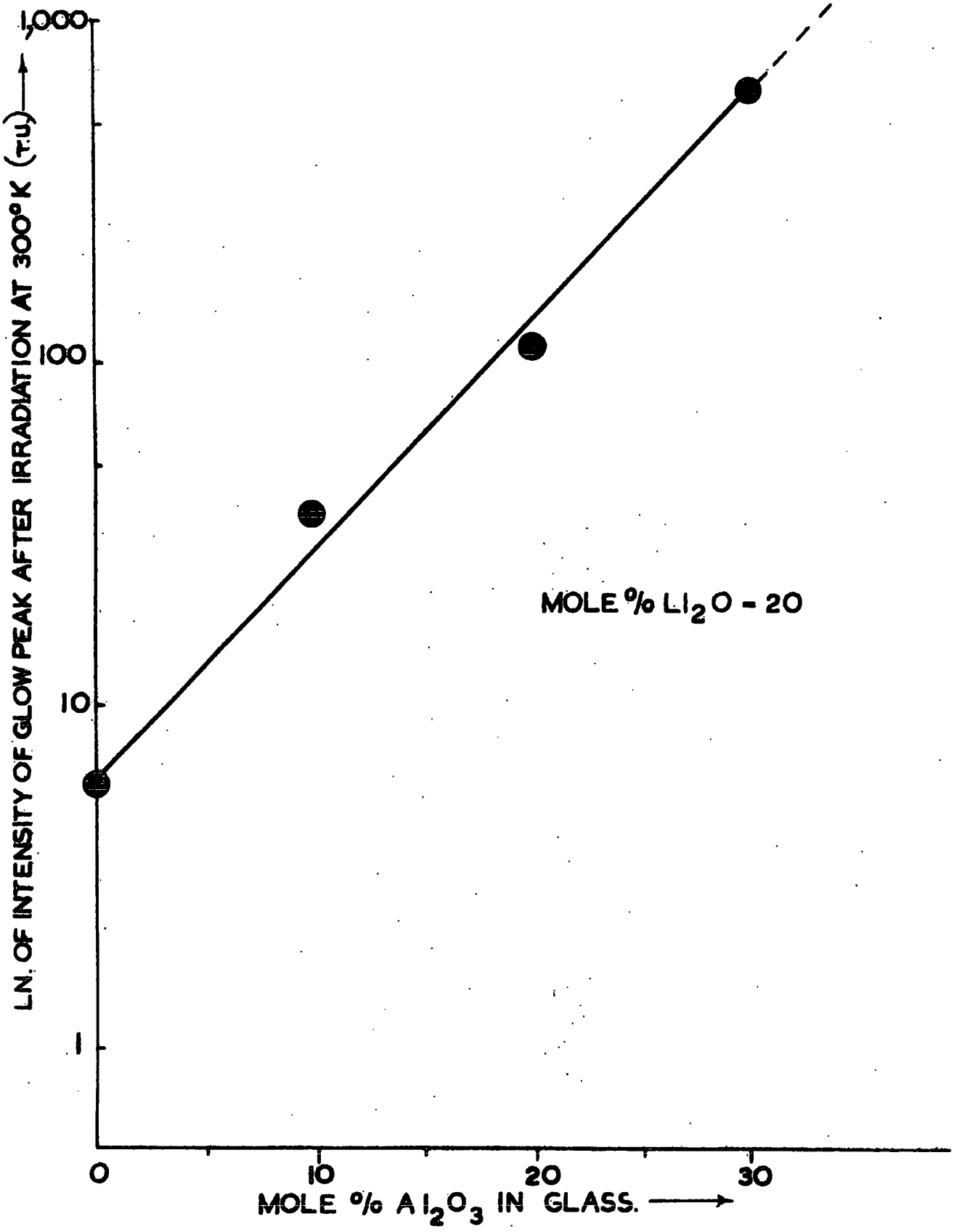

FIG 4. 5 VARIATION OF THERMOLUMINESCENCE PEAK INTENSITY WITH BASE GLASS COMPOSITION.

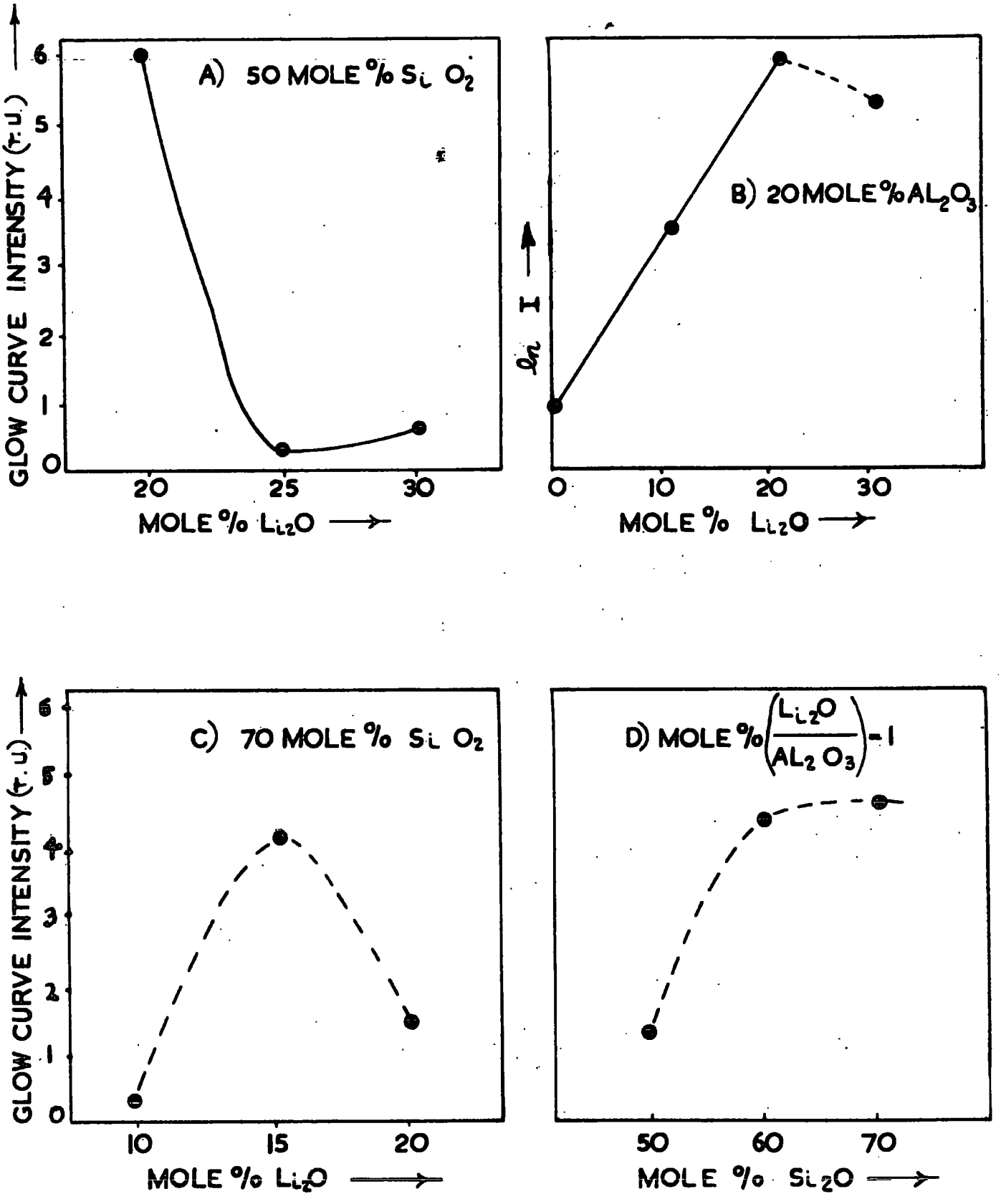

FIG 4.6 GLOW CURVE INTENSITY IN (L.A.S.) GLASS AFTER IRRADIATION AT 300K, WITH VARIATION IN THE GLASS COMPOSITION.

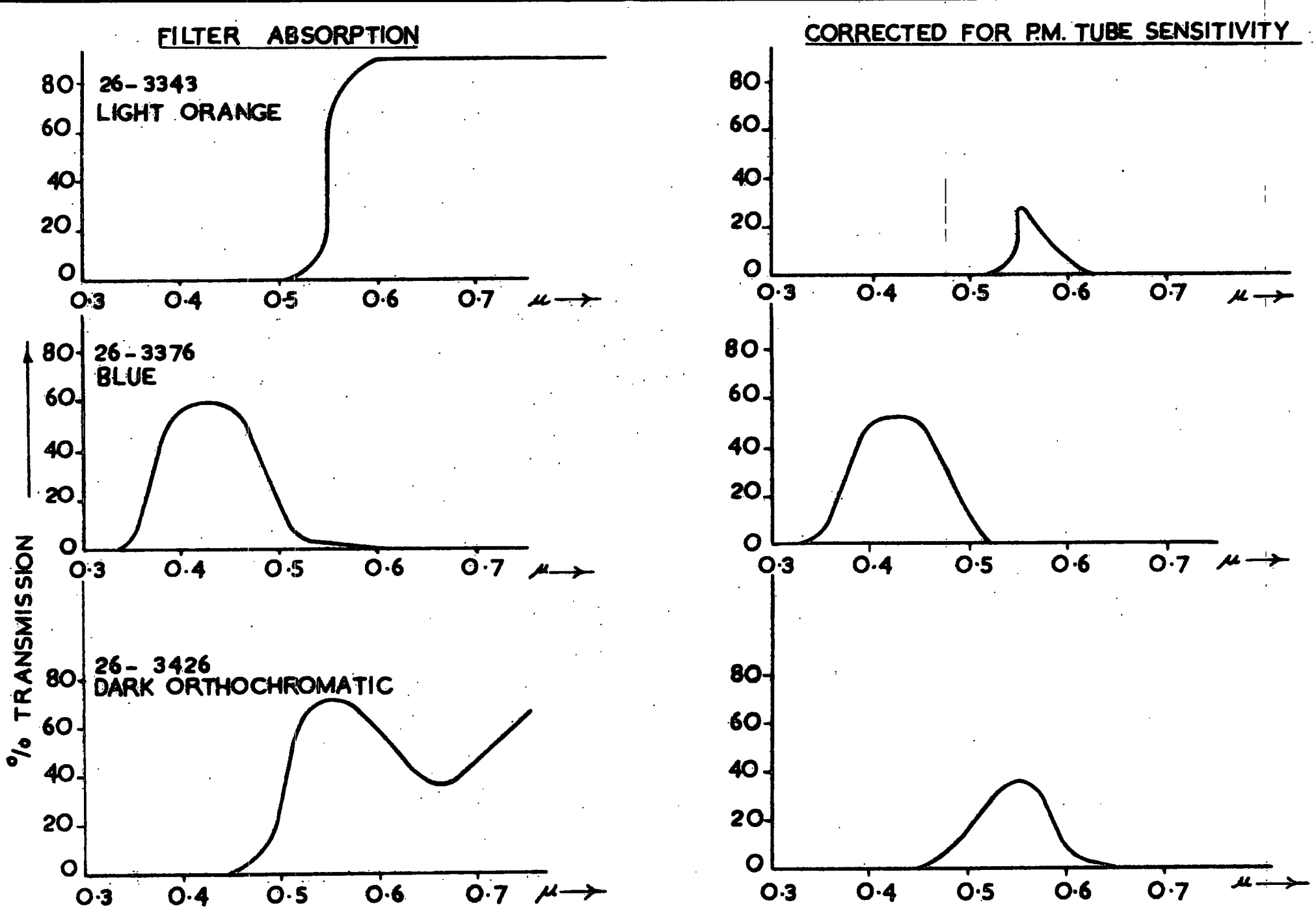

FIG 4.7 OPTICAL CHARACTERISTICS OF FILTERS.

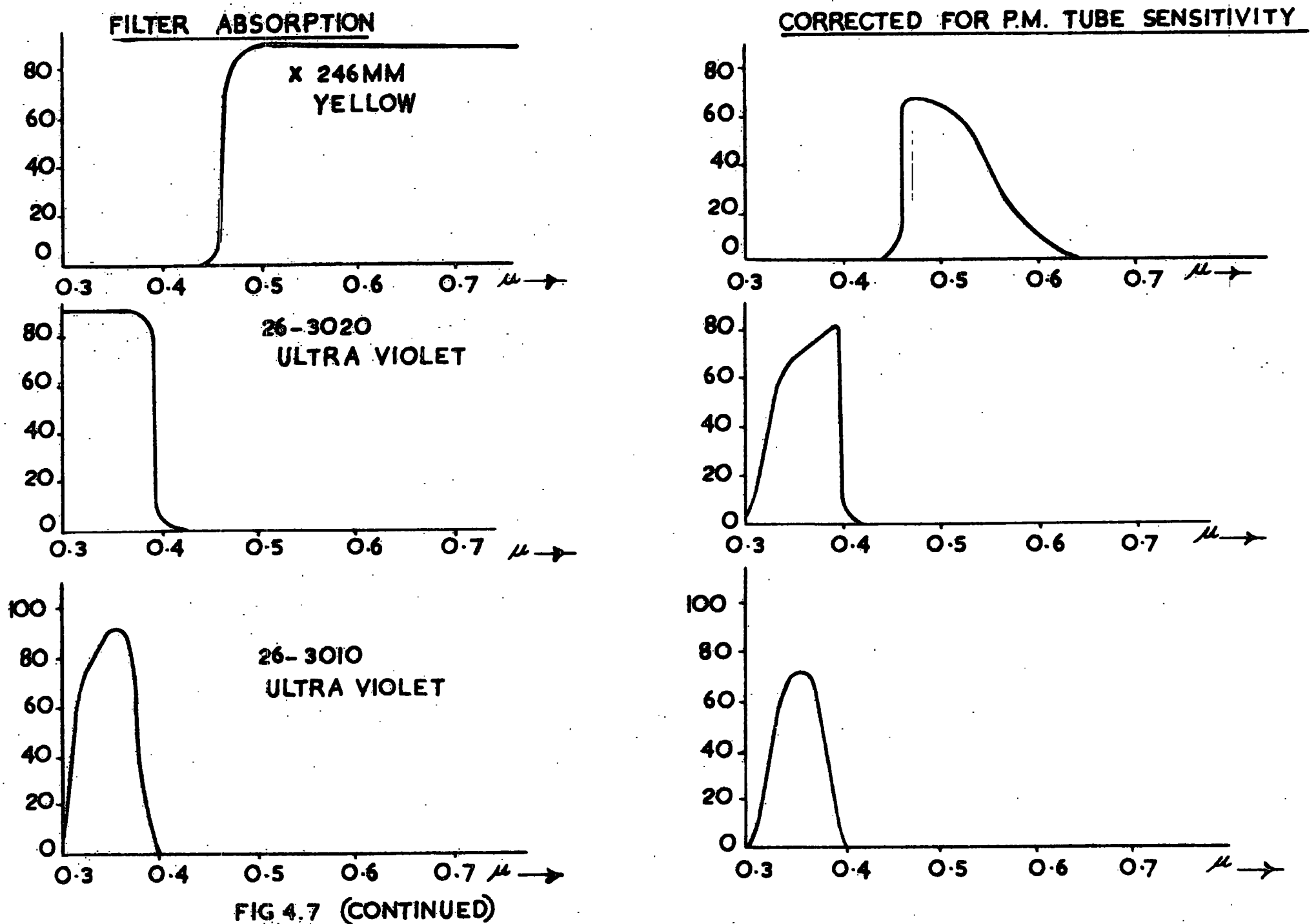

FIG 4.7 (CONTINUED)

The peak intensities after correction for the photo multiplier spectral sensitivity led to the graphs in Fig. (4.8). It can be seen that the lower temperature peak has a more complex structure than the similar 260 K and 433 K peaks. These latter peaks have a single broad component in the 6,000 A region of the spectrum whilst the 150 K peak appears to have an additional ultra-violet component.

These curves can be compared with the X-ray fluorescence intensities of sample 1022 at 77 K and room temperature given in Fig. (4.9)(4.10) respectively. The saturated X-ray fluorescence curves for sample 1022 using no filter (1), a u-v filter (2) and an orange filter (3) are shown in Fig. (4.11). From the above it is evident that the trap populations involved in the recombination process are altered appreciably as the temperature varies.

In an attempt to correlate the effect of additives to the base glass the decay of the X-ray induced luminescence at 77 K was observed. The results for L.A.S. are shown in Fig. (4.12) and the effect of adding Gd_2O_3 and TiO_2 is shown in Fig. (4.13). Incorporation of TiO_2 is seen to reduce the long time component and this can not be accounted for by a simple re-absorption by the titanium ion as titanium has been shown to produce absorption in the ultra-violet region. Fig. (4.12) shows that absorption nearer 6,000 A would be more appropriate to produce the observed long time component reduction.

It is also important to note that the luminescence efficiency

Fig 4.8

SPECTRAL DISTRIBUTION OF THERMOLUMINESCENCE FOR SAMPLE L.A.S. 1022 AFTER X-RAY IRRADIATION AT 77K

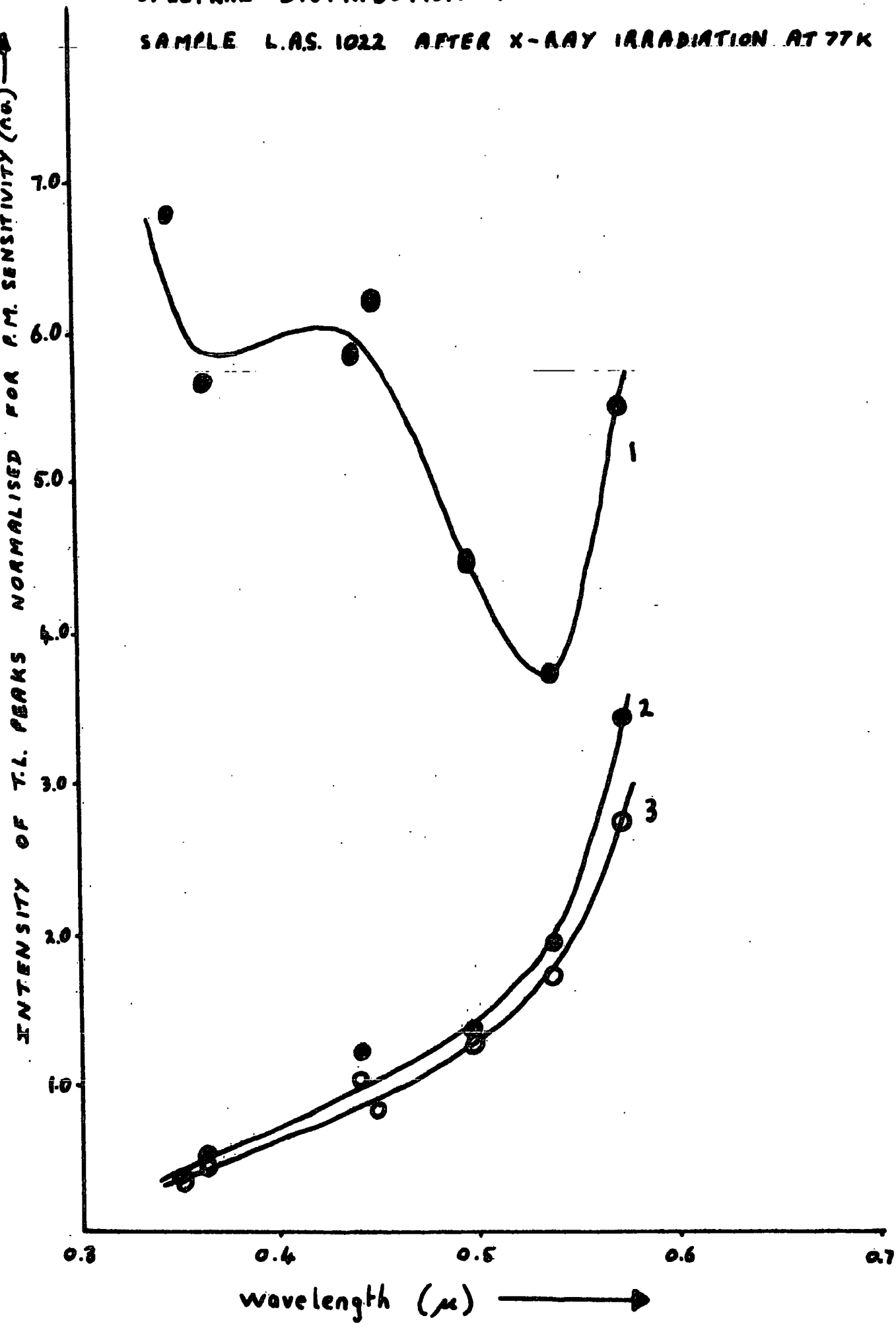

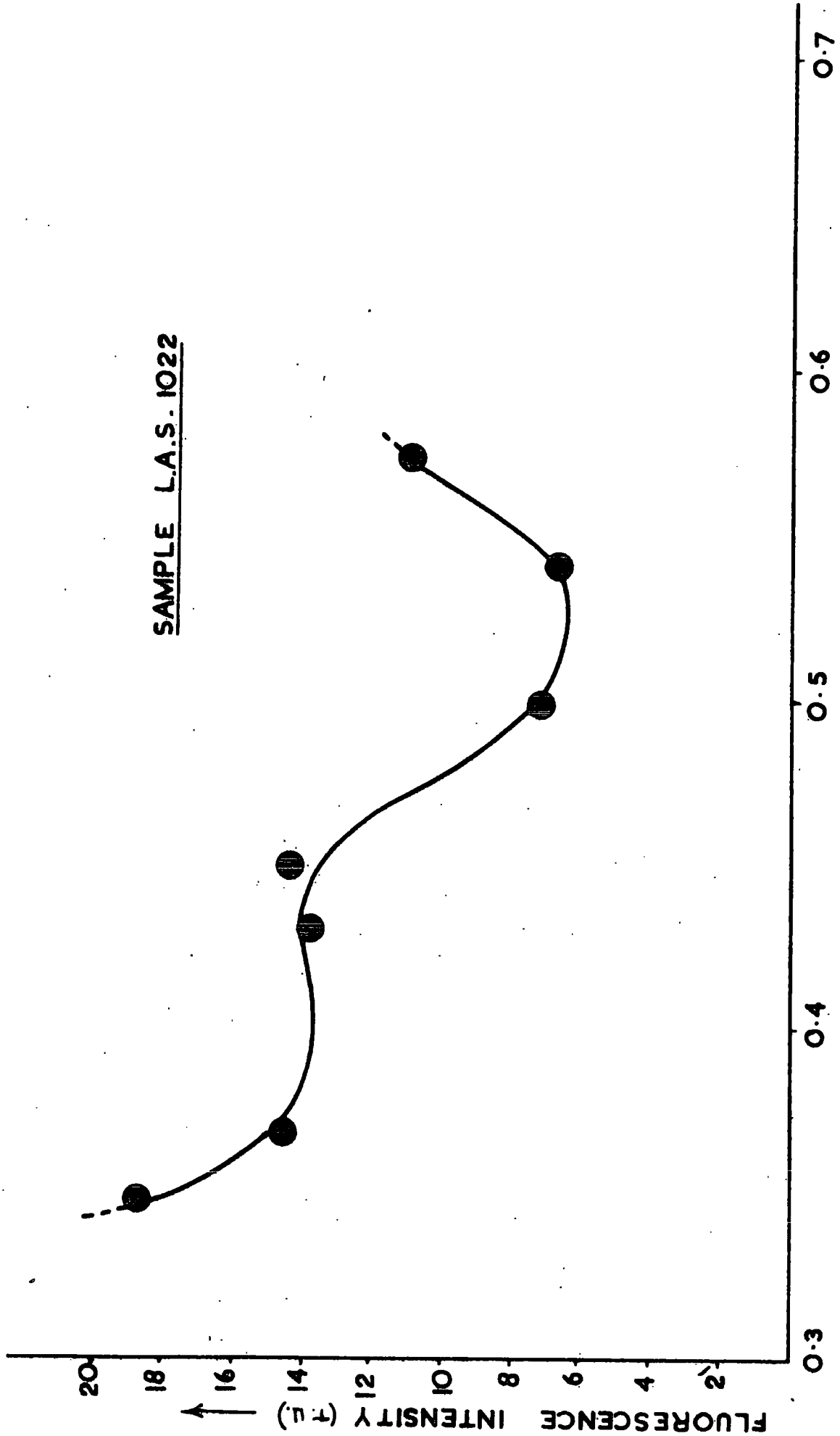

FIG 4.9 X-RAY FLUORESCENCE AFTER 5 MINS. IRRADIATION AT 77K.

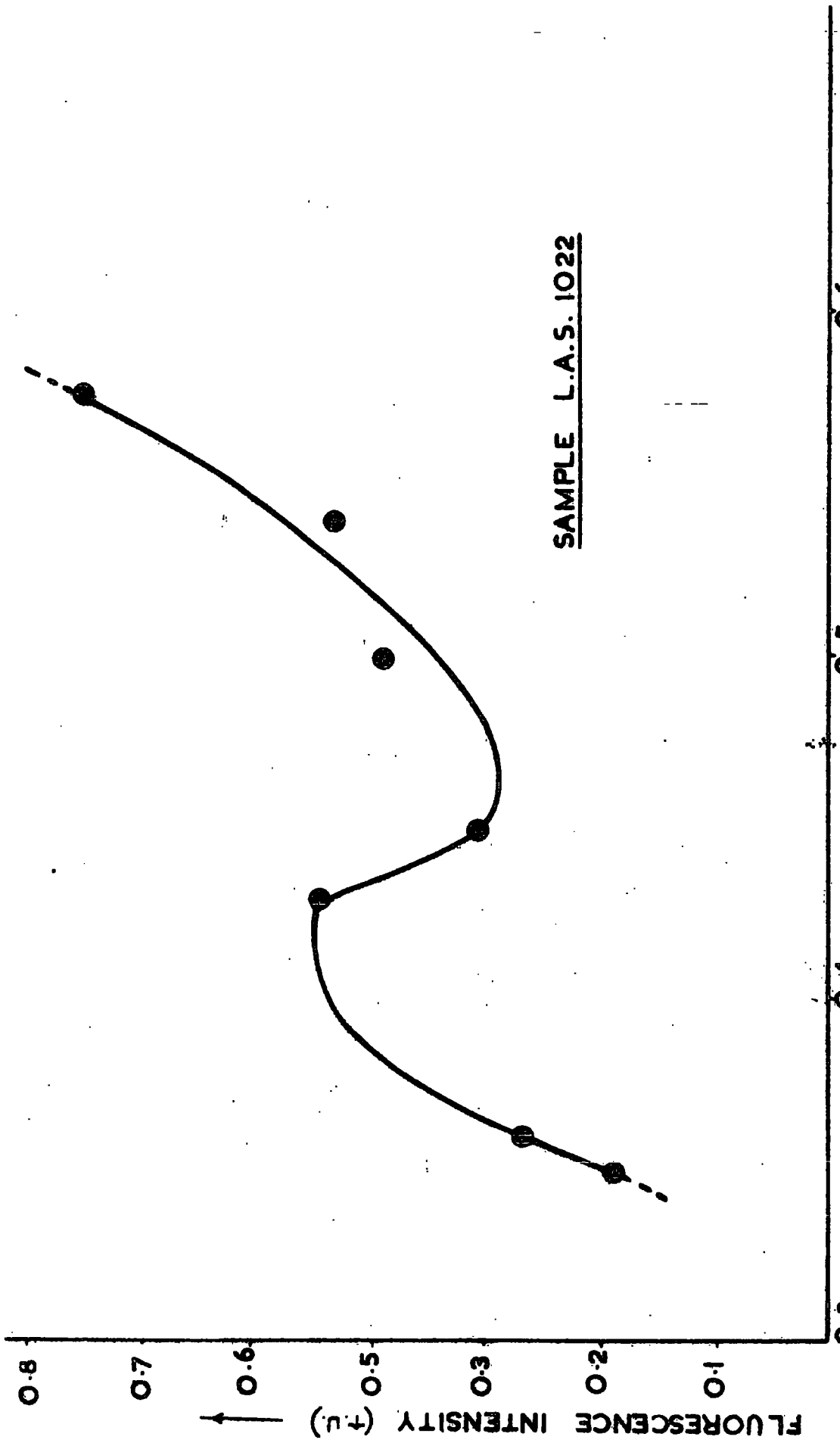

FIG 4.10 SPECTRAL DISTRIBUTION OF X-RAY FLUORESCENCE AT 300K.

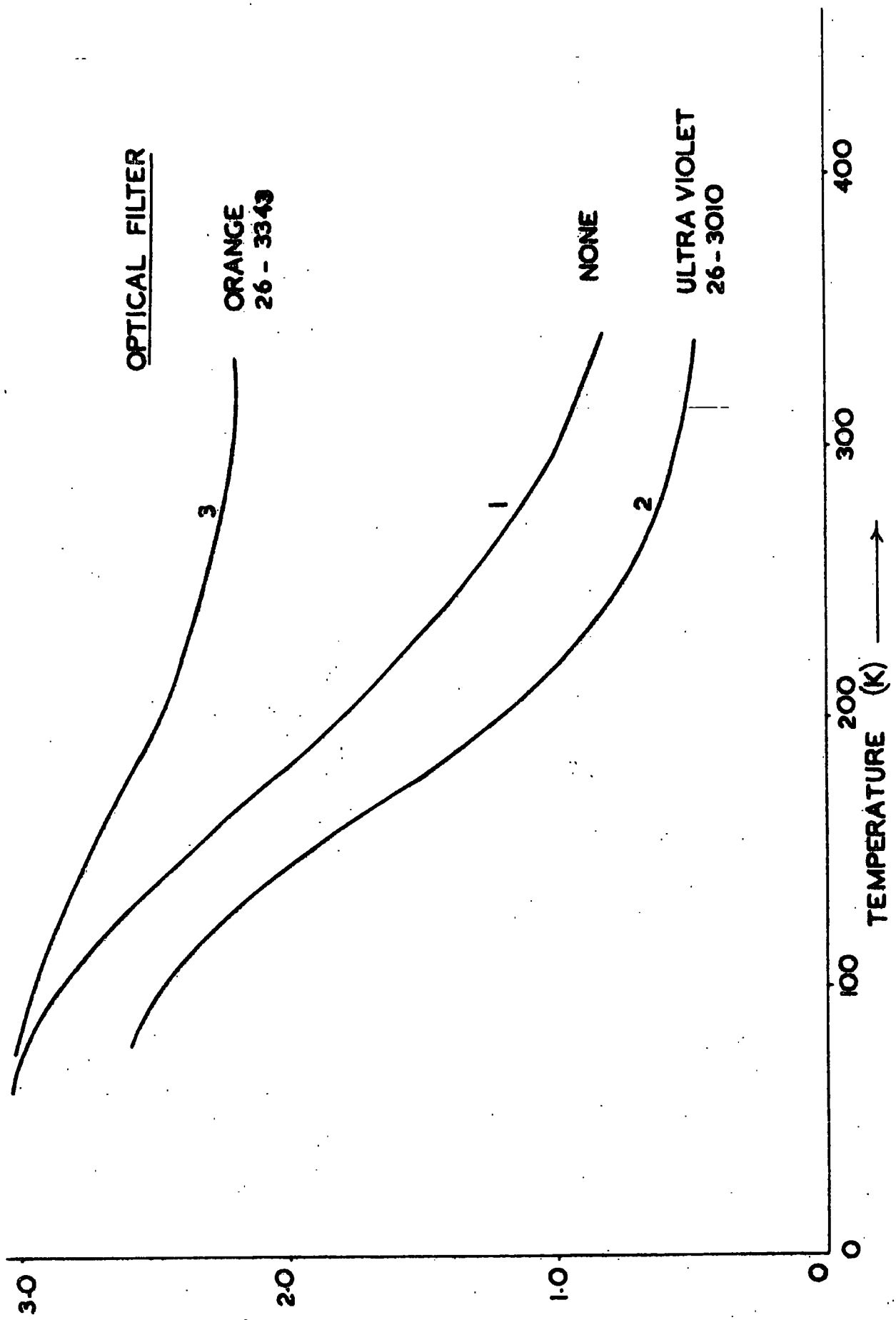

FIG 4.11 SATURATED X-RAY FLUORESCENCE FOR L.A.S. 1022

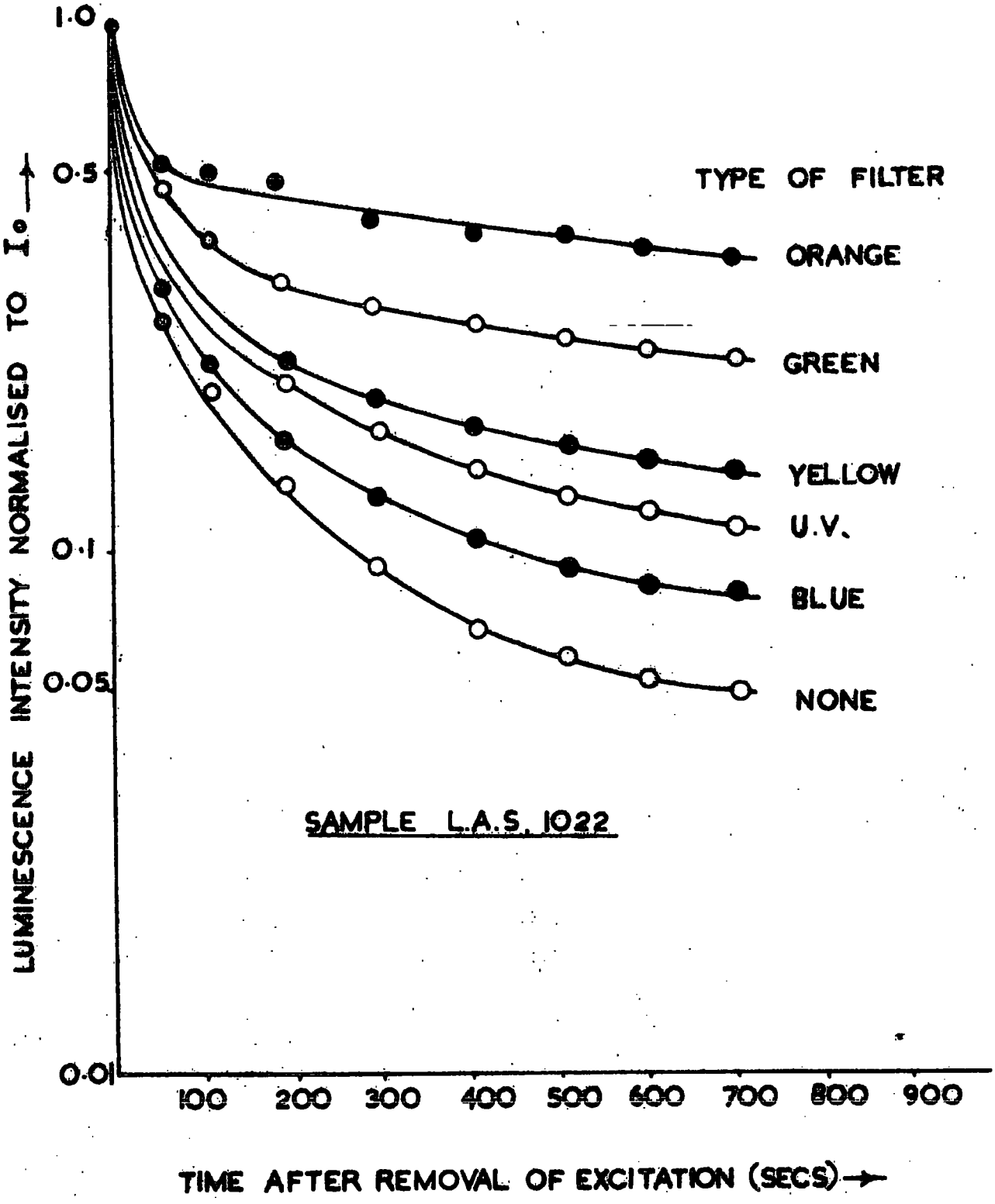

FIG 4.12 LUMINESCENCE DECAY OBSERVED THROUGH VARIOUS OPTICAL FILTERS.

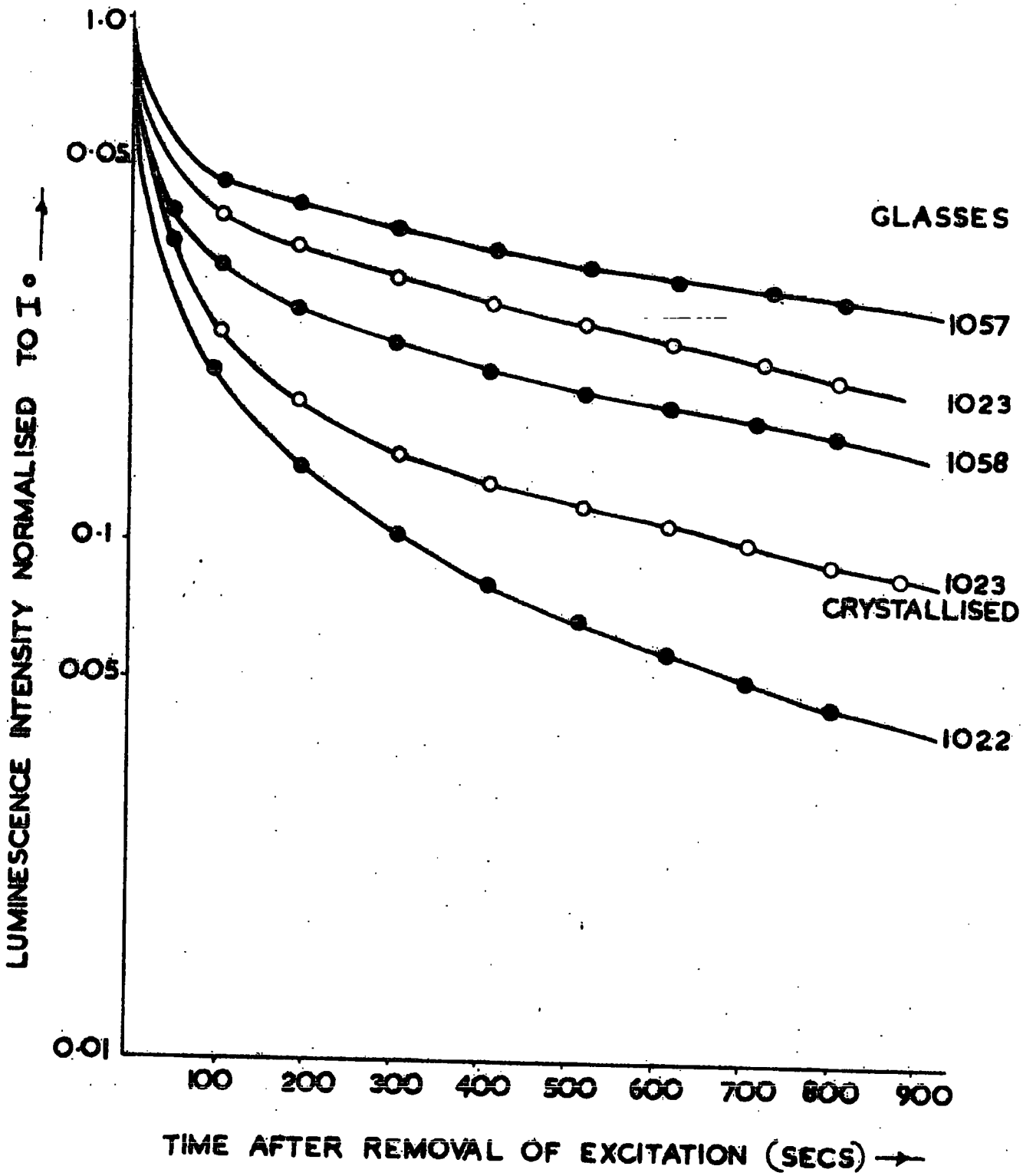

FIG 4.13 LUMINESCENCE DECAY AFTER X-RAY IRRADIATION AT 120K FOR 5 MINS.

with X-ray excitation showed a marked increase with reduction of temperature from room temperature to 77 K in all the L.A.S. glasses except those with an Al/Li ratio greater than one. In this case little or no increased efficiency with reduction of temperature was found. These facts reveal information relevant to the construction of a model for the defects, which is necessary if luminescence is to prove a useful method of studying the environment of additives in the glass.

Difficulty was found when an attempt was made to measure the thermoluminescence of the glasses after heat treatment because either the specimens fractured or TiO_2 had to be incorporated to enhance nucleation, with the resulting quenching of the glow peak. However, measurements were obtained for low concentrations of TiO_2 with and without Gd_2O_3. Observation of the glow curves of powdered specimens was not possible with the equipment used. For sample L.A.S. 1022 no change was observed after heating to 800°C for one hour although a marked amount of crystallisation was observed both visibly and by X-ray diffraction. Room temperature irradiation of L.A.S. 1057 (0.1% TiO_2 and 1% Gd_2O_3) after heating to 800°C for one hour produced a marked increase in the glow peak intensity at 480 K. This may be associated with the reduction in the quenching ability of the titanium, caused by changes in the titanium environment during crystallisation.

4.2.3 Discussion

The addition of Gd_2O_3 to L.A.S. 1022 produced an increase in the three base glass thermoluminescence peaks observed. However, the

similar relative magnitudes and not greatly different temperatures of the peaks, suggest that the gadolinium is not directly associated with the defects. This conclusion is also supported by the observations on N.S. glass. It must be stated that the temperature of all the glow peaks in the L.A.S. glasses were slightly increased, when gadolinium was present, indicating that the electron traps had become more stable.

One of the most interesting features of the glow curve results was the quenching found whenever titanium was present. It is well known that transition ions can give rise to thermoluminescence quenching due to the existence within these ions of energy levels which allow non-radiative decay processes to occur. Although expected, the quenching efficiency of the titanium was remarkably high and was thought to be due in part to a process other than the existence of non-radiative energy losses. Observation of the glow curves when titanium was present, which was possible if less than 0.5% TiO_2 was present, showed that the two low temperature peaks were unchanged in position but that the higher temperature peak was resolved into two components. An explanation of this is suggested as the existence of two locations for the titanium ion w.r.t. the base glass defect which produces the high temperature peaks.

It is noted that similar thermoluminescence peaks occur in various glasses i.e. sodium silicate and borosilicate glasses observed and from fused silica reported in the literature. Hence as suggested elsewhere (4.14) the defects have been associated with

Si-O bonds and non-bridging oxygen ions. The association with Li and Al ions would thus appear to be indirect. A model may be proposed in which Li and Al are in the second co-ordination sphere of the basic silicon defect producing ion. As the basic defects appear to be common to silicate glasses a Ti-O-Si scheme is suggested for the titanium location. The two different sites required may be of the form

1.

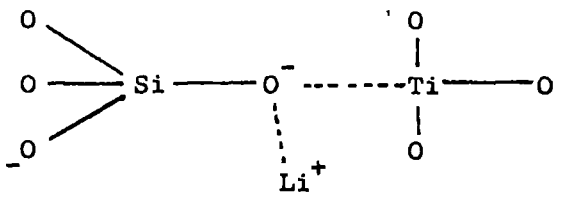

2.

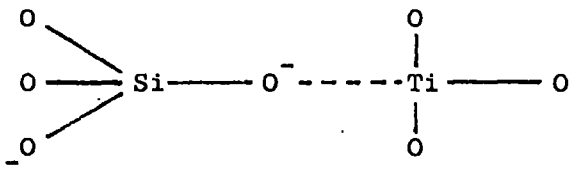

analogous to the base glass defects suggested by Sidorov and Tyul'kin (4.15) for two component silicate glass.

It can be seen that when both gadolinium and titanium are present the two low temperature peaks are unchanged. The stabilizing effect found when only gadolinium was present is counteracted by the presence of titanium. This gives an indication of a possible interaction between these two ions. When both ions are present a new high temperature glow peak occurs with maximum intensity at 460 K which resembles neither base glass nor base glass with either ion added separately. A possible explanation is again the association of the gadolinium and titanium

ions which removes the effect of Gd on the low temperature peaks. Also if this complex is located near the base glass defect giving rise to the high temperature glow curve, a distortion of the environment could account for this new peak at 460 K. It is suggested that all the high temperature peaks are associated with a similar basic defect variously distorted by the proximity of gadolinium or titanium ions or of both these ions in the form of a local Gd - Ti complex.

In an attempt to clarify the nature of the basic defects produced in the L.A.S. glasses, glow curves were obtained from a variety of compositions in this system. As already outlined in section 4.2.2 there is a correlation of the high temperature peak with the aluminium concentration and of the low temperature peak with the lithium content. It is thus possible to associate the high temperature peak with a positive ion Al^{3+}, Ti^{3+}, or Gd^{3+} substituted for silicon in a basic tetrahedral co-ordination. The rare earth ion in particular is likely to distort the local environment considerably, as is evident in the previous discussion in Chapter 3. However, the effect on the nearest silicon atom, which is most likely to be the seat of the basic defect should be similar for these three ions. The small size and resulting high field gradients in the proximity of the lithium ions can be responsible for the much lower energies involved in the low temperature traps.

Observation of the luminescence with continuous X-ray irradiation showed that reducing the temperature of the specimen from 300 K to 77K produced a marked increase in the luminescence

efficiency in all glasses except those in which the Al/Li ratio exceeded 1. In this case very little or no increase in efficiency was found as the temperature was lowered. An explanation of this is suggested later in terms of an exchange between two hole traps that are thought to be responsible for the visible emission.

The special distribution of the thermoluminescence peaks for L.A.S. 1022 show that the high temperature peaks have one component compared with the more complex low temperature emission. A similar change in spectral emission was observed in the X-ray fluorescence intensity of L.A.S. glasses when cooled from 300 K to 77 K. From this it can be concluded that electrons thermally released from traps during thermoluminescence are liberated into a 'conduction band'. The electrons are then free to undertake similar recombination processes in the glow and in the X-ray fluorescence experiments. This is evident from Fig. (4.2) which shows the saturated X-ray fluorescence intensity variation with temperature. It thus becomes necessary to consider the hole traps with which the electrons recombine to establish the nature of this dual emission process. The simplest way to explain the observed phenomenon is to have two hole traps which are placed above the valence band as shown in Fig. (4.14). It can be considered that during the excitation period many electrons are removed from regions close to the valence band to produce these holes. During the excitation it is also likely that many electrons will be removed to the conduction band and then held in traps below this band. So a situation will exist in which electrons are in excited states and holes exist in the valence band and in the two

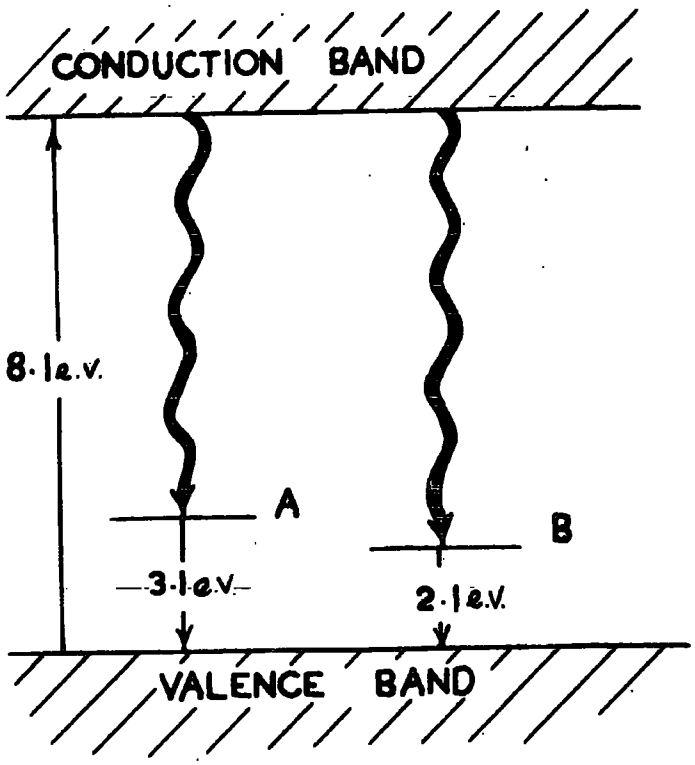

FIG 4.14 SCHEMATIC DIAGRAM OF HOLE TRAPS

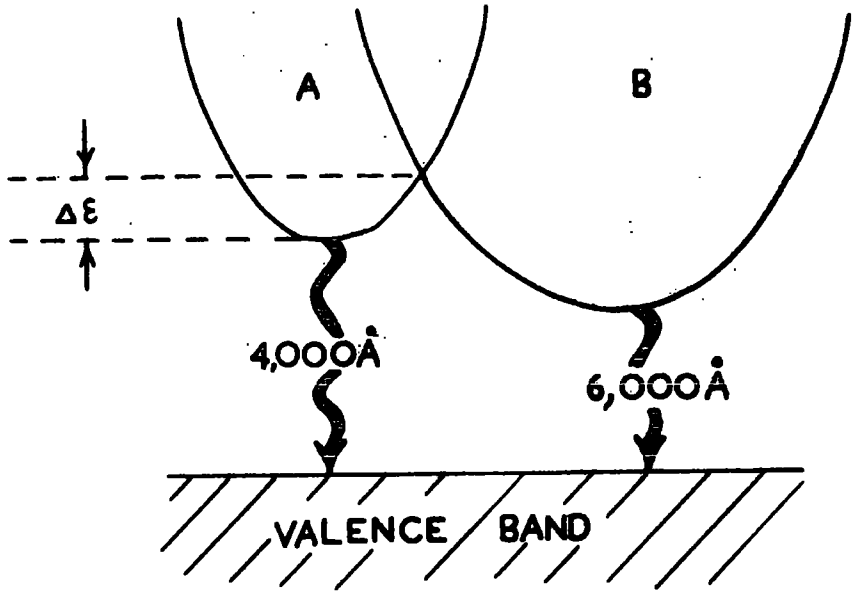

FIG 4.15 CONFIGURATIONAL DIAGRAM OF HOLE TRAPS

traps A and B. The recombination can then be considered to take place by the transition indicated in Fig. (4.14). From the results it would appear that transition of the electrons from A and B to the valence band corresponds to the 4,000 A (3.1 ev) and 6,000 A (2.1 ev) emissions respectively. The valence to conduction band gap can be estimated from the optical absorption cut off for fused silica which is known to be 8.1 ev. If this is correct then a transition from the conduction band to the A and B traps should be observable. However, this transition would have an energy in the region of 5 - 6 ev which is outside the range of the photomultiplier used.

Consideration must now be given to the change in the spectral emission with temperature. In Fig. (4.15) a configurational diagram is suggested for the hole traps A and B. At temperatures at which the thermal energy exceeds $\Delta\epsilon$, electrons entering trap A will have a finite probability of transfer to site B. Hence the 4,000 A emission will be effectively quenched above this temperature. As the temperature is reduced below this value the quenching is removed and the 4,000 A emission observed. In order for the transfer process to be efficient, as is found in glasses, the defects A and B should be in reasonably close proximity.

If the luminescence decay from sample L.A.S. 1022 after irradiation at 100 K is observed through various filters, the form of the decay is seen (see Fig. 4.12) to change; the short component being reduced as the wavelength of the filter increases. The short period decay component is in the ultra violet region and the larger component is in the region of 6,000 A. Two different

time constants would be expected if the model proposed above is correct, with A having the long time component w.r.t. B. Titanium addition to the glass is also found to effect this decay as is shown in Fig. (4.13) and can be understood by considering the titanium as a simple filter. Absorption produced by various concentrations of titanium in the base glass is shown in Fig. (4.16). It can be seen that with increasing TiO_2 content the absorption progresses from the U.V. into the visible region. It can also be seen that an optical filter with this absorption can produce the changes observed in the decay when titanium is present. So it would appear that at least part of the T.L. quenching by the incorporation of TiO_2 is due to a simple re-absorption process followed by non-radiative transfer. However, the 6,000 A component can not be reduced by this mechanism and an alternative suggestion must be made.

Most of the models previously suggested for the defect centres place the hole on the non-bridging oxygen ion whilst the electron is associated with a silicon ion. Non-bridging oxygen ions are produced, in a silica matrix by the inclusion of monovalent ions. The presence of tripositive ions in the glass results in the reduction of the number of non-bridging oxygens produced by the monovalent ions, by allowing local charge compensation.

So it is reasonable to assume that the presence of titanium can reduce the number of non-bridging oxygens and hence reduce the overall number of A and B sites. This could also explain the results found for the various base glasses with excess aluminium. The number of A and B sites would then be reduced when the aluminium ions

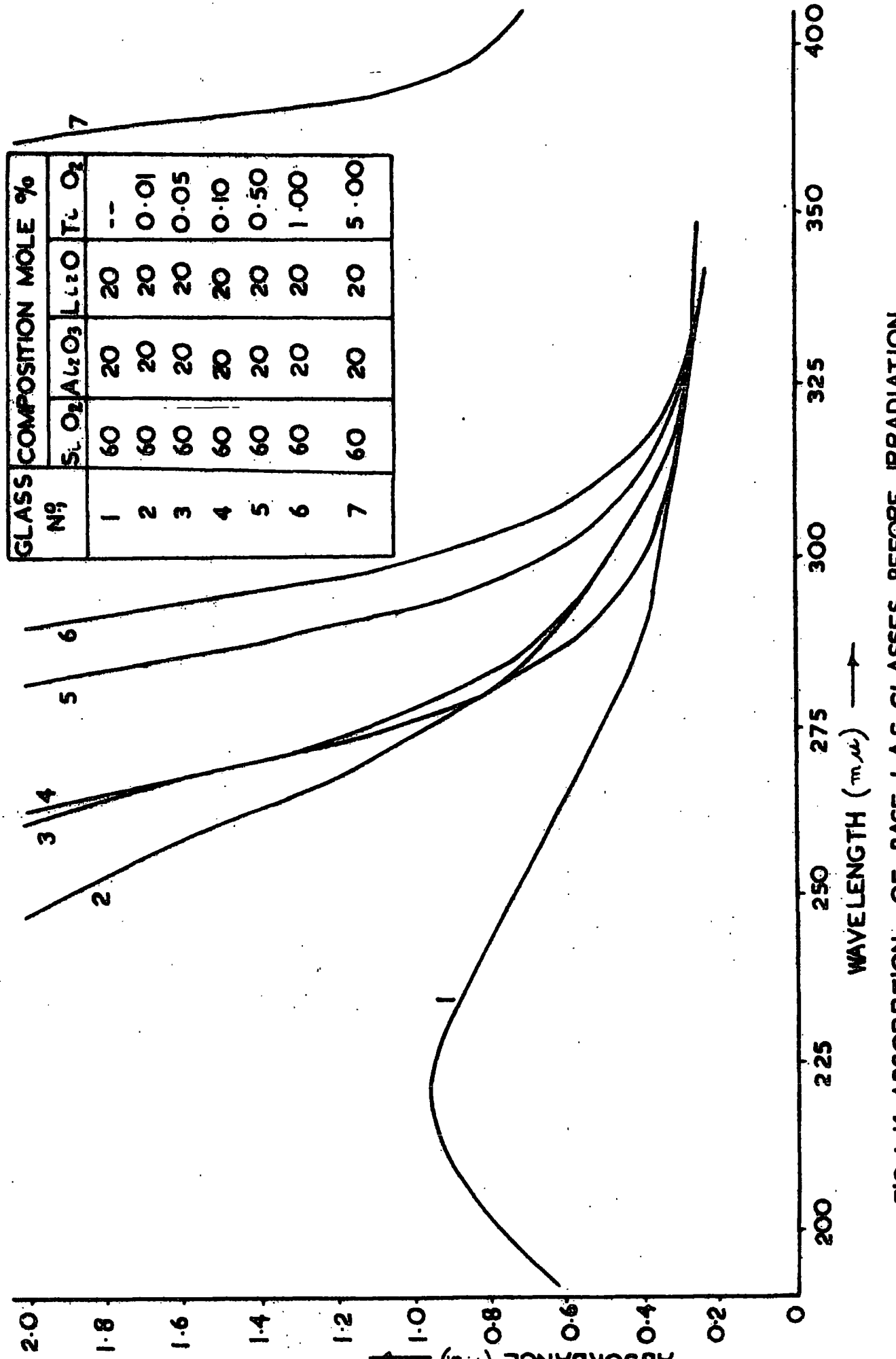

FIG 4.16 ABSORPTION OF BASE L.A.S. GLASSES BEFORE IRRADIATION

are not locally charge compensated by lithium ions. Models for the A and B sites developed by J.W.H. Schreurs (4.15) are as shown below:

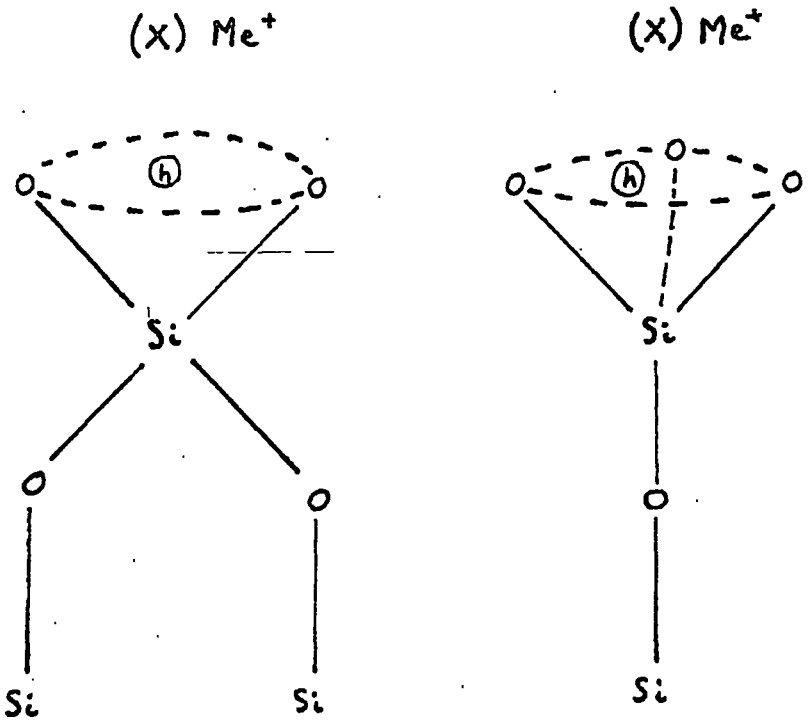

Fig 4.7

The increased thermoluminescence of the L.A.S. 1057 and L.A.S. 1023 glasses after heat treatment indicates a reduction in the quenching action of the titanium. This could be due to the development of crystalline regions in which the titanium is absent.

The results obtained by observing defects have not shown the existence of more than one site for the gadolinium ion. The indirect association of the defect centres with the gadolinium ion prohibited the clarification of this problem. Evidence did suggest that a Gd-Ti complex may be responsible for certain results, and that this

association is likely to be near the defect which is related to the aluminium ion.

4.3 X-ray Induced Electron Spin Resonance

4.3.1. Results

Electron spin resonance observations were carried out on all the specimens and as stated earlier only those containing gadolinium showed a resonance before irradiation. This is taken as evidence of the lack of titanium in the paramagnetic Ti^{3+} state and also of the absence of any other paramagnetic impurities.

After irradiation the base L.A.S. glass gave a distinct resonance which could be resolved into a component with an effective g value of 2.004 and one with $g \approx 2.01$; hereafter referred to as the α and β components respectively. These lines corresponded to the appearance of a dark brown colouration in the samples which are discussed in the next section.

The α and β components of the e.s.r. were observed in all the L.A.S. glasses after irradiation except those containing gadolinium where the absorption produced by the presence of the rare earth ion effectively masked observation of these induced defect resonances. After crystallisation of the samples followed by irradiation there was no appreciable change in these base glass resonances indicating that either the defects are produced within well ordered domains in the glass and hence do not change on crystallisation, or that the defects are in the glassy state which is not completely removed by the crystallisation procedure. As similar resonance absorption has

been attributed to the orientation of ionic sites found in crystalline quartz (4.17) and since no diminution of the e.s.r. intensity was noticed, the former hypothesis appears most likely.

Incorporation of titanium into the L.A.S. base glass, followed by irradiation, produced an additional resonance line with $g \approx 1.94$. This resonance increased rapidly with the initial addition of TiO_2 but above 1.0% the intensity of the $g \approx 1.94$ to the α and β component absorption remained constant. There was a slight indication that the titanium associated line ($g \approx 1.94$) increased in width as the concentration of this ion increased. However, after crystallisation this resonance in the glass with 0.1% TiO_2 was removed, whilst in the 5.0% TiO_2 containing glass there was no change.

Crystallisation of glasses containing gadolinium and titanium led to a reduction in the Gd^{3+} absorption intensity and allowed observation of the base glass irradiation defect and the titanium associated line.

These results are summarised in Fig. (4.18)

4.3.2. Discussion

It has been shown (4.15) that in a binary lithium or sodium silicate glass the X-ray induced α and β components in the e.s.r. absorption can be attributed to the formation of hole traps on non-bridging oxygen ions. This has been confirmed by Mackey et al. (4.18). The similarity of the resonances found here for lithium alumina silica glasses suggests that the same holes

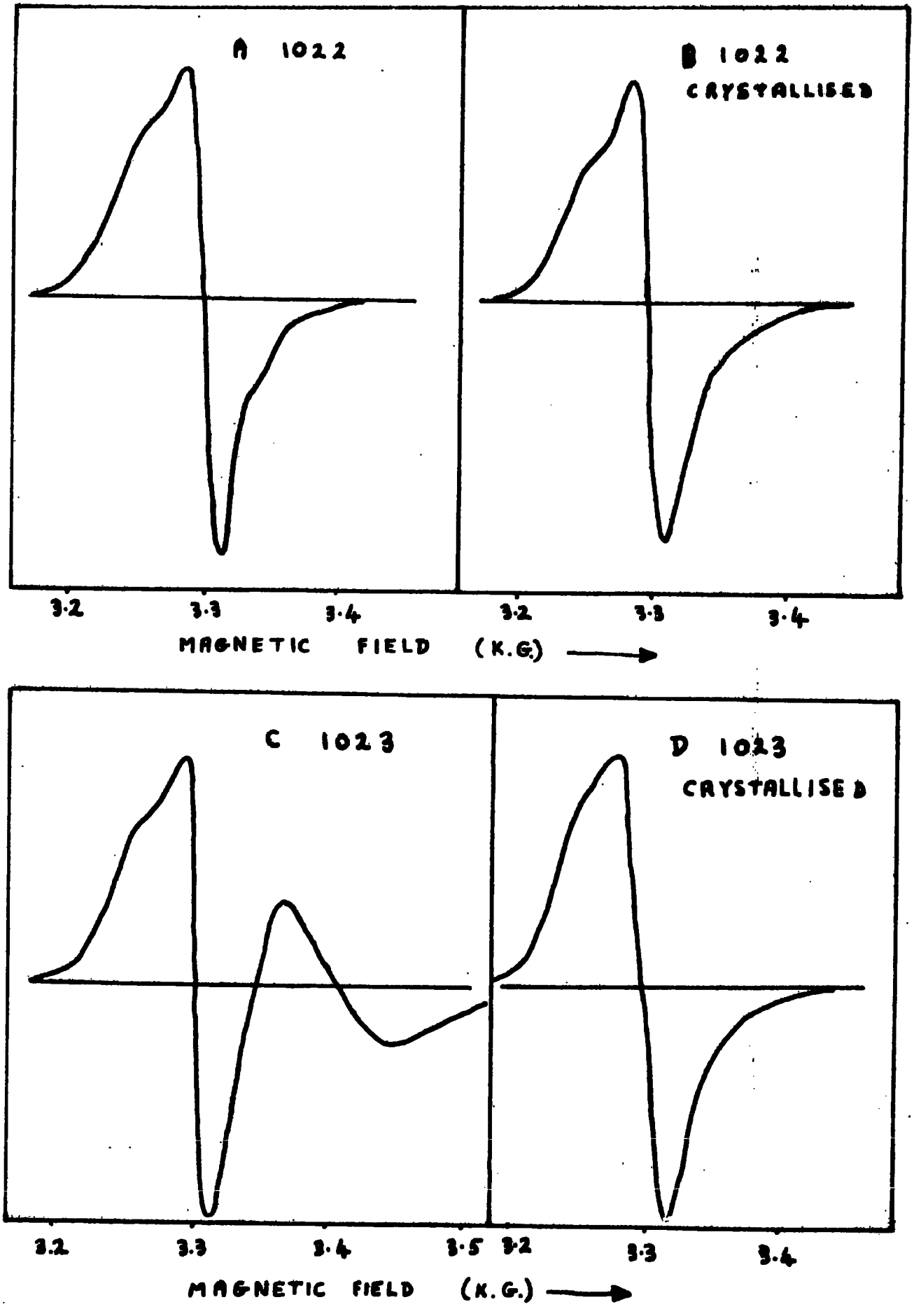

Fig 4.18 E.S.R. SIGNALS FROM IRRADIATED L.A.S. GLASSES

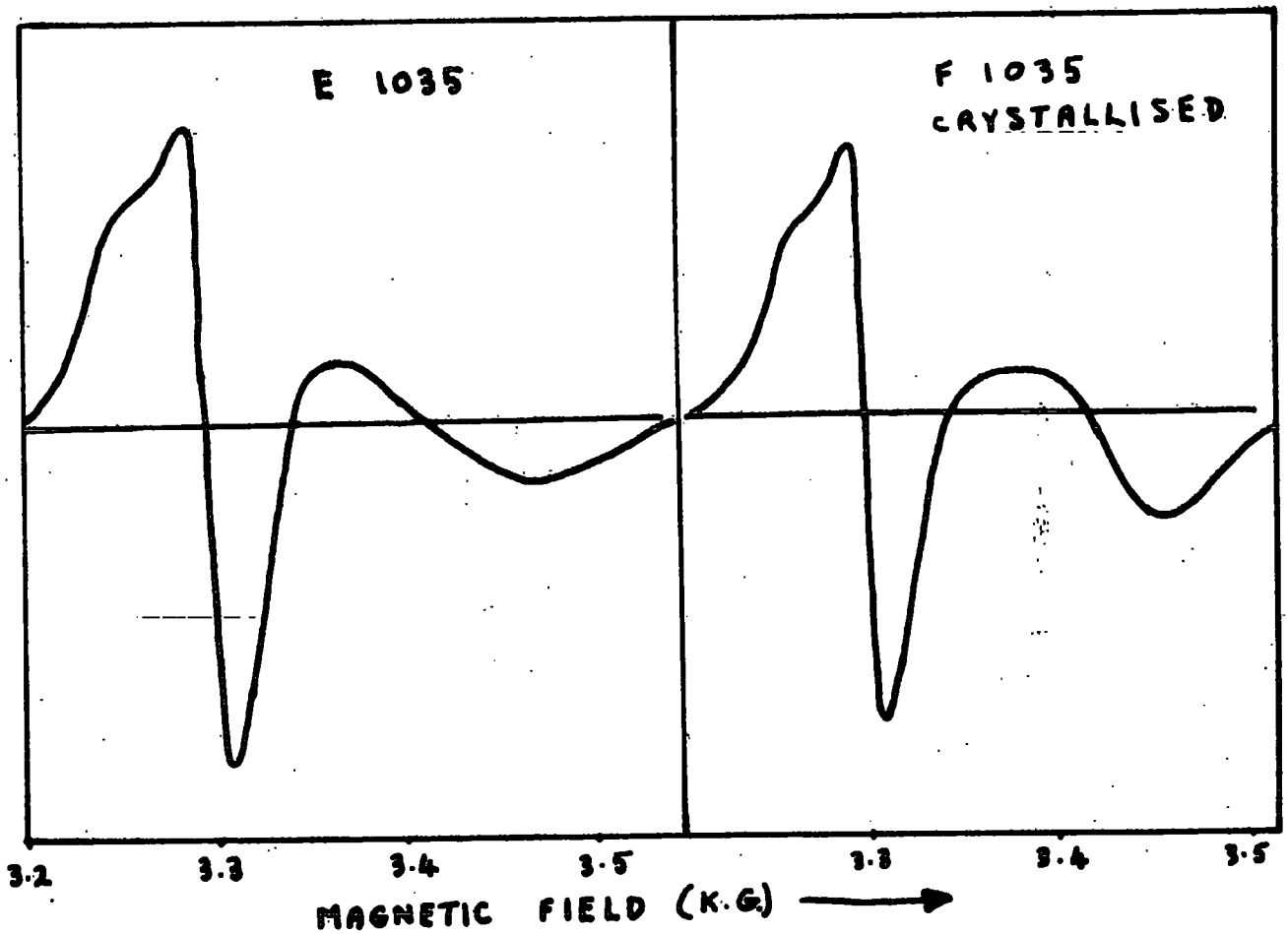

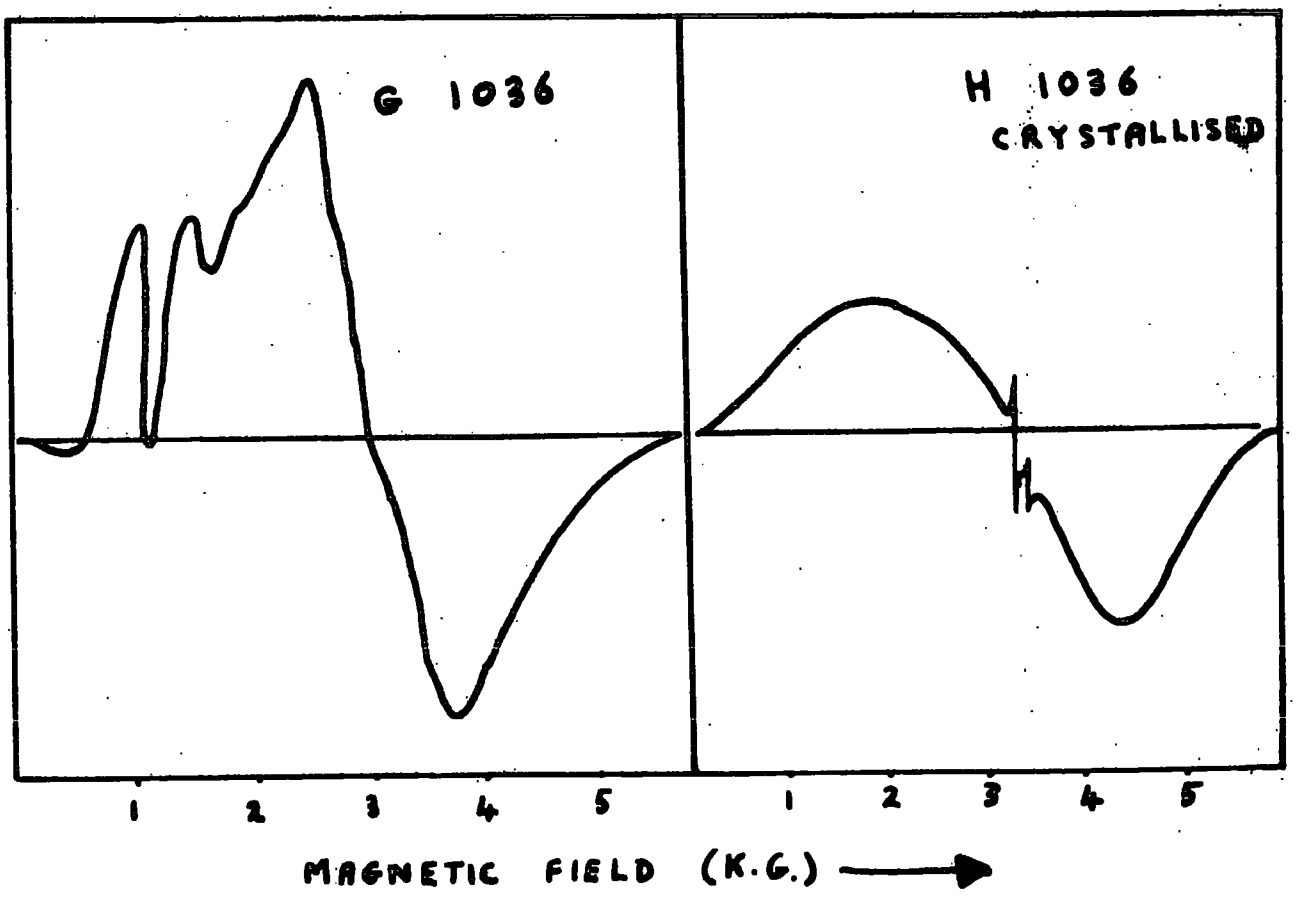

Fig 4.18 CONTINUED

on non-bridging oxygen ions are responsible for the observed effects. Again the two models of Fig. (4.17) may be used to explain the existence of two different hole traps on non-bridging oxygens ions. The remarkable insensitivity of the resonance to crystallisation may be due in part to the broad nature and lack of resolution of the absorption in this region.

The increase of the Ti^{3+} resonance for initial additions of titanium and then a constant ratio for the $g \approx 1.94$ to the base glass defects for titanium concentrations above 1.0%, can be explained by the fact that for every electron trapped by a titanium ion an equivalent hole must be formed. This hole is most likely to be associated with a non-bridging oxygen ion. Initially lithium ions will compete for the electrons but above a small fraction of titanium the Ti^{4+} ion predominates due to its greater cross section for electron capture.

4.4. Optical Phenomena

4.4.1. Results

All the base glasses gave very little absorption in the visible region of the spectrum, however, a broad optical absorption was found below 3,250 A. The absorption of various L.A.S. glass compositions is shown in Fig. (4.19) and there is an indication of two separate peaks, one at 2,150 A and the other at 2,350 A. It was found that these two absorptions are symmetric when the $Li_2O:Al_2O_3$ ratio is one i.e. when all the tri-positive aluminium ions can be locally charge compensated by monovalent lithium ions. When there is an excess of Al_2O_3 or

of lithium oxide there is a resulting charge imbalance and the optical absorption below 3,250 A becomes non-symmetric.

No systematic change was found in the intensity of the 2,150 A and 2,350 A absorptions with base glass composition, except that for a given percentage of SiO_2 minimum absorption always occurred for a Li_2O/Al_2O_3 ratio of 1.0, as shown in Fig. (4.20).

Addition of titanium changes the absorption of L.A.S. glass producing an apparent optical absorption edge which moves to longer wavelengths with increasing TiO_2 concentration. This is shown in Fig. (4.16) whilst in Fig. (4.21) the wavelength for a given absorption (representing the absorption edge) is plotted against the TiO_2 concentration and shows an exponential dependence. This corresponds to a slight darkening in appearance of the glass samples.

Addition of Gd_2O_3 produced no change in the broad absorption in the ultra-violet region, except for the appearance of the sharp absorption lines shown in Fig. (4.22). When both gadolinium and titanium are present the titanium absorption masks any effect of the Gd_2O_3.

In the low energy infra-red region, absorption occurs due to ionic bond vibrations. The absorption for some L.A.S. glasses in the 2.5 to 40 μ region is shown in Fig. (4.23) and was not changed appreciably by the addition of TiO_2, Gd_2O_3 or both. Several broad peaks were observed at 8.8, 10.2, 14 and 22 μ which have been attributed to vibration of Si-O type bonds. After the L.A.S. glasses containing titanium plus gadolinium and titanium alone

GLASS No.	COMPOSITION MOLE %		
	SiO_2	Al_2O_3	Li_2O
1	80	0	20
2	70	15	15
3	50	20	30
4	50	30	20
5	50	25	25
6	70	10	20
7	60	20	20

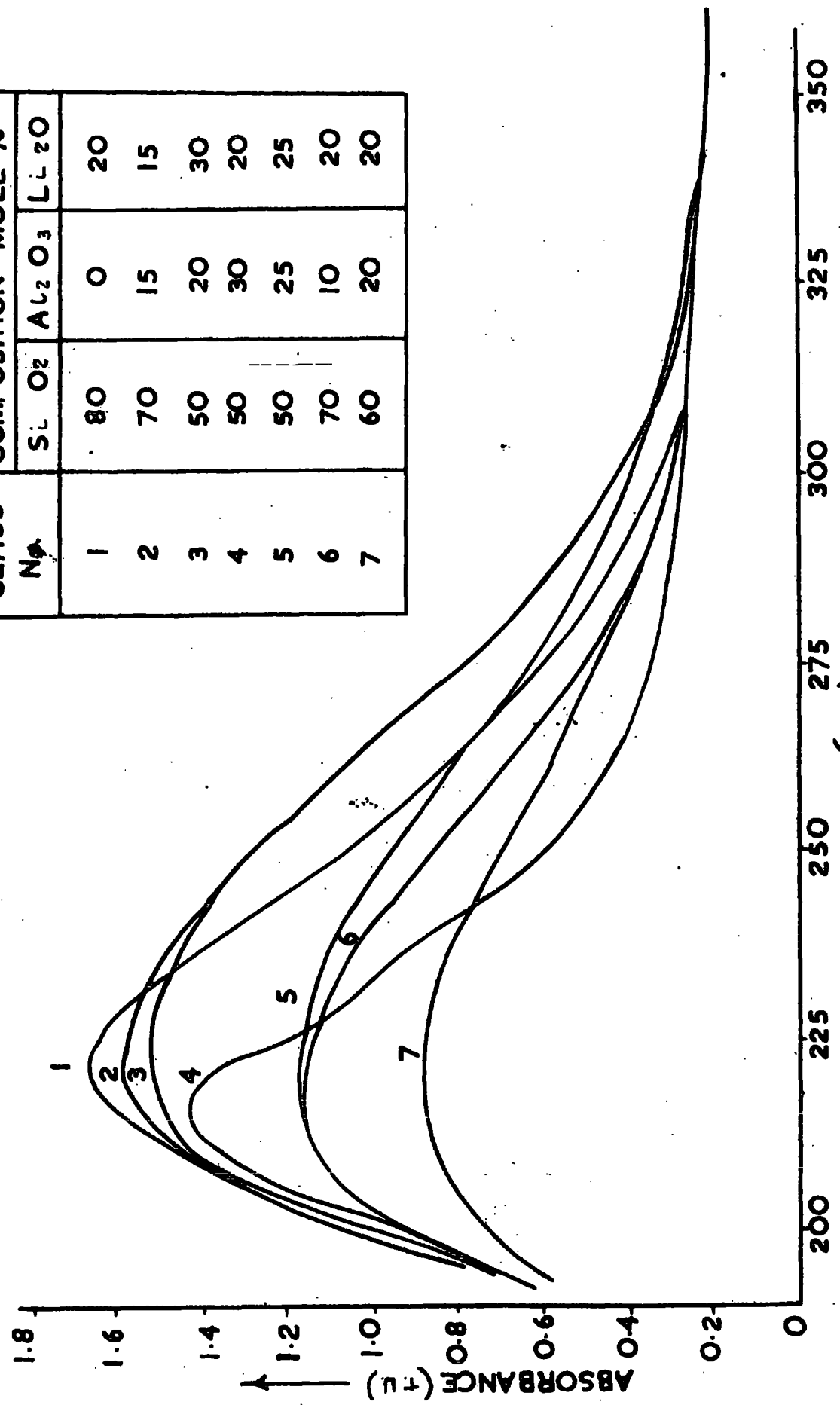

FIG 4.19 ABSORPTION OF BASE L.A.S. GLASSES BEFORE IRRADIATION.

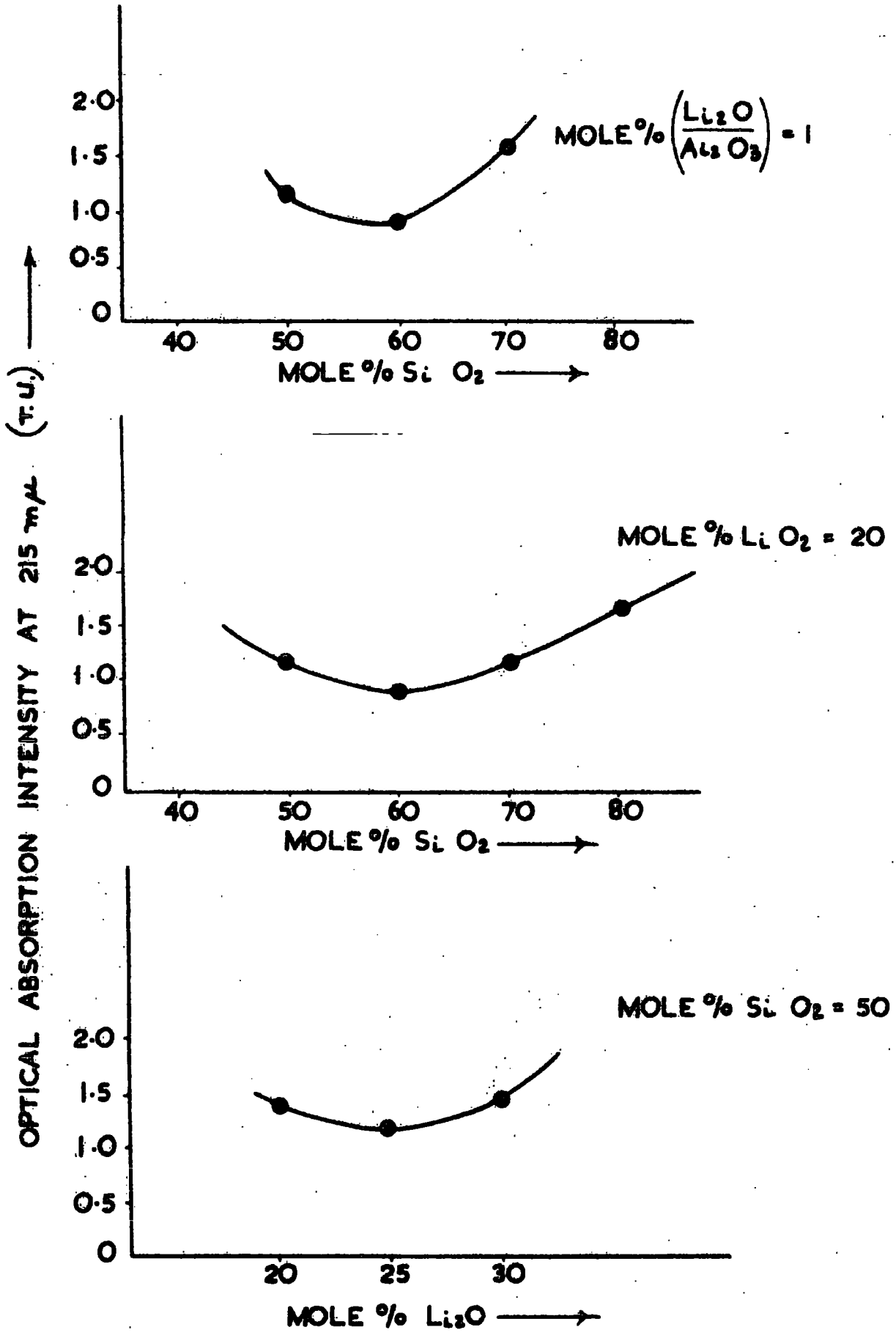

FIG 4.20 RELATIVE OPTICAL ABSORPTION IN L.A.S. BASE GLASSES.

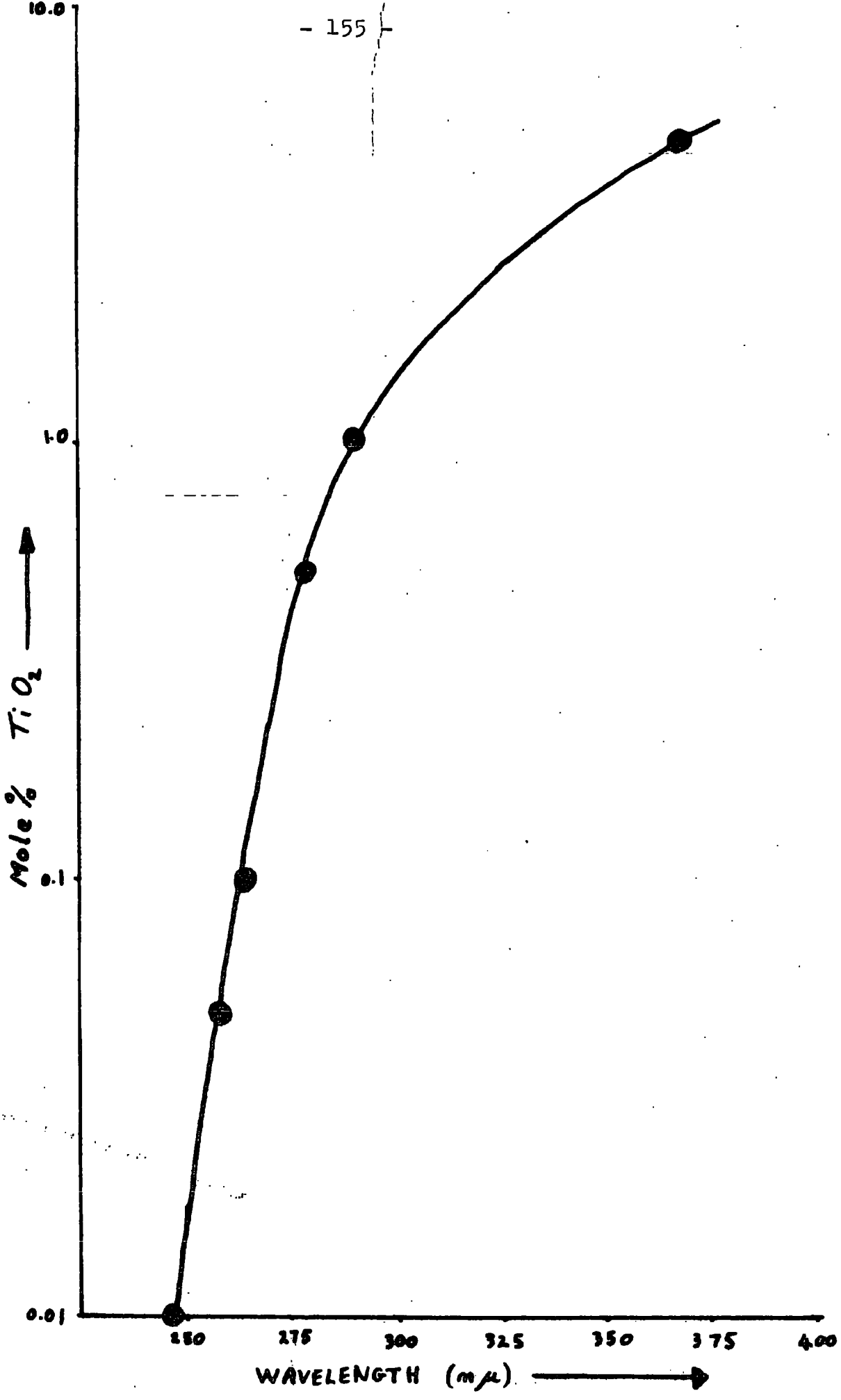

Fig 4.21 ABSORPTION AS A FUNCTION OF TiO_2 CONCENTRATION IN L.A.S. GLASS

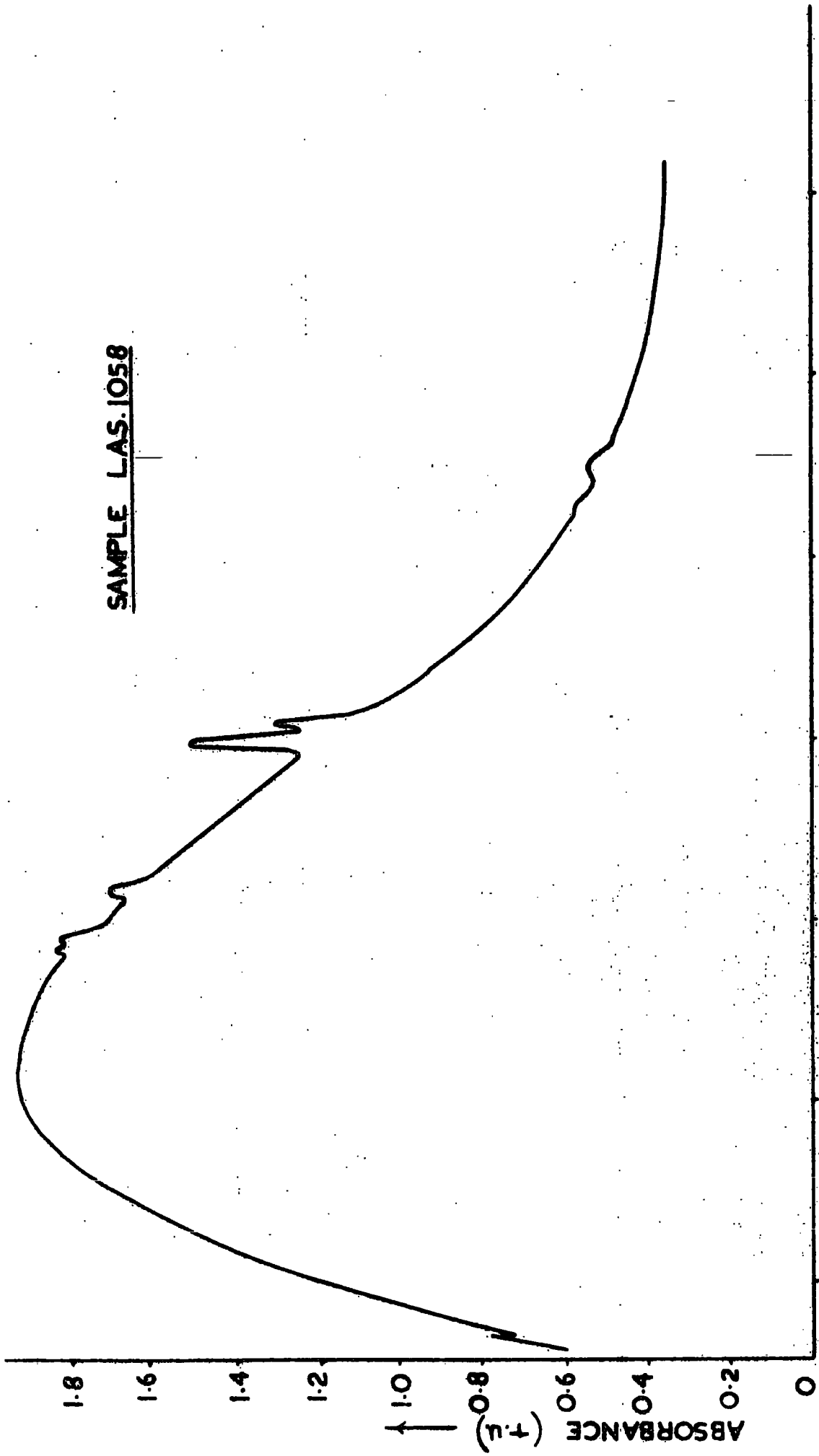

FIG 4.22 ULTRAVIOLET ABSORPTION OF GADOLINIUM CONTAINING GLASS

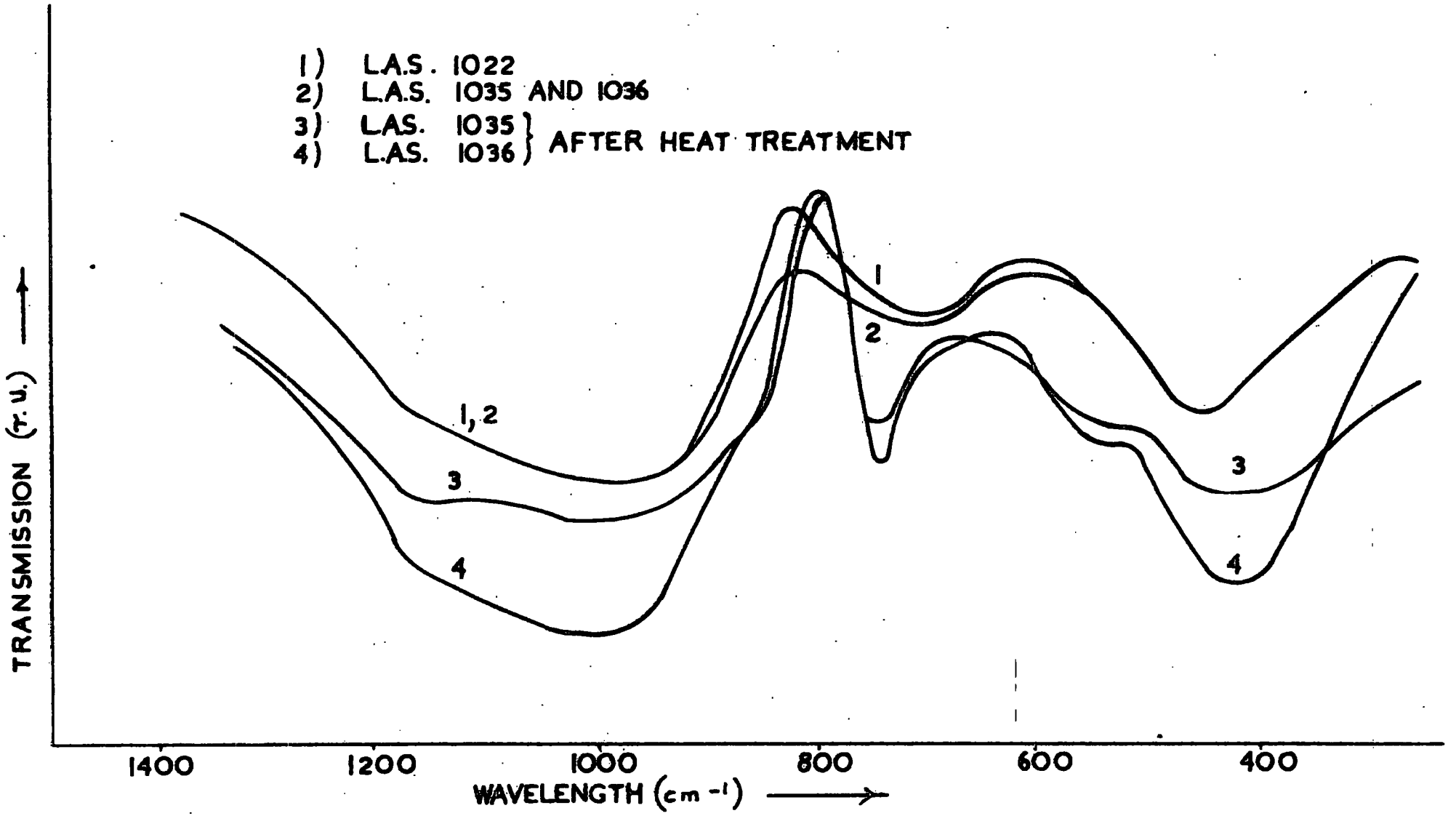

FIG 4.23 OPTICAL ABSORPTION OF GLASSES USING KBr PELLET TECHNIQUE

were subjected to heat treatment and became crystallised, narrowing of the bands and an indication of more structure in the 13.5 and 25 μ peaks was observed. This is shown in Fig.(4.23).

In an attempt to correlate the thermoluminescence observations, optical absorption spectra were taken of samples after they had been subjected to a period of X-ray irradiation. The results for the base L.A.S. 1022 glass and for this base glass with 5% TiO_2 are shown in Fig. (4.24).

These results were obtained both before (curve 1) and after (curve 2) X-ray irradiation at 295 K. The difference between the two curves is also shown (curve 3) and represents the absorption by the X-ray induced defects. This consists of two absorption bands at 2.1 - 2.2 e.V. and 3.1 - 3.2 e.V. for the specimen containing no titania and of a broad band in the region of 1 - 3 e.V. for the specimen with titania. There appears also to be a slight optical absorption in the 3,500 A and 6,000 A region for 1022 after extended irradiation periods. Absorption in the 3,500 A and 6,000 A region is also observed before irradiation with thick samples. The optical absorption of the L.A.S. 1022 glass specimen after irradiation at 77 K is shown in Fig. (4.25) for various temperatures up to room temperature. In this diagram the absorption at room temperature has been subtracted.

4.2.2. Discussion

The two components of the optical absorption found in the L.A.S. base glasses at 2,150 A and at 2,350 A can be compared with

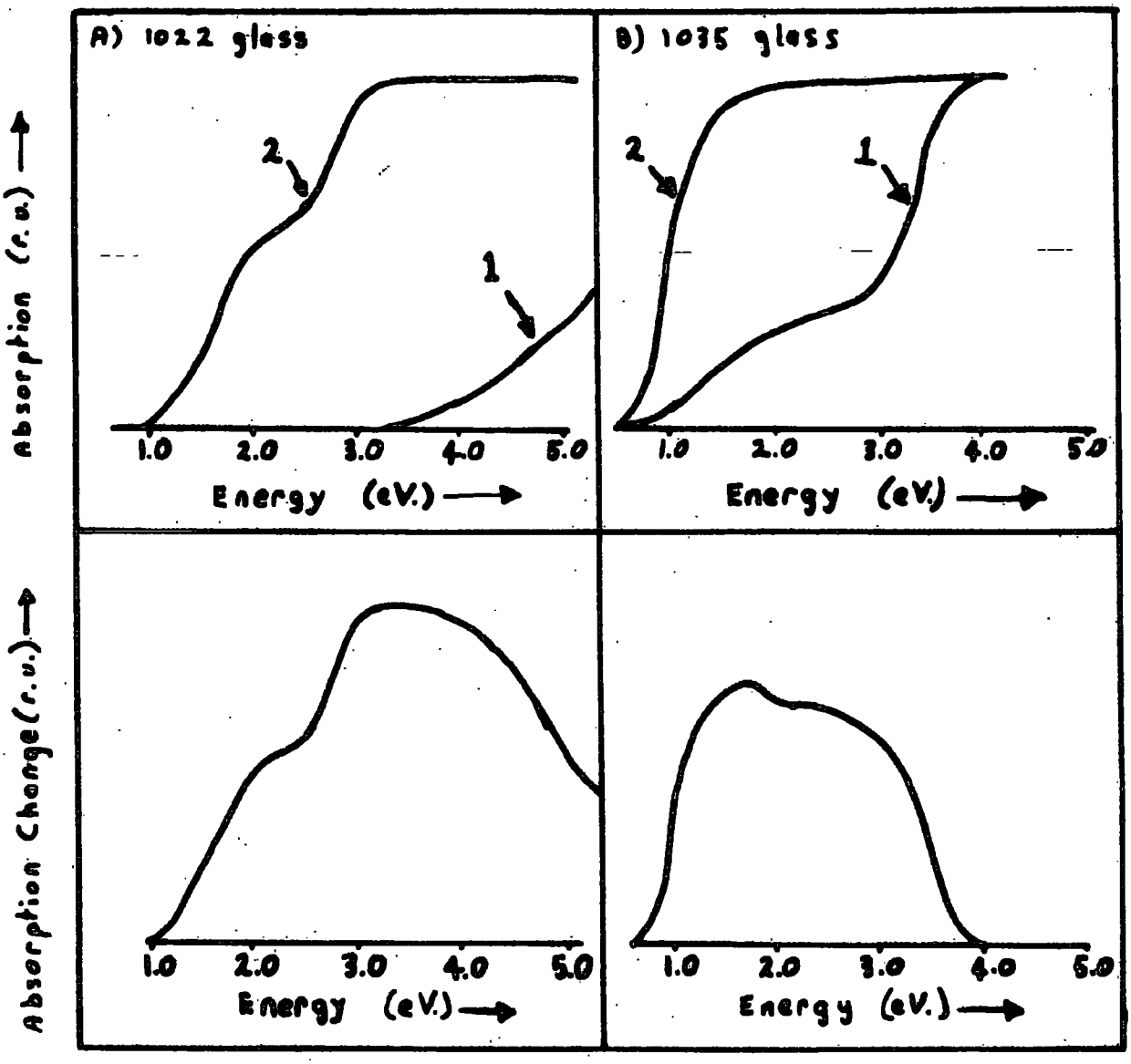

Fig 4.24 ABSORPTION DIFFERENCE BEFORE AND AFTER IRRADIATION FOR TWO L.A.S. GLASSES

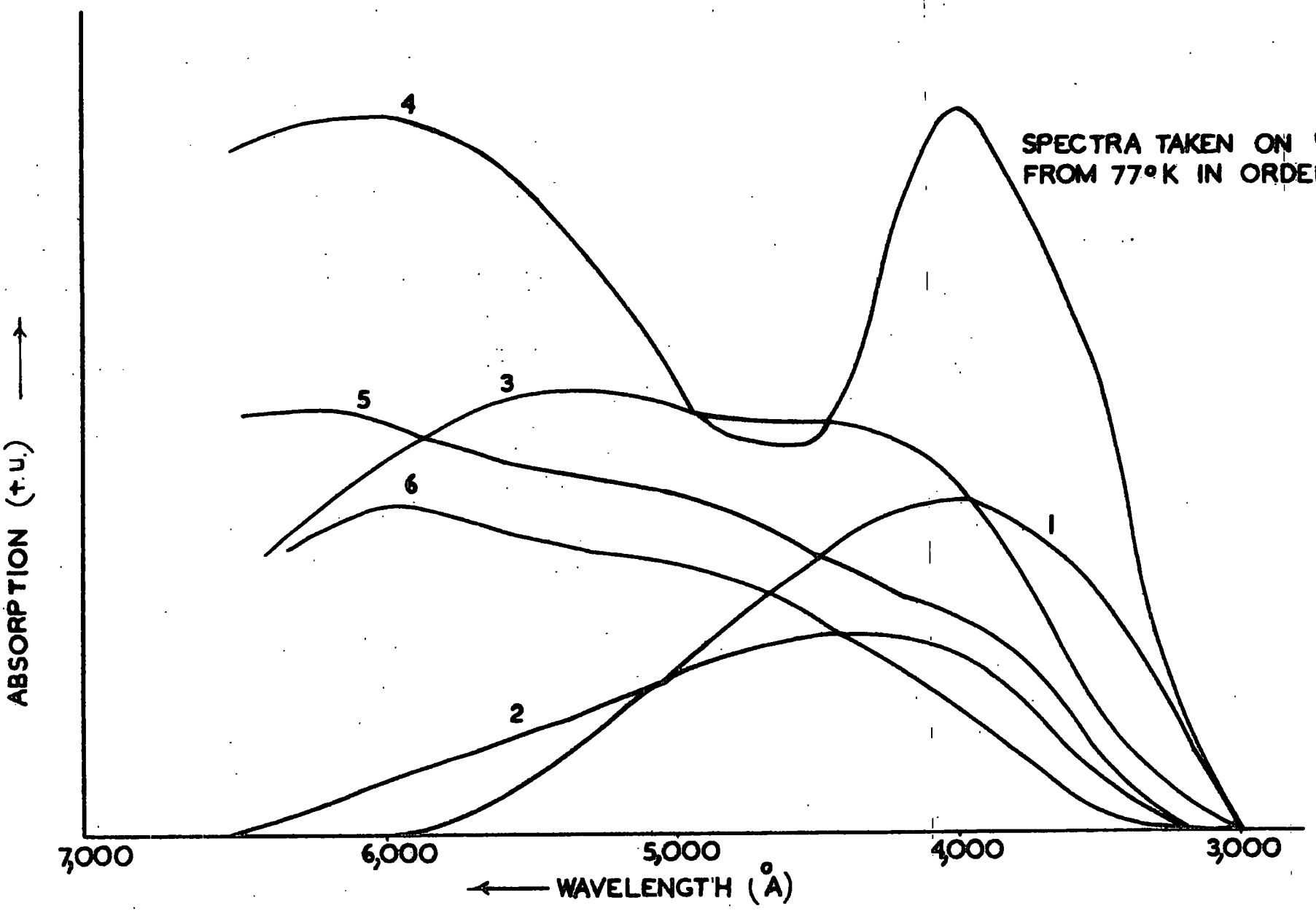

FIG 4.25 OPTICAL ABSORPTION OF LAS. 1022 AFTER IRRADIATION AT 77°K

the 2,260 A (β) and 2,380 A (α) absorptions found in additively coloured KI and attributed (4.19) to perturbations of the exciton states which produce the first fundamental absorption band of the crystal. The perturbation is caused by the proximity of an F centre (β -band) or a negative ion vacancy (α -band). So in glass it is suggested that the base glass edge absorption (8.1 e.V. in pure SiO_2) is modified near local ionic fluctuations producing increased positive and negative charges to give rise to the two absorptions near the optical absorption edge. This would agree with the fact that minimum absorption in this region was found when the Li_2O/Al_2O_3 was such as to allow local charge compensation. The increased optical absorption produced by the presence of titanium may be due to a small fraction of this ion in the Ti^{3+} state which is known to result in an absorption at 3,500 A, however, this ionic state was not detected by e.s.r. before irradiation as mentioned in Chapter 3. The absorption in the ultra-violet region caused by the presence of gadolinium has been identified as due to transitions of the Gd^{3+} ion. This is shown in Fig. (4.26) in which a comparison is made between the glass absorptions and those of the gadolinium ion in a $LnCl_3$ crystal. Three principal absorptions in the infra-red region for silicate glasses have been found at 1050 cm^{-1}, 780 cm^{-1} and 475 cm^{-1} (4.20). These have been attributed to the silicon-oxygen stretching mode within the SiO_4 tetrahedra (4.21) the intertetrahedral Si stretching mode and the Si-O bending modes respectively. In the L.A.S. glasses the 1050 cm^{-1}, Si-O stretching mode has a double component which may be assigned to an Al-O-Si bond vibration. It is also possible to correlate the absorption band at 700 cm^{-1} in

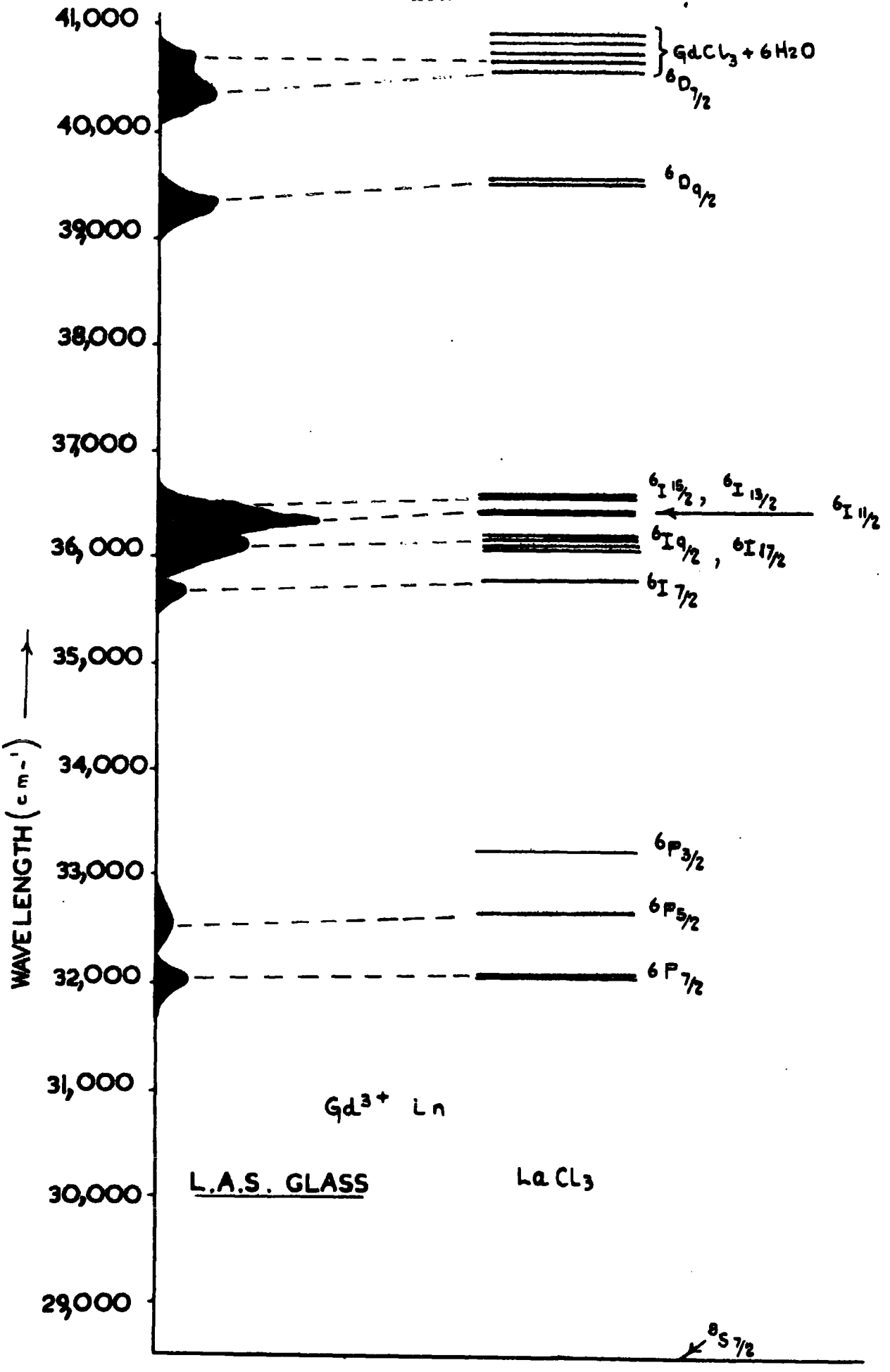

FIG 4.26 ABSORPTION LINES FOR SAMPLE L.A.S. 1058

the L.A.S. glasses to the intertetrahedral Si stretching mode. The resolution of this absorption is seen to be reduced by the incorporation of TiO_2 or Gd_2O_3 in agreement with the results of Ferraro et al. (4.20). This reduction is thought to be due to the destruction of Si - O - Si bridges by the incorporation of Na_2O and a similar bridging bond destruction is suggested when TiO_2 is added to the glass. With heat treatment this particular absorption becomes enhanced which would be expected as the development of a crystalline phase requires bonds to be formed between tetrahedra. When Gd_2O_3 is present in addition to the TiO_2 the enhancement of this absorption is less.

The 460 cm^{-1} absorption found in the L.A.S. glasses is thought to be associated with the Si - O bond bending modes by a direct comparison with the 475 cm^{-1} absorption found in sodium silicate glasses and attributed to this mode. When the glass containing TiO_2 is crystallised this absorption appears to have a double structure with peaks at 420 cm^{-1} and 550 cm^{-1}.

The optical absorption produced by X-ray irradiation is due to trapped electrons and holes, and whilst the absorption induced in the ultra-violet region is due to the former, the latter produces absorption in the visible region. This classification has been extensively studied (4.22) in sodium silicate glasses, and can be directly applied to the L.A.S. glasses as the basic silicon tetrahedra are thought to be only slightly modified. From the optical absorption measurements made after the L.A.S. glass was irradiated at 77 K some deductions can be made about the stability of the X-ray induced traps. It is evident from Fig. (4.15) that

the trap producing optical absorption at 4,000 A is unstable at room temperature and this is seen to agree with the deductions made from the thermoluminescence results.

CHAPTER 5

GENERAL CONCLUSIONS

The role of titanium in the production of glass ceramics depends upon the glass composition. For the 20 mole % lithia, 60 mole % silica, 20 mole % alumina glass studied, it would appear that phase separation does not play a part in titanium nucleation. No titanate compounds were detected during the initial crystallisation process from which it is concluded that the precipitation of a titanate compound to act as a nucleation centre is unlikely. Titanium does reduce the viscosity of a glass melt which allows easier atomic re-arrangement and this is no doubt a significant factor in the crystallisation process.

The suggestion that titanium is attached to non-bridging oxygen ions at the periphery of well ordered domains would agree with the observations made in the glass composition.

Firstly the effect of the addition of gadolinium to the glass was found not to effect the titanium nucleation but did reduce the crystal growth rate. This would be the case if gadolinium ions were located in the glassy regions, when nucleation is thought to begin at the well ordered domains. Crystal growth inhibition can then be explained by the interaction of titanium and gadolinium as the crystal front advances. Extended heat treatment results in a change in the gadolinium site occupation, discussed in Chapter 3, and appears

to be due to a gadolinium-titanium interaction which would occur at the crystal/glass interface.

A multiple site occupation is suggested for gadolinium in the glass matrix from an interpretation of electron spin resonance results with the spin Hamiltonian:-

$$\mathcal{H}(S) = g_o \beta \; H.S + D\left(S_z^2 - \tfrac{1}{3}S(S+1)\right) + \left(E(S_x^2 - S_y^2)\right)$$

The solution of this hamiltonian has allowed all the major features of the experimental results to be found. To obtain a reasonable fit between calculated and experimental results two crystal field values for the gadolinium ion environment are required. In the lithium aluminium silicate glasses the main site for gadolinium has a crystal field with $D \approx 0.018\ cm^{-1}$ and $E \approx 0.005\ cm^{-1}$ whilst a site also occurs with $D \approx 0.065\ cm^{-1}$ and $E \approx 0.025\ cm^{-1}$.

When the glass lattice is changed the relative occupation of these two sites changes. An increase in the high g value component of the electron spin resonance absorption corresponding to an increase in the relative number of high crystal field sites. This is particularly noticeable when the glass lattice containing the gadolinium is changed to sodium borosilicate.

The observation of X-ray irradiated defects is also in agreement with the idea of local well ordered domains existing within the glass. E.S.R. results showed that the defects, thought to be due to silicon-oxygen tetrahedra, with an electron in a

meta-stable position, were unchanged after crystallisation. If well ordered regions did not exist a narrowing or a reduction in intensity of the defect lines would be expected after crystallisation. From the optical absorption and thermoluminescence work it is evident that a forbidden energy gap exists in the glass as well as in the crystalline state. Recent work (5.1) has shown that an amorphous material can give rise to such a band gap if local well ordered regions exist with dimensions of the order of 100 A. Unfortunately this is just below the detection limit of the electron microscopy techniques employed.

If the crystal growth inhibition found to be produced by the presence of gadolinium in the lithium aluminium silicate glasses is due to the presence of gadolinium in the interstitial (high crystal field) site, an increased inhibition may be found in glass systems which favour this interstitial site. Although advantageous nucleation properties of a gadolinium containing titanate glass-ceramic have been found, to enable this to be developed requires more extensive tests. Especially relevant would be the effect of the rare earth purity and the measurement of the physical properties of the glass-ceramic produced.

APPENDIX 1

Computer Programmes

The programmes given were used on the I.B.M. 360/67 computer of the Universities of Durham and Newcastle upon Tyne.

CONTENTS

DIAG

```
 1    (SUBRG):
 2   DIAG:PROC OPTIONS (MAIN);
 3   DCL(A(N,N),R(N,N))BIN FLOAT CONTROLLED;
 4   DCL(N,MV) FIXED BIN,DATA FILE STREAM INPUT;
 5   DCL(B(N,N),E(N,N) FLOAT CONTROLLED,DATA FILE STREAM INPUT;
 6    DCL(IND) FIXED BIN;
 7    DCL(F(N,N),G(N,N)) FLOAT CONTROLLED,DATA FILE STREAM INPUT;
 8    DCL YY FIXED BIN INITIAL(0);
 9    DCL(MMM)FLOAT;
10    DCL(ZZZ)FLOAT;
11    DCL(INCH)FIXED BIN;
12    DCL(NNN,COUNT)FIXED BIN;
13    DCL XX FLOAT;
14    DCL(MIN,MAX)FLOAT;
15    DCL(SUM(501))FLOAT;
16    DCL(Y,Q)FLOAT;
17    DCL(P,M,T,INCT)FLOAT;
18   DCL(C(N,N),D(N,N))BIN FLOAT CONTROLLED;
19   DCL(INDD)FIXED BIN;
20   DCL(MAXH,DF,EF)FLOAT;
21   DCL(H,I,J,K,L,S)FIXED BIN;
22    DCL Q FIXED BIN;
23    PUT LIST('DATA FORM:MIN,MAX,T(INIT),INCT,P(INIH),MAXH,
       IND(=1(0))');
24   PUT LIST('G VALUE .....DF.....EF');
25   PUT SKIP;
26    GET LIST(MIN,MAX);
27   GET LIST(T,INCT,P,MAXH);
28    PUT DATA(T,INCT,P,MAXH);
29   PUT SKIP;
30   GET LIST(INDD);
31    GET LIST(Q);
32    PUT DATA(INDD,Q);
33   GET LIST(DF,EF);
34   PUT LIST(DF,EF);
35    GET LIST(INCH);
36   PUT SKIP;
37   GET FILE(DATA) LIST(N,MV);
38   ALLOCATE A;
39   ALLOCATE B;
40   ALLOCATE C;
41   ALLOCATE D;
42   ALLOCATE E;
43   ALLOCATE R;
44   ALLOCATE F;
45   ALLOCATE G;
46   M=P
47   DO I=1 TO N;
48   DO J=1 TO N;
49    GET FILE(DATA) LIST(B(I,J));
50   END;
51   END;
```

```
52    B=B*DF;
53    DO I=1 TO N;
54    DO J=1 TO N;
55   GET FILE(DATA) LIST(E(I,J));
56   END;
57   END;
58    E=E*EF;
59   DO I=1 TO N;
60   DO J=1 TO N;
61   GET FILE(DATA) LIST(F(I,J));
62   END;
63   END;
64    G=F;
65   L2:P=M;
66    COUNT=0;
67    AGAIN: F=G;
68    F=0.0935*P*0.5*F*SIN(T);
69    A=B+E+F;
70   C=0;
71    COUNT=COUNT+1;
72   DO J=1 TO N;
73    C(J,J)=0.0935*P*(4.5-J)*COS(T);
74    END;
75   A=A-C;
76   D=A;
77   CALL MSDU(A,R,N,MV);
78    DO K=1 TO 8;
79   DO L=1 TO 8;
80    XX=A(K,K)-A(L,L);
81    IF XX< MIN THEN GO TO FRED;
82    IF XX> MAX THEN GO TO FRED;
83    SP=2.64575*(R(1,K)*R(2,L)+R(7,K)*R(8,L))
84    +3.46410*(R(2,K)*R(3,L)+R(6,K)*R(7,L))
85    +3.87298*(R(3,K)*R(4,L)+R(5,K)*R(6,L))
86    +4.0*R(4,K)*R(5,L);
87    SM=2.64575*(R(2,K)*R(1,L)+R(8,K)*R(7,L))
88    +3.46410*(R(3,K)*R(2,L)+R(7,K)*R(6,L))
89    +3.87298*(R(4,K)*R(3,L)+R(6,K)*R(5,L))
90    +4.0*R(5,K)*R(4,L);
92    W=SP**2+SM**2;
93    W=W*(2*SIN(T)+COS(T));
94    IF W < 0.0001 THEN GO TO FRED;
95    PUT SKIP;
96    PUT LIST('H VALUE');
97    PUT EDIT(P)(F(5,2));
98    PUT EDIT('ANGLE=',T)(A(8),F(5,2));
99    PUT SKIP
100   PUT LIST('EIGEN VALUES ARE');
101   PUT SKIP;
102   PUT LIST(A(K,K),A(L,L),K,L,P,T);
103   PUT EDIT('TRANSITION PROB=',W)(X(5),A(18),F(9,4));
104   NNN=COUNT;
105   SUM(NNN)=SUM(NNN)+W;
106   PUT SKIP;
107   FRED:END;
108   END;
```

```
   115.5  Y=MAXH-0.02;
   117     IF P > Y THEN GO TO L4;
   118    IF P > MAXH THEN GO TO L4;
   121     ZZZ=INCH/50;
   122     P=P+ZZZ;
   123    GO TO AGAIN;
   131     L4:IF T > 1.49 THEN GO TO L3;
   133     T=T+INCT;
   134    GO TO L2;
   135     L3:DO NNN=1 TO COUNT;
   136     MMM=NNN/50;
   138     PUT LIST(MMM,SUM(NNN));
   139     PUT SKIP;
   140     END;
END OF FILE
```

MSDU

```
1     MSDU:PROCEDURE (A,R,N,MV);
2     DECLARE
3         (I,IND,J,L,M,MV,N)
4         FIXED BINARY,
5         ERROR EXTERNAL CHARACTER (1),
6         (A(*,*),R(*,*),ANORM,ANRMX,THR,U,Y,SINX,
7         SINX2,COSX,COSX2,SINCS,FN)
8         BINARY FLOAT;
9     ERROR='0';
10     IF N < = 1
11    THEN DO;
12        ERROR='1';
13        GO TO FIN;
14        END;
15    FN=N;
16    IF MV=0
17    THEN DO;
18          DO I=1 TO N;
19            DO J=1 TO N;
20            R(I,J)=0;
21            END;
22          R(I,I)=1;
23          END;
24        END;
25    ANORM=0;
26        DO I=1 TO(N-1);
27          DO J=(I+1 ) TO N;
28          ANORM=ANORM+A(I,J)*A(I,J);
29          END;
30        END;
31    IF  ANORM < = 0. 0
32    THEN GO TO SORT;
33    ANORM=1.414* SQRT(ANORM);
34    ANRMX=ANORM*1.0E-6/FN;
35    IND=0;
36    THR=ANORM;
37    S10:
38       THR=THR/FN;
39    S20:
40       L=1;
41    S30:
42       M=L+1;
43    S40:
44       IF ABS(A(L,M))> =THR
45       THEN DO;
46          IND=1;
47          U=0.5*(A(L,L)-A(M,M));
48          Y=-A(L,M)/SQRT(A(L,M)*A(L,M)+U*U);
```

```
49          IF U< 0.0
50          THEN Y=-Y;
51          SINX=Y/SQRT(2.0*(1.0+(SQRT(1.0-Y*Y))));
52          SINX2=SINX*SINX;
53          COSX=SQRT(1.0-SINX2);
54          COSX2=COSX*COSX;
55          SINCS=SINX*COSX;
56            DO I=1 TO N;
57            IF I < L
58            THEN DO;
59              IF I < M
60              THEN DO;
61                U=A(I,L)*COSX-A(I,M)*SINX;
62                A(I,M)=A(I,L)*SINX+A(I,M)*COSX;
63                A(I,L)=U;
64                END;
65              END;
66          ELSE IF I > L
67          THEN DO;
68            IF I < M
69            THEN DO;
70              U=A(L,I)*COSX-A(I,M)*SINX;
71              A(I,M)=A(L,I)*SINX+A(I,M)*COSX;
72              END;
73            ELSE IF I > M
74            THEN DO;
75              U=A(L,I)*COSX-A(M,I)*SINX;
76              A(M,I)=A(L,I)*SINX+A(M,I)*COSX;
77              END;
78            IF I ¬ =M
79            THEN A(L,I)=U;
80            END;
81          IF MV=0
82          THEN DO;
83            U=R(I,L)*COSX-R(I,M)*SINX;
84             R(I,M)=R(I,L)*SINX+R(I,M)*COSX;
85            R(I,L)=U;
86            END;
87          END;
88        U=2.0*A(L,M)*SINCS;
89        Y=A(L,L)*COSX2+A(M,M)*SINX2-U;
90        U=A(L,L)*SINX2+A(M,M)*COSX2+U;
91        A(L,M)=(A(L,L)-A(M,M))*SINCS+A(L,M)*(COSX2-SINX2);
92        A(L,L)=Y;
93        A(M,M)=U;
94        END;
95      IF M ¬ = N
96    THEN DO;
97          M=M+1;
98          GO TO S40;
99          END;
```

```
   100     IF L ¬ =(N-1)
   101     THEN DO;
   102         L=L+1;
   103         GO TO S30;
   104         END;
   105     IF IND =1
   106     THEN DO;
   107         IND=0;
   108         GO TO S20;
   109         END;
   110     IF THR > ANRMX
   111     THEN GO TO S10;
   112     SORT:
   113         DO I=1 TO N;
   114           DO J=1 TO N;
   115           IF A(I,I) < A(J,J)
   116           THEN DO;
   117             U=A(I,I);
   118             A(I,I)=A(J,J);
   119             A(J,J)=U;
   120             IF MV=0
   121             THEN DO;
   122               DO L= 1 TO N;
   123               U=R(L,I);
   124               R(L,I)=R(L,J);
   125               R(L,J)=U;
   126               END;
   127             END;
   128           END;
   129         END;
   130     END;
   131     FIN:
   132     RETURN;
   133     END;
END OF FILE
```

BERT

```
      SUBROUTINE REDSK(IPOS,INC,IVAL)
      ML=(IPOS-1)/1600
      LK=IPOS-1600*ML
      IL=ML+INC
      READ(IL'LK)IVAL
      RETURN
      END


      SUBROUTINE START(K,L)
      CALL CHUNG(J)
      IF(J)1,2,2
1     K=(J+1)/256+255
      L=J-256*(K-256)
      RETURN
2     K=J/256
      L=J-256*K
      RETURN
      END


      SUBROUTINE WRISK(IPOS,INC,IVAL)
      ML=(IPOS-1)/1600
      LK=IPOS-1600*ML
      IL=ML+INC
      WRITE(IL'LK)IVAL
      RETURN
      END


      INTEGER TITLE (60),COUNT
      REAL NOMU,LAMDA,MULT
      DIMENSION N(2),ICH(4),K2(2),MAXPO(400),ITEM(8645)
      EQUIVALENCE (ICH(4),N(2))
      DATA MULT/1.0084/
      DEFINE FILE 1(1600,1,U,MILK),2(1600,1,U,MILK),
      3(1600,1,U,MILK),4(1600,1,U,MILK),5(1600,1,U,MILK),
      6(1600,1,U,MILK)
      DATA PI/3.141592654/
      K2(1)=1
      K2(2)=4
      I3=200
```

```
      PIO2=0.5*PI
      J=0
      KJ=0
      I1=0
      JK=1
      JJJ=1
      READ(2,  1)TITLE,LAMDA,NOMU,MAX1,IR
    1 FORMAT(40A2,/,20A2,2F10.0,215)
      CALL CHUNG(I,J)
    2 DO    3 I=1,2
      JJA=2*(I-1)+1
    3 CALL START(ICH(JJA),ICH(JJA+1))
      IF(ICH(4)-221)14,4,14
    4 DO    7 I=1,3
      IF(ICH(I)-16)7,7,5
    5 ICH(I)=ICH(I)-16
      IF(ICH(I)-10)7,6,6
    6 ICH(I)=ICH(I)-10
    7 CONTINUE
      I2=100*ICH(1)+10*ICH(2)+ICH(3)
      IF(I3-I2)9,9,8
    8 I3=I2
    9 IF(JK*(I2-I1))10,13,13
   10 JK=-JK
      KL=(JK+3)/2
      GO TO (11,12),KL
   11 KJ=KJ+1
   12 CALL WRISK(KJ,K2(KL),J)
   13 I1=I2
      J=J+1
      ITEM(J)=I2
      GO TO    2
   14 K3=J
      WRITE(3,   15)
   15 FORMAT(1H1)
      WRITE(3,   16)TITLE
   16 FORMAT(1X,60A2,//)
      AA=LAMDA+0.00005
      BB=NOMU+0.05
      WRITE(3,   17)AA,BB,MAX1,IR
   17 FORMAT(10H LAMBDA=,F8.4,//,16H SIZE OF STEP = ,F5.1,8H
      MICRONS ,'/1/,' FIRST PEAK IS BASED ON',I4,//,'
      PEAK HEIGHT =',I3,//)
      KJ=KJ-1
      ISUF=0
      L=0
   18 K=L+1
      L=K
      CALL REDSK(K,K2(1),NPO)
      IMAX=ITEM(NPO)
   19 CALL REDSK(L,K2(2),IL2)
      MIN=ITEM(IL2)
      IF((IMAX-MIN)-IR)20,23,23
```

```
      PIO2=0.5*PI
      J=0
      KJ=0
      I1=0
      JK=1
      JJJ=1
      READ(2,  1)TITLE,LAMDA,NOMU,MAX1,IR
    1 FORMAT(40A2,/,20A2,2F10.0,215)
      CALL CHUNG(I,J)
    2 DO    3 I=1,2
      JJA=2*(I-1)+1
    3 CALL START(ICH(JJA),ICH(JJA+1))
      IF(ICH(4)-221)14,4,14
    4 DO    7 I=1,3
      IF(ICH(I)-16)7,7,5
    5 ICH(I)=ICH(I)-16
      IF(ICH(I)-10)7,6,6
    6 ICH(I)=ICH(I)-10
    7 CONTINUE
      I2=100*ICH(1)+10*ICH(2)+ICH(3)
      IF(I3-I2)9,9,8
    8 I3=I2
    9 IF(JK*(I2-I1))10,13,13
   10 JK=-JK
      KL=(JK+3)/2
      GO TO (11,12),KL
   11 KJ=KJ+1
   12 CALL WRISK(KJ,K2(KL),J)
   13 I1=I2
      J=J+1
      ITEM(J)=I2
      GO TO    2
   14 K3=J
      WRITE(3,   15)
   15 FORMAT(1H1)
      WRITE(3,   16)TITLE
   16 FORMAT(1X,60A2,//)
      AA=LAMDA+0.00005
      BB=NOMU+0.05
      WRITE(3,   17)AA,BB,MAX1,IR
   17 FORMAT(10H LAMBDA=,F8.4,//,16H SIZE OF STEP = ,F5.1,8H
      MICRONS,/1/,' FIRST PEAK IS BASED ON',I4,//,'
      PEAK HEIGHT =',I3,//)
      KJ=KJ-1
      ISUF=0
      L=0
   18 K=L+1
      L=K
      CALL REDSK(K,K2(1),NPO)
      IMAX=ITEM(NPO)
   19 CALL REDSK(L,K2(2),IL2)
      MIN=ITEM(IL2)
      IF((IMAX-MIN)-IR)20,23,23
```

```
20    L=L+1
      IF(L-KJ)21,21,28
21    CALL REDSK(L,K2(1),IL2)
      MAX=ITEM(IL2)
      IF (IMAX-MAX)22,19,19
22    IMAX=MAX
      NPO=IL2
      K=L
      GO TO   19
23    J=K
24    J=J-1
      IF(J)26,26,25
25    CALL REDSK(J,K2(2),IL1)
      MIN=ITEM(IL1)
      IF((IMAX-MIN)-IR)27,26,26
26    ISUF=ISUF+1
      MAXPO(ISUF)=NPO
      GO TO   18
27    CALL REDSK(J,K2(1),IL1)
      MAX=ITEM(IL1)
      IF(IMAX-MAX)18,24,24
28    CONTINUE
      WRITE(3,  29)
29    FORMAT(7X,'POSITION',6X,'VALUE',7X,'MILLIMETRES',11X,'D')
      DO   39 I=1,ISUF
      IZZ=0
      MM=MAXPO(I)
      I2=ITEM(MM)
      DO   32 IL=1,2
      IZ=2*IL-3
      M=MM
30    M=M+IZ
      IF(M)32,32,31
31    I4=ITEM(M)
      IF((I2-I4)-2)30,30,32
32    N(IL)=M
      MM=(N(1)+N(2))/2
      I4=ITEM(MM)-I3
      GO TO (33,36),JJJ
33    COUNT=I
      IF(I4-MAX1)39,39,34
34    JJJJ=MM
      JJJ=2
      WRITE(3,   35)I4
35    FORMAT(12X,'O',9X,I3,27X,'INFINITY')
      GO TO   38
36    IM=MM-JJJJ
      AMM=IM
      AM=AMM*NOMU*0.001
      AMM=AM*PI/720.0
      AMM=LAMDA/(2.0*SIN(AMM))+0.0005
      AM=AM+0.0005
      DK=MULT*(AMM-0.0005)+0.0005
      WRITE(3,   37)IM,I4,AM,AMM,DK
```

```
37    FORMAT(9X,I4,9X,I3,10X,F7.3,2(10X,F8.3) )
38    IZZ=1
39    MAXPO(I)=IZZ*MM
      JN=ISUF-COUNT+1
      WRITE(3,   40)JN
40    FORMAT(//,'NO OF PEAKS= ',I3)
      AJJJJ=JJJJ
      AJJ=AJJJJ-300.0
      CALL SCALF(0.01,0.01,AJJ,0.0)
      CALL FPLOT(+2,AJJ,1000.0)
      CALL FPLOT(0,AJJ,0.0)
      CALL FPLOT(+1,-200.0,+50.0)
      DO   41 KLK=1,2
      L1=30*(KLK-1)+1
      L2=L1+29
      XS=FLOAT(JJJJ-220+20*KLK)
      CALL FCHAR(XS,+50.0 ,0.15,0.1,PI02)
41    WRITE(7,  42)(TITLE(LKL),LKL=L1,L2)
42    FORMAT(30A2)
      NMI=5000/NOMU
      LOOP=(K3-1)/NMI+2
      DO   43 KIK=1,LOOP
      XCOOR=FLOAT(NMI*(KIK-1))+AJJJJ-15.0
      IVAL=5*(KIK-1)
      CALL FCHAR(XCOOR,-25.0,0.10,0.1,0.0)
43    WRITE(7,  44)IVAL
44    FORMAT(I3)
      DO   47 II=COUNT,ISUF
      I=ISUF-II+COUNT
      IF(MAXPO(I))47,47,45
45    MA=MAXPO(I)
      IV=ITEM(MA)
      VI=FLOAT(IV+25)
      AMA=FLOAT(MA)
      CALL FPLOT(-2,AMA,VI)
      DO   46 JK=1,2
46    CALL POINT(3)
      CALL FPLOT(1,AMA,VI)
47    CONTINUE
      CALL FPLOT(+1,0.0,0.0)
      CALL FPLOT(-2,0.0,0.0)
      CALL DATSW(0,IGOR)
      GO TO (48,49),IGOR
48    WRITE(3,  15)
      WRITE(3,  16)TITLE
49    L=1
      NN=25
      M=(K3-1)/25
      NREM=K3-25*M
      DO   53 I=1,M
50    DO   51 J=1,NN
      NO=25*(I-1)+J
      TITLE(J)=ITEM(NO)
      XNO=NO
      Y=TITLE(J)
```

```
   51     CALL FPLOT(O,XNO,Y)
          GO TO (52,53),IGOR
   52     WRITE(3,  56)I,(TITLE(J),J=1,NN)
   53     CONTINUE
          GO TO(54,57),L
   54     IF(NREM)57,57,55
   55     L=2
          NN=NREM
          I=M+1
          GO TO   50
   56     FORMAT(1X,26(I3,1X))
   57     CALL EXIT
          END
END OF FILE
```

REFERENCES

CHAPTER 1

1. 1 Mackenzie, J.D. Modern Aspects of the Vitreous State 1. 1 (1960)

1. 2 Weyl, W.A. & Marboe, E.C. Glass Industry Vol.41 8 Aug. (1960)

1. 3 Zachariasen, W.H. J.Amer. Chem.Soc. 54 3841 (1932)

1. 4 Porai-Koshits, E.A. The Structure of Glass 5(1966)

1. 5 Evans, P L. & King, S.V. Nature 212, 1353 (1966)

1. 6 Bell, R.J. & Dean, P. Nature 212, 1354 (1966)

1. 7 Stookey, S.D. U.S. Pat. 2,920,971 (1960)

1. 8 Beals, M.D. The Glass Ind. Dec. (1963) P.679-694

1. 9 Turnbull, R.C. & Lawrence, W.G. J.of Am. Ceram.Soc.Vol.35(2) 1952, 48 - 53

1.10 Janakirama Rao, Bh.V, Phys. & Chem.of Glasses Vol.4 No.1 Feb. 1963

1.11 Vogel, W. Structure of Glass 6 114 (1966)

1.12 Doherty, P.E., Lee, D.W. & Davies, R.S. J. of Am. Ceram. Soc. Vol.50 No.2 77-81

1.13 Martin, F.W. Phys. & Chemistry of Glasses Vol.6 No.4 Aug. 1965, 143-146

1.14 Barry, T.I. et al. J. Materials Science 4,7 (1969)596-612 and J. Materials Science 5 (1970) 117-126

1.15 Sakka, S. & Mackenzie, J.D. J. of non-crystalline solids 1,107 (1969) (and references therein)

1.16 Barry, T.I. & Lay, L.A. Reactiv. Sol. Proc.Int.Symp. (1968 publ.1969, J.W. Mitchell ed.) 685-694

1.17 Sands, R.H. Phys. Rev. 99 1222 (1955)

1.18 Castner, T.(Jr.)., Newell, G.S., Holton, W.C. & Slichter, C.P. J. Chem.Phys. 32,668 (1960)

1.19 Rogerson, P.S. Mineralogical Magazine Vol.37 No.291 Sept. 1970 p. 741-758

1.20 Mann, M.M. (1969) Ph.D. Thesis. University of Southern California

1.21 Rice, D.K., & Deshazer, L.G. Phys.Rev. Vol. 186 No.2 Oct. 1969 387-392

1.22 Nicklin, R.C. Ph.D. Thesis, Nov 1967 Iowa State University.

1.23 Van Wieringen, J.S. & Katz, A. 1957 Philips Res. Rept.12 432-454

1.24 Byurganovskaya, G.V. & Orlov, N.F. 1962 Optics and Spectroscopy 12, 151-154

1.25 Schulman, J.H. & Compton, W.D. 1962 Colour Centres in Solids, pp 368-384 (MacMillan Co., New York)

1.26 Karapetyan, G.O. & Reishakhrit, A.L. 1967 Izv. Akad. Nauk .. SSSR,.. Neorg.Mater 3, 217

1.27 Mackey, T.H., Boss T.W. and Kopp, M. 1970 Phys. And Chem. of Glasses 11, 205-212

1.28 Stroud, J.S., Schreurs, J.W.H. and Tucker, R.F. 1965 Proceedings of 7th InternationalCongress on Glass, Belgium, pp 7-24

1.29 Sidorov, T.A., Tyulkin, V.A. and Aksenov, Z. 1967 Prd. Spectrosk 7, 778-782

1.30 Sidorov, T.A., Tyulkin, V.A. and Aksenov, Z. Dokl Akad. Nauk SSSR 175 1094-1096 (1967)

CHAPTER 2

2. 1 Clinton, D., Mercer, R.A. and Miller R.P. J. Mat.Sci. 5(1970) 171-181

2. 2 Debye, P. Ann. Physik, 46,809 (1915)

2. 3 Van Vleck, (1940) Phys. rev. 57,426

2. 4 Van Vleck, (1948) Phys. rev. 74,1168

2. 5 Pryce, M.H. and Stevens, K.W.H. (1950) Proc. Phys.Soc. A,63,36

CHAPTER 3

3. 1 Clinton, D., Mercer, R.A., Miller, R.P. Mater.J. Sci. 5(1970) 171

3. 2 Rogers, P.S.. Minerological Magazine 37 (1970) 291

3. 3 Vojnovich, T. and Mcgee, T.D. J.Am.Ceramic Vol.52 7 July (1969) 386-392

3. 4 Van Vleck, J.H. & Penney, W.G. Phil.Mag. 17,961 (1934)

3. 5 Abragam, A. and Pryce, M.H. Proc. Roy.Soc. 205 (1951 A) 135

3. 6 Slater, J.C. Quantum Theory of Atomic Structure Vol. 1, McGraw-Hill, Ch.11 (1960)

3. 7 Stevens, K.W.H. Proc. Phys. Soc. (London) A65 (1952) 209

3. 8 Bleaney, B. & Stevens, K.W.H. Rept. Progr. Phys. 16 (1953) 108

3. 9 Hutchings, M.T. Solid State Physics 16 (1964) 227-271

3.10 Abragam, A. & Bleaney, B. Electron Paramagnetic Resonance of Transition Ions, International Series of Monographs on Physics. Clarendon Press Oxford (1970)

3.11 Pake, G.E. (P.33) Paramagnetic Resonance. W.A. Benjamin Inc., New York, (1962)

3.12 Yarif'yanov ,N.S., Timerov R.Kh. & Usacheva, N.F. F.Zika Iverdaga Tela, 4. 11 (1962) 3344

3.13 Chepleva, I.V., Lazukin, V.N., & Dembovskii, S.A. Izvestiya Akademii Nauk. SSSR, Neorganicheskie, Materialy 4, 11 (1968) 1927

3.14 Nicklin, R.C. Ph.D. Thesis, Nov.(1967) Iowa State University

3.15 Koster, G.F. & Statz, H. Phys. Rev. 113, 2(1959) 445

3.16 Statz, H. & Koster, G.F. Phys. Rev. 115, 6(1959) 1568

CHAPTER 4

4. 1 Shulgin, B.V., Taylor, K.N.R., Hoaksey, A. and Hunt, R.P. 1972 J. Phys. C. Solid State Phys. Vol. 5 1716 - 1726

4. 2 Herring, A.P., Dean, R.W., and Drobnick, J.K. 1968 Rept. Am. Ceram. Soc. 70th Annual Meeting Glass Discussion Chicago, April 24, 1968

4. 3 Karapetyan, G.O., and Reishakhrit, A.L. Izv. Akad. Nauk. SSSR Neorg. Mater. 3, 217 (1967)

4. 4 Gurney, R.W. and Mott, N.F. Trans. Farad Soc. 35(1939) 69

4. 5 Bieringer, R.J., and Montgomery, C.G. Phys. Rev. B Vol. 2 12 Dec. 1970 pp 4988 - 4994

4. 6 Fritzsche, H. J. Non.Crystalline Solids 6(1971) 49-71

4. 7 Urbach, F. Akad. Wiss Wien Ber. 11A (1930) 139,363

4. 8 Randall, J.T., and Wilkins, M.H.F. Proc.Roy.Soc. A 184 (1945) 366-380, 390-407

4. 9 Bonfiglioli, G. 'Thermoluminescence of geological materials' Academic Press London (1968) p 15-25

4.10 Yokota, R. Phys. Rev. 91(1953) 1013

4.11 Kikuchi, T. J. Phys. Soc. Japan 13,5(1958) 526-531

4.12 Shalgaonkar, C.S. and Narlikar, A.V. J. Mat. Sci. 7(1972) 1465-1471

4.13 Medlin, W.L. J. of Chem. Phys. 38,5(1963) 1132-1145

4.14 Barry, T.I., Clinton, D., Lay, L.A., Mercer, R.A., and Miller, R.P. J. Mat. Sci. 5(1970) 117-126

4.15 Sidorov, T.A. and Tyul'Kin, V.A. Izv. Akad.Nauk.SSSR Neorg. Mater. 2,11 (1966) 2033-2038

4.16 Schreurs, J.W.H. J. Chem. Phys. 47,2 (1967) 818-830

4.17 Weeks, R.A. J. Appl.Phys. 27,11 (1956) 1376-1381

4.18 Mackey, J.H., Boss, J.W. and Kopp, M. Phys. Chem. Glasses 11,6(1970) 205-212

4.19 International Series of Monographs on Solid State Physics, Colour Centers in Solids, P.104. Schulman and Compton Pergamon Press (1963)

4.20 Ferraro, J.R., Hazdra, J.J. and Boettner, W. J. Chem. Phys. 57,11 (1972) 4540-4542

4.21 Ferraro, J.R. and Manganani, M. Phys. Chem.Glasses (to be published)

4.22 Stroud, J.S., Schreurs, J.W.H. and Tucker, R.F. 7th International Congress on Glass, Brussels, June 28-July 3, (1965) 7-24

J. Phys. C: Solid State Phys., Vol. 5, 1972. Printed in Great Britain.

Optical characteristics of Tb^{3+} ions in soda glass

B V SHULGIN†, K N R TAYLOR, A HOAKSEY and R P HUNT
Physics Department, University of Durham, Durham, UK

MS received 16 December 1971, in revised form 30 March 1972

Abstract. The optical properties of terbium doped soda glass have been investigated as a function of terbium concentration. The properties studied in this work were the excitation, luminescence and absorption spectra and the luminescence decay times. In the case of short wavelength excitation, the absorption occurs in the glass matrix and is followed by energy transfer to the Tb^{3+} ions. At long wavelengths the efficiency of energy transfer between Tb^{3+} ions by dipole–dipole interaction is small up to quite high concentrations of terbium in the glass. However, above approximately 1 wt% Tb the intensity of the luminescent $^5D_4 \rightarrow {}^7F_j$ transitions increases very rapidly with terbium concentration. It is suggested that in this range energy transfer occurs between the ions of a Tb^{3+} ion pair by means of an exchange–dipole interaction.

1. Introduction

Increasing interest has been shown in recent years in the properties of the rare earth ions in glasses, both in terms of the theoretical and practical aspects of the glasses (Karapetyan and Reishakhrit 1967, Rindone 1966). A considerable amount of this work is concerned with the concentration dependence of both the luminescence and luminescence decay time, in particular for glasses doped with Tb^{3+} ions (Kovaleva *et al* 1966, Karapetyan and Lunter 1966, Reisfeld *et al* 1969). It is generally believed that the mechanism of energy transfer between the rare earth ions in such a matrix is one involving dipole–dipole interactions. Early observations in our laboratory have suggested that for terbium concentrations greater than about 0·6 to 1·0 wt% in soda glass a mechanism of energy transfer involving exchange–dipole interactions begins to occur.

In the present work we have investigated the optical properties of Tb^{3+} ions in a soda glass matrix. These have primarily been concerned with the luminescence behaviour and have included measurements of the excitation and emission spectra, the concentration dependence of these spectra and the luminescence intensity and the luminescence decay times associated with the Tb^{3+} ions. The effects of temperature on the luminescence and the energy storage after x ray irradiation have also been examined. In order to establish the mechanisms of energy loss in the specimens the absorption spectra were obtained between 300 nm and 6000 nm.

† At present working at Durham with the support of a British Council Scholarship. Permanent address: Urals Polytechnical Institute, Sverdlovsk, USSR.

2. Experimental

The samples were prepared by melting together 0·1 kg quantities of the base glass plus terbium oxide. The composition of the base glass is given in table 1 and the terbium oxide concentrations used varied from 0·1 wt% to 11·6 wt%. The melting was

Table 1. Composition of the base soda glass

Oxide	SiO_2	Na_2O	CaO	Al_2O_3	Others
wt%	70·8	16·4	5·0	2·5	≃ 5

performed in either platinum or quartz crucibles at 1300 °C for 3 hours. After melting, the specimens were cooled to 600 °C at a rate of 200 °C per hour and left at this temperature for 10 to 12 hours, before cooling to room temperature.

The luminescence, absorption and thermoluminescence (glow curve) spectra were obtained using a specially designed cryostat capable of working in the temperature range from 80 K to 860 K in conjunction with an Optika spectrophotometer. The heating rate used in the glow curve measurements was 2·5 degrees per second. The luminescence spectra were obtained with photoexcitation at a wavelength of 365 nm using a high pressure mercury lamp. The luminescence spectra obtained from the Optika were corrected for the quantum efficiency of the detectors used in this spectrophotometer.

The luminescence decay times were determined using either a mercury source modulated with a rotating shutter (pulse duration 0·4 ms) or a Zenon flash tube (pulse duration 5 μs). The luminescence emission intensity was measured using a conventional EMI 9514B photomultiplier, amplifier and oscilloscope system after passing through either a 540–560 nm filter or the Optika used in a monochromator mode.

3. Results and discussion

3.1. Excitation, luminescence and absorption spectra

The excitation spectrum of Tb^{3+} ions, measured for the emission at 553 nm is shown in figure 1. This is similar in form to the results obtained by Herring *et al* (1968) and consists of the following bands:

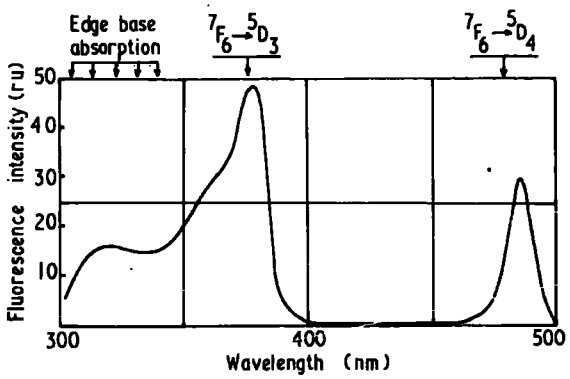

Figure 1. The excitation spectrum of a soda glass specimen containing 8·16 wt% Tb for the $^5D_4 \rightarrow {}^7F_j$ transitions obtained by measuring the wavelength dependence of the emission for excitation at 553 nm.

Table 2. (*a*) The details of the observed transitions for all the specimens used in this work

296 K, λ_{exc}, 365 nm			Concentration of Tb in soda glasses (wt %)									
			0·095		0·9		4·35		8·16		11·6	
λ nm	ν cm^{-1}	Transition	I	$\Delta_{\frac{1}{2}}$ (nm)	I	$\Delta_{\frac{1}{2}}$ (nm)	I	$\Delta_{\frac{1}{2}}$ (nm)	I	$\Delta_{\frac{1}{2}}$ (nm)	I	$\Delta_{\frac{1}{2}}$ (nm)
382	26178	$^5D_3$–$^7F_6$	—	—	—	—	—	—	—	—	100	590 cm^{-1}
416	24038	$^5D_3$–$^7F_5$	25	—	20·0	—	—	—	16·67	9	16·7	520 cm^{-1}
438	22831	$^5D_3$–$^7F_4$	18·4	—	21·6	—	32	—	13·51	8	26·0	—
444	22522	$^5D_3$–$^7F_4$	12·1	—	15·4	—	22	—	8·24	8	20·9	—
459	21786	$^5D_3$–$^7F_3$	4·66	—	8·16	—	5·83	—	4·08	8	9·3	380 cm^{-1}
474	21097	$^5D_3$–$^7F_2$	—	—	1·60	—	—	—	4·5	—	10	—
488	20492	$^5D_4$–$^7F_6$	4·85	19·6 ± 2·8	12·3	17·8	108·0	18·2	443·2	18·2	1800	18·2
497	20121	$^5D_4$–$^7F_6$	2·24		7·01		79·10		343·3		1463	
544	18382	$^5D_4$–$^7F_5$	14·2	16 ± 2	31·8	15	551·14	15	2136	15	6761	15
553	18083	$^5D_4$–$^7F_5$	27·0		39·5		672·30		2540		7230	
586	17065	$^5D_4$–$^7F_4$	—	—	5·33	—	—	—	393·4	—	1008	—
596	16778	$^5D_4$–$^7F_4$	—	—	—	—	—	—	252·9	—	609	—
620	16129	$^5D_4$–$^7F_3$	—	—	—	—	—	—	89·4	—	206	—

Table 2. (*b*) Halfwidths of the lower energy levels of the Tb^{3+} ions in the 11·6 wt % sample at room temperature

Level		$^5D_4$	$^7F_0$	$^7F_1$	$^7F_2^+$	$^7F_3$	$^7F_4(1)$	$^7F_4(2)$	$^7F_5(1)$	$^7F_5(2)$	$^7F_6(1)$	$^7F_6(2)$	$^7F_6$ General
Energy (cm^{-1})	26200	20500	(6000)	(5600)	5100	4360	3700	3430	2400	2100	370	0	0
$\Delta\nu$(cm^{-1})	380	490	—	—	~ 300	290	440	430	410	420	310	320	570 ± 25

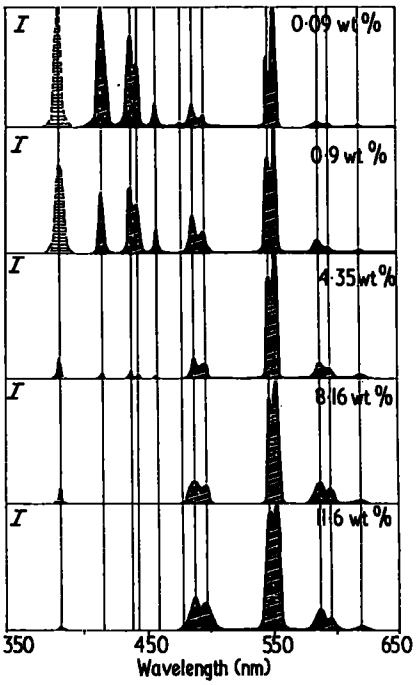

Figure 4. The variation in the form of the luminescence spectrum of the terbium doped glasses as a function of concentration. The intensities have been normalized to the peak at 554 nm. The mercury 365 nm emission line was used to excite the luminescence.

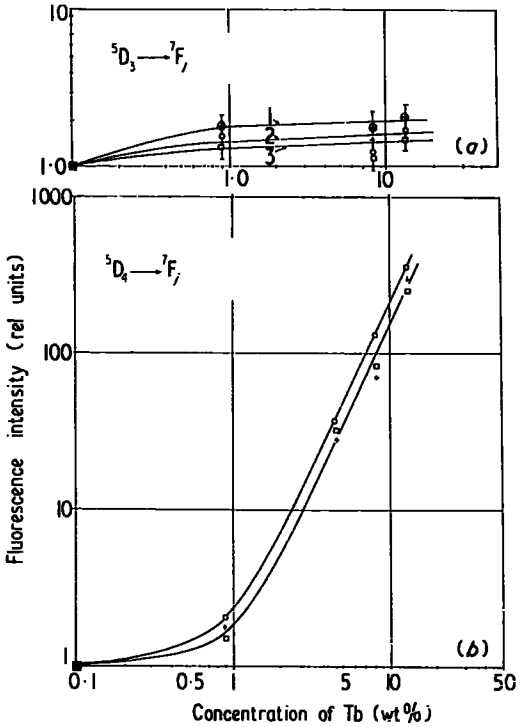

Figure 5. The concentration dependence of the luminescence intensity in terbium doped glasses for (*a*) the $^5D_3 \rightarrow {}^7F_j$ transitions: curve 1, 459 nm; curve 2, 444 nm; curve 3, 438 nm; (*b*) the $^5D_4 \rightarrow {}^7F_j$ transitions: + 488 nm; ○ 544 nm; □553 nm.

The efficiency derived this way is small ($\simeq$ 10%) for the 11·6 wt% Tb sample and consequently it is difficult to account for the sharp increase in the luminescence intensity of the $^5D_4 \rightarrow {}^7F_j$ transition in terms of the dipole–dipole model. Consequently we assume that on increasing the terbium concentration from 0·6–1·0 wt% to 11·6 wt% terbium the mechanism of energy transfer between the Tb^{3+} ions becomes a dipole exchange interaction. In the case of a single Tb^{3+} ion the $^5D_4$ state is excited by a nonradiative relaxation from the $^5D_3$ level. This is shown diagrammatically by 'A' in figure 8. In the case of a pair of coupled ions a further method of excitation of the $^5D_4$

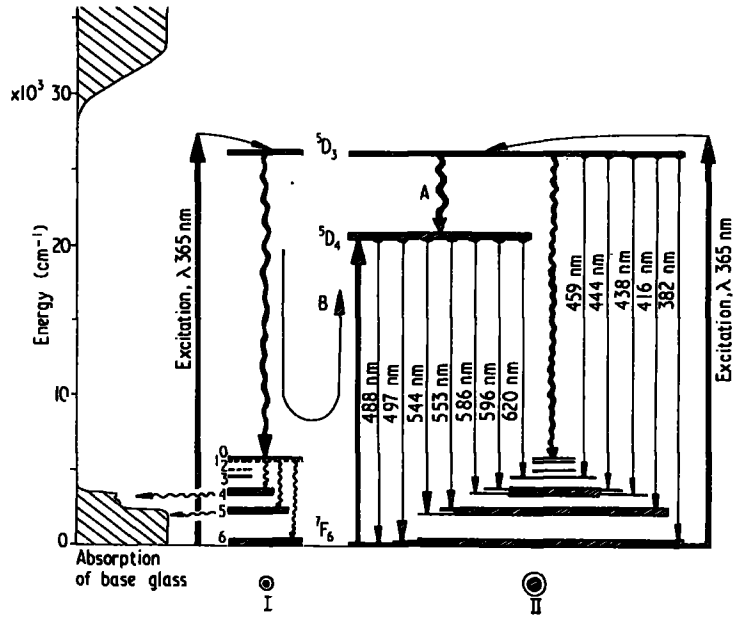

Figure 8. A schematic representation of the luminescence process of Tb^{3+} in soda glass showing both the single ion and ion pair interactions. The glass absorption spectrum is also shown to give a relative scale for the transitions.

level is possible. This occurs through a dipole exchange interaction mechanism shown as 'B' in figure 8. The energy separation of the $^7F_6 \rightarrow {}^5D_4$ and the $^7F_{0,1} \rightarrow {}^5D_3$ levels in the terbium ions are essentially the same. In the isolated ion the $^5D_3 \rightarrow {}^6F_{0,1}$ transition is experimentally found to be predominantly nonradiative and the energy of this transition is rapidly dissipated into the lattice. In the case of a pair of coupled ions however, the energy of the $^5D_3 \rightarrow {}^7F_{0,1}$ transition ($\simeq 25000\,cm^{-1}$) of one ion is absorbed by the $^5D_4$ levels of the second ion, allowing the more probable $^5D_4 \rightarrow {}^7F_j$ transitions to occur. The remaining energy associated with transitions within the ^7F_j manifold is either dissipated directly to the lattice (wavy lines in figure 8) or radiated as an infrared component of the luminescence.

A simplified version of the energy level model is reproduced in figure 9*a* where A is an isolated Tb^{3+} ion and B a pair of coupled Tb^{3+} ions. The $N_{j,a}$, $N_{j,b}(j = 2, 3)$ represent the number of Tb^{3+} ions in the different excited states. The subscripts *a* and *b* are used to distinguish the ions in the pair. The transitions between the different excited states are indicated by arrows and the radiative transitions with which we are presently concerned are labelled L_A and L_B. In the case of a noninteracting ion the basic kinetic equation describing level 2*a*, is,

$K'_{quench}(c)$ is also shown in this figure along with the concentration dependence of the luminescence.

3.3. Thermoluminescence and thermal quenching

After x ray irradiation the terbium doped specimens show a yellow colouration and a distinct glow peak is observed on heating. In figure 10*a* are presented the experimental glow curves for irradiation periods of 3 and 5 hours respectively for the 8·16 wt%

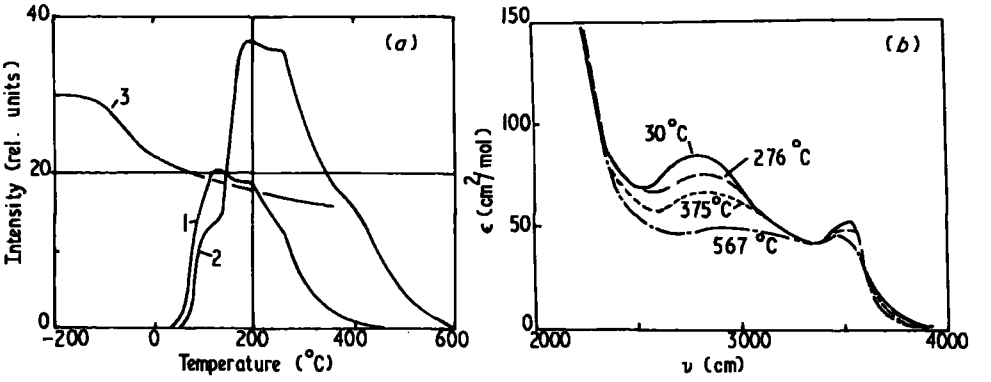

Figure 10. (*a*) The thermoluminescence (curves 1 and 2) and thermal quenching (curve 3) of the luminescence of the Tb^{3+} ions in soda glass. Curve 1, 3 h irradiation. Curve 2, 5 h irradiation. (*b*) The infrared absorption spectra for soda glass at different temperatures (after Scholze and Dietzel 1955).

sample. After heating to 500 °C visual inspection of the sample showed that the colouration had disappeared. The broad glow peaks in figure 10*a* appear to contain a series of separate peaks at 110, 190, 250, 350 and 405 °C, and while the position of these is independent of the irradiation period, the intensities of the higher temperature peaks increase with increasing irradiation. If we make a crude estimate of the trap depths (ϵ) from the positions of these peaks, using the formula

$$\epsilon = T_p/500\,\text{eV}$$

where T_p is the peak position in K, we obtain trap depths of 0·77, 0·93, 1·05, 1·25 and 1·35 eV.

We suggest that the thermoluminescence peaks and the observed colouration are connected with the same defects (electron traps) within the glass matrix. Further the nature of these defects appears to be understood. The analysis of the temperature dependence of the infrared absorption spectra for soda glass (see figure 10*b*) by Scholze and Dietzel (1955) shows that the destruction of the bound hydroxyl groups occurs in the same temperature region (30 to 600 °C) as the thermoluminescence output. Consequently it is proposed that the bound hydroxyl groups are the least stable regions in the glass structure and the defects appearing after x ray irradiation are connected with these bound groups. Annealing of these defects then leads to the glow peaks observed.

Finally, it is important to notice that the luminescence of Tb^{3+} in these glasses persists to quite high temperatures but shows a quenching phenomenon in the vicinity of the glow peaks. The experimental variation of the total luminescence with temperature

JOURNAL OF MATERIALS SCIENCE 8 (1973) 203–211

E.s.r. during crystallization in Gd^{3+} doped lithium-aluminium-silicate glasses

R. P. HUNT, K. N. R. TAYLOR
Physics Department, University of Durham, Durham City, UK

Measurements of the electron spin resonance spectrum have been made in a Gd^{3+} doped lithium-aluminium-silicate glass at various stages during the crystallization of the glass. The crystallization was induced by heat-treatment at various temperatures and took place either from the surface or from nucleation centres produced by the presence of TiO_2 in the glass.

The changes in the resonance spectra have been interpreted in terms of the stability of the gadolinium sites. In the presence of titanium, it is suggested that complexes are formed in the glass which involve both titanium and gadolinium ions.

Supporting measurements show that the presence of these complexes is also detectable from the more conventional structural and thermal characterization of the glasses.

1. Introduction

In recent years the volume of work being undertaken in an attempt to establish the nature of the glassy state has increased rapidly. In particular, electron spin resonance techniques have been used to provide information about environments of paramagnetic probe ions in the glass and about the phase transition from the glass to the crystalline state [1-6]. In this latter respect, the increasing development of glass ceramics has emphasized the importance of understanding the role played by nucleating agents in producing these materials. The most commonly used agent at the present time is TiO_2 although many other materials may be used for this purpose.

There are considerable differences of opinion concerning the mechanism of nucleation and subsequent crystallization [7-9] and it is by no means clear whether the Ti^{3+} ions surround the developing crystallites or are taken up substitutionally, i.e. into the β-spodumene and β-eucryptite lattices of the lithium-aluminium-silicate (LAS) ceramics, for example.

All the electron spin resonance work referred to above has made use of various transition metal ions as the structure sensitive probe with which to investigate the initial stages of crystallization. Little use appears to have been made of the 4f ions of the lanthanide series however, a fact which may be associated with the reduced effects of the crystal field on these ions compared with the 3d-transition metal ions. It is possible that there is less distortion of the glass structure about a 4f impurity ion than there is about a 3d since the 4f electrons are deeply buried in the ion and consequently well screened from the crystalline electrostatic field. This is not the case for the 3d ions and it may be necessary with these to allow for some distortion of the surrounding glass matrix when evaluating the Hamiltonian for the system. As a result of this the lanthanide ions may prove more satisfactory structure sensitive probes provided that the effects of crystallization are large enough to be resolved and provided that the observed spectra are capable of interpretation. This latter point is also true for the transition metal ions of course.

Early resonance work on lanthanide ions in glass was carried out by Garif'yanov [10], Chepeleva [11] and Nicklin [12] using the Gd^{3+} ion in glass matrixes which had not been heat treated. A common feature of this work was the appearance of high g-value resonances ($g \simeq 4$ and $g \simeq 6$) in addition to the $g = 2$ resonance to be expected for the S-state ion. To our knowledge such low field transitions for the Gd^{3+} ion have most frequently been reported for glassy hosts and rarely for gadolinium substituted into a crystal lattice, although as the works of Abraham

TABLE I The composition of the various glasses used in this investigation

Glass no.	SiO_2	Al_2O_3	Li_2O	TiO_2	Gd_2O_3	MgO	CaO	BaO	Na_2O	K_2O
1022	60	20	20	—	—	—	—	—	—	—
1035	60	20	20	5.0	—	—	—	—	—	—
1036	60	20	20	5.0	1.0	—	—	—	—	—
1058	60	20	20	—	1.0	—	—	—	—	—
1000	70.8	2.4	—	—	1 → 20	2.4	5.0	1.8	16.4	1.6

et al [13, 14] and Darby [15] have shown, once a strong crystal field environment lifts the restrictions on the transition selection rules ($\Delta m = \pm 1$) then many high g-value resonances should be observable. The removal of these selection rules occurs because of the admixing of the wave functions caused by the large electrostatic interaction.

We have recently examined the effects of crystallization on these resonances for surface nucleated crystal growth of glasses containing no titania and for bulk nucleation caused by the addition of TiO_2 to the glass melt. This work has shown that the behaviour of the individual resonances is sensitive to the presence of titania and the results are described in the following.

2. Experimental

Various glasses were prepared from high purity Li_2CO_3, Al_2O_3, SiO_2, TiO_2 and Gd_2O_3 by heating 100 g quantities of the well-mixed constituents at 1450°C for 8 h. Homogeneity was improved by intermediate crushing and remelting. Nucleation and crystallization were induced by further heat-treatment in the temperature range from 600 to 900°C. This heat-treatment was carried out in two ways, either by heating at a fixed temperature in this range after warming directly from room temperature or alternatively by heating in this range after a previous preheating treatment (nucleation) at a lower temperature. These different methods lead to two different types of crystallization behaviour, as is well known for the lithium-aluminium-silicate system [16]. Differential thermal analysis (DTA) was used to establish the nucleation and crystallization temperatures required for these heat-treatments.

The glasses prepared for this examination are listed in Table I, in which the detailed compositions are given.

The crystallographic structure of the heat-treated glasses was determined using conventional Debye-Scherrer X-ray diffraction techniques and the percentage crystallization estimated either from the relative intensities of the dominant lines of these diffraction patterns or from low magnification electron micrographs obtained from carbon replicas of the surfaces of freshly broken chips of the glasses.

Electron spin resonance measurements were made using a conventional X-band reflection spectrometer with field modulation at 180 Hz.

2.1. Structural and related data

The differential thermal analysis results showed the presence of two endotherms in the glasses containing titanium, but only one in the base glass LAS 1022. The low temperature endothermic peak T_N, for the titanium doped glasses, is thought to correspond to the nucleation process [17] and occurs some tens of degrees below the dominant exothermic, crystallization peak T_c. The lower peak is at least an order of magnitude smaller than the crystallization peak and as a result the nucleation transition was frequently difficult to detect.

Fig. 1 shows the DTA results for the LAS 1022, LAS 1035 and LAS 1036, specimens and there are two features which are evident from these results. First the presence of 5 at. % TiO_2 in the glass causes the crystallization temperature to be lowered by approximately 50°C and at the same time the width of the corresponding peak in the DTA output is drastically decreased. Secondly, if as little as 1 at. % Gd_2O_3 is added to the glass in addition to the 5 at. % TiO_2 the temperature of crystallization is immediately returned to the value corresponding to the base glass and the transition region is again broadened. The nucleation temperature however, is essentially unchanged between the glasses containing only titanium and those containing both titanium and gadolinium.

As indicated earlier two methods were used for crystallization of the glass, either direct crystallization at some temperature or a nucleation treatment followed by crystallization at a higher temperature. In both of these techniques the

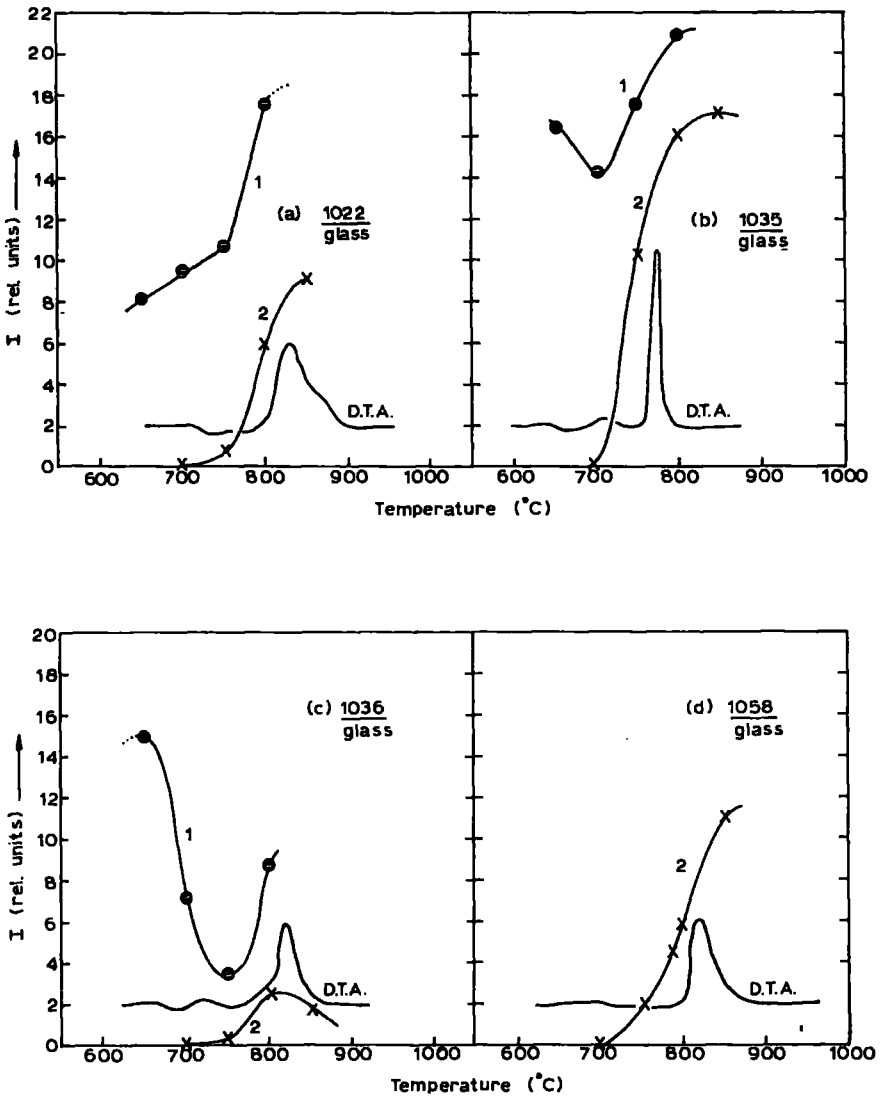

Figure 1 DTA and degree of crystallization of glasses 1022, 1035, 1036 and 1058. Curves 2 represents the degree of crystallization in samples held for 1 h at these temperatures whilst curves 1 are for samples after a subsequent heating at 850°C for 1 h.

X-ray diffraction patterns showed the presence of only the β-eucryptite phase and as Table II shows, the derived lattice parameters are essentially insensitive to the titanium or gadolinium additions.

The extent of crystallization and the crystallite size were found to depend strongly upon the composition however, for a given heat-treatment. The degree of crystallization, as estimated from the intensities of several of the diffraction lines for standard sample and exposure conditions, are shown in Fig. 1, superimposed on the DTA output. For a single heat-treatment, little crystallization was detected at temperatures less than those corresponding to the crystallization peak. Above T_c however, the percentage crystallization rose rapidly before passing through a maximum. Again there is a marked difference between the LAS 1035 (TiO_2 only) and LAS 1036 (TiO_2 + Gd_2O_3) glasses; for the latter composition the maximum amount of the crystalline phase was almost an order of magnitude less than

TABLE II Derived lattice parameters of glasses crystallized for 1 h at 850°C after nucleation (for 1 h) at the temperatures shown.

	Sample heated for 1 h at these temperatures followed by 1 h at 850°C											
	650°C			700°C			750°C			800°C		
	a	*c*	A.V.	*a*	*c*	A.V.	*a*	*c*	A.V.	*a*	*c*	A.V.
1022	5.26	11.17	267.6	5.18	10.98	255.1	5.25	10.97	261.8	5.21	11.08	260.5
1035	5.27	10.94	263.1	5.40	11.15	281.6	5.23	11.23	266.0	5.11	11.00	248.7
1036	5.24	11.10	263.9	5.28	11.13	268.7	5.20	10.96	256.6	5.25	11.03	263.3

A.V. = unit cell volume.
a, *c* dimensions are in Å and A.V. is in Å^3.

that for the specimens containing only TiO_2.

Further evidence for the inhibition of the crystallization process by gadolinium comes from the results obtained for specimens subjected to a double heat-treatment. The glasses containing TiO_2 both show a double peak in the percentage crystallization curves in agreement with other workers [18], however when Gd_2O_3 is also added to the glass the amount of crystallization developed by the second heating at temperatures above 700°C is much less than for the glasses containing only TiO_2. This is clearly seen in Fig. 1 and it is evident that while the nucleation efficiency appears to be unaffected by the addition of gadolinium, the subsequent crystallization is severely inhibited by its presence. Surprisingly, however, the LAS 1058 specimens, containing Gd_2O_3 only, showed quite extensive crystallization after the single heat-treatment.

The electron micrographs also showed these differences, the grain size in the LAS 1035 glasses being greater than that in the LAS 1036 glasses for comparable heat-treatment.

2.2. Electron spin resonance

E.s.r. absorption was anticipated only for those glasses containing Gd^{3+} ions. However, specimens of all the glasses prepared were examined in order to eliminate the possible existence of impurity resonances (for example from Fe^{3+}) which might interfere with the Gd^{3+} spectra. Resonances were never found in any specimen which did not contain gadolinium, a feature which also confirmed that the titanium ions in the LAS 1035 and LAS 1036 specimens were in the non-magnetic Ti^{4+} state. In a later phase of the work the titanium ions were deliberately converted to the Ti^{3+} state by solarization with X-rays, and under these conditions sharp and intense absorptions were observed in the vicinity of $g = 2.0$. The nature of these results will be described in a later publication and it is necessary here to comment only on the fact that in the present work the absence of these Ti^{3+} resonances in the glasses containing titania may be taken as evidence for the existence of only non-magnetic Ti^{4+} ions in these glasses. Consequently any possible influence of these ions on the observed spectrum due to cross relaxation phenomena can be ruled out. In further support of this conclusion, the temperature dependence of the spectra for glasses containing both gadolinium and titanium ions was not typical of that to be expected for a resonance spectrum dominated by cross relaxation [19].

The resonance spectra for three gadolinium concentrations (0.09, 0.2 and 1.0 at. %) were examined in preliminary measurements in order to determine the optimum conditions for the present investigation. The general form of the spectra in the range from $H = 0$ to 8 kOe is the same for all the compositions with relatively sharp resonances at $g \simeq 5.9$ and 4.3 and a much broader high intensity resonance with its centre field corresponding to $g \simeq 2.0$. This is shown for glass LAS 1058 (1.0 at. % Gd) in Fig. 2. There is also evidence of some further structure associated with this large peak in the vicinity of $g = 2.0$ but it has so far proved impossible to resolve this satisfactorily. The location of the Ti^{3+} resonance observed in titanium containing samples after X-ray irradiation is indicated in this figure. There is no evidence for this resonance in this material, before irradiation.

The only variation evident from decreasing the gadolinium concentration is associated with the broad central resonance which decreases in intensity but there is no change in its half-width.

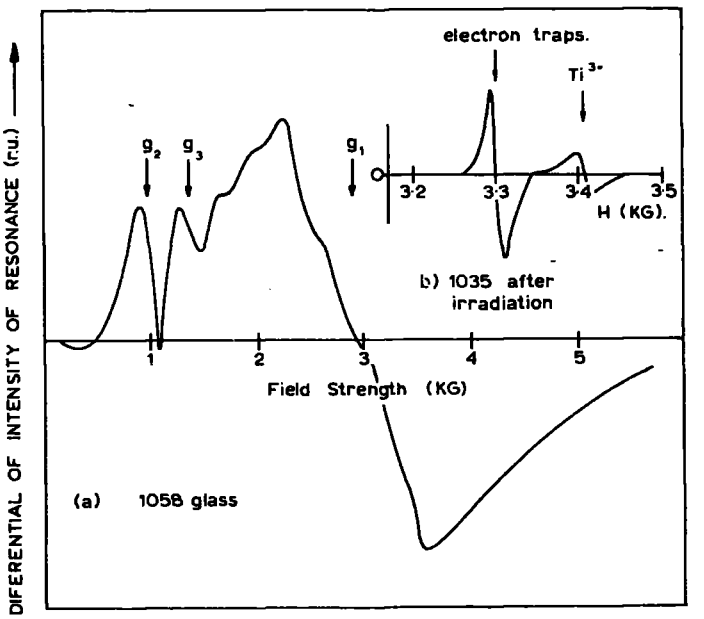

Figure 2 Differential of e.s.r. signal for glasses (a) 1058 (b) 1035 after X-ray irradiation.

There is no corresponding change in the higher g-value line intensities and again the half-widths are independent of composition, consequently we can assume that there are no appreciable interactions between the Gd^{3+} ions leading to exchange narrowing of the lines in the concentration studied. These features are typical of those found by earlier workers with gadolinium doped glasses and we have used a 1.0 at. % gadolinium concentration employed in the previous investigations of other workers and direct comparison of the various sets of results should therefore be more meaningful.

The resonance spectrum of the 1 at. % Gd^{3+} sample (Fig. 2) is similar to that found by these earlier workers [10-12] using other types of glass matrix.

It was found that after heat-treatment the intensities of the g_2 and g_3 resonances (see Fig. 2) decrease with respect to the g_1 resonance as the heat-treatment temperature is increased above about 600°C. This decrease, which is shown in Fig. 3, occurred for both the LAS 1036 (Gd and Ti doped) and LAS 1058 (Gd doping only) glasses. However, the detailed variation of the intensity ratio of the g_2 and g_3 resonances (I_2/I_3) depends upon the composition of the glass under investigation. For the LAS 1058 glasses, increasing the temperature of heat-treatment led to a sudden increase in I_2/I_3 above about 800°C. This temperature corresponds to the onset of surface nucleated crystallization as described earlier. Fig. 4 shows the variation of this ratio with increasing heat-treatment temperature. Fig. 4 also shows the behaviour of the glasses containing both titanium and gadolinium for which the results are obviously different, the I_2/I_3 ratio decreasing with increasing nucleation heat-treatment temperature. Comparison with the DTA and crystallization data of Fig. 1 suggests that these variations in the intensity ratio are associated with the onset of crystallization, differences occurring due to the different methods of nucleation.

3. Discussion

The changes caused in the transition temperatures by the addition of TiO_2 and Gd_2O_3, either separately or together, to the glass melts are evident from the results given in Fig. 1. The normally wide range of the crystallization transition at T_c is appreciably narrowed by the addition of TiO_2 in agreement with other workers, and corresponds to an increase in the crystallization efficiency caused by the action of the titanium ions as nucleating agents. As mentioned earlier the precise role played by these ions is not yet understood. With gadolinium

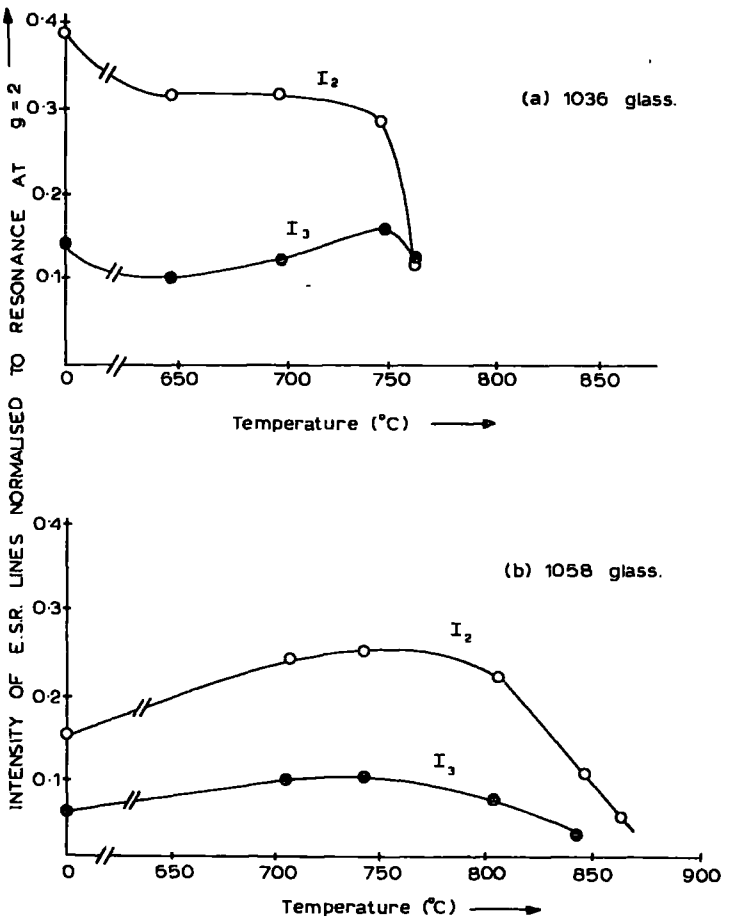

Figure 3 Relative intensities of high g-value resonances in glasses (a) 1036 (b) 1058 with heat-treatment.

doping alone the results are similar to those for the base glass LAS 1022, however, it is remarkable that in the LAS 1036 glasses the effects of the addition of 5% TiO_2 have been almost completely negated by the simultaneous addition of 1% Gd_2O_3. The crystallization temperature is comparable to that in glasses containing no TiO_2 and the range over which crystallization occurs is correspondingly larger. The nucleation temperature is little affected by the presence of the gadolinium ions however.

There is clear evidence from the X-ray data of a double peak in the dependence of the amount of crystallization on heat-treatment temperature for glasses containing TiO_2 subjected to the two stage heat-treatment. This is in agreement with other workers [18], the initial peak corresponds to nucleated crystal growth; whilst the second peak is due to a rapid crystal growth in the specimen in which the lower viscosity allows a much easier path for either bulk or surface crystallization. We will refer to these peaks as the nucleation and crystallization peaks respectively. It is remarkable, however, that with both gadolinium and titanium ions present the crystallization peak is greatly diminished compared with the results for specimens containing only titanium. There seems to be no comparable effect on the nucleation peak, and it appears that while the Ti^{4+} ions can perform their role in bringing about nucleation in the presence of gadolinium, the presence of this latter ion inhibits the subsequent crystal growth about the nucleation centres. The action of the gadolinium in this respect is very efficient since only 1% Gd_2O_3 greatly reduces the effects of 5% TiO_2.

The mechanism of this desensitization is unclear, as the action of the TiO_2 alone is not yet

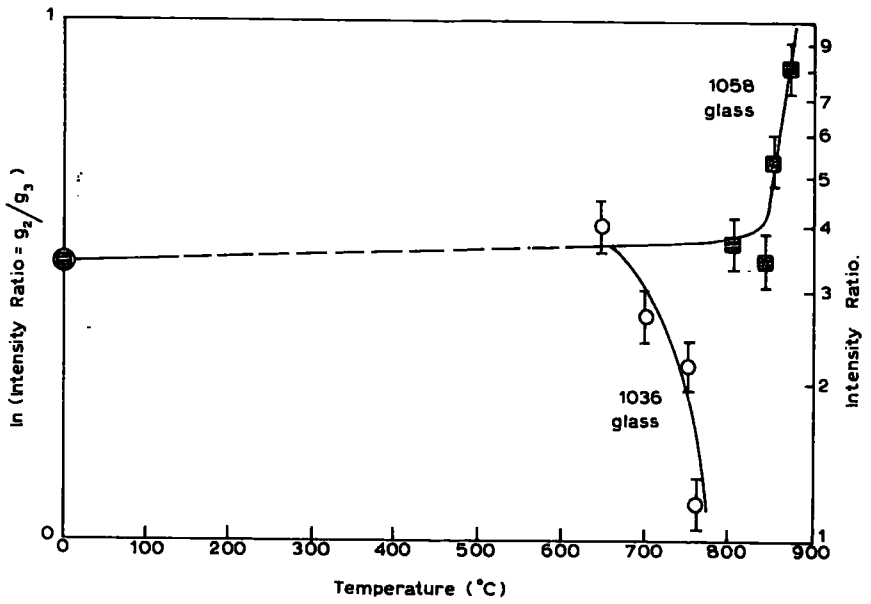

Figure 4 A comparison of the ratio of intensities of resonances at $g \approx 5.8$ (g_1) to $g \approx 4.3$ (g_2) for Gd in glass 1058 and 1036 varying with heat-treatment for 1 h at the temperatures shown.

understood. If the titanium ions are taken up substitutionally into the growing crystal phase, as some workers believe, the action of gadolinium must be to prevent the titanium ions entering the lattice. This can occur either by changing their valence through an electron transfer process or alternatively by forming complexes including at least the $Ti^{4+\,(or\,3+)}$ and Gd^{3+} ions such that the affinity of the titanium ions for these complexes is greater than that for the growing crystal. Other workers take the view that the titanium ions reduce the lattice stability on a shell surrounding the growing crystals and so allow the glass-crystal transition to occur more easily by atomic diffusion. In this case the action of the gadolinium must be to increase the stability of the glass matrix either by adopting the role of a network former or again by forming Ti-Gd complexes which are capable of screening the effects of the Ti^{4+} ions from the glass structure. Such complexes would require an extremely efficient interaction between the two types of ion as they are in the ratio of 1 (Gd):5 (Ti). There is, however, considerable evidence from other studies that some interaction does occur. These include differences in the optical absorption spectrum of solarized LAS 1036 and LAS 1035 glasses and changes in the thermoluminescence and luminescence behaviour caused by the addition of TiO_2 to glasses containing Gd_2O_3, only. The results of these measurements will be described elsewhere.

Interpretation of the resonance spectra for the specimens which have not been subjected to a heat-treatment (see for example Fig. 2) represent a considerable problem in themselves. The existence of the $g = 2$ resonance is to be expected for the Gd^{3+} ion, which has an $S_{7/2}$ ground state, and the very great width of the corresponding resonance can readily be attributed to the random orientation of the applied magnetic field with respect to the symmetry axes of the "crystal field" environment about the gadolinium ion. The low field resonances corresponding to $g = 4.3$ and 5.9 are less readily explained.

In principle we can adopt the conventional spin-hamiltonian

$$\mathcal{H}_S = g\,\mu_B\,H\,.\,S + \mathcal{H}_{CF} \qquad (1)$$

to describe the splitting of the ground state J-manifold for probe ions situated in the electrostatic field associated with the surrounding host ions. However the $\mathcal{H}_{CF}$ term contains the well-known (see for example [20]) factors α, β and γ which are identically zero for a pure S-state ion.

Consequently any observed splitting must be derived from second order effects [21] using an effective crystal field hamiltonian of the form

$$\mathscr{H}_{CF} = S.D.S \ (= \sum B_n^m O_n^m) \qquad (2)$$

where D is a tensor arising from the second order effects of the fine structure interaction. D and g are then used as disposable parameters for fitting the observed data.

While this approach may be used satisfactorily in single crystal systems its application to polycrystals is more difficult since the observed spectra then contain spatial averages over all possible crystallite orientations relative to the applied field. The situation is even worse in a glass matrix where it is not at all certain that the paramagnetic resonance probe sites are identical. At best one can probably assume similar co-ordinations for the probes but the interatomic spacing of the ions in the immediate vicinity of the probe will differ from ion to ion. Consequently a second average must be made in attempting to reproduce the observed resonances and analysis in this way may be of little value unless a great deal of structural information is known about the glass matrix.

If one persists in employing the spin-hamiltonian approach to account for the main resonance of the glasses containing Gd^{3+}, the high g-value resonances may be considered as forbidden ($|\Delta M_S| > 1$) transitions, which may not be fitted by Equation 1 and we must invoke the presence of strong crystal field effects to remove the limitation imposed by the selection rules. The low field transitions are then effectively those between the crystal field split doublets of the $J = 7/2$ state. Alternatively, however, we can use the method of analysis described by Koster and Statz [22, 23] since the matrix elements contained in the expression for the oscillator strengths suggest that a great many transitions may occur between the eight levels, including some at very low field values. The hamiltonian used in this treatment is formed by using basis wave functions of the correct symmetry and Koster and Statz have shown that the matrix elements of $\mathscr{H}_z$ between two states Γ_i and Γ_j may be written.

$$\langle\Gamma_i|\mathscr{H}_z|\Gamma_j\rangle = \mu_B g_1^{ij}[H_x U_x^1 + H_y U_y^1 + H^2 U_z^1] + \mu_B g_2^{ij}[H_x U_x^2 + H_y U_y^2 + H_z U_z^2] \qquad (3)$$

where the g^{ij}'s are fitting parameters and the U's are matrices which have been derived once and for all for many symmetries by Koster and Statz. The zero field splittings are assumed to exist *ab initio* and the level separations are then also used as fitting parameters. Unlike the spin hamiltonian approach the g-values are not related by simple constants and there is, in consequence, considerably more flexibility in fitting observed resonances using this method.

Unfortunately, random orientation of the distorted environments about the Gd^{3+} ions again make spectra interpretation extremely hazardous and until such time as a satisfactory means of analysis of e.s.r. spectra in glasses is developed it is probably more useful to attempt to employ the characteristics of the resonance spectra themselves (i.e. line width, resonance field and line intensity) as a means of obtaining information indicating possible correlations between the structural and electronic properties of glasses.

The most sensitive features of the spectrum of Fig. 2 are the low field resonances and as we have seen the relative intensities of these lines vary with heat treatment, the detailed variation depending upon the composition. The line widths and resonance fields are essentially constant however. If we take the increase in the I_2/I_3 ratio with heat-treatment temperature observed for the LAS 1058 glasses as the normal behaviour then the sudden drop in this quantity in the titanium containing, LAS 1036 glasses must be taken as a further indication of an interaction between the Gd^{3+} and Ti^{4+} ions.

The initial problem in the interpretation of the variation of the e.s.r. spectra is then one of establishing whether the observations are associated with a single type of gadolinium site or with two or more sites whose stability is associated with the degree and type of crystallization.

If the spectrum arises from a single atomic environment the low field resonances must arise from transitions between the strongly hybridized doublets of the $J = 7/2$ manifold. It is then difficult to see why the presence of titanium ions during crystallization should affect one of the resonance lines more than another. The most likely mechanism for such an effect would be a cross relaxation process but as we have seen the possibility of this seems to be small. It is possible, of course, that at Gd^{3+} sites which have a Ti^{4+} ion in the nearest neighbour shell, the change in the crystal field symmetry is sufficient to change the eigenfunctions of the levels involved in the low field transitions and hence the transition probability between them. Changes of this type

however, would normally be accompanied by changes in the energies of the levels concerned and consequently in the resonance field values. As this is not observed we must assume that the changes are such as to leave the average resonance position the same or alternatively that a two site model is to be preferred.

In this latter case, it is convenient to consider the $g = 5.4$ and 4.3 resonances as being the low field transitions at the two sites in question. The structural evidence described earlier suggests that on crystallization with titanium present, the gadolinium and titanium ions may become jointly involved in complexes in the crystallizing glass. If this is so, then the zero field splitting of the ground state may be modified by the presence of the quadrivalent titanium ions as described in the previous section. These changes will depend on the location of the Ti^{4+} ions with respect to the symmetry axis of the local electrostatic field at the Gd^{3+} site.

Under these conditions the observed changes in the resonance line intensities would seem to suggest that (i) titanium is incorporated into one site in preference to another or (ii) that the crystal field is less sensitive to the presence of Ti^{4+} at one of the sites compared to the other or finally (iii) that the Gd^{3+} ions are ejected from one of the sites as crystallization develops. The complexes involved in these sites are almost certainly associated with non-bridging oxygen ions in the silicate matrix as considered by Barry *et al* [1-3].

At the present time it is not possible to differentiate between the models as more information is needed about the environments of the two types of "impurity" ions introduced into the matrix. It would seem to us, however, that the multiple-site case is perhaps to be preferred and the problem remaining is related to the establishment of the detailed structure of the complexes themselves, their relation to the glass as a whole and their behaviour during crystallization.

References

1. T. I. BARRY, *J. Mater. Sci.* **4** (1969) 485.
2. T. I. BARRY, D. CLINTON, L. A. LAY, R. A. MERCER, and R. P. MILLER, *ibid* **4** (1969) 596.
3. *Idem, ibid* **5** (1970) 117.
4. D. LOVERIDGE and S. PARKE, *Phys. Chem. Glasses* **12** (1971) 19.
5. H. W. DE WIJN and R. F. VAN BALDEREN, *J. Chem. Phys.* **46** (1967) 1381.
6. T. A. SIDOROV and V. A. TYUL'KIN, *Izvestiya Akademii Nauk SSSR, Neorganicheskie Materialy* **2** (1966) 2033.
7. T. I. BARRY, L. A. LAY, and R. P. MILLER, *Faraday Discuss.* **50** (1970) 214.
8. V. A. BLINOV, *J. Mater. Sci.* **4** (1969) 461.
9. R. D. MAURER, Proceedings of the fourth all-union conference on the glassy state, Leningrad, in "The Structure of Glass" vol. 6. Consultants Bureau New York, (1966) 111.
10. N. S. GARIF'YANOV, R. KH. TIMEROV, and N. F. USACHEVA, *Fizika Tverdovo Tela* **4** (1962) 3344.
11. I. V. CHEPELEVA, V. N. LAZUKIN, and S. A. DEMBOVSKII, *Izvestiya Akademii Nauk SSSR, Neorganicheskie, Materialy* **4** (1968) 1927.
12. R. C. NICKLIN, Ph.D. Thesis, November (1967) Iowa State University.
13. M. M. ABRAHAM, L. A. BOATNER, C. B. FINCH, E. J. LEE, and R. A. WEEKS, *J. Phys. Chem. Solids* **28** (1967) 81.
14. M. M. ABRAHAM, E. J. LEE, and R. A. WEEKS, *ibid* **26** (1965) 1249.
15. M. I. DARBY, *J. Chem. Phys.* (to be published).
16. P. E. DOHERTY, D. W. LEE, and R. S. DAVIS, *J. Amer. Ceram. Soc.* **50** (1966) 77.
17. D. CLINTON, R. A. MERCER, and R. P. MILLER, *J. Mater. Sci.* **5** (1970) 171.
18. P. S. ROGERS, *Mineral. Mag.* **37** (1970) 291.
19. A. ABRAGAM and B. BLEANEY "Electron Paramagnetic Resonance of Transition Ions" (Clarendon Press, Oxford, 1970).
20. W. LOW, "Paramagnetic Resonance in Solids" (Solid State Physics, Suppl. 2, Academic Press, New York, 1960).
21. J. W. ORTON, "Electron Paramagnetic Resonance" (ILIFFE, London, 1968).
22. G. F. KOSTER and H. STATZ, *Phys. Rev.* **113** (1959) 445.
23. H. STATZ and G. F. KOSTER, *ibid* **115** (1959) 1568.

Received 10 July and accepted 30 August 1972.

K.N.R. Taylor, B.V. Shulgin, R.P. Hunt

Afterglow E.P.R. and Optical Absorption Spectra of Gadolinium Doped Silica Glasses After X-ray Irradiation

Published Zh. Prikl. Spectrosk 13, 1973.

К. Н. Р. Тейлор*, Б. В. Шульгин, Р. П. Хант*

Термовысвечивание, спектры ЭПР и оптического поглощения рентгенизованных силикатных стекол, активированных гадолинием

В настоящее время проявляется большой интерес к изучению оптических и электронных свойств редкоземельных ионов в стеклах [1,2]. Имеется ряд работ, посвященных исследованию люминесценции силикатных стекол, Раман-спектров и спектров оптического поглощения [1-6], однако термовысвечивание силикатных стекол, активированных р.з.э., изучено недостаточно полно. В данной работе предоставлены результаты измерения характеристик термовысвечивания (ТВ), ЭПР и оптического поглощения рентгенизованных натриевых силикатных (НС) и литиевых алюмосиликатных (ЛАС) стекол, активированных гадолинием и обсуждается роль титана как центра стабилизации дефектов в этих основах.

Методика и результаты эксперимента. Объектами исследования были многокомпонентные стекла типа:

$1,64\,Na_2O \cdot 0,24\,Al_2O_3 \cdot 7,08\,SiO_2 \cdot 1\,M_nO_m \cdot 0,1\,Gd_2O_3$ – НС,

$2\,Li_2O \cdot 2Al_2O_3 \cdot 6\,SiO_2 \cdot 0,1\,Gd_2O_3$ – ЛАС и ЛАС+0,5 TiO_2

Здесь M_nO_m – окислы щелочных и щелочноземельных элементов. Кривые термовысвечивания и спектры оптического поглощения изучаемых стекол получены с использованием спектрофотометра типа Optika ИК в сочетании со специальным криостатом. Скорость нагрева при ТВ составляла ~ 2,0 град/сек. Рентгенизованные образцы (Со-анод, 20кв, 5 часов) имели серовато-сиреневую окраску.

---

* Дарэмский университет, физический факультет, г. Дарэм, Англия

Спектры ЭПР наблюдались с помощью стандартного 3см спектрометра с частотой модуляции магнитного поля 180 гц.

Спектр свечения гадолиния в исследуемых стеклах состоит из одной полосы при 313-315нм, причем интенсивность свечения в ЛАС-стекле была в 5-7 раз выше, чем в НС-стекле, вследствие меньшего поглощения излучения в ЛАС-основе. Для стекол типа ЛАС и НС, подвергнутых рентгенизации, наблюдается ТВ в области температур 60-500°С, рис.1. Общий максимум ТВ расположен в температурном интервале 250-350°С, однако на кривой ТВ можно выделить несколько слабо разрешенных максимумов при 110, 190, 260, 350, 405 и 450°С (последнее весьма приближенно). Для стекол с титаном (ЛАС+0,5 TiO_2) не было обнаружено ТВ с помощью нашей аппаратуры.

Окрашивание стекол при рентгенизации приводит к изменению их спектров поглощения. На рис.2а показаны спектры поглощения ЛАС-стекла до облучения (кривая 1), после облучения (кривая 2) и разность этих кривых поглощения (3), которая характеризуется двумя максимумами при 2,1-2,2эв и 3,1-3,2эв. На рис.2б представлены аналогичные данные для стекла с титаном. Видно, что после облучения в спектре поглощения ЛАС+0,5 TiO_2 появляется широкая полоса в области 1÷3эв. При нагревании стекла НС и ЛАС обесцвечиваются, стекла с титаном не обесцвечиваются вплоть до температур 500°С.

Сигналы ЭПР для Gd^{3+} в НС- и ЛАС-стеклах до и после облучения аналогичны таковым, наблюдаемым в других основах [7]. Для Gd^{3+} в ЛАС-стекле они представлены на рис. 3а, а для ЛАС+0,5 TiO_2 - на рис.3б. Сигнал ЭПР состоит из широкой полосы с g-фактором, примерно равным двум и нескольких других полос с g=2,3; 2,6; 4,3 и 5,8. В стеклах с титаном возрастает интенсивность полос

с более высоким значением g-фактора. Рентгеновское облучение (рис.3, кривые 2, 3, 5, 6), приводящее к образованию дефектов в стеклянной матрице, вызывает появление дополнительного дублетного сигнала ЭПР с g-фактором равным 2,01 для ЛАС и $g_1 = 2{,}01$ и $g_2 = 1{,}93$ для ЛАС+0,5TiO_2. Поскольку широкая гадолиниевая полоса в спектре ЭПР (кривые 2 и 5) затрудняла расшифровку сигналов ЭПР, связанных с наведенными при облучении дефектами, были использованы рентгенизованные образцы стекол, не содержащие гадолиний (кривые 3 и 6 на рис.3).

Обсуждение результатов. Между кривыми термовысвечивания, спектрами ЭПР и спектрами оптического поглощения в облученных ЛАС- и НС-стеклах существует определенная корреляция, обусловленная единой природой дефектов, образующихся в результате облучения.

Термовысвечивание. Для решения вопроса связаны ли пики ТВ в исследуемых стеклах непосредственно с Gd^{3+} было изучено ТВ для Pr^{3+}, Sm^{3+}, Tb^{3+} и Dy^{3+} в НС-стекле, рис.1. Из рисунка видно, что положение пиков ТВ практически не зависит от типа активирующего р.з. иона. (Пик ТВ при 450°С [redacted] наблюдается только для гадолиния, повидимому, ввиду высокой интенсивности свечения последнего). Таким образом, электронные ловушки, ответственные за пики ТВ в исследуемых многокомпонентных силикатных основах, связаны с дефектами в стеклянной матрице, а Ln^{3+}-ионы служат эффективными люминесцентными индикаторами, позволяющими обнаружить и оценить глубину этих ловушек. Глубина этих ловушек оказалась равной 0,77; 0,93; 1,05; 1,25; 1,35; 1,44эв (использовалась формула Урбаха). Средняя глубина наиболее заполненных ловушек, соответствующих основным наиболее интенсивным пикам ТВ, равна 1,0 и 1,3эв. Наши данные по ТВ качественно согласуются с результатами, полученными ранее другими авторами [5, 6], например, в γ-облученных неактивированных натриево-кальций (цинк)-силикатных стеклах также наблюдалось ТВ в области 200-300°С.

Опыты по ТВ не позволяют однозначно установить тип (электронный или дырочный) и природу центров захвата электронов. Они могут быть связаны, как предполагают авторы [5,6] с такими дефектами в решетке стекла, как атомы натрия, захватившие электрон, или с дырочными центрами на концевом немостиковом атоме кислорода типа $\geqslant Si - O^{\oplus}$ (I) или $\geqslant Si - O^{\oplus} \ldots Me^{+}$ (II). Ранее было показано, что слабым звеном в структуре силикатных стекол являются связанные гидроксильные группы [8]. Отжиг дефектов, обусловленных ионами гидроксила, происходит, как оказалось, в том же температурном интервале, что и ТВ (60÷600°С). Это позволяет предположить, что центры захвата электронов, возникающие в НС- и ЛАС-стеклах при рентгенизации, формируются прежде всего в ослабленных местах стеклянной матрицы вблизи связанных гидроксильных групп. Возможно, это центры типа $\geqslant Si - (OH)^{-}$

Спектры оптического поглощения и ЭПР. В спектрах оптического поглощения облученных ЛАС-стекол наблюдаются полосы с максимумами 565-590нм (2,1÷2,2эв) и 390-400нм (3,1-3,2эв). В НС-стеклах максимумы полос поглощения оказываются сдвинутыми в длинноволновую область. По аналогии с данными для других силикатных основ [5,6] можно предположить, что наблюдаемые полосы поглощения обусловлены атомами натрия, захватившими электрон. Обесцвечивание стекол, происходящее при нагревании, связано с рекомбинацией электронов, покидающих атомы натрия, с дырочными центрами. Энергия, выделяющаяся в результате рекомбинации может передаваться центрам свечения, в нашем случае ионам Ln^{3+}. Рекомбинация электронов может происходить также непосредственно с центрами свечения. Между центрами окраски и ловушками, обеспечивающими ТВ, можно установить корреляцию, если последние рассматривать как ловушки электронного типа. Это изображено на рис.4. Полоса 300-400нм в спектре поглощения соответствует ловушкам с глубиной ~1,0эв, а полоса 565-590нм - ловушкам с глубиной 1,35эв. Однако степень соответствия

при данных методах исследования установить трудно.

Сравнивая данные ЭПР и оптического поглощения, можно заметить, что центры окраски в облученных НС- и ЛАС-стеклах, связаны с дефектами, обеспечивающими появление ЭПР сигнала с $g \approx 2{,}01$. По аналогии с работой [5] предполагается, что α-компонента сигнала с $g \approx 2{,}01$ соответствует полосе поглощения 565-590нм, а β-компонента этого сигнала - полосе 390-400нм. Тем самым предполагается, что природа дефектов, проявляющихся при ТВ, ЭПР и оптическом поглощении НС и ЛАС-стекол прямым или косвенным путем связана с дырочными центрами на концевых немостиковых атомах кислорода типа I или II.

<u>Влияние TiO_2 на ТВ, ЭПР и оптическое поглощение</u>. Добавление 5% TiO_2 к ЛАС-стеклу, как было отмечено выше, вызывает увеличение интенсивности сигнала ЭПР с g-фактором 5,8. Поскольку резонанс с $g \approx 5{,}8$ для Gd^{3+} обычно связывается с высоко ассимметричными нерегулярными позициями Gd^{3+} ионов в стекле [7], можно считать, что присутствие Ti^{4+} ионов стабилизирует такие состояния Gd^{3+} ионов в процессе кристаллизации. Аналогичным образом присутствие TiO_2 стабилизирует возникающие при рентгенизации дефекты, характеризующиеся полосой поглощения в области 1-3эв и ЭПР сигналом с $g = 2{,}01$ и $g = 1{,}93$. Облученные стекла с титаном не обесцвечиваются вплоть до температур 500°С. Отжиг дефектов, связанных с введением TiO_2, происходит при более высоких температурах порядка 700-800°С (энергия активации ~2эв) вследствие чего ТВ в области температур 60-500°С (энергия активации 0,65-1,4эв) не наблюдается.

В заключение следует отметить, что способность НС- и ЛАС-стекол к светозапасанию при рентгенизации, характеризующаяся высокой энергией активации (1,3-1,4эв), может быть использована при разработке дозиметров мягкого рентгеновского излучения.

K.u.R. Taylor. [illegible] R Hunt.

Термовысвечивание, спектры ЭПР и оптического поглощения рентгенизованных силикатных стёкол, активированных гадолинием.

Реферат.

В работе представлены результаты измерения характеристик высокотемпературного термовысвечивания (ТВ) (60-500°С), ЭПР и оптического поглощения рентгенизованных натриевых силикатных и литиевых алюмосиликатных стёкол, активированных гадолинием. Пики ТВ наблюдаются при температурах 110, 190, 260, 350, 405, 450 °С. Добавление TiO_2 (5%) полностью уничтожает ТВ в этом температурном интервале и стабилизирует центры окраски в рентгенизованных кварцевых стеклах. Сигнал ЭПР облучённых стёкол характеризуется двумя линиями с $g = 2{,}01$ и $1{,}97$ (последнее в случае образцов с титаном). Обсуждается природа дефектов и корреляция между спектрами ЭПР, термовысвечиванием и спектрами оптического поглощения.

Подписи к рисункам в статье К.Н.Р.Тейлора, Б.В.Шульгина, Р.П.Ханта, «Термовысвечивание, спектры ЭПР и оптического поглощения рентгенизованных силикатных стёкол, активированных гадолинием».

Рис.1. Кривые термовысвечивания рентгенизованных НС и ЛАС-стёкол, содержащих р.з. ионы.

Рис.2. Спектры поглощения стёкол типа ЛАС и ЛАС + $0{,}5TiO_2$.

Рис.3. Спектры ЭПР. а - ЛАС-стекло, б - ЛАС + $0{,}5TiO_2$. 1,4 - до облучения, 2,5 - после облучения, 3,6 - после облучения для стёкол без гадолиния.

Рис.4. Уровни локализации электронов в ЛАС-стекле.

К.Н.Р.Тейлор, Б.В.Шульгин, Р.П.Ханта

Термовысвечивание, спектры ЭПР и оптического поглощения рентгенизованных силикатных стёкол, активированных гадолинием.

Аннотация

В работе представлены результаты измерения характеристик высокотемпературного высвечивания (60-500°С), ЭПР и оптического поглощения рентгенизованных натриевых силикатных и литиевых алюмосиликатных стёкол, активированных гадолинием. Единая природа наведённых дефектов обуславливает корреляцию между оптическими и ЭПР-данными. Обсуждается роль титана, как центра стабилизации дефектов в этих основах.

Литература

1. Г.О.Карапетян,А.Л.Рейшахрит.Изв.АН СССР.Неорг.материалы 3,217, 1967.
2. G.E.Rindove,Luminescence of Inorganic Solids.Akad.Press,N.Y.ed. P.Goldberg.1966,p.419.
3. Т.А.Сидоров,Ж.П.С.9,992,1968.
4. R.Eisfeld,A.Honigbaum,G.Michaeli.Isr.J.of Chem. 7,613,1969.
5. Т.А.Сидоров,В.А.Тюлькин,В.А.Аксёнов.Д АН СССР 175,1094,1967.
6. Т.А.Сидоров,В.А.Тюлькин,В.А.Аксёнов.Ж.П.С.7,778,1967.
7. И.В.Чепелева,В.Н.Лазуркин,С.А.Дембовский.Изв.АН СССР,Неорг. материалы 4,1927,1968.
8. H.Scholze,A.Dietzel.Naturwiss. 42,342,1955.

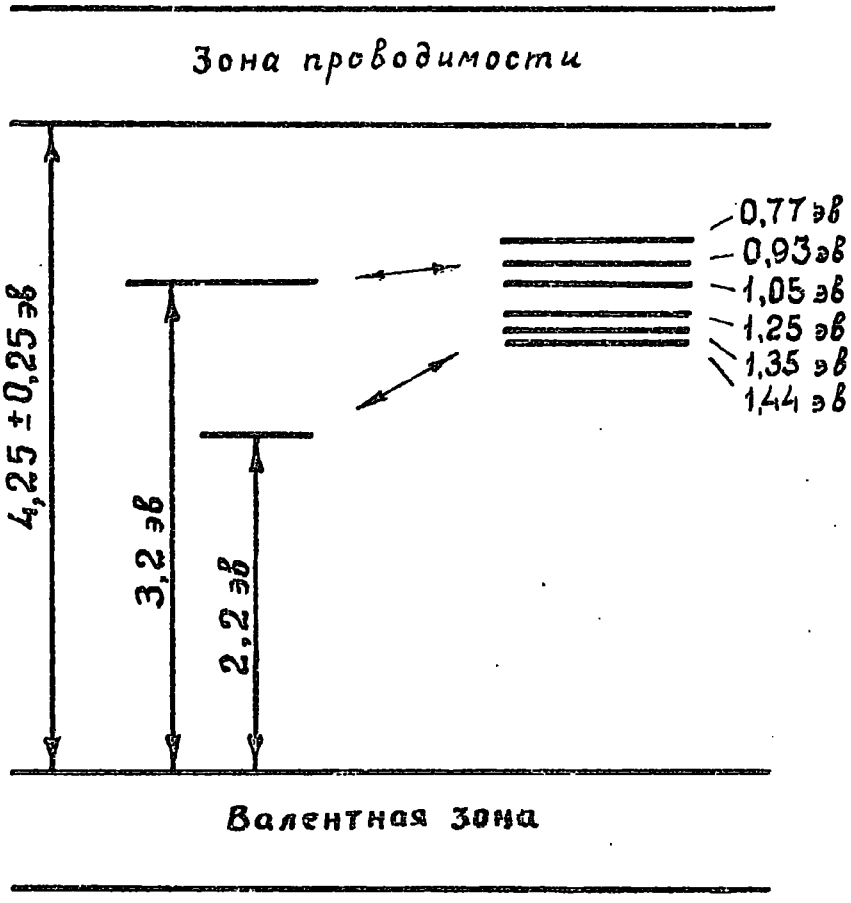
Зона проводимости
4,25 ± 0,25 эв
3,2 эв
2,2 эв
0,77 эв
0,93 эв
1,05 эв
1,25 эв
1,35 эв
1,44 эв
Валентная зона

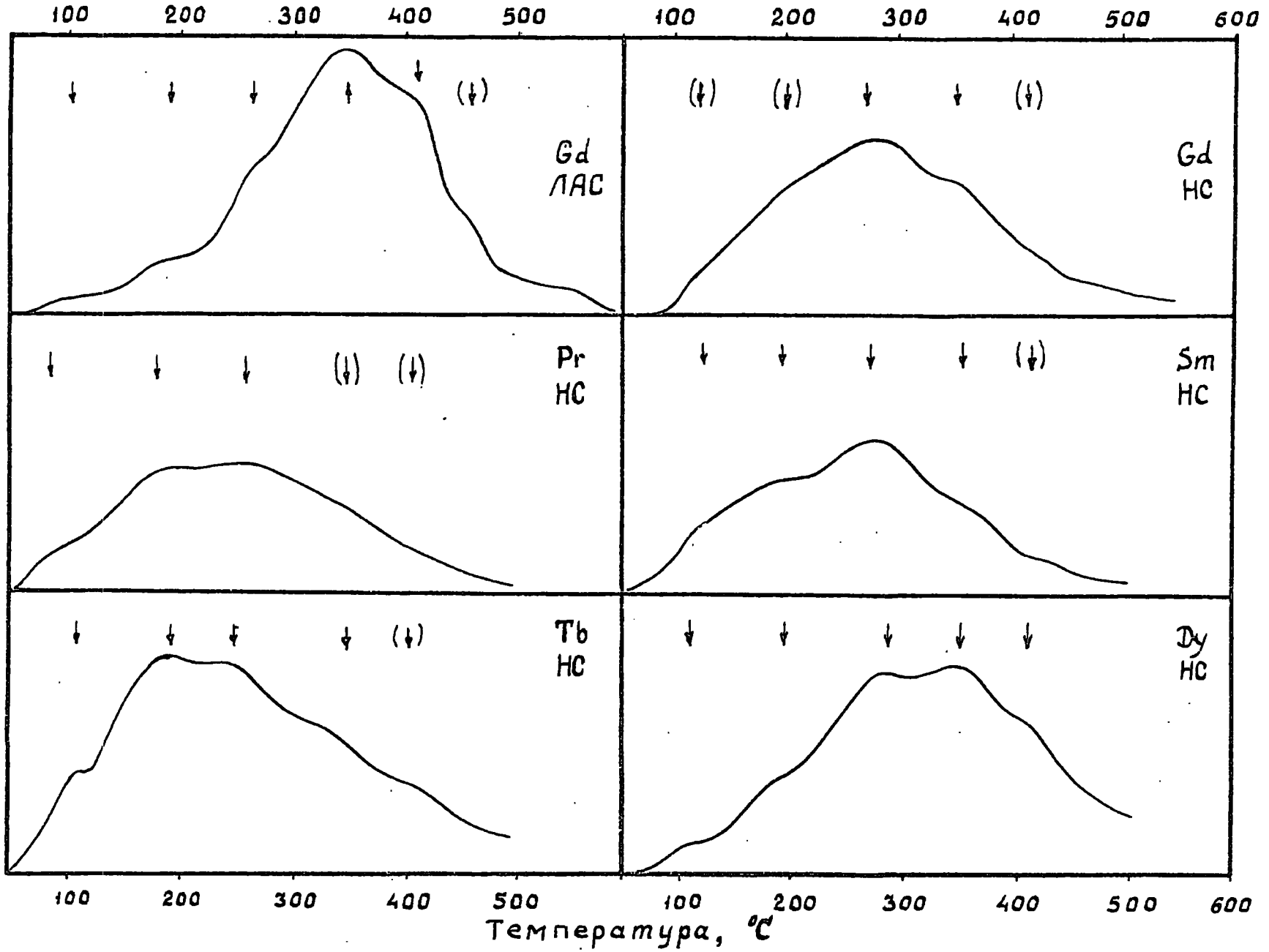
100
200
300
400
500
600
Gd
ЛАС
Gd
НС
Pr
НС
Sm
НС
Tb
НС
Dy
НС
Температура, °C

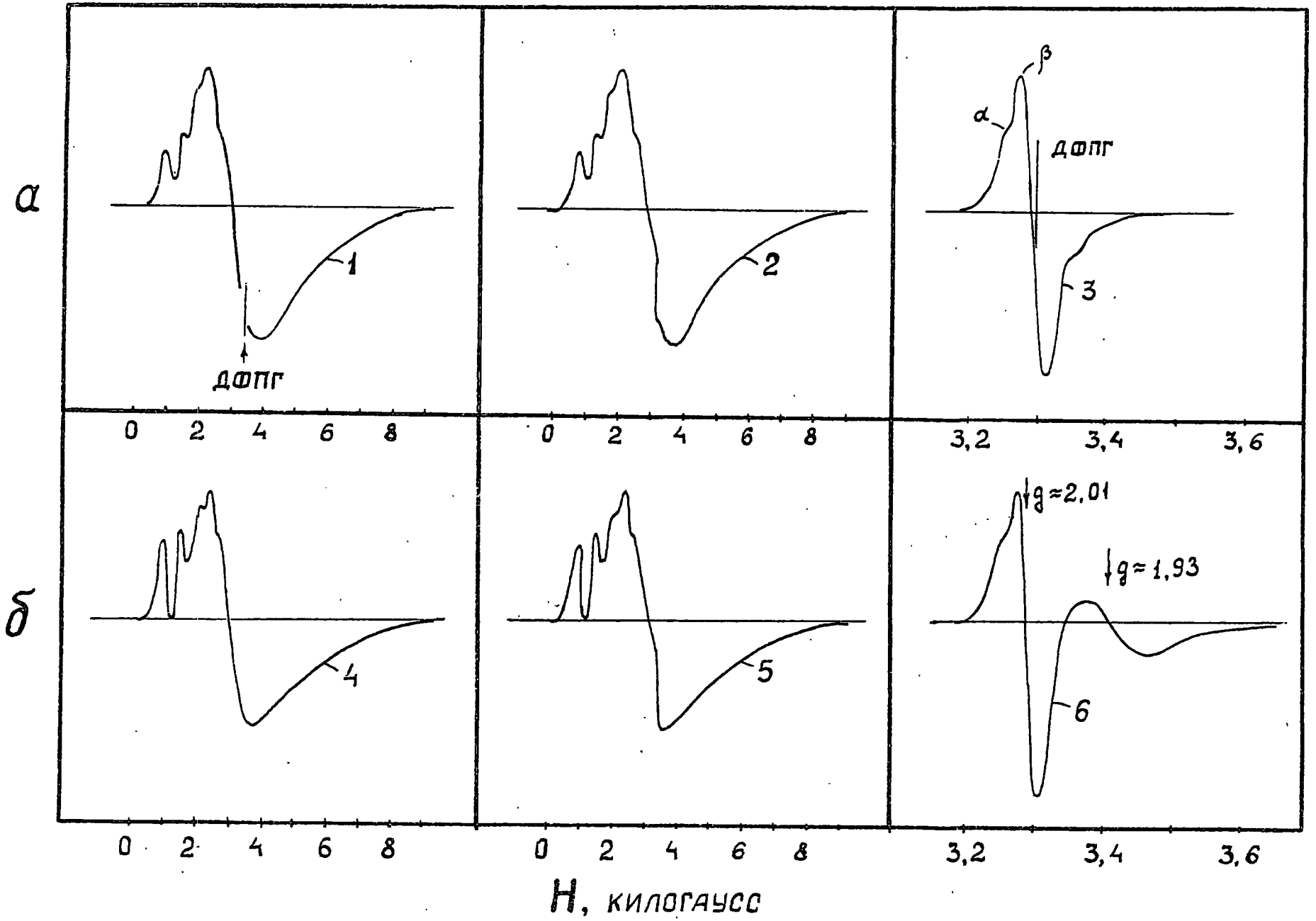
а
б
1
2
3
4
5
6
ДФПГ
α
β
g≈2,01
g≈1,93
0 2 4 6 8
3,2 3,4 3,6
H, килогаусс